Quantitative Evaluation of Redox Processes in Intact Rat Lungs and Endothelial Cells and the Effect of Hyperoxia

Zhuohui Gan
Marquette University

QUANTITATIVE EVALUATION OF REDOX PROCESSES IN INTACT RAT LUNGS AND ENDOTHELIAL CELLS AND THE EFFECT OF HYPEROXIA

by

Zhuohui Gan, B.S., M.S.

A Dissertation submitted to the Faculty of the Graduate School,
Marquette University,
In Partial Fulfillment of the Requirements for
The Degree of Doctor of Philosophy

Milwaukee, Wisconsin

December 2011

ABSTRACT
QUANTITATIVE EVALUATION OF REDOX PROCESSES IN INTACT RAT LUNGS AND ENDOTHELIAL CELLS AND THE EFFECT OF HYPEROXIA

Zhuohui Gan, B.S., M.S.

Marquette University, 2011

A common initial treatment of hypoxemia in patients with lung failure secondary to acute lung injury (e.g., adult respiratory distress syndrome) is oxygen (O_2) therapy (hyperoxia). However, prolonged O_2 therapy causes lung O_2 toxicity, which can further impair lung functions. The rat model of lung O_2 toxicity replicates key features of human lung O_2 toxicity. In addition, rats develop tolerance or susceptibility to 100% O_2 by pre-exposing them to 85% O_2 (hyper-85) or 60% O_2 (hyper-60) for 7 days, respectively. Therefore, the long-term objectives of this study are to elucidate mechanisms involved in rat tolerance of 100% O_2, and to further understanding of the mechanisms involved in lung O_2 toxicity. In this work, the effects of rat exposure to hyperoxia on targeted lung cytosolic/mitochondrial redox enzymes with pro- or anti-oxidant properties were evaluated using indicator dilution methods. The effect of hyperoxia on mitochondrial membrane potential ($\Delta\Psi_m$) in cultured endothelial cells was also evaluated using an approach developed in this study. Computational modeling was used for quantitative analysis data from intact lungs or cultured endothelial cells, and for estimation of parameters descriptive of the activities of targeted enzymes and $\Delta\Psi_m$. The results revealed an increase in the lung activity of NAD(P)H:quinone oxidoreductase 1 (NQO1) in hyper-85 and hyper-60 rats, a decrease in the lung activity of NADH:ubiquinone reductase (complex I) in rats exposed to 85% O_2 for >24 hours and an increase in the lung activity of Q-cytochrome c reductase (complex III) in hyper-85 rats. Exposure of endothelial cells to 95% O_2 for 48 hours did not alter $\Delta\Psi_m$ but increased its sensitivity to mitochondrial uncouplers. These results suggest that the decrease in the activity of complex I might be an early manifestation of an adaptive response to 100% O_2; and the increase in the activity of complex III might be important to this adaptive response. Thus, complexes I and III could serve as non-invasive indices of lung O_2 toxicity or tolerance using clinical imaging methods, or as therapeutic targets for protecting against lung O_2 toxicity.

ACKNOWLEDGEMENTS

Zhuohui Gan, B.S., M.S.

I dedicate this dissertation to my parents, my sister and all other my family members, who have been a source of great exuberance and support.

I sincerely thank my advisor Dr. Said Audi whose guidance, support and dedication have been critical to my study. I can say without exaggeration, every paragraph in this dissertation reflects the guidance and support from my advisor. Sincere thanks to Dr. Anne Clough, Dr. David Roerig, Dr. Elizabeth Jacobs, and Dr. John LaDisa for serving on the dissertation committee and providing insight into numerous challenges along the way.

I extend my gratitude to Dr. Robert Molthen, Dr. Steven Haworth, Dr. Gray Krenz, Dr. Marilyn Merker, Madhavi Ramakrishna, Qingping Wu, and Shelley Baumgardt for their help with the experiments and lab collaboration. And also I extend my gratitude to Dr. Lonber and Xiaoqian Liu for the western blot analysis of NQO1 for this study. Here, I express my specific gratitude to Robert Bongard who not only taught me experimental skills but also provided a great help for the completion of this study.

I thank Marquette University for the opportunity to work on this project and to obtain my doctoral degree. I extend my heartfelt gratitude to all those who have contributed, directly and indirectly, to the completion of this dissertation.

TABLE OF CONTENTS

LIST OF TABLES

LIST OF FIGURES

CHAPTER 1. INTRODUCTION AND BACKGROUND

1.1 Acute Lung Injury and O_2 Toxicity

Acute lung injury (ALI) and its most severe form acute respiratory distress syndrome (ARDS) are characterized by inflammation of the lung parenchyma leading to impaired gas exchange function, hypoxemia (low blood PO_2) and possibly resulting in multiple organ failure (Clark & Lambertsen, 1971; Fisher, Forman & Glass, 1984; Freeman & Crapo, 1981). ARDS is one of the most frequent causes of admission to intensive care units (ICU), with around 190,000 cases per year in the USA and a 35% ~ 45% mortality rate (Phua et al., 2009; Ragaller & Richter, 2010). Major causes for ARDS include sepsis, pneumonia, major trauma, toxins, shock, multiple transfusions, inhalation injury, lung transplant, severe burns, ionizing radiation, and chemotherapeutic agents (Cehovic, Hatton & Fahy, 2009). An important aspect of the pathogenesis of ARDS is compromise of the barrier properties of the pulmonary capillary endothelium and alveolar epithelium, which leads to pulmonary edema and hypoxemia (low blood PO_2) (Clark & Lambertsen, 1971; Crapo, Barry & Foscue, 1980). Thus the most common initial treatment for ARDS is O_2 therapy (normobaric hyperoxia) to restore blood PO_2 to close to its normal level.

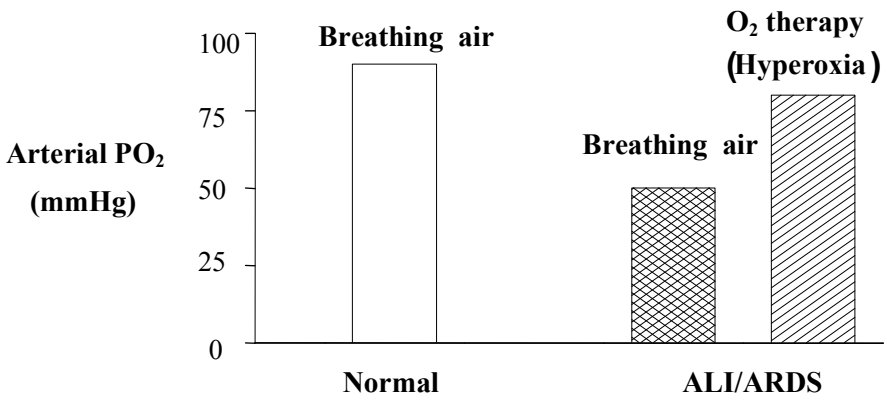

Figure 1. 1 O_2 therapy increased arterial PO_2 of ARDS patients close to the normal level.

Although high O_2 therapy initially improves arterial blood PO_2 (Figure 1.1), sustained exposure to high O_2 is limited by its lung O_2 toxicity, which can further impair lung functions. Currently, there is no effective way to mitigate the toxic effects of supplemental O_2 therapy.

The lung injury caused by normobaric hyperoxic therapy is progressive. Early clinical aspects of lung O_2 toxicity include coughing, altering in mucociliary movement, and reflecting tracheobronchitis (Clark & Lambertsen, 1971). With time, these tracheal symptoms become more intense. Behnke et al. showed that after 4 hours of 100% O_2 exposure, pulmonary symptoms such as substernal pain first appear (Behnke, Johnson & Poppen, 1935). Clark et al. showed that exposure to supraphysiological concentrations of O_2 (> 50%) for prolonged periods (> 13 hours) impair pulmonary functions (Clark & Lambertsen, 1971). After 24-hour exposure to high O_2 (> 50%), functional changes such as a decrease in vital capacity, a decrease in pulmonary compliance, a decrease in the pulmonary diffusing capacity for carbon monoxide, and absorption atelectasis are observed (Welch, Morgan & Clamann, 1963; Clark & Lambertsen, 1967; Caldwell, Lee & Schildkraut, 1966; Carvalho, Depaula & Schettino, 1998). Hyperoxia-induced decreases in alveolar volume, capillary volume, and alveolar and capillary surface densities may be explained by the increase in alveolar tissue and particularly of the interstitium, alveolar capillary

proliferation, absorption atelectesis and rupture of some alveolar septa (Kapanci, Tosco & Eggermann, 1972; Hyde & Rawson, 1969; Carvalho, Depaula & Schettino, 1998). The decrease in carbon monoxide diffusing capacity may be due to an increase in air-blood barrier thickness which is caused by swelling of epithelial and endothelial cells, fibroblastic proliferation, fibrin deposition, and increased numbers of lining cells in the alveolar lumina (Kapanci et al., 1972; Hyde & Rawson, 1969). The above early pulmonary changes are reversible if the host is returned to normal PO_2 before the symptoms become more serious (Clark & Lambertsen, 1971). However, for those subjects exposed to hyperoxia for prolonged periods such as ARDS patients, the above cellular and structural changes eventually result in the development of bronchopneumonia, pulmonary edema, and progressive hypoxemia. Time of onset of the above changes varies with the inspired PO_2 and exposure period (Joffe 1969, Hyde & Rawson, 1969).

1.2 Animal Models of O_2 Toxicity

To evaluate the time course, severity and pathogenesis of lung O_2 toxicity, several animal models of hyperoxic lung injury including rats, mice, rabbits have been developed (Clark & Lambertsen, 1967, Crapo et al., 1980, Hayatdavoudi, O'Neil & Barry, 1981, Ho et al., 1996, Matute-Bello 2008). The rat model mimics several aspects of lung O_2 toxicity observed clinically (Kapanci et al., 1972; Hyde & Rawson, 1969; Crapo et al., 1980). Hyperoxia-induced histological changes observed in man that have also been observed in rats include an increase in the thickness of air-blood barrier, an increase in the number of interstitial cells, a decrease in capillary surface area, a decrease in pulmonary capillary blood volume and alveolar volume, and the damage of endothelial cells (Crapo et al., 1980).

For rats, the severity of hyperoxic lung injury is dependent on PO_2 level and exposure

period (Crapo et al., 1980). For instance, rats exposed to > 95% O_2 die within 60 to 72 hours, but rats exposed to 85% O_2 or 60% O_2 can survive for a prolonged period of time. However, among animal models, rats are unique in that, after exposed to 85% O_2 for 5-7 days, they develop tolerance or adaptation to the otherwise lethal effects of exposure to >95% O_2 as evidenced by an increase in their survival in subsequent exposure to 100% O_2 environment (Figure 1.2). This tolerance is not observed in other rodents, but a similar tolerance occurs in humans (Capellier, Maupoil & Boussat, 1999). Interestingly, rats exposed to 60% O_2 for 5-7 days become more susceptible to 100% O_2 as evidenced by a decrease in their survival in subsequent exposure to 100% O_2 (Figure 1.2).

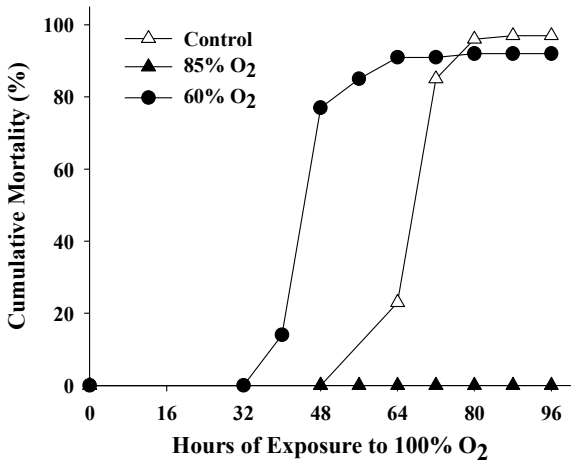

Figure 1. 2 Cumulative mortality of rats exposed to 100% O_2. Δ, control animals kept in air before exposed to 100% O_2; ▲, animals exposed to 85% O_2 for 7 days before being exposed to 100% O_2; ●, animals exposed to 60% O_2 for 7 days before being exposed to 100% O_2. (Reproduced from Figure 1 in Hayatdavoudi et al., 1981 which is available online at http://jap.physiology.org/content/51/5/1220.full.pdf)

Studies by Crapo et al. (1980) and Hayatdavoudi et al. (1981) provide detailed descriptions of histological and morphometric changes in lungs of rats exposed to lethal (100% O_2), adaptive (85% O_2) and susceptible (60% O_2) hyperoxia.

No significant structural changes are observed in lungs of rats exposed to 100% O_2 for up

to 40 hours (Figure 1.3) compared with rats exposed to room air (normoxic rats) (Crapo, Freeman & Bary, 1983). However, by 60 hours there is a 30% loss in pulmonary capillary endothelial cells and cell surface, lung infiltration of phagocytic leukocytes and other cells, and an increase in the thickness of air-blood barrier. Rats that survive 60 hours of exposure to 100% O_2 experience additional loss of pulmonary capillary endothelial cells and edema, which lead to further increase in the thickness of air-blood barrier, pleural effusion, severe hypoxemia, and death within 72 hours.

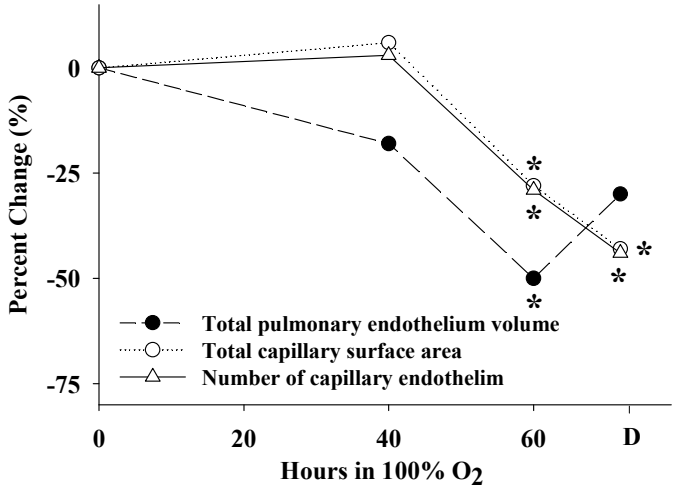

Figure 1. 3 Alterations in pulmonary capillary endothelial cell volume, surface area and number in response to rat exposure to 100% O_2 for up to 72 hours. * indicates a significant difference from that of normoxic rats ($P<0.05$). D is the time of death of rats and occurred at a mean of 66 hours of exposure. (Reproduced from Figure 1 in Crapo et al., 1983 which is available online at http://www.the-aps.org/publications/tphys/legacy/1983/issue3/170.pdf.)

For rats exposed to 85% O_2 for 72 hours, lung histological and/or morphometric changes are undetectable although the sequence of events leading to lung O_2 toxicity has presumably begun (Crapo et al., 1980). However, by 5 days, histological and morphometric changes similar to those observed after 60 hours of exposure to 100% O_2 are observed. By 7 days, the inflammation is still evident and the lungs have lost more endothelial cells, but pleural effusion and respiratory function impairment have substantially subsided and longer exposure lead to an adapted steady

state without further progression of toxic manifestation. Moreover, the rats start to gain body weight (Crapo et al., 1980; Hayatdavoudi et al., 1981). Figure 1.4 outlines the different stages of the development of lung O_2 toxicity in rats exposed to 85% O_2. During the initiation phase (0-2 days), an increase in the formation of reactive oxygen species is observed and the expression of inflammatory factors is increased, while histological and morphometric changes are not detectable (Crapo et al., 1983). During inflammatory phase (3~5 days), the lung experiences significant structural, cellular and functional changes, in addition to significant loss of body weight due to a decrease in food/water intake. The adaptation phase (>5 days) is characterized by no further loss of endothelial cells, reversal of pulmonary functional impairment, and an increase in body weight.

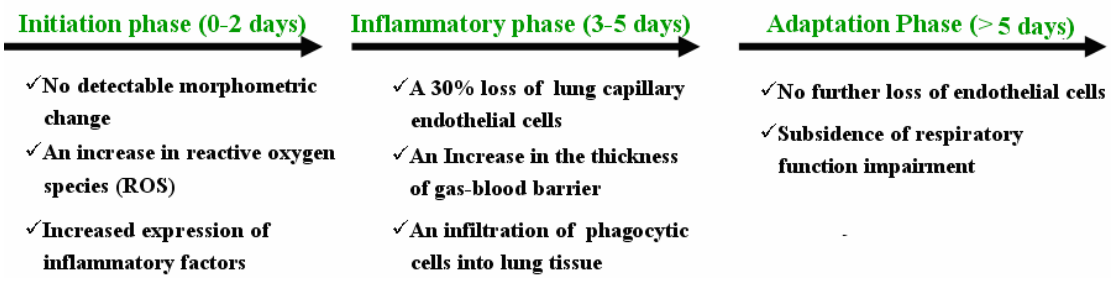

Figure 1. 4 Rat lung biochemical and structural changes during the three phase of O_2 toxicity associated with exposed to 85% O_2 (Crapo et al., 1980; Hayatdavoudi et al., 1981).

For rats exposed to 60% O_2 for 7 days, there is a decrease in the volume of endothelial cells and the arithmetic mean thickness of endothelial cells (Crapo et al., 1980, Hayatdavoudi et al., 1981). No further morphologic changes are observed following rat exposure to 60% O_2 for up to 64 days. Interestingly, rats exposed to 60% O_2 for 7 days become more susceptible to 100% O_2 (Figure 1.2) (Crapo et al., 1980; Hayatdavoudi et al., 1981).

Based on the histological and functional changes, for all above O_2 levels, the pulmonary capillary endothelium is a primary site of O_2 toxicity. The loss of pulmonary endothelial cells is an important characteristic of lung O_2 injury. Previous studies indicated that rats exposed to 85% O_2

increased cyanide-resistant O_2 consumption as a measure of the rate of reactive oxygen species (ROS) formation, primarily in endothelium (Crapo & Tierney, 1974). The production of ROS can be associated with direct endothelium injury, demonstrated by increased LDH release in O_2 challenged endothelial cells (Crapo & Tierney, 1974; Crapo et al., 1980; Hayatdavoudi et al., 1981). Previous studies also reported some differences in ultra-structure among the rats exposed to 100% O_2, 85% O_2 and 60% O_2, especially the significant differences in the response of the pulmonary endothelium. For instance, rats exposed to 100% O_2 exhibited lethal changes in the capillary endothelial cells manifested by pyknotic nuclei, swelling of the perinuclear cisternae, the rough endoplasmic reticulum and mitochondria, and the consequent rupture of plasma membrane. Necrosis of the capillary endothelial cells was a major event and was accompanied by an apparent stagnation of blood flow in capillary lumens. No adaptive changes were apparent. In marked contrast, rats exposed to 85% O_2 for 7 days exhibited some adaptive changes such as hypertrophy of capillary endothelial cells instead of simple swelling, a significant decrease in capillary lumen and a significant increase in the thickness of endothelial cells and total tissue volume (Hayatdavoudi et al., 1981; Crapo et al., 1980). In rats exposed to 60% O_2 for 7 days, there was no significant difference in the total tissue volume and the capillary lumen; however the thickness of endothelial cells was decreased significantly (Hayatdavoudi et al., 1981; Crapo et al., 1980). These results suggest that the pulmonary capillary endothelium is not only a primary target of O_2 toxicity, but also a likely important site in which biochemical adaptation to O_2 toxicity occurs (Crapo et al., 1980). Elucidating the factors that contribute to O_2 toxicity and tolerance has the potential to further understanding of the mechanisms involved in initiating lung O_2 toxicity and for identifying potential targets/mechanisms for mitigating the toxic effects of O_2 therapy on lung tissue.

CHAPTER 2. PRESENT STATUS OF PROBLEM, OBJECTIVES AND SPECIFIC AIMS

2.1 Biochemical Mechanisms of Lung O_2 Toxicity

Although the mechanisms resulting in pulmonary hyperoxic injury are not fully understood, there is ample evidence that the deleterious effects of high O_2 are the results of increased formation of ROS such as O_2^-, H_2O_2 and hydroxyl radical (Freeman & Crapo, 1981; Sander et al., 1993). Studies have suggested that mitochondrial electron transport chain NADH:ubiquinone oxidoreductase (complex I) and coenzyme Q-cytochrome c reductase (complex III) are important sources of ROS under hyperoxic conditions (Crapo & Tierney, 1974; Freeman & Crapo, 1981; Sander et al., 1993; Brueckl et al., 2006). At normal PO_2 level, cells can scavenge ROS via enzymatic (e.g., superoxide dismutase, catalase, glutathione reductase) and non-enzymatic (e.g., vitamins C and E) anti-oxidants. The increase in the formation of ROS under hyperoxic conditions has been suggested to overwhelm the cellular anti-oxidant mechanisms and cause various cytotoxic effects, including lipid peroxidation, damage to protein structures, dysfunction of enzymes, DNA strand breakage, and ultimately cell death (Rourke, Cortassa & Aon, 2005; Brueckl et al., 2006). This can compromise the barrier properties of the endothelial and epithelial cells and can result in lung edema, impaired gas exchange function, and hypoxemia. Moreover, the increase in ROS formation can initiate other cell responses that may be important to the pathogenesis of lung O_2 toxicity such as the increase in the expression of vascular adhesion molecules (e.g., P-selectin) which can result in the recruitment of phagocytic cells into the lung tissue (Brueckl et al., 2006).

2.2 Biochemical Mechanisms of Rat Tolerance and Susceptibility to Lethal O_2 Levels

Previous studies, predominantly in lung tissue homogenate, have suggested that classic antioxidant enzymes such as superoxide dismutase (SOD), catalase, and glutathione peroxidase protect against lung O_2 toxicity (Crapo et al., 1980; Hayatdavoudi et al., 1981; Wang, Manevich & Feinstein, 2004). For instance, an increase in overall activity of CuZn-SOD was reported in lung tissue homogenates of rats exposed to 85% O_2 for 7 days, but not in lung tissue homogenates of rats exposed to 100% O_2 for 60 hours (Ho, Dey & Crapo, 1996). Although the activities of these enzymes do increase in lung homogenates of rats adapted to the lethal effects of > 95% O_2, they do not appear to account for all aspects of this adaptive response. For instance, Coursin et al. reported a significant increase in the activities of these classic anti-oxidant enzymes in lung homogenates of rats exposed to 65% O_2 for six weeks (Coursin, Cihla & Will, 1987). However, these rats were more susceptible to the lethal effects of > 95% O_2 than normoxic rats.

The anti-oxidant enzyme peroxiredoxin 6 (Prdx6) has also been suggested to play a role in protection from O_2 toxicity (Manevich & Fisher, 2005; Fatma et al., 2009). Prdx6 catalyzes the reduction of H_2O_2 and hydroperoxides to H_2O by utilizing glutathione. Studies have shown that over-expression of Prdx6 confers some protection against oxidative stress by prolonging the survival of mice in lethal hyperoxia, and genetic inactivation of this enzyme increases sensitivity of mice to O_2 toxicity (Wang et al., 2004).

An important aspect of lung O_2 toxicity is edema. Na^+/K^+-ATPase and Na^+ channels play a key role in clearing edema via active transport of Na^+. A study by Factor et al. (2000) suggests that over-expression of Na^+/K^+-ATPase in rats improves alveolar fluid clearance and protects rats against O_2 toxicity as measured by the increase in the time these rats survive in a > 95% O_2

environment. However, a study by Nici et al (1991) shows an increase in Na^+/K^+-ATPase expression in lung homogenate of rats exposed to 100% O_2 for 60 hours, which die within 74 hours of exposure to 100% O_2. The results of this study suggest that the increase in the expression of Na^+/K^+-ATPase is not sufficient to protect against lung O_2 toxicity or explain the adaptation induced by rat exposure to 85% O_2 for 7 days.

The induction of phase II enzymes such as the cytosolic enzyme NAD(P)H:quinone oxidoreductase 1 (NQO1) has been suggested to play a role in rat tolerance of > 95% O_2 (Cho et al., 2002). The induction occurs via the anti-oxidant response element (ARE) mediated by an increase in the rate of ROS formation (Cho et al., 2002). In addition to its role as a phase II enzyme, NQO1 has been suggested to provide additional protective effects including regeneration of endogenous and exogenous antioxidants, scavenging of superoxide (O_2^-), and competition with one-electron quinone reductases. The competition with one-electron quinone reductases mitigates the effects of semiquinone formation and subsequent redox cycling (Cadenas 1995; Siegel & Ross, 2000; Siegel et al., 2004).

Several studies have evaluated the role of NQO1 in protection against pulmonary O_2 toxicity with mixed results (Whitney & Frank, 1993). Whitney et al. found that treatment with dicumarol (NQO1 inhibitor) or the induction of NQO1 did not significantly diminish or improve the survivability of adult rats exposed to lethal O_2 levels. The results with dicumarol treatment may be in part because dicumarol has such a high affinity for plasma proteins that only a small fraction would be taken up by the lung in vivo (Audi et al., 2005).

Cho et al. (2002) showed that mice deficient in the transcription factor Nrf2, which is involved in the induction of NQO1, had significantly lower lung NQO1 mRNA expression and

were significantly more sensitive to hyperoxia (> 95% O_2 for 72 hours) than wild type mice. Furthermore, they showed that exposure of wild type mice to hyperoxia increased their lung homogenate NQO1 activity.

Another important strategy that cells may follow to protect against lung hyperoxic injury is to mitigate the activities of ROS sources including mitochondrial complexes I, III and IV (Figure 2.1). Campian et al. (2007) found that HeLa cells exposed to 80% O_2 for 3 days (HeLa-80) decreased by ~50% intracellular ROS production and increased the activity of cytochrome c oxidase (complex IV) by ~100%. These results suggested that the increase in complex IV might act to deplete upstream electron-rich intermediates responsible for ROS production, and hence induce a tolerance to hyperoxia (Campian, Qian & Gao, 2004; Campian, Gao & Qian, 2007). Campian's studies indicated that it was possible to make cells tolerant to hyperoxia by manipulation of ROS sources instead of anti-oxidant defense (Campian et al., 2007).

Brueckl et al. (2006) evaluated the sources of ROS in isolated perfused rat lungs ventilated with hyperoxic gas (70% O_2). They demonstrated a hyperoxia-induced increase in ROS production in pulmonary capillary endothelial cells that was rotenone inhibitable. Moreover, they demonstrated that this early hyperoxia-induced increase in endothelial complex I ROS production leads to an increase in intracellular calcium which stimulates calcium dependent activation and translocation of Rac1 in endothelial cells from the cytoplasm to the plasma membrane. This in turn leads to activation of endothelial NAD(P)H oxidase, which becomes the main source of hyperoxia-induced endothelial ROS production after 30 min of lung ventilation with 70% O_2. These early hyperoxia-induced increases in endothelial ROS production and intracellular endothelial calcium may initiate various cellular responses including an increase in the expression

of vascular adhesion molecules (e.g., P-selectin). The increase in the expression of vascular adhesion molecules can result in the recruitment of inflammatory cells into the lung tissue as seen in lungs of rat exposure to hyperoxia (85% O_2) for > 72 hours. These results suggest that the early hyperoxia-induced increase in endothelial ROS production via complex I may be important to the initiation of the gross lung structural and functional changes associated with rat exposure to hyperoxia (85% O_2) for > 72 hours.

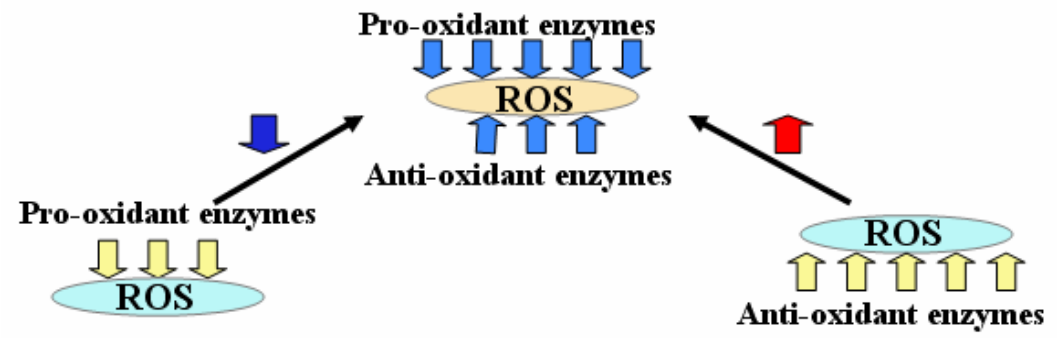

Figure 2. 1 Possible strategies that cells may follow to protect against hyperoxic lung injury.

2.3 Mitochondrial Membrane Potential and Hyperoxia

Mitochondria play an important role in cell physiology and pathology such as ATP synthesis, regulation of intracellular calcium, production of ROS, apoptosis, and other cellular functions (Nicolls & Budd, 2000; Duchen, Surin & Jacobson, 2003). Mitochondrial functions involve the maintenance of the proton electrochemical potential (Δp) which is made up of a mitochondrial membrane potential ($\Delta\Psi_m$) dominantly across inner mitochondrial membrane and a small pH gradient (Nicolls & Budd, 2000), $\Delta p = \Delta\Psi_m - 60\ \Delta pH$. A typical Δp is comprised of a 150 mV $\Delta\Psi_m$ and a ΔpH of −0.5 (Nicolls & Budd, 2000). Thus, $\Delta\Psi_m$ is the dominant component of Δp.

$\Delta\Psi_m$ is an important indicator of mitochondrial function and a measure of the energetic state of the cell, and oxidative stress has been show to alter $\Delta\Psi_m$ in cultured cells (Huang, Yappert

& Jumblatt, 2008). The collapse of $\Delta\Psi_m$ is an early signal of cell apoptosis or necrosis and a change in $\Delta\Psi_m$ represents cellular abnormity. Since the pulmonary capillary endothelium is a primary and early target of lung O_2 toxicity and the loss of endothelial cells due to necrosis is one of the important changes after prolonged hyperoxic exposure, it would be useful to determine the effect of hyperoxia on endothelial $\Delta\Psi_m$. As mentioned above, the mitochondrial electron transport chain is the main source of ROS under hyperoxic conditions. Previous studies have demonstrated that the rate of mitochondrial ROS production is inversely proportional to $\Delta\Psi_m$ (Huang et al., 2008). For instance, human lens epithelial cells grown under hyperoxic conditions (80% O_2) for 24 to 36 hours showed a reduction in $\Delta\Psi_m$ as compared to cells grown under a normoxic environment for the same time period (Huang, Yappert & Jumblatt, 2008). This decrease in $\Delta\Psi_m$ was concomitant with an increase in mitochondrial ROS production. This hyperoxia-induced decrease in $\Delta\Psi_m$ is consistent with the decrease in $\Delta\Psi_m$ observed in cultured human lens epithelial cells treated with H_2O_2 (Huang et al., 2008). The effect of hyperoxia on the $\Delta\Psi_m$ in pulmonary endothelial cells has not been evaluated.

2.4 Objectives and Specific Aims

J. Lorrain Smith described pulmonary O_2 toxicity for the first time in 1889. Since then, a large number of studies on mechanisms of lung O_2 toxicity and tolerance have been carried out (Clark & Lambertsen, 1967; Welch et al., 1963; Crapo et al., 1980; Hayatdavoudi et al., 1981; Ho et al., 1996; Gomi & Matsuo, 2002). These studies have predominantly focused on evaluating the effect of hyperoxia on the activities of anti-oxidant enzymes in lung tissue homogenates. Hyperoxia-induced changes in the activities of redox enzymes, predominantly in lung tissue homogenates, have been demonstrated (Crapo et al., 1980; Hayatdavoudi et al., 1981; Wang et al.,

2004). However, the factors that contribute to rat tolerance of 100% O_2 following exposure to 85% O_2 for 5-7 days are still not fully understood.

Previous studies, predominantly in lung tissue homogenates, have suggested that redox enzymes, among other factors, play a role in rat tolerance and susceptibility to 100% O_2 (Crapo et al., 1980; Audi et al., 2005; Campian et al., 2007). However, the results of these in vitro studies do not necessarily predict hyperoxic-induced changes in the activities of redox enzymes in an intact lung. This is because potential changes in key aspects of the enzyme environment in an intact lung (e.g., availability of electron donors, competing redox enzymes, tissue permeation of electron acceptors, tissue perfusion) that may influence redox enzyme kinetics are not preserved. Studies evaluating the activities of redox enzymes in intact lungs have lagged behind studies in lung tissue homogenates, in part because of the complexity of the intact lung. Recent studies have demonstrated the utility of the multiple indicator dilution method (MID) and redox active probes for evaluating the activities of cell surface, cytoplasmic, and mitochondrial redox enzymes in the intact lungs (Audi et al., 2005, 2008).

MID usually involves the bolus injection or finite pulse infusion of indicators or probes into the organ's arterial inlet, followed by measurements of their concentrations in the venous effluent as a function of time. The indicators usually include a vascular indicator and a test indicator, which is a substrate for the targeted metabolic function(s) of interest (e.g. redox enzyme). The interactions of the test indicator with these metabolic function(s) on passage through the organ result in characteristic differences between test indicator concentration in venous effluent-time curve and vascular indicator concentration in venous effluent-time curve. The information content of data resulting from MID can be complex because, in addition to the

targeted metabolic function(s), several other factors can influence the amount of indicator that is removed and/or modified on passage through the lung. These include organ perfusion (e.g., perfused capillary surface area, capillary transit time distribution), and reactions taking place in the blood (e.g., plasma protein binding). With appropriate experimental design and indicators, the indicator dilution data contain information about all these processes. Interpretation of this data necessitates the use of mathematical models based on hypotheses regarding the processes responsible for all mechanisms of indicator disposition on passage through the organ. The resulting kinetic model parameters include measures of the activities of the metabolic function(s) of interest.

MID can provide information about the activities of redox enzymes in cells accessible to redox active probes from the vascular space, presumably dominated by capillary endothelial cells since these cells are in direct contact with the blood and account for a large fraction (up to 50% in normoxic lungs) of total lung cells. This is important since the pulmonary endothelial cell is the primary target of O_2 toxicity and a potential site where biochemical adaptation to O_2 toxicity occurs (Crapo et al., 1980).

The work described in this dissertation utilizes MID as well as mathematical modeling to quantitatively evaluate the effect of rat exposure to 85% O_2 on the activities of cytosolic (NQO1) and mitochondrial (complexes I and III) redox enzymes, as well as the rate of lung H_2O_2 release during the initiation phase (12-24 hours) and adaptation phase (5-7 days) of rat exposure to 85% O_2.

Due to the importance of $\Delta\Psi_m$ to cellular bioenergetics, several approaches have been developed to probe $\Delta\Psi_m$ in intact cells (Ward, Rego & Frenguelli, 2000; Duchen et al., 2003;

Huang et al., 2007). Generally speaking, these approaches make use of fluorescent cationic dyes such as Rhodamine 123 (R123), tetramethylrhodamine methyl ester (TMRM) which have been shown to accumulate in mitochondria driven in part by $\Delta\Psi_m$ (Ward et al., 2000; Huang et al., 2007). These approaches, which are based on the Nernst equation, do not account for other factors that determine the cellular disposition of these dyes, including multi-drug efflux pump P-glycoprotein (Pgp) for which these dyes are known substrates, and plasma membrane potential ($\Delta\Psi_p$). In addition, these approachs measure intracellular dye fluorescence, and hence are confounded by the fact that these dyes tend to undergo self-quenching at the high concentrations attained in mitochondria due to aggregation. Therefore, one of the objectives of this work is to develop a quantitative approach for evaluating $\Delta\Psi_m$ in intact cells that overcomes the limitations of existing methods.

2.4.1 Targets

a. NAD(P)H : Quinone Oxidoreductase 1 (NQO1)

Using MID and mathematical modeling, Audi et al. (2003) demonstrated that the redox active quinone compound duroquinone (DQ) is reduced to durohydroquinone (DQH_2) on passage through the pulmonary circulation of the isolated perfused rat lung, wherein DQH_2 appears in the venous effluent. Inhibitor studies reveal that NQO1 is the dominant reductase involved in the reduction of DQ, and the capacity of the lung to reduce DQ to DQH_2 was shown to be a measure of lung NQO1 activity (Audi et al., 2005; Audi et al., 2008; Lindemer, Bongard & Hoffmann, 2011). Rat exposure to 85% O_2 for 21 days, as a model of pulmonary oxidative stress, increases the capacity to reduce DQ to DQH_2 in the pulmonary circulation, as well as lung tissue NQO1

activity and protein level (Audi et al., 2005). On the other hand, rat exposure to 85% O_2 for 48 hours, which is not long enough to make rats tolerance to the lethal effects of 100% O_2, has no effect on the capacity of the lung to reduce DQ, or on tissue homogenate NQO1 activity and protein level (Audi et al., 2008).

Therefore, one of the questions addressed in this study is whether the measured increase in NQO1 activity after rat exposure to 85% O_2 for 21 days is detectable after rat exposure to 85% O_2 for 7 days as measured by the capacity of a lung to reduce DQ. An affirmative result would be consistent with a role of NQO1 in protection against O_2 toxicity.

b. Mitochondrial Complexes I and III

Mitochondria is the most important site of ATP synthesis via the electron transport chain. Electrons are delivered through the mitochondrial electron transport chain during energy transduction, while a small fraction (2-5%) of electrons leak to O_2 prematurely, forming the O_2 free radical superoxide and further dismutating into H_2O_2 or other radicals (Muller 2000; Andreyev, Kushnareva & Starkov, 2005). The electron transport chain components complexes I and III are reported as the important sites where ROS are formed (Chen, Vazquez & Moghaddas, 2003; Muller, Liu & Remmen, 2004; Campian et al., 2004). The proposed site of ROS formation at complex I is its NADH dehydrogenase located on the matrix side of inner membrane (Chen et al., 2003; Muller et al., 2004). There are two possible sites of ROS formation at complex III : the quinol-oxidizing (Q_o) center which orients the intermembrane space and the quinone-reducing (Q_i) center which is located in the inner membrane facing mitochondrial matrix. Compared with complex I, the inhibition of complex III results in more ROS generation (Chen et al., 2003; Muller et al., 2004). Limiting electron flow into complex III can mitigate mitochondrial ROS production.

On the other hand, the inhibition of complex IV, which is the downstream component of complex III, enhances electron leak and ROS generation at complexes I and III (Chen et al., 2003).

Few studies have evaluated the effect of hyperoxia on the activities of mitochondrial complexes I, III and IV. Brueckl et al. (2006) exposed rats to 70% O_2 and measured the formation of H_2O_2 in pulmonary endothelium in situ using the membrane-permeable probe 2,7-dichlorofluorescein (DCF). Paradies et al. (2004) showed that increased formation of ROS under hyperoxic conditions decreased complex I activity in bovine heart submitochondrial particles due to the oxidation of the inner mitochondrial membrane phospholipid cardiolipin. Cardiolipin is required for electron transfer in complex I and to prevent the proton leakage at complex I. Thus the oxidation of cardiolipin might result in an increase in ROS production at complex I due to an increase in electron leakage. The study by Campian et al. (2004, 2007) showed a ~2-fold increase in the activity of complex IV in wild-type Hela cells after exposure to 80% O_2 for 3 days.

Recently, Audi et al. (2008) demonstrated the capacity of the rat lung to reduce the redox active quinone compound coenzyme Q_1 (CoQ_1) to its hydroquinone (CoQ_1H_2) form, and to oxidize CoQ_1H_2 to CoQ_1 on passage through the pulmonary circulation. Inhibitor studies revealed that mitochondrial complex I and NQO1 are the dominant sites of CoQ_1 reduction on passage through the lung, and that mitochondrial complex III is the dominant site of CoQ_1H_2 oxidation. Hyperoxic studies show that rat exposure to 85% O_2 for 48 hours decreases the overall lung capacity to reduce CoQ_1 to CoQ_1H_2 predominately due to a ~ 50% decrease in the capacity of complex I mediated CoQ_1 reduction with no effect on lung complex III activity as measured by the capacity of the lung to oxidize CoQ_1H_2 to CoQ_1 (Audi et al., 2008). Therefore, an important objective of this study is to determine whether a change in the activity of complex III could occur after rat exposure to 85% O_2

for 7 days as measured by the capacity of a lung to oxidize DQH_2 or CoQ_1H_2. Another important objective is to determine how early the decrease in the activity of complex I, as measured by the capacity of a lung to reduce CoQ_1, after rat exposure to 85% O_2 occurs, and whether the decrease in lung complex I activity detected after 48 hours of rat exposure to 85% O_2 is maintained following rat exposure to 85% O_2 for 7 days.

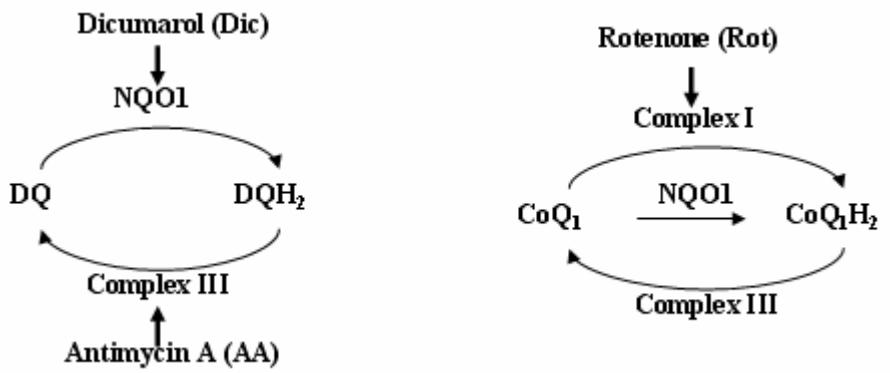

Figure 2. 2 Metabolism of quinone compounds and the inhibitors.

c. Mitochondrial Membrane Potential

Rhodamine dyes such as rhodamine 123 (R123), tetramethyrhodamine ethyl ester (TMRE) are one of the earliest and most widely used probes for monitoring $\Delta\Psi_m$ in isolated mitochondria and intact cells because of their availability and relatively high fluorescence quantum yield (Nicolls & Budd, 2000). The most common approach for evaluating $\Delta\Psi_m$ in intact cells using rhodamine has involved fluorescence detection using fluorescence microscopy or laser confocal microscopy (Nicolls & Budd, 2000; Duchen et al., 2003). This general approach has been confounded by the tendency of rhodamine to undergo quenching due to aggregation at concentrations > 5 μM, which may be attained in mitochondria, and by the potential for photo bleaching and/or photo-induced cell injury (Nicolls & Budd, 2000; Solaini, Sgarbi & Lenaz, 2007; Zhang, Huang & Carson, 2001). Moreover, this general approach provides indices of $\Delta\Psi_m$, such as

probe total cellular fluorescence or mitochondrial fluorescence, rather than an estimate of $\Delta\Psi_m$ in mV. Because of the logarithmic form of the Nernst equation, a change in $\Delta\Psi_m$ results in a much larger change in the measured probe cellular or mitochondrial fluorescence (Nicolls & Budd, 2000). Furthermore, this approach is sensitive to the binding of rhodamine to mitochondria, which can lead to overestimation of $\Delta\Psi_m$ (Solaini et al., 2007). In addition, most of the previous approaches for evaluating $\Delta\Psi_m$ in cells do not account for the fact that rhodamine dyes are substrates of the multi-drug efflux transporter P-glycoprotein (Nicolls & Budd, 2000; Huang et al., 2007). Thus, one of the objectives of this work is to develop a quantitative approach for evaluating $\Delta\Psi_m$ in cultured BPAEC. This approach could be utilized in future studies for evaluating the effect of hyperoxia on $\Delta\Psi_m$ in intact lungs.

d. Hydrogen Peroxide (H_2O_2)

Since an increase in the formation of ROS plays a key role on lung O_2 toxicity, the measurement of ROS generation could be important. In a previous study, a decrease in the activity of complex I is demonstrated in lungs of rats exposed to 85% O_2 for 48 hours (Audi et al., 2008). This might be important since Brueckl et al. (2006) suggested that an increase in ROS production by complex I may be important to the initiation of the gross lung structural and functional changes associated with rat exposure to hyperoxia (85% O_2) for > 72 hours. Thus studies are needed to evaluate the effect of the depression in complex I activity observed in hyperoxic lungs on ROS production.

The primary ROS formed in mitochondria is superoxide (O_2^-) which can not cross the mitochondrial membrane due to its charge. The formation of O_2^- is measured in purified submitochondrial particles or mitochondria (Chen et al., 2003; Campian et al., 2004). Intracellular

O_2^- can convert to H_2O_2 quickly due to the existence of intracellular SOD such as mitochondrial MnSOD, cytosolic CuZn-SOD (Suzy & Serpil, 2001; Brand 2010). H_2O_2 can permeate cellular membranes rapidly (Bienert, Schjoerring and Jahn, 2006; Wilhelm, Vankova & Maxova, 2003) and has a much longer half-life (Bienert et al., 2006). Thus, for intact cells, H_2O_2 usually is measured as an index of O_2^- formation (Campian et al., 2004; Brueckl et al., 2006).

Though H_2O_2 can be produced by pyruvate dehydrogenase (PDH), 2-oxoglutarate dehydrogenase (OGDH) directly (Brand 2010), in most cases, the initial ROS product is O_2^- which can be scavenged and converted into H_2O_2 (Suzy & Serpil, 2001; Brand 2010). Thus, the production of H_2O_2 is usually associated with the production of O_2^-. The mitochondrial electron transfer chain is the major source of O_2^- where mitochondrial complex I and complex III are two primary sites of O_2^- formation (Muller 2000; Chen et al., 2003). Other sites of O_2^- production include complex II, complex IV, PDH, OGDH, glycerol 2-phosphate dehydrogenase (GPDH), NADPH oxidase, and monoamine oxidases (Muller 2000; Chen et al., 2003; Andreyev et al., 2005; Brueckl et al., 2006; Brand 2010). The production of H_2O_2/O_2^- can be stimulated by hyperoxia, hypoxia, and inhibitors such as antimycin A, endotoxin (Brueckl et al., 2006; Minamiya 1995; Song, Al-Medhi & Fisher, 2001; Wilhelm et al., 2003). The produced H_2O_2 can be scavenged by antioxidant enzymes such as glutathione peroxidase and catalase (Barja 2002; Brand 2010).

Fluorescent probes such as amplex red (AR), ortho-phenylenediamine dihydrochloride (o-PD), 2,7-dichlorofluorescein (DCF), and homovanillic acid are widely used to estimate the formation of H_2O_2 (Kinnula, Everitt & Whorton, 1991; Zhou, Diwu & Panchuk, 1997; Wilhelm et al., 2003; Chen et al., 2003; Campian et al., 2007). Several studies have measured the production

or release rate of H_2O_2 in submitochondrial particles, mitochondria or cells using homovallic acid, AR, DCF or o-PD (Kinnula et al., 1991; Zhou et al., 1997; Chen et al., 2003; Campian et al., 2004; Heumüller, Wind & Barbosa, 2007). Few studies have been carried out to estimate the rate of H_2O_2 release or production in isolated perfused lungs (Al-mehdi, Shuman & Fisher, 1997a; Song, Al-mehdi & Fisher, 2001, Brueckl et al., 2006). Al-mehdi et al. (1997a) developed a method to estimate intracellular release of H_2O_2 from perfused lung using o-PD, but the effect of hyperoxia was not evaluated. Brueckl et al. (2006) used DCF and fluorescent microscopy to measure the formation of H_2O_2 in rat pulmonary endothelial cells in situ. Labinskyy et al. (2006) applied the same method to measure the formation of H_2O_2 but in rat carotid arteries. Song et al. (2001) measured H_2O_2 in the endothelial cells of perfused rat lung under ischemia conditions using AR by microscope. Though these methods were able to detect lung H_2O_2 formation or release, Al-mehdi's method (1997) had a relatively low sensitivity and Brueckl's method (2006) did not provide the rate of H_2O_2 formation.

Therefore, one of addressed aims of this study is to develop an apporach to evaluate the rate of H_2O_2 release from perfused rat lungs. Compared with DCF and o-PD, amplex red (AR) is reported as a more specific and sensitive probe of H_2O_2 (Zhou et al., 1997; Chen et al., 2003; Brand 2010). Therefore, in this study, AR is selected as the probe of H_2O_2 to estimate the lung rate of H_2O_2 release utilizing MID.

2.4.2 Specific Aims

The long-term objectives of this work are to elucidate the underlying mechanisms of rat tolerance to 100% O_2, and to further understanding of the mechanisms involved in lung O_2 toxicity.

The specific aims are:

Specific Aim # 1:

Determine the effect of rat exposure to 85% O_2 for 7 days (Hyper-85) on the activities of cytosolic (NQO1) and mitochondrial (complexes I and III) redox enzymes in intact lungs.

Hypothesis:Exposure of rats to 85% O_2 for 7 days will increase the activity of NQO1, decrease the activity of complex I, and increase the activity of complex III in the intact lung, and that measurements of the activities of these redox enzyme in hyper-85 lungs can provide critical insights into their potential roles in conferring tolerance to 100% O_2.

Specific Aim # 2:

Determine how early following rat exposure to 85% O_2 does mitochondrial complex I activity decrease in the intact lung and determine the effect of rat exposure to 85% O_2 on lung rate of H_2O_2 release.

Hypothesis:Lung mitochondrial pro-oxidant enzyme complex I is highly sensitive to rat exposure to 85% O_2, and that a decrease in lung complex I activity is an early index of the initiation phase of lung O_2 injury.

Specific Aim # 3:

Develop an approach for quantitative assessment of mitochondrial membrane potential ($\Delta\Psi_m$) in intact cultured endothelial cells by measuring the disposition of Rhodamine dyes in the extracellular medium.

Hypothesis: $\Delta\Psi_m$ plays a dominant role in the disposition of rhodamine dyes in the intact cultured endothelial cells, and that measurements of rhodamine concentrations in the extracellular medium provide sufficient information to estimate $\Delta\Psi_m$ in intact cells.

CHAPTER 3. EXPERIMENTAL METHODS

3.1 Probes and Inhibitors

3.1.1 Redox Active Quinone Compounds: Probe to Estimate the Activity of NQO1, Complex I and III

Quinone compound 2,3,5,6-tetramethyl-1,4-benzoquinone (duroquinone, subsequently referred to as DQ) and coenzyme Q_1 (CoQ_1), the homology of coenzyme Q_{10}, are selected as the probes for enzyme NQO_1, complex I and III.

DQ and CoQ_1 are redox active compounds that have been used to probe pulmonary endothelial surface and the activity of intracellular redox enzymes due to their high water and lipid solubility, as well as their flow-limited character, availability and ability to be substrates of one or more of the targeted enzymes (Merker, Audi & Lindemer, 2007; Audi et al., 2008). NQO1 plays a dominant role in DQ reduction to its two-electron reduction product durohydroquinone (DQH_2) on a single passage through the rat pulmonary circulation (Audi et al., 2003; Lindemer et al., 2011) and complex III is the dominant enzyme mediating the oxidation of DQH_2. A NQO1 contribution to CoQ_1 reduction has been identified and the protective effect of CoQ_1 in complex I dysfunction has been attributed to non NQO1-mediated CoQ_1 reduction followed by CoQ_1H_2 oxidation at complex III (Merker et al., 2007; Audi et al., 2008). Thus, CoQ_1 and its reduced form CoQ_1H_2, DQ and its reduced form DQH_2 are useful for probing the activities of NQO1, complex I and complex III in intact lungs using MID.

3.1.2 Amplex Red: Probe to Estimate the Amount of H_2O_2

10-acetyl-3,7-dihydroxyphenoxazine (Amplex red, subsequently referred to as AR) is a colorless membrane-impermeable probe of H_2O_2. In the presence of peroxidase such as

horseradish peroxidase (HRP) or myeloperoxidase (MPO), AR can react with H_2O_2 quickly, resulting in H_2O and high-intensity fluorescent resorufin as described below (Zhou et al., 1997).

$$AR + H_2O_2 \xrightarrow{Peroxidase} resorufin + H_2O$$

AR is highly selective for H_2O_2 compared with other probes such as DCF which can react with other ROS. The oxidized product of AR, resorufin which can be measured fluorometrically or spectrophotometrically, has a high quantum yield (54,000 M^{-1} cm^{-1}). Thus, the sensitivity of AR to detect H_2O_2 could be as low as nM using its fluorescence. (Zhou 1997, Song 2001). However, measuring resorufin using a fluorometric assay is limited by the fact that resorufin undergoes self-quenching when its concentration is greater than 5 uM. This self-quenching property of resorufin does not affect its absorbance spectrum and hence measuring resorufin spectrophotometrically is not limited by its concentration (Zhou et al., 1997). Compared with other dyes such as dihydrorhodamine and dihydrofluorescein, AR has a relatively slow auto-oxidation rate and is resistant to photobleaching (Zhou et al., 1997). For these reasons, AR has been widely used as an extracellular probe of H_2O_2 in cultured cells and in isolated lungs (Song et al., 2001; Chen et al., 2003; Zhou et al., 1997; Heumüller et al., 2008). In this study, AR was used to estimate the rate of H_2O_2 released from lung tissue into perfusate by the measurement of the absorbance of produced resorufin.

3.1.3 FAPGG: Probe to Estimate Perfused Surface Area

N-[3-(2-Furyl) acryloyl]-Phe-Gly-Gly (FAPGG) is used to evaluate the rate constant of ACE-mediated FAPGG hydrolysis as an index of perfused capillary surface area.

FAPGG is a membrane-impermeable substrate of angiotensin converting enzyme (ACE). When the perfusate containing FAPGG passes through the lung, ACE located on the cellular

surface hydrolyzes FAPGG into FAP and GG. Since the activity of ACE on a unit surface area is stable, the measurement of FAPGG in the venous efflux can be used to evaluate the rate constant of ACE-mediated FAPGG hydrolysis.

The linear steady state rate of ACE-mediated FAPGG hydrolysis passage through a perfused lung is represented as a permeability-surface area product (*PS*, ml/min) defined by the following equation:

$$PS = -F\ln(1-E)$$

where $E = steady-state\ extraction\ ratio = \frac{3}{2}\frac{abs1-abs2}{abs1}$; *abs1* is the absorbance value of FAPGG sample before the hydrolysis reaction, *abs2* is the absorbance value of FAPGG sample after the hydrolysis reaction, and F is the perfusate flow (Audi et al., 2005). In the present study, *PS* is considered to be an index of perfused capillary endothelial surface area in intact rat lungs (Audi et al., 2003, 2005, 2008).

3.1.4 Rhodamine Dyes: Probe to Monitor Mitochondrial Membrane Potential in Cultured Cells

Rhodamine 123 (R123) is one of several monovalent cationic fluorescent dyes widely used as the probe for monitoring $\Delta\Psi_m$ in isolated mitochondria and intact cells. R123 is widely used because of its relatively high fluorescence quantum yield. However, R123 tends to undergo self-quenching at concentrations > 5 μM which results in a nonlinear relationship between the fluorescence and its concentration. Because of the relatively large $\Delta\Psi_m$, and the tendance of R123 to aggregate in mitochondria, the concentration of R123 in mitochondria is ususally thousands of times that in the extracellular medium. Therefore, even the addition of a low concentration to the extracellular medium could result in mitochondrial concentrations > 5 μM. At this high

concentration, R123 tends to undergo self-quenching. To avoid the effect of the self-quenching, R123 fluorescence in extracellular medium, which is low enough, instead of R123 fluorescence in mitochondria was measured and used for the model fitting in this study. Tetramethylrhodamine ethyl ester (TMRE) is an analogue of R123, but with a higher membrane permeability and lower cell toxicity (Farkas, Wei & Febbroriello, 1989; Ward, Rego & Frenguelli, 2010). In this study, TMRE was used to validate $\Delta\Psi_m$ estimated using R123.

3.1.5 Inhibitors of the Targeted Enzymes – NQO1, Complex I, III and IV

Rotenone (Rot) is a lipophilic chemical which can cross cellular membranes easily. It inhibits the transfer of electrons from the iron-sulfur center in complex I to ubiquinone and thus can be used as an inhibitor of complex I (Li, Ragheb & Lawler, 2003). Antimycin A (AA) binds to the Q_i site of complex III in the cytochrome b subunit and blocks the flow of electrons from semiquinone to ubiquinone in the Q-cycle of complex III in oxidative phosphorylation. So AA inhibits the electron transport pathway, thus prevents the consumption of O_2 and disrupts the proton gradient across the inner membrane (Huang, Cobessia & Tung, 2005; Park, Han & Kim, 2007). Potassium cyanide (KCN) is a potent inhibitor of the cellular respiration, acting on mitochondrial cytochrome c oxidase (complex IV) and blocking the production of ATP (Seddon & Mcvitte, 1974). Dicumarol is a coumarin-derived natural compound which is used clinically due to its anticoagulant properties. The best defined action of dicumarol is the inhibition of NQO1 by competing with NAD(P)H at the pyridine nucleotide binding site (González, Ariza & Villalba, 2007). But it can also exert its effects through mechanisms unrelated to NQO1 such as inhibiting glutathione peroxidase II (Mays & Benson, 1992), affecting stability of microtubules (Madari 2003) or impairing the electron transport chain (González et al., 2007).

These inhibitors were utilized in this study to differentiate the contributions of their corresponding targeted enzymes on the metabolism of quinone probes.

3.1.6 Inhibitors for the Factors Affecting the Cellular Disposition of Rhodamine Dyes

Carbonyl cyanide m-chlorophenylhydrazone (CCCP) is a potent mitochondrial uncoupler which inhibits oxidative phosphorylation by dissipating the proton gradient across the inner mitochondrial membrane and thus dissipating $\Delta\Psi_m$ (Kim 2004; Park, Jo & Pak, 2002). 9,10-dihydro-5-methoxy-9-oxo-4-acridine-Carboxamide (GF120918) is a specific inhibitory modulator of P-glycoprotein (Pgp) which is a multi-drug efflux pump for many chemicals including rhodamine dyes (Seral, Michot & Chanteux, 2003; Krishna & Mayer, 2000). A buffer containing a high concentration of potassium (138 mM) is used to dissipate $\Delta\Psi_p$ by inhibiting potassium channels across the plasma membrane (He & Curry, 1995).

These inhibitors were utilized in this study to differentiate the contributions of their corresponding targets to the cellular disposition of rhodamine probes.

3.2 Multiple Indicator Dilution Method (MID) and Lung Infusion

MID has been used to assess the kinetics of transport and metabolism of substrates in intact organs such as liver, brain, heart and lung. The indicators are introduced into the organ inflow as a rapid bolus or a pulse of finite duration, and then their concentrations are measured in the organ's venous effluent as a function of time. The information content of data resulting from MID can be complex because, in addition to the metabolic processes of interest occurring within the tissue, other factors such as organ kinematics. The binding to protein can also influence the amount of indicator that is removed and/or modified on passage. Therefore, an interpretation of

these data necessitates the use of mathematical models based on the hypotheses regarding the processes responsible for all mechanisms of indicator disposition on passage through the organ. The resulting kinetic model parameters include measures of the activities of metabolic processes of interest.

Generally speaking, MID data do not provide information about the specific types of cells affecting the reduction of a redox active probe such as DQ on passage through the lung. However, resulting DQ MID data would be expected to provide information about the activities of NQO1 in cells accessible to DQ from the vascular space, presumably dominated by the pulmonary capillary endothelium with its large surface area and direct contact with the blood. In this study, MID is used to measure the lung capacity to reduce the redox active probes such as duroquinone (DQ) and coenzyme Q_1 (CoQ_1), and the lung capacity to oxidize their reduced forms (DQH_2 and CoQ_1H_2) on passage through the pulmonary circulation. For each probe, the general approach is to measure the rate of appearance in the venous effluent of the probe's reduced form (DQH_2 or CoQ_1H_2) during the arterial infusion of the probe's oxidized form (DQ or CoQ_1), and the oxidized form during the arterial infusion of the reduced form. This approach is carried out in the absence or presence of one or more inhibitors of the targeted redox enzymes. The resulting data provide information about the activities of the targeted redox enzymes in the intact rat lungs. Figure 3.1 shows schematic diagram of lung ventilation-perfusion system for single pass MID studies.

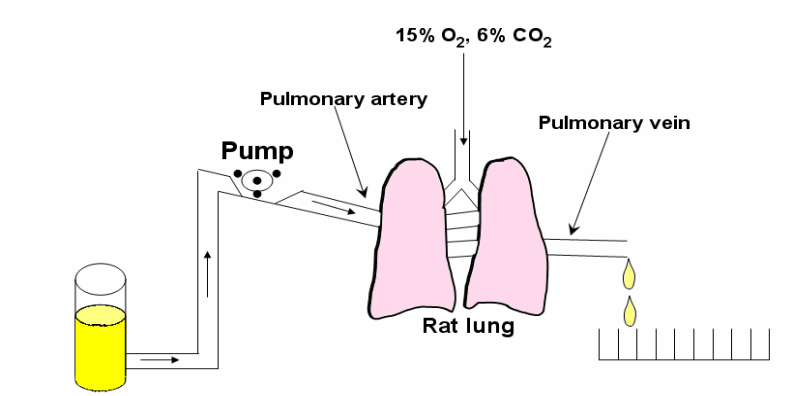

Figure 3. 1 Schematic diagram of lung ventilation-perfusion system with MID application.

3.3 Mathematical Models

In this study, either MID infusion experiment or the measurement of the fluorescence of extracellular rhodamine includes multiple processes which affect the distribution or metabolism of probes. Thus, the acquired data can not be used to estimate the activities of targeted enzymes directly. To interpret the data quantitatively and estimate parameters of interest such as the activity of targeted enzyme, mathematical models which describe the related biological system are required. In the following section, a kinetic model to describe the processes affecting the distribution or metabolism of quinone probes during passage through an intact lung is introduced as an example.

3.3.1 Example: Kinetic Model for Redox Metabolism of Quinone during Passage Through Lung

Quinone(s) are substrates for redox enzymes NQO1, complex I and complex III. Utilizing MID, we are able to evaluate the redox metabolism of quinone compounds in an intact lung. For quantitative interpretation of the resulting data, a kinetic model that not only accounts for quinone tissue and vascular interactions but also the distribution of capillary transit times is needed (Audi et al., 2004, 2005, 2008).

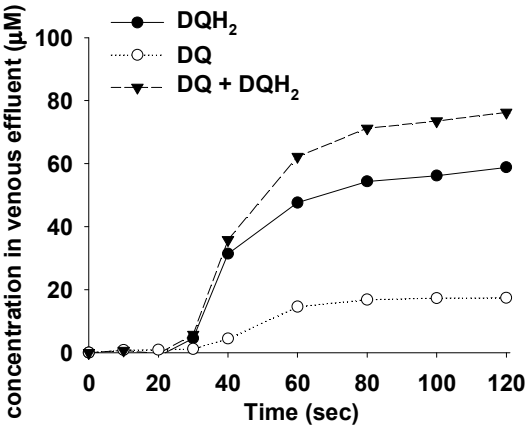

Figure 3. 2 Time course of DQ/DQH_2 concentration in the venous effluent during 100 μM DQ infusion experiment passage through an intact rat lung.

Figure 3.2 shows the time course of DQ/DQH_2 concentration in the venous effluent during 100 μM DQ arterial infusion passage through an intact rat lung using the MID method described in 3.2. The efflux of DQ/DQH_2 are the net results of multiple factors, including i) quinone and hydroquinone interactions with competing nonlinear tissue redox processes, ii) quinone and hydroquinone interactions with protein (i.e., BSA) in the vascular and tissue spaces, and iii) capillary perfusion kinematics (i.e., a heterogeneous distribution of capillary transit times, $h_c(t)$).

A previously developed whole lung kinetic model for the pulmonary disposition of quinones and hydroquinones could be utilized to quantitatively interpret this data (Audi et al., 2004, 2005, 2008). The model consists of a capillary region that accounts for quinone (Q) and hydroquinone (QH_2) tissue and vascular interactions, and conducting arteries and veins. The capillary region has a distribution of capillary transit times, $h_c(t)$ (Ramakrishna et al., 2010). The capillary region is modeled as parallel non-interacting capillary elements with transit times distributed according to $h_c(t)$ (Figure 3.3).

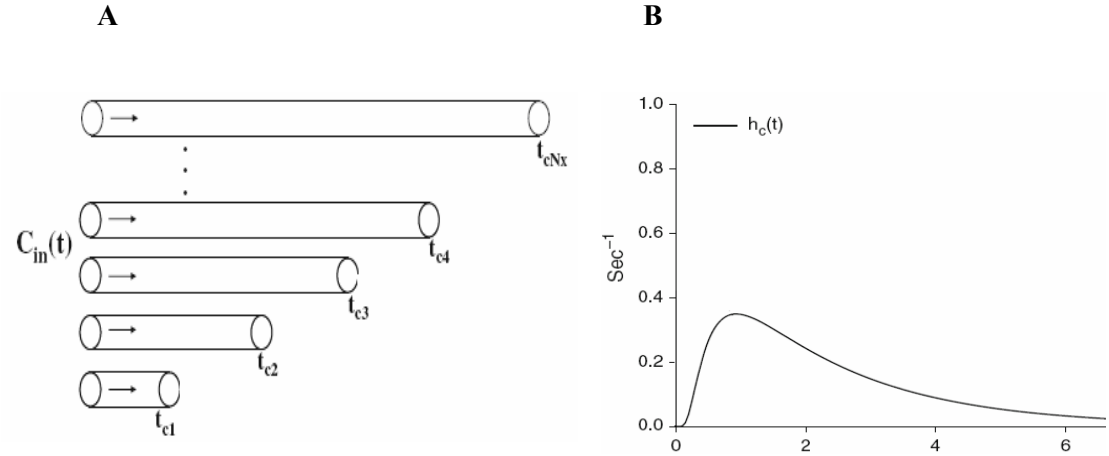

Figure 3. 3 Parallel pathways corresponding to capillaries with different transit time. $C_{in}(t)$ is an input function of infused probe and $t_{ci}(s)$ are the times for the perfusate passage through given length capillaries. B: Approximation of the function form of the capillary transit time distribution $h_c(t)$ for normoxic lungs.

A single capillary element consisting of a vascular region and its surrounding lung tissue region with volumes V_c (ml) and V_e (ml), respectively (Figure 3.4). Within the vascular region, quinone (Q) and hydroquinone (QH_2) participate in nonspecific and rapidly equilibrating interactions with the perfusate albumin (BSA). The free (i.e., not BSA bound) vascular concentrations of Q and QH_2 can freely permeate into the tissue region from the vascular region. Within the tissue region, Q is reduced via NQO1, complex I, and an other reductase(s), and QH_2 is oxidized via mitochondrial complex III. These reduction and oxidation processes are assumed to follow Michaelis-Menten kinetics, where V_{max} and K_m represent the maximum reduction or oxidation rate and Michaelis-Menten constant, respectively. For a given redox process, V_{max} is then a measure of the activity of that process in the intact lung. All nonspecific Q and QH_2 interactions in the vascular and tissue spaces are assumed to follow the law of mass action (Audi et al., 2005, 2008).

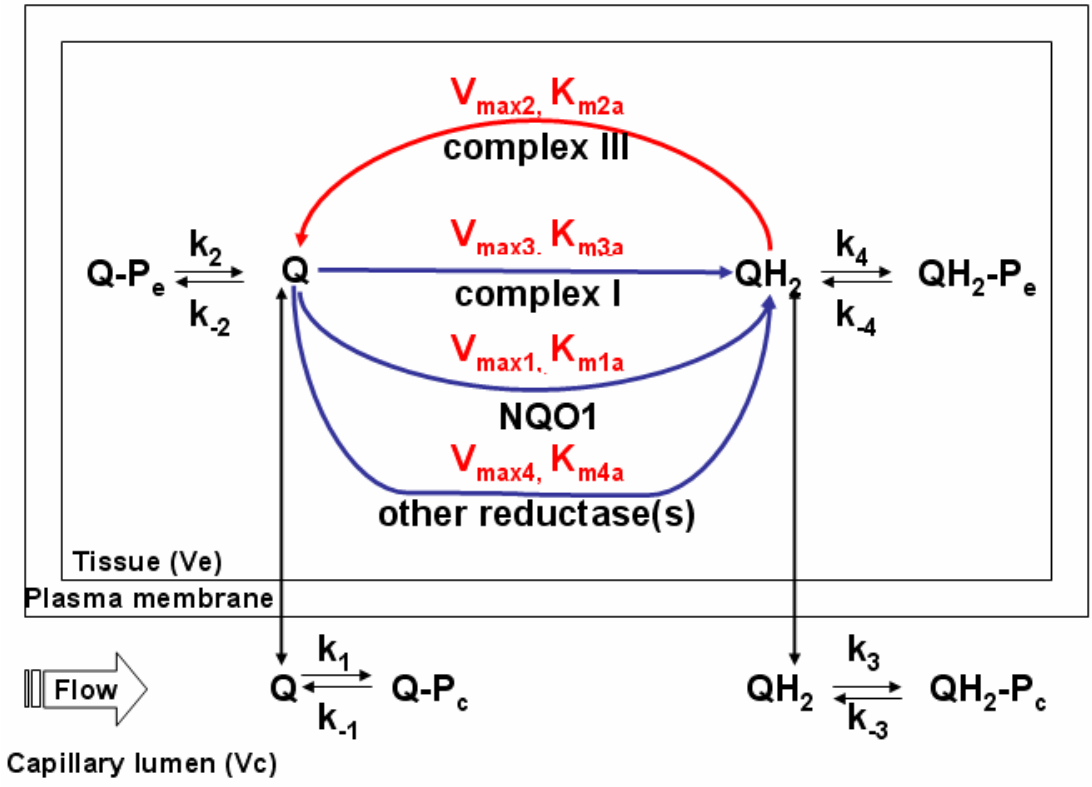

Figure 3. 4 Schematic representation of quinone redox metabolism passage through single capillary. V_{max1}, V_{max2}, V_{max3} and V_{max4} are the respective maximum rates for quinone reduction via NQO1, hydroquinone oxidation via complex III, quinine reduction via complex I and quinine reduction via other reductases. K_{m1a}, K_{m2a}, K_{m3a} and K_{m4a} are the apparent Michaelis-Menten constants for NQO1, complex III, complex I and other reductases. Q, Q-P_e, and Q-P_c represented free, albumin-bound and tissue protein-bound quinone respectively. QH_2, QH_2-P_e, and QH_2-P_c represented free, albumin-bound and tissue protein-bound hydroquinone respectively. k_1, k_2, k_3 and k_4 were bound rate constants for the interactions of Q-BSA, Q-tissue protein, QH_2-BSA and QH_2-tissue protein. k_{-1}, k_{-2}, k_{-3} and k_{-4} were bound rate constants for the interactions of Q-BSA, Q-tissue protein, QH_2-BSA and QH_2-tissue protein.

Based on the single capillary element model depicted in Figure 3.4, the species balance equations descriptive of spatial and temporal variations in the concentrations of Q and QH_2 in the vascular volume (V_c) and tissue volume (V_e) are

$$\frac{\partial \overline{Q}}{\partial t}+W\left(\frac{V_c}{V_c+V_{F1}}\right)\frac{\partial \overline{Q}}{\partial x}=\frac{1}{V_c+V_{F1}}\left(-\frac{V_{\max 1}\overline{Q}}{K_{m1a}+\overline{Q}}-\frac{V_{\max 3}\overline{Q}}{K_{m3a}+\overline{Q}}-\frac{V_{\max 4}\overline{Q}}{K_{m4a}+\overline{Q}}+\frac{V_{\max 2}\overline{QH_2}}{K_{m2a}+\overline{QH_2}}\right) \quad \text{(E3.1)}$$

$$\frac{\partial \overline{QH_2}}{\partial t}+W\left(\frac{V_c}{V_c+V_{F2}}\right)\frac{\partial \overline{QH_2}}{\partial x}=\frac{1}{V_c+V_{F2}}\left(\frac{V_{\max 1}\overline{Q}}{K_{m1a}+\overline{Q}}+\frac{V_{\max 3}\overline{Q}}{K_{m3a}+\overline{Q}}+\frac{V_{\max 4}\overline{Q}}{K_{m4a}+\overline{Q}}-\frac{V_{\max 2}\overline{QH_2}}{K_{m2a}+\overline{QH_2}}\right) \quad \text{(E3.2)}$$

where W = convective transport velocity = L/ $\bar{t}_c$; x = 0 and x = L are the capillary inlet and outlet,

respectively; $\bar{t}_c$ is the capillary mean transit time; Q(x,t), and QH_2(x,t) are vascular concentrations of free quinone (Q) and hydroquinone (QH_2) forms, respectively, at distance x from the capillary inlet at time t; $\overline{Q} = \alpha_1$ Q and $\overline{QH_2} = \alpha_3$ QH_2 are the total (free + BSA bound) vascular concentrations of Q and QH_2, respectively; α_1 = 1 + (Q bound fraction/ Q free fraction) and α_3 = 1 + (QH_2 bound fraction/ QH_2 free fraction) are constants which account for the rapidly equilibrating interactions of Q and QH_2 with the 5% BSA perfusate calculated from the fractions of Q and QH_2 bound to BSA obtained by ultrafiltration (Audi et al., 2003). V_{max1}, V_{max2}, V_{max3} and V_{max4} are the respective maximum rates of quinone reduction via NQO1, hydroquinone oxidation via complex III, quinone reduction via complex I and quinone reduction via other reductase(s). K_{m1a}, K_{m2a}, K_{m3a} and K_{m4a} are the respective apparent Michaelis-Menten constants for quinone reduction via NQO1, hydroquinone oxidation via complex III, quinone reduction via complex I and quinone reduction via other reductase(s). $V_{F1} = (\alpha_2 / \alpha_1) V_e$ and $V_{F2} = (\alpha_4 / \alpha_3) V_e$ are the respective virtual volumes of the distributions for Q and QH_2, where α_2 and α_4 are the constants which account for the rapidly equilibrating interactions of Q and QH_2 with lung tissue sites (P_e) of association, respectively. For DQ and DQH_2, α_1 =25 and α_3=4. For CoQ_1 and CoQ_1H_2, α_1 =14.6, and α_3=16.5 (Audi et al., 2005, 2008). These values were determined by centrifugal ultrafiltration.

Equations E3.1 - 3.2 are for a single capillary element. For the lung model, the effect of the distribution of capillary transit time ($h_c(t)$) on the plasma concentrations and the redox status of Q and QH_2 on passage through the pulmonary circulation was taken into consideration (Audi et al., 2003, 2008). Most of the dispersion within the lung vascular region is due to the capillary bed (Ramakrishna et al., 2010). Thus, Q and QH_2 transit through the arteries and veins are represented by a shifted impulse function, where the shift was the plasma mean transit time through the arteries

and veins determined as previously described (Ramakrishna et al., 2010). To provide the whole organ output Q and QH_2, the outputs for all transit times were summed, weighted by $h_c(t)$ as previous described (Audi et al., 2003, 2005, 2008; Dawson et al., 2003). The activities of targeted enzymes could be quantitatively estimated by fitting the above model to the experiment data such as data in Figure 3.2.

3.3.2 MATLAB

To implement the kinetic model in 3.3.1, a mathematical programming software is required to numerically integrate the model's system of coupled non-linear partial differential equations. MATLAB ("MATrix LABoratory") is a tool for numerical computation, especially array-based data. The programming efficiency of MATLAB is quite high compared to other language such as FORTRAN or C. MATLAB has its own function library which contains hundreds of functions and thus makes it easier for the users to solve numerical problems. However, as an interpreted language, the computation efficiency of MATLAB is relatively low compared to FORTRAN or C. To overcome this shortcoming when a large number of computations is needed, MATLAB supplies a gateway function to support C or Fortran functions, so that the user can use Fortran or C functions in MATLAB easily. In this study, the mathematical models were solved in MATLAB due to its portability, usability, extendibility and abundant functions. When a large number of computations were required, C functions were embedded through an MATLB-C gateway function in order to improve computation efficiency.

3.4 Statistics

The number of animals used in each condition was determined using power analysis (a

power >85), which determines the minimum number of lungs needed to obtain valid and meaningful results. t-test was used to compare two groups of data statistically. For multiple groups of data, one-way ANOVA was used for statistical comparison. For the comparison of single parameter in 2 groups such as V_{max} of complex I for normoxic lungs and hyper-85 lungs, $\Delta\Psi_m$ estimated by R123 data and TMRE data, a modified one side t-test is utilized. Briefly, the normalized variances of distribution for 2 groups are calculated and scaled with weights from their corresponding inverse information matrices. The difference of parameters from 2 groups is then divided by the square root of the sum of variances of disturbance and the resulting t value is showed below,

$$t = \frac{P_1 - P_2}{\sqrt{\frac{E_1 \times VD_1}{DF_1} + \frac{E_2 \times VD_2}{DF_2}}}$$

where P_1, P_2 are the values of same parameters from different groups. VD_1 and VD_2 are the variances of distribution which are the sum of squared variances. DF_1 and DF_2 are their degrees of freedom. E_1 and E_2 are the scalar weights from corresponding inverse information matrices. $P<0.05$ is considered the criterion for statistical significance.

CHAPTER 4. LUNG ACTIVITIES OF NQO1, MITOCHONDRIAL COMPLEXES I AND III AFTER EXPOSURE OF RATS TO 85% O_2 FOR 7 DAYS

4.1 Introduction

It is known that rats exposed to 85% O_2 for 7 days, but not rats exposed to 85% O_2 for 2 days develop a tolerance of 100% O_2 (Crapo et al., 1978, 1980). Previously, Audi et al. demonstrated that rat exposure to 85% O_2 for 48 hours, decreased lung complex I activity by ~50% with no effect on lung activities of complex III or NQO1 (Audi et al., 2008). These results stimulated the following question. Are the activities of these enzymes changed in rats exposed to 85% O_2 for 7 days? Thus, This work was to evaluate the effect of rat exposure to 85% O_2 for 7 days (hyper-85) on lung tissue activities of cytosolic NQO1 and mitochondrial complexes I and III in the isolated perfused lung. The activities of NQO1, complex I, and/or complex III in the intact lung can be measured using indicator dilution methods with the redox-active quinone compounds duroquinone (DQ), coenzyme Q_1 (CoQ_1) and their hydroquinones as test indicators. The general approach involved pulse infusion of each quinone (DQ or CoQ_1) or its hydroquinone (DQH_2 or CoQ_1H_2) into the arterial inflow of isolated perfused lungs from rats exposed to room air (normoxic) or 85% O_2 for 7 days, and then the venous efflux rate of hydroquinone during quinone infusion and vice versa was measured. This protocol was carried out over a range of quinone/hydroquinone concentrations, and in the absence or presence of one or more inhibitors of NQO1, complex I, and complex III. A previously developed kinetic model for the pulmonary disposition of these quinones and their hydroquinones (Audi et al., 2008) was used for estimating parameters descriptive of the activities of the targeted redox enzymes in normoxic and hyper-85 lungs.

4.2 Materials and Methods

Materials

Duroquinone (DQ) and Coenzyme Q1 (CoQ_1) were purchased from Sigma Chemical Company (St. Louis, MO). Durohydroquinone (DQH_2) and CoQ_1 hydroquinone (CoQ_1H_2) were prepared by reduction of DQ or CoQ_1 with potassium borohydride (KBH_4). Bovine serum albumin (Standard Powder, BSA) was purchased from Serologicals Corp (Gaithersburg, MD). Standard NQO1 and NQO1 antibody were purchased from Santa Cruz Biotechnology Co (Santa Cruz, CA). Beta actin antibody was purchased from Abcom (Cambridge, MA). Pierce* ECL Western Blotting Substrate was purchased from Thermo Scientific (Rockford, IL). Rabbit-anti-mouse IgG1 antibody and other reagent grade chemicals not mentioned above were purchased from Sigma Chemical Company.

4.2.1 Hyperoxic Exposure

For normoxic lung studies, male Sprague-Dawley rats (275 to 325 g; Charles River) were exposed to room air. For the hyperoxic lung studies, age matched rats were housed in a Plexiglas chamber (13W x 23L x 12H inches) maintained at ~ 85% O_2 (hyper-85), balance N_2, for 7 days with free access to food and water (Audi et al., 2008). The total gas flow was 3.5 liters/min, and the chamber CO_2 was maintained at < 0.5 %. The temperature within the chamber was maintained at 20-22^{o}C using a custom built cooling system. The chamber was opened every other day for 15 min to weigh the animals, place them in a clean cage, and replace food, water, and CO_2 absorbent. The protocol was approved by the Institutional Animal Care and Use Committees of the Zablocki Veterans Affairs Medical Center and Marquette University (Milwaukee, WI).

4.2.2. Isolated Perfused Lung Preparation

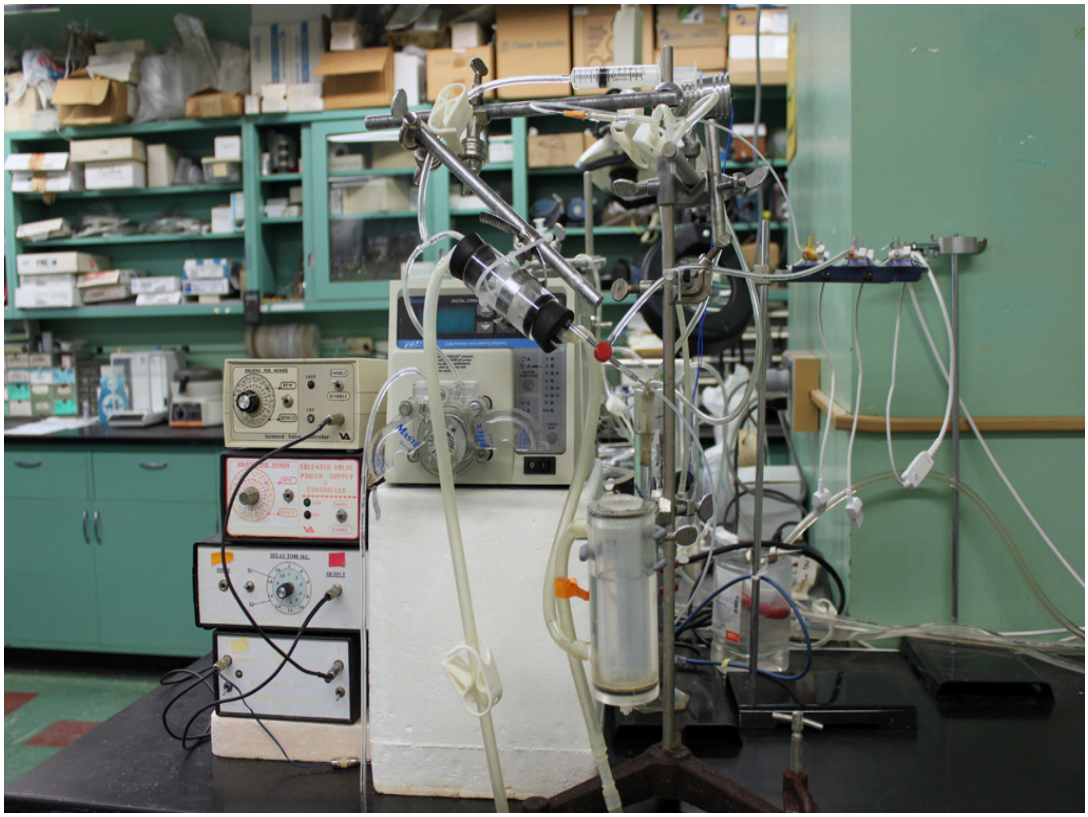

Figure 4. 1 Lung perfusion-ventilation system.

Rats were anesthetized with pentobarbital sodium (40 mg/kg body wt. i.p.), the trachea was then clamped, the chest was opened and heparin (0.7 IU/g body wt.) was injected into the right ventricle (Audi et al., 2008). A 1 ml blood sample was collected for measurement of aortic blood hematocrit. The pulmonary artery and the trachea were then cannulated, and the pulmonary venous outflow was accessed via a cannula in the left atrium. The lung was then removed from the chest and attached to a ventilation and perfusion system (Figure 4.1). The control perfusate contained 4.7 mM KCl, 2.51 mM $CaCl_2$, 1.19 mM $MgSO_4$, 2.5 mM KH_2PO_4, 118 mM NaCl, 25 mM $NaHCO_3$, 5.5 mM glucose, and 5% fatty-acid free bovine serum albumin (BSA) (Audi et al., 2003). The single pass perfusion system (Figure 4.1) was primed (Masterflex roller pump) with the control perfusate maintained at 37^{o}C and equilibrated with 15% O_2, 6% CO_2, balance N_2

resulting in perfusate PO_2, PCO_2 and pH of ~105 Torr, 40 Torr, and 7.4, respectively. Initially, control perfusate was pumped through the lung until the lung was evenly balanced and venous effluent was free of blood. The lung was ventilated (40 breaths/min) with end-inspiratory and end-expiratory pressures of ~ 6 and 3 mmHg, respectively, with the above gas mixture. The pulmonary arterial pressure was referenced to atmospheric pressure at the level of the left atrium and monitored continuously during the course of the experiments. The venous effluent pressure was atmospheric pressure.

For the quinone/hydroquinone pulse infusion experiments described below, the lung was removed at the end of the experiment and weighed to obtain lung wet weight. The lung was then dried and weighed again to obtain dry weight and wet/dry weight ratio.

4.2.3 Lung Experimental Protocols

To determine the DQ reduction capacity of the lung, four 135-second long sequential arterial pulse infusions at DQ concentrations of 50, 100, 200, and 400 μM were carried out with a perfusate flow of 10 ml/min. For each pulse infusion, a venous effluent sample (1 ml) was collected between 130 ~ 135 seconds after the initiation of the pulse infusion. An infusion for 130 seconds is long enough for the venous effluent concentrations of DQ and DQH_2 to reach the steady state (Audi et al., 2005; Audi et al., 2003). Between pulse infusions, the lung was perfused with 30 ml of fresh perfusate to wash the lung and perfusion system of any remaining traces of DQ and/or DQH_2 (Audi et al., 2005). For some of the lungs, the 400 μM DQ pulse infusion was repeated after lung treatment with the NQO1 inhibitor dicumarol (400 μM).

To determine the capacity of NQO1-mediated DQ reduction on passage through the pulmonary circulation, each lung was perfused for 5 min with perfusate containing antimycin A (AA, 10 μM, complex III inhibitor) or potassium cyanide (KCN, 2 mM, complex IV inhibitor) to inhibit complex III mediated DQH_2 oxidation (Boveris, Oshino & Erecinska, 1971). This was followed by four successive DQ pulse infusions, as above DQ infusion, with the inhibitor present throughout the infusion protocol.

To evaluate the capacity of complex III mediated DQH_2 oxidation on passage through the pulmonary circulation, each lung was perfused for 5 min with perfusate containing dicumarol or dicumarol plus rotenone (complex I inhibitor, 20 μM) (Audi et al., 2003; Audi et al., 2005; Audi et al., 2008). This was followed by four 135-second sequential arterial pulse infusions at DQH_2 concentrations of 50, 100, 200, and 400 μM at a flow of 10 ml/min, with the inhibitors present throughout the infusion protocol. A 1 ml venous effluent sample was collected between 130 and 135 seconds after initiation of each pulse infusion. For some of the lungs, the 400 μM DQH_2 infusion was repeated after lung perfusion with AA to inhibit complex III mediated DQH_2 oxidation. The flow rate was determined in previous studies by the maximum of the dynamic range when the activities of targeted enzymes were decreased by the application of inhibitors.

To determine the CoQ_1 reducing capacity of the lung, four 45-second long sequential arterial pulse infusions at CoQ_1 concentrations of 25, 50, 100, 200, and 400 μM were carried out with a perfusate flow of 30 ml/min. This flow was chosen to optimize the sensitivity of this assay for an increase/decrease in complex I activity. For each pulse infusion, a venous effluent sample (1 ml) was collected between 43 and 45 seconds after initiation of the pulse infusion. At this flow, infusion for 42 seconds is long enough for the venous effluent concentrations of CoQ_1 and

CoQ_1H_2 to reach the steady state (Audi et al., 2008). Between pulse infusions, the lung was perfused with 30 ml of fresh perfusate to wash the lung and perfusion system of any remaining traces of CoQ_1 and/or CoQ_1H_2 (Audi et al., 2008).

The CoQ_1 reducing capacity of the lung is the net result of lung CoQ_1 reduction capacity and CoQ_1H_2 oxidation capacity. To determine CoQ_1 total lung reduction capacity, the lung was perfused for 5 min with perfusate containing AA or KCN to inhibit complex III mediated CoQ_1H_2 oxidation (Boveris et al., 1971). This was followed by five 45-second sequential arterial pulse infusions at CoQ_1 concentrations of 25, 50, 100, 200, and 400 μM at a flow of 30 ml/min, with the inhibitor(s) present throughout the infusion protocol. The same protocol but using rotenone as the inhibitor of complex I was applied to determine complex I mediated reduction capacity. The CoQ_1 pulse infusions in the presence of dicumarol, which is the inhibitor of NQO1, was applied to determine the lung NQO1 mediated reduction capacity, and the CoQ_1 pulse infusions in the presence of dicumarol and rotenone was applied to determine the reduction capacity of other reductase(s).

To evaluate the capacity of complex III mediated CoQ_1H_2 oxidation on passage through the pulmonary circulation, each lung was perfused for 5 min with perfusate containing dicumarol plus rotenone to minimize CoQ_1 reduction (Audi et al., 2003, 2005, 2008). This was followed by five 45-second sequential arterial pulse infusions at CoQ_1H_2 concentrations of 25, 50, 100, 200, and 400 μM at a flow of 30 ml/min, with the inhibitors present throughout the infusion protocol. A 1 ml venous effluent sample was collected between 42 and 45 seconds after initiation of each pulse infusion. For some of the lungs, the 400 μM CoQ_1H_2 infusion was repeated after lung perfusion with AA to inhibit complex III mediated CoQ_1H_2 oxidation.

To determine perfused lung surface area, a 150 μM 20-second pulse infusion of the angiotensin converting enzyme (ACE) substrate N-[3-(2-Furyl) acryloyl]-Phe-Gly-Gly (FAPGG) was carried out at a perfusate flow of 30 ml/min (Audi et al., 2005). Two 1 ml venous effluent samples were collected between 16 and 20 seconds after the start of the FAPGG infusion (Audi et al., 2005, 2008).

4.2.4 Determination of Quinone (DQ, CoQ_1) and Hydroquinone (DQH_2, CoQ_1H_2) Concentrations in Venous Effluent Samples

For a given quinone compound, the concentrations of its oxidized and reduced forms in each venous effluent sample were determined as previously described using the extinction coefficients of 0.0143 μM^{-1} cm^{-1} for CoQ_1, 0.00229 μM^{-1} cm^{-1} for CoQ_1H_2, 0.02164 μM^{-1} cm^{-1} for DQ and 0.0017 μM^{-1} cm^{-1} for DQH_2 (Audi 2005, Audi 2008). Briefly, venous effluent samples were centrifuged (13,500 g) for 1 min. For each sample, 100 μl of the resulting supernatant was added into a micro tube containing 0.8 ml ice-cold ethanol and 10 μl potassium ferricyanide (12.1 mM in water) which oxidized hydroduroquinone to quinone or 10 μ1 EDTA (1 mM in water) to minimize auto-oxidation of hydroquinone. The tubes were mixed on a vortex mixer followed by centrifugation at 13,500 g for 7 min. A perfusate sample that had passed through the lungs but contained no probe was treated in the same way to be used as the blank for absorbance measurements. The absorbance values were measured at 275 nm for CoQ_1 or CoQ_1H_2 and 265 nm for DQ or DQH_2 using a Beckman DU 7400 spectrophotometer. Sample concentrations of probes (in μM) were calculated from the absorbance values of the fully oxidized (abs1) and EDTA-treated supernatant (abs2).

For DQ or DQH_2 infusion,

$$[DQH_2]_{in\ venous\ effluent} = \frac{abs1 - abs2}{0.02164 - 0.0017} \text{ and } [DQ]_{in\ venous\ effluent} = \frac{abs1}{0.02164} - [DQH_2] \quad \text{(E4.1)}$$

For CoQ_1 or CoQ_1H_2 infusion,

$$[CoQ_1H_2]_{in\ venous\ effluent} = \frac{abs1 - abs2}{0.0143 - 0.00229} \text{ and } [CoQ_1]_{in\ venous\ effluent} = \frac{abs1}{0.0143} - [CoQ_1H_2] \quad \text{(E4.2)}$$

At steady state, 92 ± 3 (SD) % and 95 ± 4 (SD) % of the infused DQ and DQH_2, respectively, were recovered in the total venous effluent as DQ + DQH_2, with the loss attributable primarily to binding of both forms to the tubing (data not shown). 93 ± 6 (SD) % and 92 ± 6 (SD) % of the infused CoQ_1 and CoQ_1H_2 were recovered in the total venous effluent as CoQ_1 + CoQ_1H_2, respectively.

The steady state efflux rates of hydroquinone (or quinone) from the lung during quinone (or hydroquinone) arterial infusion was calculated as the product of the perfusate flow and the steady state venous effluent hydroquinone (or quinone) concentrations.

4.2.5 Determination of Perfused Capillary Surface Area

A permeability-surface area product (*PS*, ml/min) is considered to be an index of perfused capillary endothelial surface area in intact rat lungs (Audi et al., 2003, 2005, 2008). PS represented by the linear steady state rate of ACE-mediated FAPGG hydrolysis passage through a perfused lung during FAPGG perfusion is defined by the equation described in chapter 3.1.3.

4.2.6 Determination of Activities of Targeted Redox Enzymes in Lung Homogenate

i. Lung homogenate NQO1 activity and Protein Expressions

Lungs were isolated and connected to the ventilation-perfusion system as described above, after which they were washed free of blood by Hank's Balanced Salted Solution (HBSS) containing 2.5% ficoll, PH 7.4. The blood-free lung was weighted, minced and homogenized

using a Ploytron tissue homogenizer on ice in a beaker containing the homogenization buffer which contained 10 mM HEPES, 3.8mM EDTA and 1% protease inhibitor cocktail, PH7.4. The volume of the homogenaiztion buffer in the beaker was 5-fold (vol/mass) of the lung wet weight.

NQO1 activity

A fraction of the above lung homogenate was centrifuged (13,500g) at 4 ^{o}C for 30 min. The supernatant was collected and stored on ice. The protein concentration was determined using Bio-Rad protein assay (Bio-Rad laboratories, Hercules, CA) using BSA as the standard. The NQO1 activity was then measured using a modified procedure of Lind et al (Lind, Cadenas & Hochstein, 1990). Briefly, the collected supernatant was diluted by 1:100 using the buffer containing 25 mM Tris·HCl. Then 50 μl diluted supernatant was added into a semimicro spectrophotometric cuvette containing 1 ml assay buffer which contained 25 mM Tris·HCl, 0.23 mg/ml BSA, 0.01% (vol/vol) tween-20, 50 μM 2,6-dichlorophenolindophenol (DCPIP), 5 μM flavin adenine dinucleotide (FAD) with or without 20 μM dicumarol, PH 7.4. The reaction was initiated by the addition of NADPH (final concentration 200 μM). The absorbance of reduced DCPIP was measured spectrophotometrically at 600 nm every 15 seconds for 10 min. The concentration of reduced DCPIP is calculated from the recorded absorbance values using an extinction coefficient of 0.021 μM^{-1} cm^{-1}. NQO1 activity (nmol DCPIP reduction min^{-1} mg $protein^{-1}$) was determined as the difference between the rate of DCPIP reduction in the presence and absence of dicumarol over the linear portion of the reaction progress curve (Audi et al., 2005, 2008).

NQO1 Protein Expression

A fraction of the above lung homogenate was centrifuged (13,500 g) at 4 ^{o}C for 30 min. A portion of the resulting homogenate supernatant was then centrifuged at 10,000 g for 15 min. The protein concentration of the resulting supernatant was determined using the BCA protein assay. Supernatant containing 25 μg protein was then subjected to sodium dodecyl sulphate-polyacrylaminde gel electrophoresis (SDS-PAGE) using MES-SDS running buffer. The proteins were then transferred to a polyvinylidene fluoride (PVDF) membrane and washed several times using a Tris buffered saline with tween-20 solution (TBST). The resulting membrane was incubated in TBST containing 5% non-fat milk at room temperature for 1 hours and then incubated in TBST containing 1:4000 dilution of NQO1 antibody (A180, Santa Cruz Biotechnology Co.) and 1:6000 beta actin antibody (AC-15, Abcam) at 4 ^{o}C overnight. The membrane was washed for several times using TBST and then incubated in TBST containing 1:12000 dilution of rabbit-anti-mouse IgG1 antibody at room temperature for 2 hours. Before imaging, the membrane was washed and then incubated in Pierce* ECL Western Blotting Substrate (Thermo Scientific, MA) for 5 min. The intensity of protein band was captured and analyzed using an Image Station 4000MM (Kodak, NY).

ii. Mitochondrial activities of complex I and complex IV

Lungs were isolated and washed free of blood with perfusate containing 2.5% Ficoll. The lungs were then weighed, minced, and homogenized as above with buffer (pH 7.2) containing 225 mM mannitol, 75 mM sucrose, 5 mM 3-[N-morpholino]propanesulfonic acid, 20 mM ethylene glycol-bis(B-aminoethyl ether)-N,N,N',N'-tetraacetic acid, 2% fatty-acid free BSA, and 0.02 ml per ml protease inhibitor cocktail set III (Calbiochem, La Jolla, CA). Lung homogenates were centrifuged at 1,500 g for 5 min at 4 °C, and the resulting supernatants were centrifuged again at

13,000 g for 30 min at 4°C to obtain a crude mitochondrial fraction (P2). The P2 fractions were washed twice by resuspension in 8 ml ice-cold homogenization buffer without BSA and then centrifuged (13,000 g for 20 min at 4°C). The final P2 fractions were resuspended in 1-ml BSA-free homogenization buffer. The protein concentrations were determined using BCA Protein Assay Kit (Thermo Scientific, MA) using BSA as the standard.

Mitochondrial complex I activity

Complex I activity was measured using a modified procedure of Lenaz et al (2004). Briefly, 20 µl thawed P2 fraction was added into a semi spectrophotometric cuvette containing 1 ml assay buffer which contains 13 mM Tris, 1.3 mM EDTA, 50 mM KCl, 2 mM KCN, 2 µM Antimycin A, 100 µM CoQ_1 and 100 µM NADH with or without 2 µM rotenone. NADH oxidation was monitored as the decrease in absorbance at 340 nm every 20 seconds for 20 min. The concentration of NADH was calculated from the recorded absorbance values using an extinction coefficient of 6.22 mM^{-1} cm^{-1}. Complex I activity (nmol NADH oxidation min^{-1} mg $protein^{-1}$) was determined as the difference between the rate of NADH oxidation in the presence and absence of rotenone over the linear portion of the reaction progress curve (Audi et al., 2008).

Mitochondrial complex IV activity

Complex IV activity was measured using a modified procedure of Storrie et al (Storrie & Madden, 1990; Audi et al., 2008). The thawed P2 fraction was diluted by 1:10 using phosphate buffer which contains 40 mM KH_2PO_4, 40 mM K_2HPO_4, 0.1% Triton X-100, PH6.2. Then 50 µl diluted mitochondrial fraction was added into 1 ml cytochrome c buffer which contains 40 mM KH_2PO_4, 40 mM K_2HPO_4, 0.1% Triton X-100 and 0.22 mM 70%-reduced cytochrome C. The reduction percentage of cytochrome c is adjusted by NaHS solution. The oxidation of reduced

cytochrome c was monitored as the decrease in absorbance at 550 nm every 20 seconds for 10 min. The concentration of reduced cytochrome c was calculated from the recorded absorbance values using an extinction coefficient of 0.0191 μM^{-1} cm^{-1}. Complex IV activity was expressed using the oxidation rate of reduced cytochrome c (nmol min^{-1} mg $protein^{-1}$).

4.2.7. Lung Histology

Lungs were isolated and washed free of blood using KRB pefusate containing 5% BSA. The lungs were then perfused with 10% buffered formalin, and the airways were also filled with the buffered formalin (~5 ml) via the trachea. The pulmonary artery and trachea were then clamped and the lungs were removed and placed in buffered formalin. The lungs were then shipped to Research Animal Diagnostic Laboratory (Columbia, MO) for the preparation of lung slices. To prepare the lung slices, the fixed lungs were subjected to dehydration and infiltration with paraffin wax, and then embedded into wax-filled block molds. The largest lobe of blocked lungs was sliced into 5 μm sections at 3 mm intervals using an automated microtome, and then were mounted onto glass slides. The sections were then stained with hematoxylin and eosin (H&E) and sealed with mounting medium and a coverslip. The prepared lung slices were then observed with a microscope at $\times 200$ magnification.

4.3 Results

4.3.1 Rat Body Weight, Lung Dry Weight, Aortic Blood Hematocrit and Perfused Capillary Surface Area

Rats lost ~14% of their pre-exposure body weight over the 7-day 85% O_2 exposure period (Figure 4.1) consistent with results from previous studies (Crapo et al., 1980). Most of this weight

loss occurred between days 2 and 6. Age-matched normoxic rats gained body weight steadily over the 7-day exposure period (Figure 4.2).

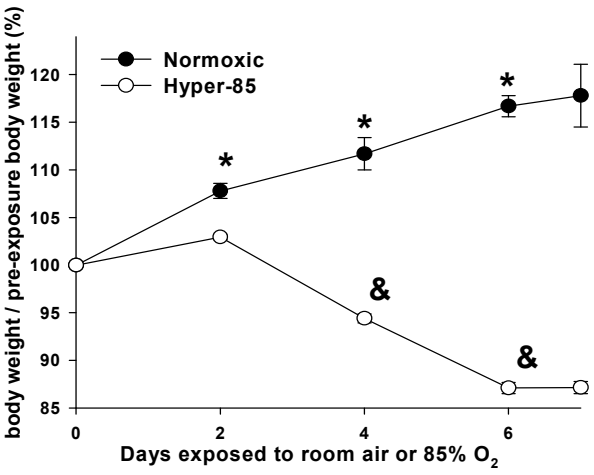

Figure 4.2 Rats body weights (as a percent of pre-exposure body weight) over 7-day exposure period to room air (normoxic) or 85% O_2 (hyper-85). Values are mean ± SE. Normalized weights at a given time are significantly different from normalized weights at the previous time point for * normoxic and & hyper-85, respectively ($P<0.05$).

Rat exposure to 85% O_2 for 7 days increased lung wet weights by ~80% (Table 4.1). There was no significant difference between wet-to-dry weight ratio compared to normoxic lungs. These results are consistent with results from previous studies (Audi et al., 2008; Crapo et al., 1980) and suggest that 85% O_2 induced increase in lung wet weight and dry weight are mostly due to increased tissue mass rather than edema.

Rat exposure to 85% O_2 increased aortic blood hematocrit by 17% as compared to normoxic lungs in agreement with that reported in previous studies (Crapo et al., 1980, 1983). Those studies suggested that this increase could be due to dehydration, consistent with the measured body weight loss in hyper-85 rats (Table 4.1). Another possible explanation is an increase in erythropoiesis. Hyper-85 rats show signs of cyanosis even in a hyperoxic environment due to an increase in the thickness of lung air-blood barrier (Crapo et al., 1978, 1980), which suggests a tendency for hyperoxemia. Hyperoxemia requires an increase in erythropoiesis to recover the capacity for systemic O_2 delivery (Semenza, 1994, 2007) which can be induced through an increase in expression of the erythropoietin gene (Ratcliffe, Ebert & Firth, 1997;

Chandel 2010).

Exposure to 85% O_2 for 7 days decreased lung *PS* (ml/min), an index of perfused capillary endothelial surface area, by 56% as compared to normoxic lungs (Table 4.1). This is consistent with the 50% decrease in capillary volume and endothelial surface area measured morphometrically (Crapo et al., 1980).

	B. W. (g)	**W. W. (g)**	**W/D**	**Hct (%)**	***PS* (ml/min)**
Normoxic	320±3	1.20±0.02	5.53±0.05	43.5±0.3	23.8±0.3
Hyper-85	269±2*	2.27±0.05*	5.70±0.04	50.4±0.4*	10.3±0.3*

Table 4. 1 Body weight (B.W.), lung wet weight (W.W.), lung wet weight/lung dry weight ratio (W/D), hematocrit (Hct), and *PS* of normoxic rats and rats exposed to 85% O_2 for 7 days (Mean ± SE), n=94 and 96 for normoxic and hyper-85 rats respectively.

4.3.2 Lung Histology

Figure 4.3 shows histological sections of a normoxic lung and a hyper-85 lung. The sections of hyper-85 lung indicate a significant increase in lung tissue content (44.9±1.5, n=6) compared with the sections of normoxic lung (25.3±1.6, n=6). An increase in the thickness of air-blood barrier and an increase in the matter found in septa in hyper-85 lung are also observed, consistent with the results of a study by Crapo et al. (Crapo et al., 1980).

4.3.3 Quinone/Hydroquinone Pulse Infusion Results

Figure 4.4 shows that rat exposure to 85% O_2 for 7 days has a differential effect on the redox metabolism of DQ and CoQ_1 on passage through the pulmonary circulation. In hyper-85 lungs, the hydroquinone efflux rates increased by 32% during DQ infusion and decreased by 25% during CoQ_1 infusion as compared to that in normoxic lungs. For each quinone, the rate of hydroquinone efflux during quinone infusion is the net result of quinone reduction to

hydroquinone and hydroquinone oxidation to quinone. Thus, the differential effect of rat exposure to 85% O_2 on DQ or CoQ_1 reduction could be due to hyperoxia-induced change in quinone reduction and/or hydroquinone oxidation. To determine the underlying mechanisms of this differential response, the effects of lung treatment with one or more inhibitors of the dominant quinone reductases or hydroquinone oxidases on the redox metabolism of DQ, CoQ_1, and their hydroquinones on passage through the pulmonary circulations of normoxic and hyper-85 lungs were evaluated.

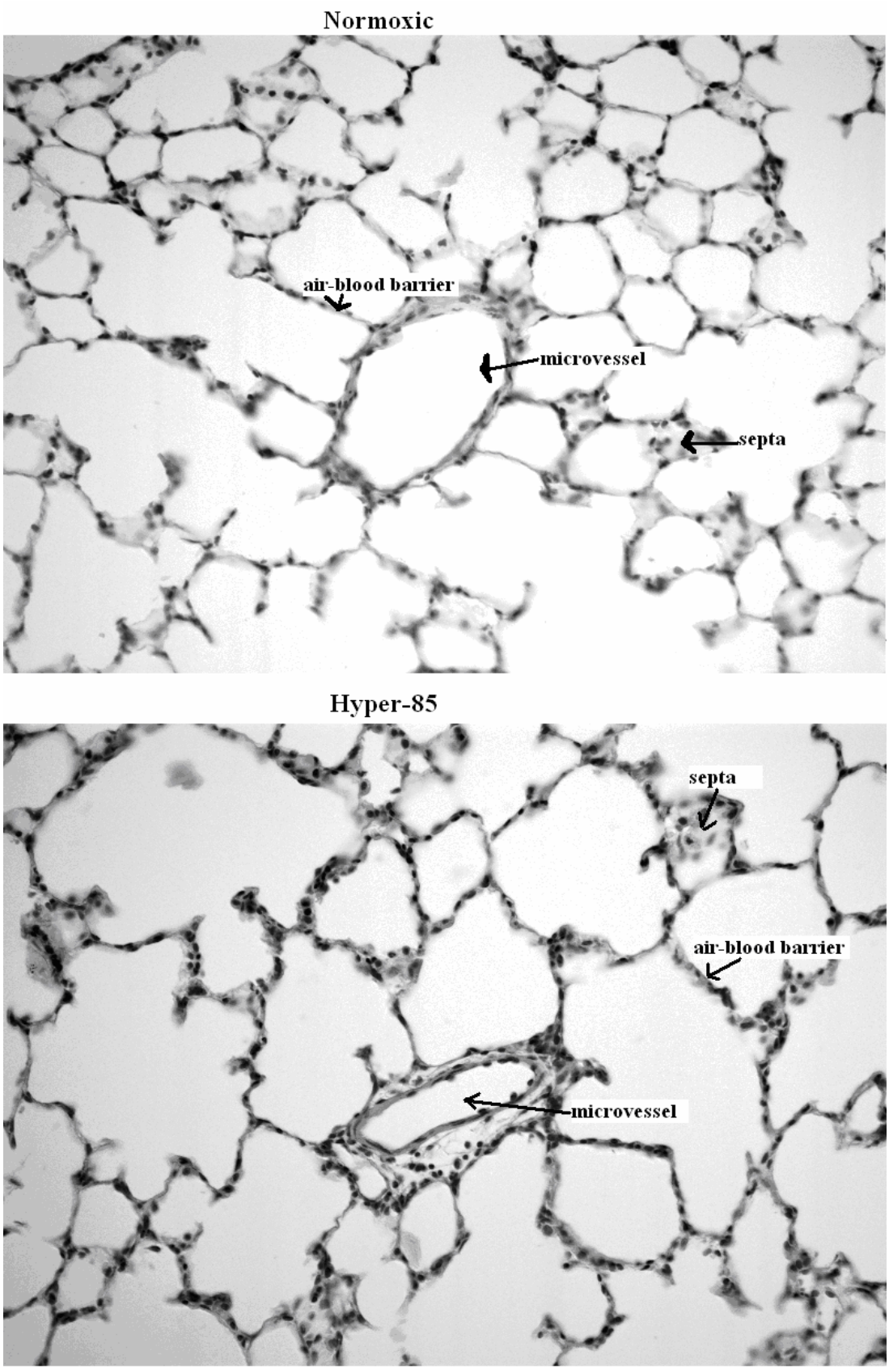

Figure 4.3 Images of histological sections of a normoxic and a hyper-85 rat lung. The magnification is x200.

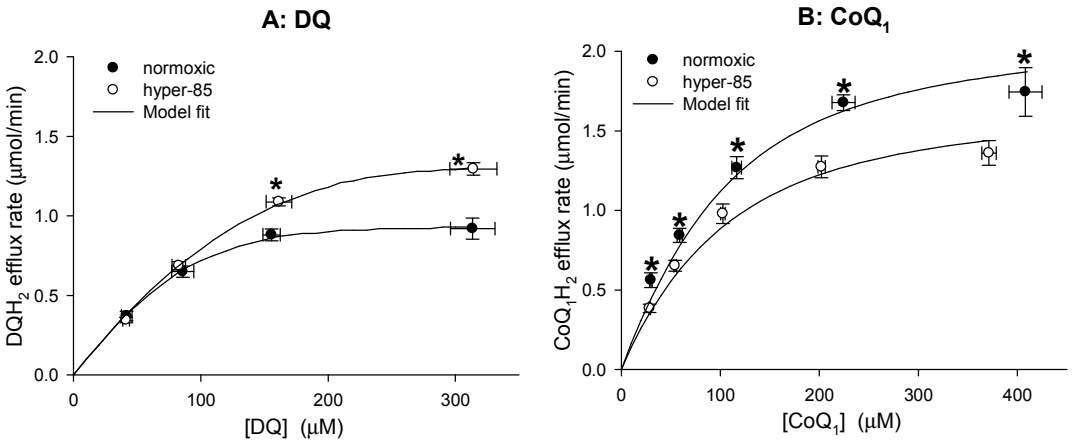

Figure 4.4 The differential effect of rat exposure to 85% O_2 for 7 days on DQ redox metabolism and CoQ_1 redox metabolism. A: the relationship between the steady state rate of DQH_2 efflux and the infused DQ concentrations during DQ arterial infusion, for normoxic lungs (n = 4), hyper-85 lungs (n = 5). B: The relationship between the steady state rate of CoQ_1H_2 efflux and the infused CoQ_1 concentrations during CoQ_1 arterial infusion, for normoxic lungs (n = 7), hyper-85 lungs (n = 11). Values are mean ± SE. * Hyper-85 rates significantly different from the normoxic rates at the same infused concentrations

Lungs treatment with dicumarol decreased the rate of DQH_2 efflux during DQ infusion by >95% during DQ infusion in both normoxic and hyper-85 lungs. This is consistent with NQO1 being the dominant reductase of DQ on passage through the pulmonary circulation (Audi et al., 2005).

The steady state rate of DQH_2 efflux during DQ infusion in the presence of AA was measured to evaluate the capacity of NOQ1-mediated DQ reduction (Figure 4.5). For both normoxic and hyper-85 lungs, the rates of DQH_2 efflux during DQ infusion were higher than those in the absence of AA (Figure 4.4 A), consistent with the inhibition of DQH_2 oxidation. Lungs treatment with AA also increased the difference in the steady state efflux rate of DQH_2 between normxoic and hyper-85 lungs at the two highest infusion concentrations (Figure 4.5) as compared to the difference in the absence of AA (Figure 4.4 A). This suggests a higher rate of DQH_2 oxidation in hyper-85 lungs as compared to normoxic lungs.

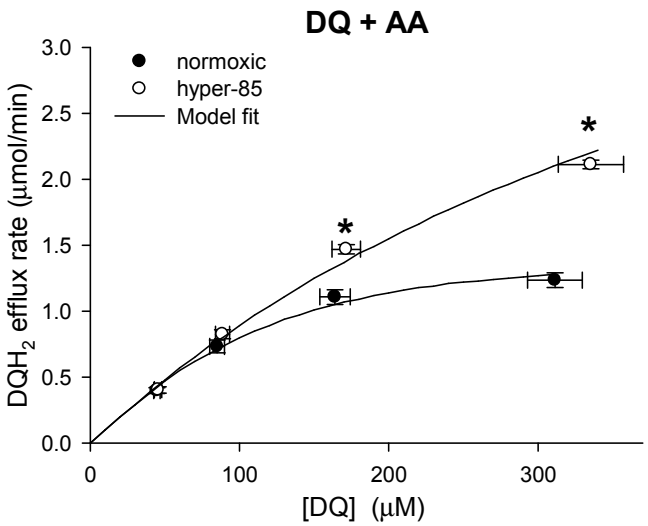

Figure 4.5 The relationship between the steady state rate of DQH_2 efflux and the infused DQ concentrations during DQ arterial infusion in the presence of AA (10 µM), for normoxic lungs (n = 5), hyper-85 lungs (n = 5). Values are mean ± SE. * Hyper-85 rates significantly different from the normoxic rates at the same infused concentrations

The steady state rate of DQ efflux during DQH_2 infusion in the presence of dicumarol was measured to evaluate the capacity of lungs to oxidize DQH_2 (Figure 4.6 A). In hyper-85 lungs, the steady state efflux rate of DQ was ~40% higher than that of normoxic lungs at the two highest infused concentrations. In the presence of AA, the efflux rate of DQ during DQH_2 infusion was nearly zero. This is consistent with complex III being the dominant DQH_2 oxidase on passage through the pulmonary circulation (Audi et al., 2005).

The rate of DQ efflux during DQH_2 infusion was measured in the presence of dicumarol and rotenone to evaluate the effect of rat exposure to 85% O_2 on mitochondrial complex III mediated DQH_2 oxidation. The complex I inhibitor rotenone was added to minimize competition between DQH_2 and reduced endogenous coenzyme Q_9 hydroquinone (CoQ_9H_2) for oxidation via complex III. For both normoxic and hyperoxic lungs, the rates of DQ efflux during DQH_2 infusion were higher in the presence of dicumarol plus rotenone than in the presence of dicumarol alone (Figure 4.6). Futhermore, for hyper-85 lungs, the steady state rates of DQ efflux during DQH_2

infusion at the two highest concentrations in the presence of dicumarol plus rotenone were about 30% higher than those in normoxic lungs. For both normoxic and hyper-85 lungs, the rate of DQ efflux during DQH_2 infusion at the highest concentration in the presence of AA along with dicumarol and rotenone was virtually zero (data not shown). This further supports that complex III is the dominant site for DQH_2 oxidation on passage through the pulmonary circulation of both normoxic and hyper-85 lungs.

As stated above, the steady state efflux rate of CoQ_1H_2 during CoQ_1 infusion was on average ~25% lower in hyper-85 lungs than in normoxic lungs over the range of infused concentrations. To evaluate the contributions of complex I and NQO1 mediated CoQ_1 reduction to this decrease, the steady state efflux rate of CoQ_1H_2 during CoQ_1 infusion were measured in the presence of rotenone, dicumarol, or rotenone plus dicumarol.

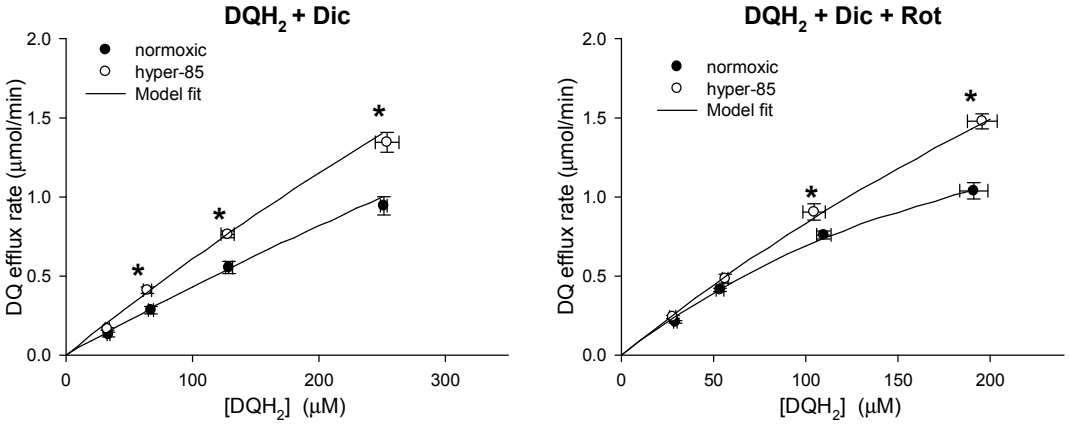

Figure 4.6 A: The relationship between the steady state rate of DQ efflux and the infused DQH_2 concentrations during DQH_2 arterial infusion in the presence of Dic (400 µM), for normoxic lungs (n = 6), hyper-85 lungs (n = 6). B: The relationship between the steady state rate of DQ efflux and the infused DQH_2 concentrations during DQH_2 arterial infusion in the presence of Dic (400 µM) and Rot (20 µM), for normoxic lungs (n = 4), hyper-85 lungs (n = 4). Values are mean ± SE. * Hyper-85 rates significantly different from the normoxic rates at the same infused DQH_2 concentrations.

Lungs treatment with rotenone decreased the efflux rate of CoQ_1H_2 by ~67% in normoxic lungs and ~46% in hyper-85 lungs, as compared to the rates in the absence of rotenone (Figure 4.7

B), consistent with complex I being a dominant site of CoQ_1 reduction (Audi et al., 2008). Moreover, lungs treatment with rotenone eliminated the difference in CoQ_1H_2 efflux rates between normoxic and hyper-85 lungs measured in the absence of inhibitors, consistent with a decrease in the capacity of complex I mediated CoQ_1 reduction in hyper-85 lungs as compared to normoxic lungs.

Lungs treatment with dicumarol decreased the efflux rate of CoQ_1H_2 in both normoxic and hyper-85 lungs, and the decrease was larger in hyper-85 lungs (~60%) than in normoxic lungs (~25%) (Figure 4.7 C). As a result, treatment of lungs with dicumarol increased the difference in CoQ_1H_2 efflux rates between normoxoic and hyper-85 lungs compared with that measured in the absence of inhibitors. This increase was consistent with an increase in the capacity of NQO1 mediated CoQ_1 reduction in hyper-85 lungs as compared to normoxic lungs. This result is also consistent with the hyperoxia-induced increase in the capacity of NQO1-mediated DQ reduction (Figure 4.5).

Figure 4.7 D shows that the steady state CoQ_1H_2 efflux rates decreased by ~85% and >95% in the presence of rotenone and dicumarol in normoxic and hyper-85 lungs, respectively. These results are consistent with the dominant role of complex I and NQO1 in CoQ_1 reduction on passage through these lungs.

To evaluate the capacity of lungs to oxidize CoQ_1H_2, the steady state rate of CoQ_1 efflux during CoQ_1H_2 infusion was measured in the presence of rotenone and dicumarol to minimize CoQ_1 reduction. Figure 4.7 F shows that the steady state efflux rate of CoQ_1 during CoQ_1H_2 infusion in the presence of rotenone and dicumarol in hyper-85 lungs was on average ~28% higher than that in normoxic lungs at the two highest infused concentrations. This result suggests an

increase in the capacity of complex III mediated CoQ_1H_2 oxidation in hyper-85 lungs as compared to normoxic lungs. Additional lung treatment with AA decreased the efflux rate of CoQ_1 to nearly zero (data not shown). This is consistent with complex III being the dominant CoQ_1H_2 oxidase on passage through pulmonary circulation (Audi 2008).

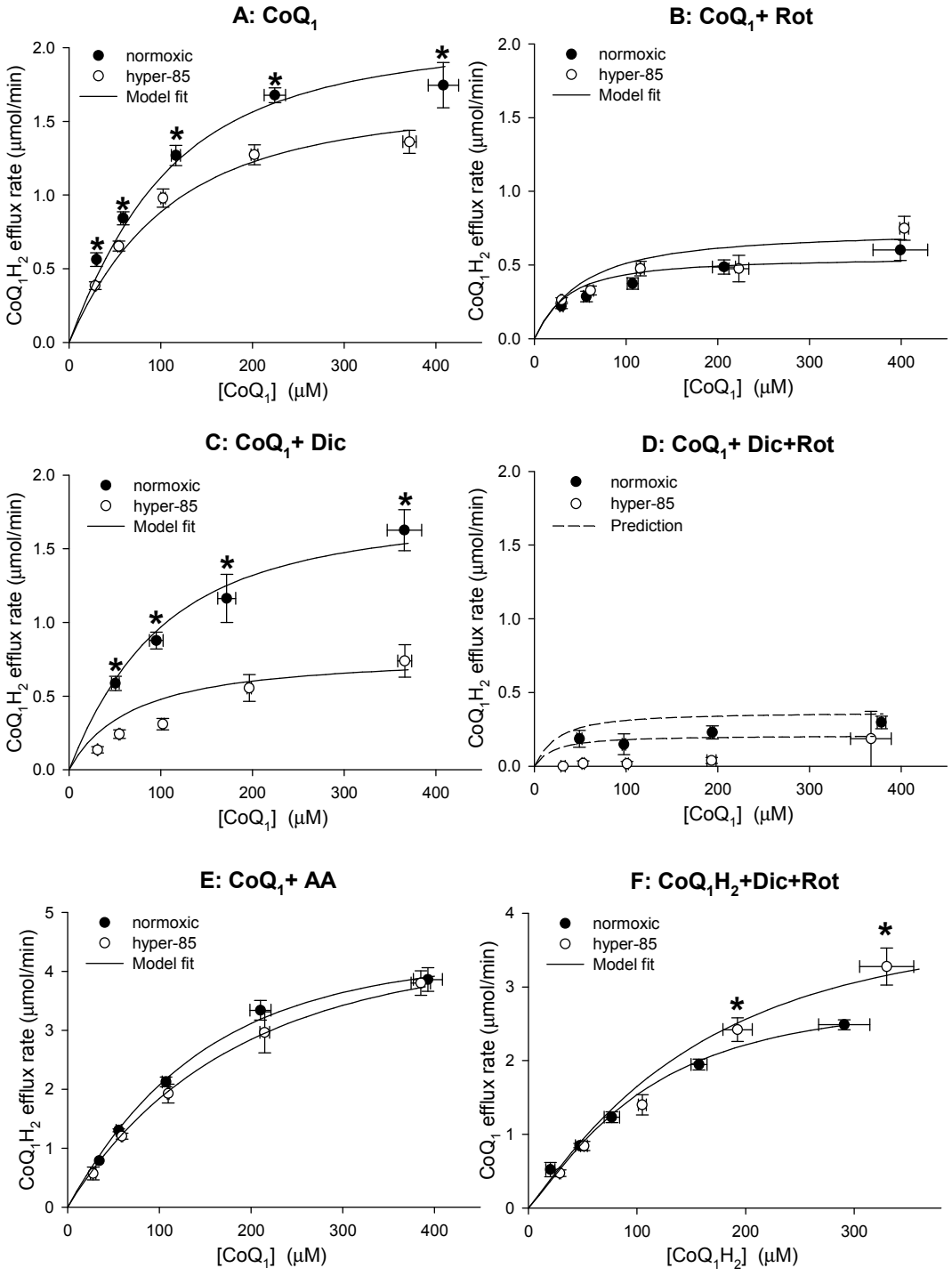

Figure 4.7 A: The relationship between the steady state rate of CoQ_1H_2 efflux and the infused CoQ_1

concentrations during CoQ_1 arterial infusion for normoxic lungs (n = 7), hyper-85 lungs (n = 11). B: The relationship between the steady state rate of CoQ_1H_2 efflux and the infused CoQ_1 concentrations during CoQ_1 arterial infusion in the presence of rotenone (Rot, 20 μM), for normoxic lungs (n = 5), hyper-85 lungs (n = 8). C: The relationship between the steady state rate of CoQ_1H_2 efflux and the infused CoQ_1 concentrations during CoQ_1 arterial infusion in the presence of dicumarol (Dic, 400 μM), for normoxic lungs (n = 4), hyper-85 lungs (n = 4). D: The relationship between the steady state rate of CoQ_1H_2 efflux and the infused CoQ_1 concentrations during CoQ_1 arterial infusion in the presence of dicumarol (Dic, 400 μM) and rotenone (Rot, 20 μM), for normoxic lungs (n = 4), hyper-85 lungs (n = 3). E: The relationship between the steady state rate CoQ_1H_2 efflux and the infused CoQ_1 concentrations during CoQ_1 arterial infusion in the presence of antimycin A (AA, 10 μM) , for normoxic lungs (n = 4), hyper-85 lungs (n = 3). F: The relationship between the steady state rate of CoQ_1 efflux and the infused CoQ_1H_2 concentrations during CoQ_1H_2 arterial infusion in the presence of dicumarol (Dic, 400 μM) and rotenone (Rot, 20 μM), for normoxic lungs (n = 6), hyper-85 lungs (n = 4). Values are mean ± SE. * Hyper-85 rates significantly different from the normoxic rates at the same infused CoQ_1 concentrations.

Treatment of lungs with AA is one approach to inhibit complex III mediated CoQ_1H_2 or DQH_2 oxidation. Another approach is to treat the lungs with the complex IV inhibitor KCN which reduces the respiratory chain and closes complex III for hydroquinone oxidation (Audi 2005, Audi 2008). Figure 4.8 shows that the efflux rate of DQH_2 was not different during DQ infusion in the presence of AA or KCN in normoxic lungs. For hyper-85 lungs, the efflux rate of DQH_2 during DQ infusion in the presence of KCN was slightly higher than that in the presence of AA at the highest infused concentration. However, for normoxic lungs, but not for hyper-85 lungs, the steady state CoQ_1H_2 efflux rates during CoQ_1 infusion in the presence of KCN were ~30% higher than that in the presence of AA (Figure 4.9). These results suggests that a different effect of KCN on CoQ_1 redox metabolism compared with AA in normoxic lungs.

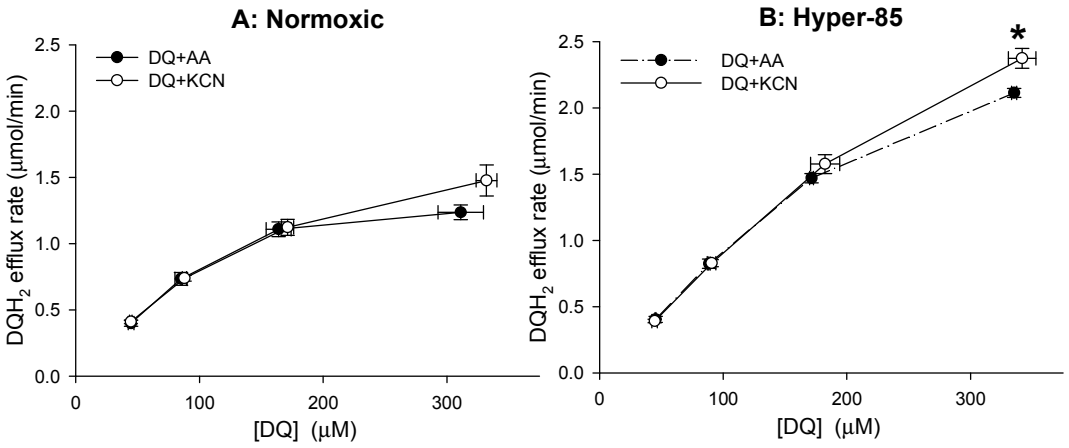

Figure 4.8 The relationship between the steady state rate of DQH_2 efflux and the infused DQ concentrations during DQ arterial infusion in the presence of AA (10 µM) or KCN (2 mM) A: normoxic lungs, antimycin A (n = 5), KCN (n = 5). B: hyper-85 lungs, AA (n = 5), KCN (n = 3). Values are mean ± SE. * rates in the presence of KCN significantly different from rates in the presence of antimycin A at the same infused DQ concentrations.

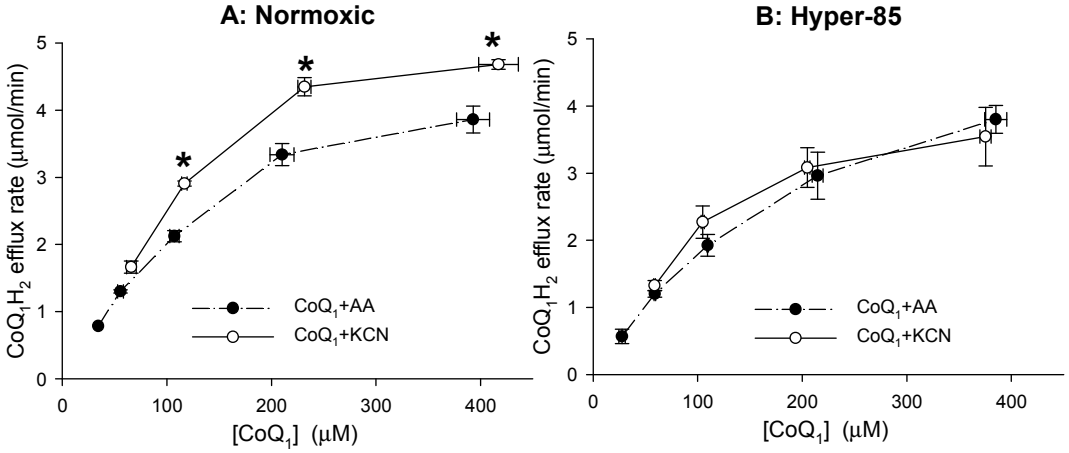

Figure 4.9 The relationship between the steady state rate of CoQ_1H_2 efflux and the infused CoQ_1 concentrations during CoQ_1 arterial infusion in the presence of AA (10 µM) or KCN (2 mM) A: normoxic lungs, AA (n = 4), KCN (n = 4). B: hyper-85 lungs, AA (n = 3), KCN (n = 4). Values are mean ± SE. * rates in the presence of KCN significantly different from rates in the presence of antimycin A at the same infused CoQ_1 concentrations.

4.3.4 Activities of NQO1, Complex I and Complex IV in Lung Homogenates

Rat exposure to 85% O_2 for 7 days increased total lung NQO1 activity by 72% (Table 4.2). This increase was eliminated when NQO1 activity was normalized to total lung protein which increased by 114% in hyper-85 lungs as compared to normoxic lungs.

	Homogenate NQO1 Activity (μmol/min/lung)	Homogenate NQO1 Activity (nmol/min/mg protein)
Normoxic	26.5 ± 1.7	670 ± 80
Hyper-85	45.6 ± 4.7*	538 ± 43

Table 4.2 Lung homogenate NQO1 activity Values are mean ± SE. n = 7 and 7 for normoxic and hyper-85 lungs, respectively. * Indicate value significantly different from the corresponding normoxic.

Table 4.3 shows that mitochondrial complex I activity per mg protein was ~50% lower in mitochondrial fractions derived from hyper-85 lungs than from normoxic lungs. On the other hand, complex IV activity per mg protein increased in hyper-85 lung homogenates by ~90% as compared to normoxic lungs (Table 4.3).

	Complex I activity (nmol/min/mg protein)	Complex IV activity (nmol/min/mg protein)
Normoxic	13.2 ± 2.3	232 ± 16
Hyper-85	6.8 ± 1.2*	439 ± 51 *

Table 4.3 Mitochondrial complexes I and IV activities. For complexes I and IV activities, n = 5 and 7 for normoxic and hyper-85 lungs, respectively. Values are mean ± SE. * Indicates value significantly different from the corresponding normoxic value.

4.3.5 Immunoblots of NQO1 in Lung Homogenate

Figure 4.10 shows examples of NQO1 immunoblots for normoxic and hyper-85 lung homogenates. Band intensities for hyper-85 lungs were on average ~ 3-fold that of normoxic lungs (Table 4.4).

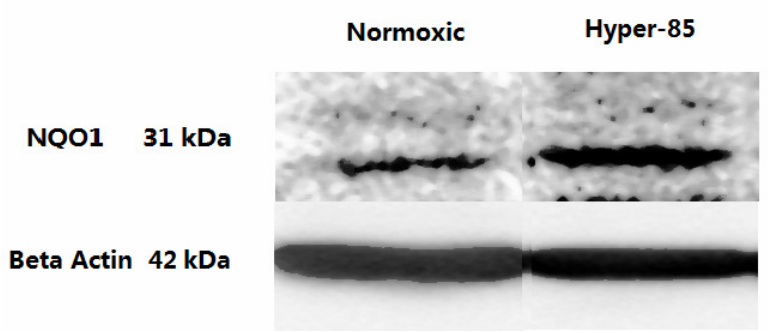

Figure 4.10 Western blots of NQO1. 1st column: normoxic rats, n=10; 2nd column: rats exposed to 85% O_2 for 7 days, n=12.

	Normoxic	Hyper-85
Band intensity	100	298±85 *

Table 4.4 NQO1 band intensities for normoxic and hyper-85 lungs. Values are mean ± SE. Normoxic lungs, n = 10; hyper-85 lungs, n = 12 respectively. * $P<0.05$. Note that for each run, the band intensity for normoxic lung was assigned an arbitrary value of 100.

4.4 Kinetic Analysis of Quinone and Hydroquinone Pulse Infusion Data

The data in Figures 4.4, 4.5, 4.6, 4.7 are the net results of multiple factors, for quantitative interpretation of these data, the whole lung kinetic model for the pulmonary disposition of quinones and hydroquinones described in chapter 3.3 was required.

The model consists of conducting arteries, veins and a capillary region that accounts for quinone (Q) and hydroquinone (QH_2) tissue and vascular interactions (Audi et al., 2005, 2008). The capillary region has a distribution of capillary transit times, $h_c(t)$ (Ramakrishna et al., 2010). For a single capillary element, the species balance equations descriptive of spatial and temporal variations in the concentrations of Q and QH_2 in the vascular volume (V_c) and tissue volume (V_e) are described in chapter 3.3.2. For the lung model, the effect of the distribution of capillary transit time ($h_c(t)$) on the plasma concentrations and the redox status of Q and QH_2 on passage through the pulmonary circulation was taken into consideration (Audi et al., 2003, 2008). To provide the whole lung output, the outputs for all transit times were summed, each weighted according to $h_c(t)$. Previously, Ramakrishna et al. determined $h_c(t)$ for normoxic rat lungs and hyper-85 lungs, and

demonstrated that rat exposure to 85% O_2 for 7 days decreased capillary mean transit time by 42% and increased the relative dispersion of $h_c(t)$ by 40% (Ramakrishna et al., 2010). These values were used in the kinetic analysis of the normoxic and hyper-85 quinone and hydroquinone pulse infusion data.

4.4.1. Kinetic Analysis of DQ/DQH$_2$ Data

For DQ/DQH_2, the relevant redox reactions are NQO1 mediated DQ reduction and complex III mediated DQH_2 oxidation. Thus, equations E3.1-E3.2 reduce to E4.3 - E4.4.

$$\frac{\partial \overline{Q}}{\partial t} + W\left(\frac{V_c}{V_c + V_{F1}}\right)\frac{\partial \overline{Q}}{\partial x} = \frac{1}{V_c + V_{F1}}\left(-\frac{V_{\max 1}\overline{Q}}{K_{m1a} + \overline{Q}} + \frac{V_{\max 2}\overline{QH_2}}{K_{m2a} + \overline{QH_2}}\right) \tag{E4.3}$$

$$\frac{\partial \overline{QH_2}}{\partial t} + W\left(\frac{V_c}{V_c + V_{F2}}\right)\frac{\partial \overline{QH_2}}{\partial x} = \frac{1}{V_c + V_{F2}}\left(\frac{V_{\max 1}\overline{Q}}{K_{m1a} + \overline{Q}} - \frac{V_{\max 2}\overline{QH_2}}{K_{m2a} + \overline{QH_2}}\right) \tag{E4.4}$$

In the absence of rotenone (complex I inhibitor), DQH_2 competes with endogenous CoQ_9H_2 for oxidation via complex III. The steady state DQ efflux rates during DQH_2 infusion in the presence of dicumarol alone appear to follow linear kinetics for the range of infused DQH_2 concentrations studied (Figure 4.5 A). Thus, in the absence of rotenone, V_{max2} and K_{m2a} in Equations (E4.3-E4.4) are substituted for with a tissue mediated DQH_2 oxidation rate k_{ox} (ml/min), resulting in the equations E4.5-E4.6.

$$\frac{\partial \overline{Q}}{\partial t} + W\left(\frac{V_c}{V_c + V_{F1}}\right)\frac{\partial \overline{Q}}{\partial x} = \frac{1}{V_c + V_{F1}}\left(-\frac{V_{\max 1}\overline{Q}}{K_{m1a} + \overline{Q}} + K_{ox}\overline{QH_2}\right) \tag{E4.5}$$

$$\frac{\partial \overline{QH_2}}{\partial t} + W\left(\frac{V_c}{V_c + V_{F2}}\right)\frac{\partial \overline{QH_2}}{\partial x} = \frac{1}{V_c + V_{F2}}\left(\frac{V_{\max 1}\overline{Q}}{K_{m1a} + \overline{Q}} - K_{ox}\overline{QH_2}\right) \tag{E4.6}$$

Since the venous effluent data are measured at the steady state, the steady-state forms of equations E4.3-E4.6 are shown below

$$WV_c \frac{\partial[\overline{DQ}]}{\partial x} = -\frac{V_{\max 1}[\overline{DQ}]}{K_{m1a} + [\overline{DQ}]} + \frac{V_{\max 2}[\overline{DQH_2}]}{K_{m2a} + [\overline{DQH_2}]} \quad \text{(E4.7)}$$

$$WV_c \frac{\partial[\overline{DQH_2}]}{\partial x} = \frac{V_{\max 1}[\overline{DQ}]}{K_{m1a} + [\overline{DQ}]} - \frac{V_{\max 2}[\overline{DQH_2}]}{K_{m2a} + [\overline{DQH_2}]} \quad \text{(E4.8)}$$

$$WV_c \frac{\partial[\overline{DQ}]}{\partial x} = -\frac{V_{\max 1}[\overline{DQ}]}{K_{m1a} + [\overline{DQ}]} + K_{ox}[\overline{DQH_2}] \quad \text{(E4.9)}$$

$$WV_c \frac{\partial[\overline{DQH_2}]}{\partial x} = \frac{V_{\max 1}[\overline{DQ}]}{K_{m1a} + [\overline{DQ}]} - K_{ox}[\overline{DQH_2}] \quad \text{(E4.10)}$$

For DQ or DQH_2 infusion, the unknown model parameters under steady-state conditions are V_{max1} (μmol/min) and V_{max2} (μmol/min), the respective maximum rates for DQ reduction via NQO1 and DQH_2 oxidation via complex III; K_{m1a} (μM) and K_{m2a} (μM), the apparent Michaelis-Menten constants for NQO1 mediated DQ reduction and complex III mediated DQH_2 oxidation, respectively; and k_{ox} (ml/min), the tissue mediated DQH_2 oxidation rate on passage through the pulmonary circulation in the absence of rotenone.

The values of these parameters for normoxic and hyperoxic lungs were estimated using the following approach. First, the values of V_{max1} and K_{m1a}, parameters descriptive of NQO1-mediated DQ reduction, were determined. This was done by fitting the steady-state solution of the lung model to the steady state rates of DQH_2 efflux during DQ infusion in the presence of antimycin A (Figure 4.5), which corresponded to setting V_{max2} to zero in Equations E4.3-E4.4. The estimated values of these model parameters are given in Table 4.5. Rat exposure to 85% O_2 for 7 days increased V_{max1} by ~200%. The estimated value of K_{m1a} was 1 μM, which was the lower bound setting for this parameter in the least squares fitting procedure (see Figure 4.5 for model fit).

	V_{max1} (μmol/min)	V_{max1} (μmol/min/g dry wt)	K_{m1a} (μM)
Normoxic	1.38± 0.07	6.4 ± 0.3	1.0
Hyper-85	4.11 ± 0.39 *	10.8 ± 0.7 *	1.0

Table 4.5 Values of model parameters descriptive of NQO1-mediated DQ reduction in normoxic and hyper-85 lungs estimated from the steady-state DQH_2 efflux rates during DQ infusion in the presence of AA. Values are mean ± SE. n = 5 for both groups. V_{max1} is the maximum DQ reduction rate; K_{m1a} is the apparent Michaelis-Menten constant. * Significantly different from normoxic.

For a given lung, the parameters descriptive of complex III-mediated DQH_2 oxidation (V_{max2} and K_{m2a}) were estimated by fitting the steady state solution of the organ model to the steady state rates of DQ efflux during DQH_2 infusion in the presence of dicumarol and rotenone, with V_{max1} was set to zero in Equations (E4.3-E4.4) to account for the presence of dicumarol. The results in Table 4.6 show that rat exposure to 85% O_2 increased V_{max2} by ~180%, with no significant effect on $K_{m2a.}$

	V_{max2} (μmol/min)	V_{max2} (μmol/min/g dry wt)	K_{m2a} (μM)
Normoxic	1.67 ± 0.10	8.7 ± 0.7	42 ± 2
Hyper-85	4.65 ± 0.36*	13.6 ± 1.8*	36 ± 11

Table 4.6 Values of model parameters descriptive of complex III mediated DQH_2 oxidation in normoxic and hyper-85 lungs estimated from the steady-state DQ efflux rates during DQH_2 infusion in the presence of dicumarol plus rotenone. Values are mean ± SE. n = 4 for both groups. V_{max2} is the maximum DQH_2 oxidation rate; K_{m2a} is the apparent Michaelis-Menten constant. * Significantly different from normoxic values.

The value of K_{ox} was estimated by fitting the solution of the steady state organ model, with V_{max1} set to zero in Equations (E4.5-E4.6), to the steady state rates of DQ efflux during DQH_2 infusion in the presence of dicumarol (Figure 4.6 A). Table 4.6 shows that rat exposure to 85% O_2 for 7 days increased the estimated value of K_{ox} by ~140% as compared to normoxic lungs.

	K_{ox} (ml/min)	K_{ox} (ml/min/g dry wt)
Normoxic	6.38 ± 0.60	27.6 ± 2.9
Hyper-85	15.2 ± 1.58*	35.0 ± 8.4

Table 4.7 Value of model parameter descriptive of the DQH_2 oxidation capacity in normoxic and hyper-85 lungs estimated from the steady-state DQ efflux rates during DQH_2 infusion in the presence of dicumarol. Values are mean ± SE. n = 6 for both groups. K_{ox} is total rate of DQH_2 oxidation on passage through the pulmonary circulation. * Significantly different from normoxic values.

A second estimate of the values of V_{max1} and K_{m1a} for normoxic and hyper-85 lungs was obtained by fitting the steady state lung model solution to the steady state rates of DOH_2 efflux during DQ infusion in the absence of inhibitors (Figure 4.4 A), with K_{ox} in Equations (E4.5-E4.6) set to the mean values in Table 4.7. The estimated values of V_{max1} for hyper-85 lungs were ~140% higher than that estimated for normoxic lungs (Table 4.8).

	V_{max1} (μmol/min)	V_{max1} (μmol/min/g dry wt)	K_{m1a} (μM)
Normoxic	1.46 ± 0.10	7.2 ± 0.8	4.4 ± 1.4
Hyper-85	3.52 ± 0.12*	10.1 ± 0.6*	6.4 ± 1.6

Table 4.8 Values of model parameters descriptive of NQO1-mediated DQ reduction in normoxic and hyper-85 lungs estimated from the steady-state DQH_2 efflux rates during DQ infusion. Values are mean ± SE. n = 6 for both groups, respectively. K_{m1a} is Michaelis-Menten constant of DQ reduction via NQO1. * Significantly different from normoxic values.

For normoxic and hyper-85 lungs, the values of V_{max1} in Table 4.8 vs. Table 4.5, i.e. estimated from the steady state rates of DQH_2 efflux during DQ infusion in the absence or presence of AA, respectively, were not significantly different. This is consistent with the dominant inhibition effect of AA being on complex III- mediated DQH_2 oxidation.

4.4.2. Kinetic Analysis of CoQ_1/CoQ_1H_2 Data

All the redox processes in Figure 3.4 contribute to the pulmonary disposition of CoQ_1 and

CoQ_1H_2 (Audi et al., 2008). Thus for CoQ_1 and CoQ_1H_2 pulse infusion data, the governing differential equations are E3.1-E3.2. The steady state forms of these equations are equations E4.11-4.12.

$$WV_c \frac{\partial[\overline{Q}]}{\partial x} = -\frac{V_{\max 1}[\overline{Q}]}{K_{m1a}+[\overline{Q}]} - \frac{V_{\max 3}[\overline{Q}]}{K_{m3a}+[\overline{Q}]} - \frac{V_{\max 4}[\overline{Q}]}{K_{m4a}+[\overline{Q}]} + \frac{V_{\max 2}[\overline{QH_2}]}{K_{m2a}+[\overline{QH_2}]} \quad \text{(E4.11)}$$

$$WV_c \frac{\partial[\overline{QH_2}]}{\partial x} = \frac{V_{\max 1}[\overline{Q}]}{K_{m1a}+[\overline{Q}]} + \frac{V_{\max 3}[\overline{Q}]}{K_{m3a}+[\overline{Q}]} + \frac{V_{\max 4}[\overline{Q}]}{K_{m4a}+[\overline{Q}]} - \frac{V_{\max 2}[\overline{QH_2}]}{K_{m2a}+[\overline{QH_2}]} \quad \text{(E4.12)}$$

where Q and QH_2 stand for CoQ_1 and CoQ_1H_2 respectively.

For CoQ_1 or CoQ_1H_2 infusion, the unknown model parameters under steady-state conditions are V_{max1} (μmol/min), V_{max2} (μmol/min), V_{max3} (μmol/min) and V_{max4} (μmol/min), the respective maximum rates for CoQ_1 reduction via NQO1, CoQ_1H_2 oxidation via complex III, CoQ_1 reduction via complex I and CoQ_1 reduction via other reductase(s) respectively; K_{m1a} (μM), K_{m2a}(μM), K_{m3a} (uM) and K_{m4a} (uM), the apparent Michaelis-Menten constants for NQO1 mediated CoQ_1 reduction, complex III mediated CoQ_1H_2 oxidation, complex I mediated CoQ_1 reduction and other reductase(s) mediated CoQ_1 reduction, respectively.

The values of these parameters were estimated by simultaneously fitting the steady-state solutions of the lung model equations to the mean values of the normoxic and hyper-85 data in Figures 4.7 A, B, C, E and F. For this fitting procedure, the Michaelis-Menten constants (intensive parameters) for the various redox enzymes were assumed to be the same for normoxic and hyper-85 lungs. On the other hand, the V_{max} values (extensive parameters) for the various redox enzymes were allowed to be different for normoxic and hyper-85 lungs. Thus, for the above fitting procedure, the number of model parameters was 12. The effect of an inhibitor was simulated by the setting the value(s) of V_{max} of the inhibitor's targeted redox enzyme to zero. Thus, in the

presence of rotenone, dicumarol, or antimycin A, V_{max3}, $V_{max1,}$ or V_{max2} was set to zero, respectively. The estimated values of the parameters for normoxic and hyper-85 lungs along with 95% confidence intervals are given in Table 4.9. A modified one-sided t-test (chapter 3.3.3) was used to determine whether the estimated V_{max} values for normoxic and hyper-85 lungs were different. The results revealed that hyper-85 lungs increased the capacity of NQO1 mediated CoQ_1 reduction by 250%, increased the capacity of complex III mediated CoQ_1H_2 oxidation by 25%, and decreased the capacity of complex I mediated CoQ_1 reduction by 35%.

The confidence intervals for the Michaelis-Menten constants for CoQ_1/CoQ_1H_2 redox processes are relatively large (as compared to the estimated parameter values). One possible reason is that the actual values of these parameters are low relative to the range of CoQ_1 concentrations achieved in this study.

To evaluate the model, the estimated values of model parameters for normoxic and hyper-85 lungs (Table 4.9) were used to predict the steady-state efflux rates of CoQ_1H_2 during CoQ_1 infusion in the presence of dicumarol and rotenone which were not used for the estimation of the model parameters. Figure 4.7 D showed that the model was able to predict these data reasonably well.

Targets	Vmax (μmol/min)		Km (μM)
	Normoxic	*Hyper-85*	
NQO1	0.50±0.37	1.76±0.56*	30.8 ± 42.3
Complex III	4.09±0.49	5.07±0.60*	31.3 ± 7.2
Complex I	2.73±0.59	1.88±0.54*	49.6 ± 33.5
Other Reductase (s)	1.37±0.61	1.13±0.63	13.7 ± 19.2

Table 4.9 Value of model parameters in normoxic and hyper-85 lungs estimated from CoQ_1/ CoQ_1H_2 infusions. Values are mean ± 95% CI. * Significantly different from normoxic.

To account for the increase in lung dry weight of hyper-85 lungs as compared to normoxic lungs, the estimated values of V_{max}(s) in Table 4.9 were normalized to lung dry weight. This normalization assumes that all lung cells are accessible to CoQ_1 and CoQ_1H_2 on passage through the pulmonary circulation (Audi et al., 2008). The normalized values are given in Table 4.10. The normalized values of V_{max1} (NQO1) for hyper-85 lungs are ~100% higher than for normoxic lungs. The normalized values of V_{max3} (complex I) for hyper-85 lungs are now ~59% lower than that for normoxic lungs. These results suggest that, even if taking the increase in the number of lung tissue cells into consideration, the increase in NQO1 activity and the decrease in complex I activity are still significant. For complex III, the normalized values of V_{max2} (complex III) for hyper-85 lungs are now ~26% lower than that for normoxic lungs. Compared with the ~25% increase in the overall lung V_{max2} for hyper-85 lungs, this significant decrease might suggest a more complex change in complex III in hyper-85 lungs compared with complex I and NQO1. For other reductase(s), there are no significant differences between the values for normoxic and hyper-85 lungs either in overall V_{max4} or V_{max4} per gram dry lung. This suggests that either other reductase(s) in hyper-85 lungs did not change or the contribution of other reductase(s) on Q-QH_2 metabolism was minor.

Targets	V_{max} (μmol/min/g)	
	Normoxic	*Hyper-85*
NQO1	2.27±1.68	4.77±1.51*
Complex III	18.6±2.23	13.7±1.63*
Complex I	12.4±2.68	5.08±1.46*
Other Reductase (s)	6.25±2.77	3.05±1.71

Table 4.10 Values of normalized maximum reaction rates in normoxic and hyper-85 lungs estimated from CoQ_1/ CoQ_1H_2 infusions. Values are mean ± 95% CI. *: Significantly different from normoxic.

4.5 Discussion and Conclusions

Rat exposure to 85% O_2 for 7 days had a differential effect on the redox metabolism of DQ and CoQ_1, with the lung DQ reduction capacity increasing by 37% and the lung CoQ_1 reduction capacity decreasing by 25%. Inhibitor studies and kinetic analysis revealed that the increase in DQ reduction capacity in hyper-85 lungs could be accounted for by a 140% increase in the maximum rate of NQO1 mediated DQ reduction (V_{max1}) and a 180% increase in maximum rate of complex III mediated DQH_2 oxidation (V_{max2}). The decrease in CoQ_1 reduction capacity in hyper-85 lungs could be accounted for by a 250% increase in the maximum rate of NQO1 mediated CoQ_1 reduction (V_{max1}), a 25% increase in maximum rate of complex III mediated CoQ_1H_2 oxidation (V_{max2}) and a 35% decrease in maximum rate of complex I mediated CoQ_1 reduction (V_{max3}). These results suggest a hyperoxia-induced increase in the activities of NQO1 and complex III, and a decrease in the activity of complex I in isolated perfused lungs.

The effect of hyperoxic exposure on NQO1

Rat exposure to 85% O_2 for 7 days increased the lung NQO1 activity as measured by the increase in the capacity (V_{max1}) of NQO1 mediated DQ reduction (~140%) or CoQ_1 reduction (~250%). Since the lung dry weight increased ~68% in rats exposed to 85% O_2 for 7 day as compared to normoxic lungs, presumably due to an increase in the number of interstitial cells, this brought into question whether the increase in NQO1 activity was simply the result of the increase in the number of lung tissue cells. Table 4.11 shows that the increase in lung dry weight is not sufficient to account for the increase in lung NQO1 activity. Both DQ and CoQ_1 data suggest an increase in NQO1 activity per gram of dry lung, by ~40% and ~110% respectively.

Western blots indicated that The expression of NQO1 in per mg lung protein of hyper-85

lungs is ~298% of that of normoxic lungs. Taking the amount of lung protein into consideration, the amount of NQO1 expression in hyper-85 lungs is about 5-fold of normoxic lungs. The increase in NQO1 expression in hyper-85 lungs might explain the increase in NQO1-mediated quinone reduction.

Although the activity of NQO1 in lung tissue homogenate increased by ~70% in hyper-85 lungs as compared to normoxic lungs, this increase disappeared when the activity was expressed by per mg of lung protein (Table 4.11). One possible reason may be that other dicumarol-inhibitable reductase(s) besides NQO1 contribute to the reduction of DCPIP which is used as the probe of NQO1 activity in tissue assay. This could be evaluated by using a different NQO1 inhibitor, such as 5-methoxy-1,2-dimethyl-3-[(4-nitrophenoxy)methyl]indol-4,7-dione (ES936), which inhibits NQO1 by an alternative mechanism (Bongard et al., 2009).

Both DQ and CoQ_1 are substrates for NQO1. Hence, a hyperoxia-induced change in lung NQO1 activity would be expected to have a proportionate change in the model parameter (V_{max1}) descriptive of the capacity of NQO1 mediated DQ and CoQ_1 reduction. Both DQ and CoQ_1 pulse infusion data suggest a hyperoxia-induced increase in lung NQO1 activity per gram of dry lung weight as compared to normoxic lungs, but DQ suggests a smaller increase (~40%) than CoQ_1 (~110%). This difference could be due to the effect of dicumarol on reductase(s) other than NQO1 (e.g. complex I) for which CoQ_1 is also a substrate (Audi et al., 2008).

NQO1	Normoxic	Hyper-85
V_{max1} (μmol/min) from DQ data [#]	1.38± 0.07	4.11 ± 0.39[*]
V_{max1} (μmol/min/ g dry weight) from DQ data [#]	6.4 ± 0.3	10.8 ± 0.7[*]
V_{max1} (μmol/min) from CoQ_1 data [#]	0.50±0.37	1.76±0.56*
V_{max1} (μmol/min/ g dry weight) from CoQ_1 data [#]	2.27±1.01	4.77±1.51*

Activity in lung homogenate (μmol/min/lung) &	26.5 ± 1.67	45.6 ± 4.74*
Activity in lung homogenate (nmol/min/mg protein) &	670 ± 80	538 ± 43
NQO1 protein expression (%) &	100	298±85*

Table 4. 11 Values of NQO1 activity estimated by different methods. #: Values are mean ± 95% CI. &: values are mean± SE. *: P<0.05. Significantly different from normoxic.

The effect of hyperoxic exposure on Complex I

The results of the CoQ_1 pulse infusion data suggest that rat exposure to 85% O_2 for 7 days decreased the activity of complex I (V_{max3}) by ~35%. This decrease is even larger (~60%) when V_{max3} is normalized to lung dry weight (Table 4.12). This result is consistent with the ~50% decrease in complex I activity (per mg protein) in lung homogenate (Table 4.12). Thus the ~50% depression in complex I activity measured by Audi et al. in lungs of rats exposed to 85% O_2 for 48 hours is maintained after 7-day exposure to 85% O_2. This suggests that the hyperoxia-induced depression in complex I activity may be an early manifestation of an adaptive response to the hyperoxic environment.

Previous studies have suggested that hyperoxia-induced decrease in complex I activity could be due to the fact that 7 out of the 45 complex I subunits are encoded by mitochondrial DNA (mDNA), which is known to be highly sensitive to ROS (Chicco & Sparagna, 2007). The decrease in complex I activity could also be through the oxidation of cardiolipin, which is important for the electron transport function of complex I.

Ratner et al. (Ratner, Starkov & Matsiukevich, 2009) demonstrated that exposure of neonatal mice to hyperoxia (75% O_2) for 72 hours decreased complex I activity by ~70%. This decrease compromises mitochondrial oxidative phosphorylation, contributes to an alveolar development arrest, and also contributes to the development of bronchopulmonary dysplasia (Ratner et al., 2009). The importance of the depression in complex I activity to O_2 toxicity was

demonstrated by treating mice with a complex I inhibitor, which resulted in an alveolar development arrest under normoxic conditions. Based on these results, Ratner et al. (2009) concluded that hyperoxia-induced decrease in complex I activity might play a key role in lung O_2 toxicity. Additional studies would be needed to evaluate the effect of this decrease in complex I activity on mitochondrial bioenergetics.

Complex I	Normoxic	Hyper-85
V_{max3} (mol/min) from CoQ_1 data #	2.73±0.59	1.88±0.54*
V_{max3} (mol/min/g dry weight) from CoQ_1 data #	12.4±1.60	5.08±1.46 *
Activity in lung homogenate (nmol/min/mg protein)&	13.2 ± 2.31	6.78 ± 1.24*

Table 4. 12 Values of complex I activity estimated by different methods. #: Values are mean ± 95% CI. &: values are mean± SE. *: P<0.05. Significantly different from normoxic.

Effect on complex III

Although rat exposure to 85% O_2 for 7 days increased the lung capacity (V_{max2}) of complex III mediated DQH_2 and CoQ_1H_2 oxidation as compared to normoxic lungs, the increase was much larger for DQH_2 (~180%) than for CoQ_1H_2 (~25%). Furthermore, the increase in V_{max2} for CoQ_1H_2 dissipated when V_{max2} was normalized to lung dry weight (Table 4.13). It is not clear what could account for this difference since both DQH_2 and CoQ_1H_2 are substrates for complex III and hence a change in complex III activity would be expected to have a proportionate change in the capacity of complex III to oxidize DQH_2 or CoQ_1H_2 on passage through the pulmonary circulation. One possible reason could be the competition between endogenous CoQ_9H_2 and CoQ_1H_2 or DQH_2 for oxidation via complex III. The advantage of DQH_2 in the competition with CoQ_9H_2 for the oxidation at complex III is that the reduction of DQ is independent of complex I, which makes the competition between DQH_2 and CoQ_9H_2 not as complex as the competition

between CoQ_1H_2 and CoQ_9H_2. The decrease in complex I activity reduces the competition from CoQ_9H_2 and hence increases the oxidation of DQH_2 via complex III. Since the formation of CoQ_1H_2 is dependent on complex I, then for CoQ_1H_2, the competition from CoQ_9H_2 changes less.

Complex III	Normoxic	Hyper-85
V_{max2} (μmol/min) from DQ data	1.67 ± 0.10	4.65 ± 0.36*
V_{max2} (μmol/min/ g dry weight) from DQ data	8.7 ± 0.7	13.6 ± 1.8*
V_{max2} (μmol/min) from CoQ_1 data	4.09±0.49	5.07±0.60*
V_{max2} (μmol/min/ g dry weight) from CoQ_1 data	18.6±1.32	13.7±1.63

Table 4. 13 Values of complex III activity estimated by different methods. Values are mean ± 95% CI.

In addition to its effects on lung activities of NQO1 and complex I and III, rat exposure to 85% O_2 for 7 days increased the activity of complex IV in lung tissue homogenates by ~90% compared to normoxic lung homogenates. Previous studies indicated that the electron transport chain complexes I and III have a tight relationship and act as a supercomplex (Genova, Bianchi & Lenaz, 2005). In addition, part of complex IV is bound to and functionally associated with complex III (van Raam et al., 2008). Thus, complexes I, III and IV might consistitute a mitochondrial supercomplex (van Raam et al., 2008). In the present study, mitochondrial electron transport chain complexes are differentially altered by rat exposure to 85% O_2 for 7 days, with the increases in the activities of complexes III and IV and the decrease in the activity of complex I. Regarding the specific relationship between mitochondrial electron transport chain components (Genova et al. 2005; Van Raam et al., 2008), the above results raise the following questions. Do these hyperoxia-induced changes in the activities of complexes I, III and IV occur simultaneously or sequentially? Do these changes occur independently or dependently? Are these changes toxic or

protective? Addressing these questions would further understanding of how the mitochondrial electron transport chain adjusts the activities of its complexes and hence its overall function in response to an oxidative stress stimulus such as hyperoxia.

Previous studies have suggested that the hyperoxia-induced increase in ROS formation plays a key role in lung O_2 toxicity. Thus, at least two potential strategies that lung cells might follow to counter this increase, either improving defenses against the increased ROS generation or improving metabolic mechansims that might suppress ROS generation in the first place (Campian et al., 2004). Of these two possibilities, preemptive suppression of ROS production would be the most effective and economical solution (Campian et al., 2004). This study indicated that rats exposed to 85% O_2 for 7 days not only increased the activities of antioxidant enzymes such as NQO1 but also changed the activities of mitochondrial ROS sources such as mitochondrial complexes I and III. Since the intracellular production of ROS by mitochondria under hyperoxia might be the most important mechanism of hyperoxic damage, manipulation of ROS generation from mitochondria could be an efficient way to counter hyperoxia-induced lung injury. The decrease in complex I activity could be a means of decreasing the production of electron-rich intermediates such as ubisemiquinone. The increases in the activities ofcomplex III and complex IV could be a means of enhancing the capacity to utilize electron-rich intermediates and hence decreasing ROS production at complex III. Future studies are needed to evaluate the effect of this increase in complexes III and IV on mitochondrial ROS production.

Lungs treatment with AA (an inhibitor of complex III) or KCN (an inhibitor of complex IV) would be expected to inhibit complex III-mediated hydroquinol oxidation completely (Seddon & Mcvitte, 1974, Lenaz 2001). Thus, one would expect no difference in the steady-state rates of

hydroquinol (DQH_2 or CoQ_1H_2) efflux during quinone (DQ or CoQ_1) infusion from lungs treated with either AA or KCN. The results show that for normoxic and hyperoxic lungs, the efflux rates of DQH_2 during DQ infusion in the presence of AA or KCN were virtually the same expect for a small but significant difference at the highest DQ infused concentration in hyper-85 lungs (Figure 4.8). The efflux rate of CoQ_1H_2 during CoQ_1 infusion in the presence of AA or KCN was also not different in hyper-85 lungs. However, for normoxic lungs, the efflux rates of CoQ_1H_2 during CoQ_1 infusion in the presence of KCN were ~30% higher than in the presence of AA (Figure 4.9). One possible reason for this difference is that KC, but not AA (Dickman & Mandel, 1990), can stimulate glycolysis (Belinsky, Kauffman & Thurman, 1989) and hence increase pyruvate availability, which in turn increases NADH supply for complex I and finally increases the rate of complex I mediated CoQ_1 reduction. The effect of such an increase in NADH availability may not be as important for complex I mediated CoQ_1 reduction in hyper-85 lungs as in normoxic lungs due to the ~50% depression in complex I activity in hyper-85 lungs. This explanation would also be consistent with the lack of difference in DQH_2 efflux during DQ infusion in the presence of AA or KCN because DQ is not a substrate for complex I which requires NADH. One possible reason for the differential effects of KCN and AA on glycolysis could be the fact that KCN but not AA is known to inhibit GSH peroxidase (Kraus & Ganther, 1980). The inhibition of GSH peroxidase would divert glucose-6-phosphate from the pentose phosphate pathway to glycolysis. Additionally, it is known that AA does not completely inhibit the electron flow from ubiquinone to cytochrome c (Lenaz 2001) and hence has a relatively weak inhibition effect on ATP production compared to KCN. Both factors suggest that KCN could stimulate more glycolysis rather than AA.

In summary, rat exposure to 85% O_2 for 7 days decreased lung complex I activity by ~50%, increased lung complex III activity by ~25%, and increased lung NQO1 activity by ~40% and ~110% for DQ and CoQ_1 respectively. The depression in lung complex I activity following rat exposure to 85% O_2 for 48 hours is maintained in rats exposed to 85% O_2 for 7 days which have developed a tolerance to 100% O_2. This suggests that the decrease in lung complex I activity might be an early manifestation of an adaptive response to hyperoxic exposure, though the decrease in lung complex I activity alone was not sufficient to induce rat tolerance to 100% O_2 in rats exposed to 85% O_2 for 48 hours. The increase in lung NQO1 activity measured after exposure to 85% O_2 for 21 days is detectable in rats exposed to 85% O_2 for 7 days. Thus, we suspect that the increase in lung NQO1 activity might be a secondary anti-oxidant response under hyperoxic exposure.

CHAPTER 5. LUNG MITOCHONDRIAL COMPLEX I ACTIVITY AND H_2O_2 RELEASE DURING THE INITIATION PHASE OF O_2 TOXICITY

5.1 Introduction

Previously, Audi et al. demonstrated that rat exposure to 85% O_2 for 48 hours decreased the overall capacity of the lung to reduce CoQ_1 to CoQ_1H_2, predominately due to a 50% depression in the capacity of complex I-mediated CoQ_1 reduction, but with no effect on the capacity of NQO1-mediated CoQ_1 reduction and the capacity of complex III-mediated CoQ_1H_2 oxidation, or lung capillary perfusion kinematics (Audi et al., 2008). The results presented in chapter 4 of this dissertation demonstrated that this decrease persists after 7 days of rats exposed to 85% O_2, which is long enough for rats to develop a tolerance of 100% O_2. Ratner et al. (2009) suggested that the depression in complex I activity is an important aspect of the initiation phase of O_2 toxicity due to its effect on cellular ATP production via oxidative phosphorylation. These results raised the following questions. How early following rat exposure to 85% O_2 does complex I activity decrease? What is the effect of this decrease in complex I activity on lung ROS production? The work described in this chapter attempts to address these questions.

To address the first question, the effects of rat exposure to 85% O_2 for 12 or 24 hours on complex I activity in lung homogenate and on complex I mediated CoQ_1 reduction on passage through the pulmonary circulation of isolated perfused lungs were evaluated. Audi et al. demonstrated that rat exposure to 85% O_2 for 48 hours had no effect on NQO1 mediated CoQ_1 reduction, complex III mediated CoQ_1H_2 oxidation or lung perfusion kinematics (Audi et al., 2008). Thus any change in CoQ_1 reduction in lungs of rats exposed to 85% O_2 for 12 hours or 24 hours was attributed to a change in complex I mediated CoQ_1 reduction and hence in complex I

activity in the intact lung.

To address the second question, a spectrophotometric method for measuring the rate of H_2O_2 release from isolated perfused rat lung using Amplex Red (AR) was developed. The general approach of the developed assay involves the recirculation of perfusate containing AR and HRP through the pulmonary circulation and the measurement of resorufin concentration in reservoir samples collected periodically during a 30-min recirculation period.

5.2 Materials and Methods

Coenzyme Q_1 (CoQ_1) was purchased from Sigma Chemical Company (St. Louis, MO). Bovine serum albumin (Standard Powder, BSA) was purchased from Serologicals Corp. (Gaithersburg, MD). Reduced CoQ_1 (CoQ_1H_2) was prepared by reduction of CoQ_1 with potassium borohydride (KBH_4) as previously described (Cadenas, Boveris & Ragan, 1977). Amplex Red (AR), horseradish peroxidase (HRP) and other reagent grade chemicals were purchased from Sigma Chemical Company.

5.2.1 Hyperoxic Exposure

Rats were exposed to 85% O_2 for 12 hours, 24 hours or 48 hours as described in chapter 4.2.1.

5.2.2 Lung Preparation

The isolated perfused rat lung preparation and the ventilation-perfusion system are described in chapter 4.2.2.

5.2.3 Lung Infusion Protocols

CoQ_1 Pulse Infusion

To determine the rate of CoQ_1 reduction on passage through the pulmonary circulation, two 45-second long sequential arterial pulse infusions at CoQ_1 concentrations of 50 and 200 μM were carried out with a perfusate flow rate of 30 ml/min. For each pulse infusion, a venous effluent sample (1 ml) was collected between 43 and 45 seconds after the initiation of the pulse infusion. Between pulse infusions, the lung was perfused with 30 ml of fresh perfusate to wash the lung and perfusion system of any remaining probes of CoQ_1 and/or CoQ_1H_2.

Perfused Capillary Surface Area

The perfused capillary surface area was determined using the ACE substrate FAPGG as described in chapter 4.2.5.

5.2.4 Characterization of AR-H_2O_2 Assay and Determination of Optimal Perfusion Conditions

To make sure that H_2O_2 or HRP does not interfere with the absorbance spectrum of resorufin, the spectra of AR, resorufin, H_2O_2, and HRP were determined in HBSS containing 10 mM HEPES. Figure 5.1 shows the absorbance spectra for amplex red (AR), resorufin, horseradish peroxidase (HRP) and H_2O_2. As expected, the absorbance peak of resorufin is at 571 nm. The absorbances of AR, HRP and H_2O_2 at 571 nm are close to zero and hence do not interfere with the resorufin absorbance.

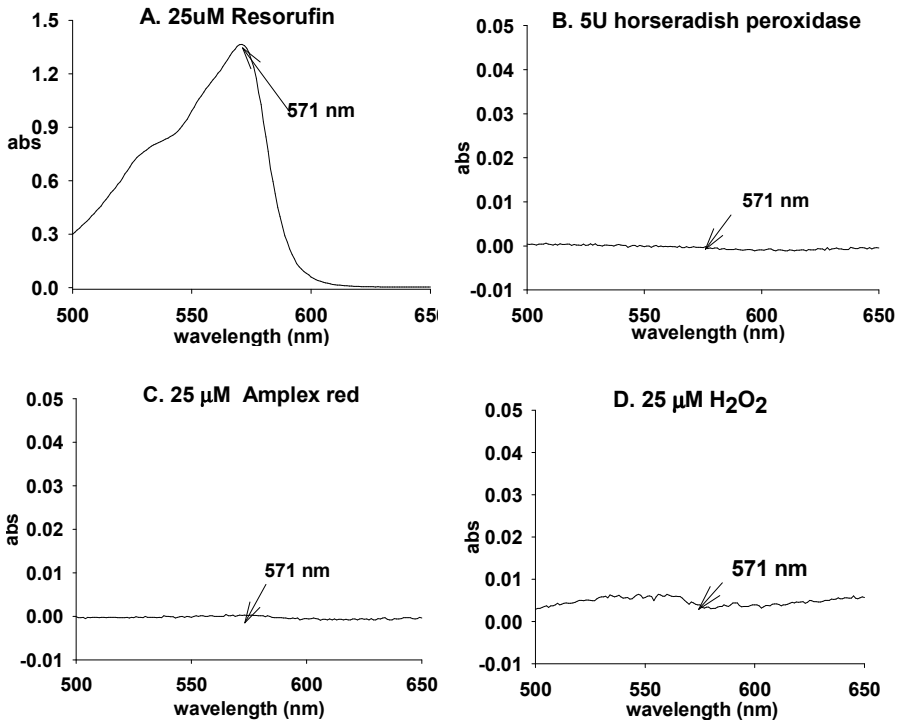

Figure 5.1 Spectra of resorufin, horseradish peroxidase, amplex red and H_2O_2 A: spectrum of resorufin. B: spectrum of horseradish peroxidase. C: spectrum of amplex red D: spectrum of H_2O_2

To check the extinction coefficient of resorufin and the linearity of AR-H_2O_2 reaction, a standard curve that represents the relationship between H_2O_2 concentration and the resulting resorufin absorbance was obtained. 1, 5, 10 or 25 nmol H_2O_2 was added into 1 ml HBSS-HEPES containing 25 nmol AR and 5U HRP, and the resulting absorbance at 571 nm was measured. The extinction coefficient was then estimated using a linear regression. To select a proper perfusate for the lung experiments, AR-H_2O_2 standard curves were obtained using the above approach in HBSS-HEPES, KRB containing 5% (mass/vol) dextran (~66 kDa) or 5% (mass/vol) BSA, the linear range and the extinction coefficient were then determined as above.

Figure 5.2 A and B are typical standard curves which show a linear relationship between the absorbance of formed resorufin at 571 nm and H_2O_2 concentration in the range 0.5-25 μM. The resulting extinction coefficient was 0.054 μM^{-1} cm^{-1} in HBSS-HEPES (Figure 5.2 A) which is consistent with previous report (Haughland, 2002), and 0.044 μM^{-1} cm^{-1} in KRB-Dex (Figure 5.2

B). In both HBSS-HEPES and KRB-Dex, the absorbance at 571 nm increased linearly with the increase in the concentration of H_2O_2. But much less absorbance at 571 nm was detected using KRB containing 5% BSA (Figure 5.2 C). This suggests that BSA itself may have H_2O_2-scanvenging property and hence interferes with the AR-H_2O_2 assay. Therefore, for lung experiments, KRB-Dex was selected as the perfusate for AR-H_2O_2 assay.

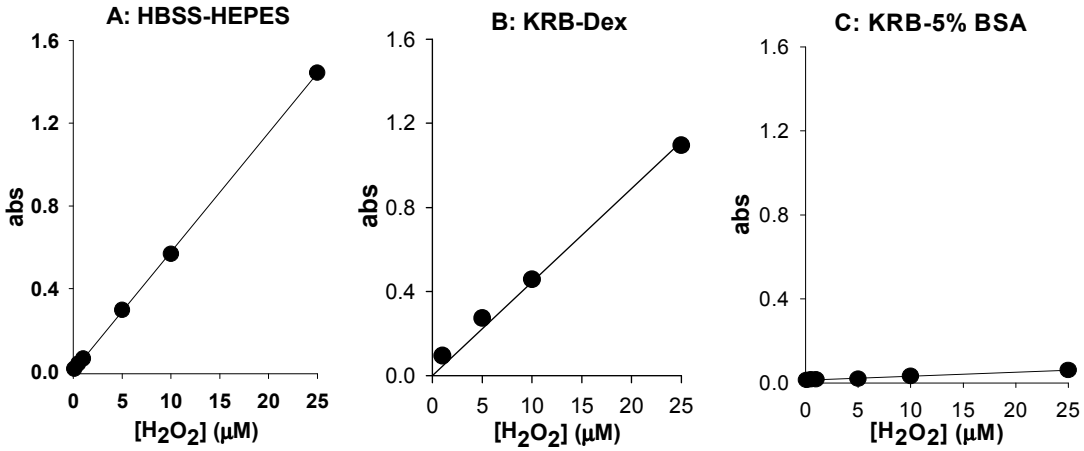

Figure 5.2 The relationship between absorbance and concentrations of H_2O_2 in different buffers. H_2O_2 was added into the cuvette with buffer containing 50 μM AR and 5U HRP. The concentration of H_2O_2 was 1 μM, 5 μM, 10 μM, 25 μM respectively. The absorbance was measured at 571 nm. A: HBSS-HEPES buffer B. KRB buffer containing 5% Dextran C: KRB buffer containing 5% BSA.

To evaluate the utility of this AR-H_2O_2 assay for determining the rate of H_2O_2 release, glucose-glucose oxidase reaction was used to produce H_2O_2 in cell-free KRB (KRB-GO) which contained 5.5 mM glucose, 0.02 U glucose oxidase, 50 μM AR, 5U HRP and 5% dextran. The resulting absorbance was measured every 20 seconds for 10 min. The rate of H_2O_2 production was estimated using linear regression based on an appropriate standard curve. Figure 5.3 A shows the time-dependent increase in the absorbance at 571 nm in cell-free KRB-GO perfusate. The estimated rate of H_2O_2 production from this glucose-glucose oxidase H_2O_2 system using AR-H_2O_2 assay was around ~2 nmol/min for 1 ml solution (2 μM/min).

To determine the sensitivity of the AR-H_2O_2 assay to metabolic inhibitors of known ROS

sources, the rate of H_2O_2 production by the glucose-glucose oxidase system was estimated in the absence and presence of 20 μM rotenone (complex I inhibitor), 10 μM antimycin A (complex III inhibitor), 1 mM apocynin (NADPH oxidase inhibitor) or 6 mM DEM (glutathione scavenger). The absorbance of a semimicro fluorescent cuvette containing KRB-GO buffer with or without an inhibitor was measured every 20 seconds in a 10-min period.

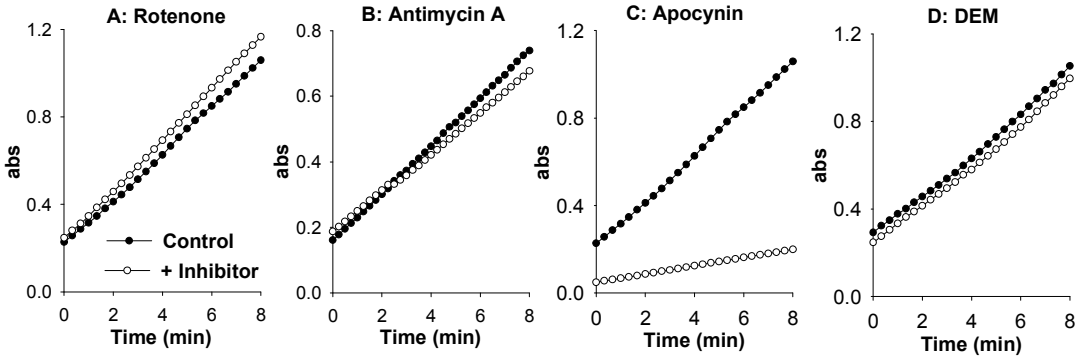

Figure 5.3 The effect of inhibitors on the formation of resorufin. KRB buffer containing 5% dextran, 25 μM AR, 5U HRP, 5.5 mM glucose, glucose oxidase with specific inhibitor was mixed well in a semi-fluorescent cuvette. A sample with the same buffer but without inhibitor was used as control and measured simultaneously. The absorbance at 571 nm was measured every 15 sec for 8 min. A: 0.02U glucose oxidase in the absence or presence of 20 μM rotenone; B: 0.015U glucose oxidase in the absence or presence of 10 M antimycin A; C: 0.02U glucose oxidase in the absence or presence of 1 mM apocynin; D: 0.02U glucose oxidase in the absence or presence of 6 mM DEM.

Figure 5.3 shows that the assay is insensitive to the presence of rotenone, antimycin A or DeM. However, apocynin decreased the detected rate of H_2O_2 production as measured by the absorbance of resorufin in the medium by ~80% (Figure 5.3 C). This decrease could be due to the effect of apocynin on glucose-glucose oxidase H_2O_2 production or on the formation of resorufin. To address this question, an AR- H_2O_2 standard curve in the buffer containing 1 mM apocynin was obtained. Figure 5.4 showed that in the presence of 1 mM apocynin, the absorbance at 571 nm of mixed AR–H_2O_2 sample was 10~20% of that of mixed samples in the absence of apocynin. This result suggests that apocynin might have an antioxidant property and hence competes with AR for H_2O_2. This result is consistent with the results of a study by Heumüller et al. in which they

evaluated the rate of resorufin formation in buffer with or without apocynin using different H_2O_2 production systems and different H_2O_2 probe including AR (Heumüller 2008). In summary, rotenone, antimycin A and DEM do not interfere with the AR-H_2O_2 assay, whereas apocynin does, presumably due to its H_2O_2 scavenging property.

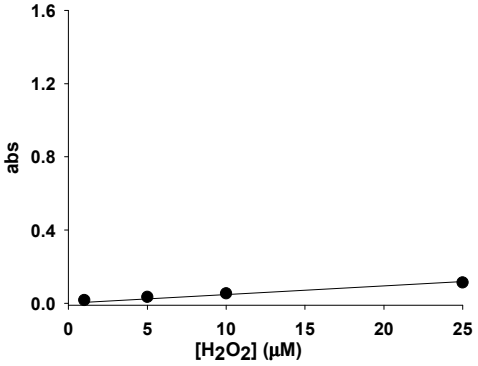

Figure 5.4 Standard curve of amplex red- H_2O_2 reaction in the presence of apocynin. The relationship between absorbance and concentrations of H_2O_2 added into the cuvette with the perfusate containing 50 μM AR, 5U horseradish peroxidase and 1 mM apocynin. The concentration of H_2O_2 was 1 μM, 5 μM, 10 μM, 25 μM respectively. The absorbance was measured at 571 nm.

5.2.5 Estimation of Lung Rate of H_2O_2 Release

Based on the results of the above bench top experiments (see the results below), KRB buffer containing 5% (mass/vol) dextran (KRB-Dex) was chosen as the perfusate for the isolated perfused lung experiments.

The following protocol was used to determine the rate of H_2O_2 release from the rat lung. Isolated lungs were washed free of blood using KRB-Dex. A 1 ml perfusate sample that had passed through the lungs but contained no AR was collected and used as the blank, after which the reservoir content was emptied and replaced with 20 ml KRB-Dex perfusate containing 50 μM AR with or without 5U of HRP. A 1 ml sample of the AR-containing KRB-Dex perfusate was removed from the reservoir prior to the start of the recirculation period. This sample was used to determine the background H_2O_2 production, and is referred below as the background sample. The remaining AR containing perfusate in the reservoir was then recirculated through the lung for a period of 30 min with the pump flow set at 10 ml/min. During the recirculation period, a 1 ml reservoir sample

was removed every 5 min. This sample was centrifuged at 13,500 g for 1 min and the absorbance of resulting supernatant was measured at 571 nm (Beckman DU7400). The sample was then added back to the reservoir to minimize the change in the total volume of perfusate in the recirculation system. To maximize the reaction rate between AR and H_2O_2, the above recirculation protocol was repeated with the addition of 5U of HRP to the perfusate. At the end of experiment, the volume of perfusate in the reservoir was measured.

Following the AR recirculation experiments, the lung was washed free of AR or resorufin and an index of perfused capillary surface area was contained as described in chapter 4.2.5.

The absorbance of resorufin in each collected sample during the recirculation period was converted to H_2O_2 concentration using an AR-H_2O_2 standard curve. The amount of H_2O_2 in the reservoir at a specific sampling time was determined as the product of H_2O_2 concentration in the reservoir sample and the corresponding reservoir volume. The lung rate of H_2O_2 release was then estimated as the slope of the relationship between sampling time and the amount of H_2O_2 in the reservoir. The absorbance values of the background sample measured at the sampling times were used to determine the background (lung independent) rate of H_2O_2 release. Thus, the lung rate of H_2O_2 release (nmol/min) was the difference between the rate determined from the reservoir samples and the background sample.

To estimate the effect of the activity of complex I on lung H_2O_2 release, the above protocol was repeated following lungs treatment with rotenone (20 μM). To estimate the sensitivity of this assay to H_2O_2 from mitochondria, the above protocol was repeated following lungs treatment with antimycin A (10 μM). The protocol was repeated in lungs ventilated with 5% CO_2 balanced O_2 to determine the dependence of the rate of H_2O_2 release on O_2 level.

5.2.6 Determination of the Activities of Complex I/IV in Lung Homogenate

The activities of complex I and complex IV in lung homogenate were measured as described in chapter 4.2.6.

5.3 Experimental Results

5.3.1 Effects of Rats Exposeure to 85% O_2 for 12, 24 or 48 hours on Body Weight, Lung Weight and Lung Perfused Capillary Surface Area

Rat exposed to 85% O_2 for 12, 24 or 48 hours had no significant difference in rat body weight, lung wet weight, lung dry weight, or perfused capillary surface area as compared to normoxic rats (Table 5.1). These results are consistent with those of Crapo et al. in which they reported that rats exposed to 85% O_2 for up to 72 hours had no detectable lung histological or morphometric changes (Crapo et al., 1980). Additionally, Block and Fisher showed that rat exposure to 100% O_2 for 48 hours had no effect on lung vascular flow distribution (Block & Fisher, 1977).

	B.W. (g)	W.W. (g)	D.W. (g)	W/D	PS (ml/min)
Normoxic	320±3.3	1.20±0.02	0.22±0.01	5.53±0.05	23.3±1.1
12 h (n=4)	313±5.1	1.28±0.13	0.23±0.01	5.59±0.22	23.0±1.3
24 h (n=7)	307±8.9	1.14±0.02	0.21±0.01	5.34±0.06	23.1±1.4
48 h (n=13)	303±4.0	1.20±0.04	0.22±0.01	5.67±0.10	26.7±3.0

Table 5. 1 Body weight (B.W.), lung wet weight (W.W.), lung dry weight (D.W.), lung wet weight/lung dry weight ratio (W/D) and *PS* of normoxic rats and rats exposed to 85% O_2 for 0, 12, 24 and 48 hours (Mean ± SE), n=94, 4, 7 and 13 respectively.

5.3.2 Effect of Rat Exposure to 85% O_2 for 12, 24, or 48 Hours on the Redox Metabolism of CoQ_1 as a Measure of Complex I Activity in the Intact Lung

Rat exposure to 85% O_2 for 24 hours or 48 hours, but not 12 hours decreased by ~20% the rate of CoQ_1 reduction on passage through pulmonary circulation at 50 μM or 200 μM CoQ_1

infusion (Figure 5.1). A previous study (Audi et al., 2008) as well as the results in chapter 4 demonstrated that the dominant oxidoreductases that determine the redox metabolism of CoQ_1 on passage through rat lungs are complex I, complex III and NQO1. Audi et al. showed that rat exposure to 85% O_2 for up to 48 hours had no effect on complex III-mediated CoQ_1H_2 oxidation, NQO1-mediated CoQ_1 reduction or capillary perfusion kinematics (Audi et al., 2005, 2008). Thuse, a change in the steady state rate of CoQ_1H_2 efflux during CoQ_1 infusion in lungs of rats exposed to 85% O_2 for 48 hours or less would be attributed to a change in complex I mediated CoQ_1 reduction and hence in complex I activity in intact lung. The results in Figure 5.1 suggest that rat exposure to 85% O_2 for 24 hours and 48 hours, but not 12 hours decreased complex I activity in intact lungs.

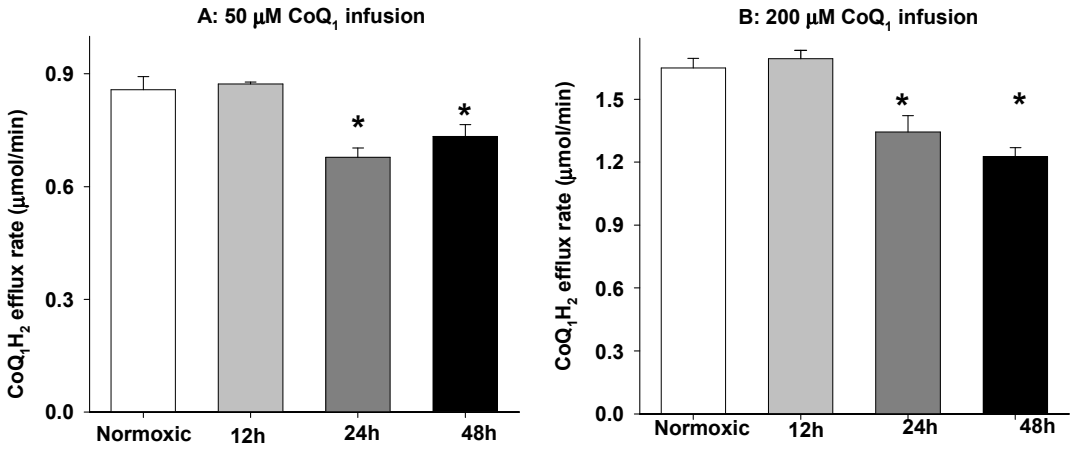

Figure 5. 5 The efflux rate of CoQ_1H_2 during 50 or 200 µM CoQ_1 infusion of rat lungs exposed to room air (n=12), 85% O_2 for 12 hours (n=4), 85% O_2 for 24 hours (n=5) and 85% O_2 for 48 hours (n=7, data from Audi et al., 2008) respectively. A: 50 µM CoQ_1 infusion B: 200 µM CoQ_1 infusion Values are mean ± SE. * Rates significantly different from the normoxic rates at the same infused CoQ_1 concentrations using one-way ANOVA ($P<0.05$).

To determine the capacity of complex I-mediated CoQ_1 reduction in lungs of rats exposed to 85% O_2 for 12, 24 or 48 hours, the lung kinetic model described in chapter 4.4 was fit to the steady state rates of CoQ_1H_2 efflux during CoQ_1 infusion at 50 and 200 µM. For this model fitting

step, the only unknown parameter was the capacity (V_{max3}) of complex I-mediated CoQ_1 reduction. Other model parameters including Michaelis-Menten constant for complex I mediated CoQ_1 reduction, Michaelis-Menten parameters for other dominant redox processes that determine the fate of CoQ_1 metabolism on passage the lung, and lung capillary transit time distribution were set at the mean values estimated for normoxic lungs (Table 4.9). Table 5.2 shows the estimated values of V_{max3} for the four groups of rats. Exposure to 85% O_2 for 24 or 48 hours decreased V_{max3}, which is a measure of complex I activity, by ~27% and ~34%, respectively.

Rats	V_{max3} (Activity of Complex I)	
	(μmol/min)	(μmol/min/g)
Normoxic	3.20±0.14	14.6±0.7
12-hour	3.12±0.07	13.6±0.3
24-hour	2.33±0.14*	11.1±0.7*
48-hour	2.10±0.18*	9.5±0.8*

Table 5.2 Estimated parameter descriptives of capacity of complex I mediated CoQ_1 reduction in normoxic rat (n=11), 12-hour 85% O_2 exposed rats (n=4), 24-hour 85% O_2 exposed rat (n=5), and 48-hour 85% O_2 exposed rats (n=7). Values are mean ± SE. * Significantly different from normoxic values using one-way ANOVA ($P<0.05$).

5.3.3 Effect of Rat Exposure to 85% O_2 for 12, 24, or 48 Hours on Complex I and Complex IV Activities in Lung Tissue Homogenate

Figure 5.6 shows that rat exposure to 85% O_2 for 12, 24 or 48 hours decreased complex I activity (rotenone-sensitive NADH oxidation) in lung tissue homogenate by ~50%. This depression in complex I activity persisted after 7 days of rat exposure to 85% O_2 as demonstrated in chapter 4.

Exposure to 85% O_2 for 24 or 48 hours had no significant effect on complex IV activity in lung tissue homogenate as compared to normoxic lungs (Figure 5.7, Table 5.3). For 12-hour exposure group, the results were not conclusive. For one batch of rats exposed to 85% O_2 for 12 hours (n=3), the activity of complex IV in lung homogenate decreased by ~50% (50.4±0.94

nmol/min/mg) as compared to normoxic lungs. However, for another two batches of rats exposed to O_2 for 12 hours (n=6), there was no difference in the activity of complex IV in lung tissue homogenates compared to normoxic lungs.

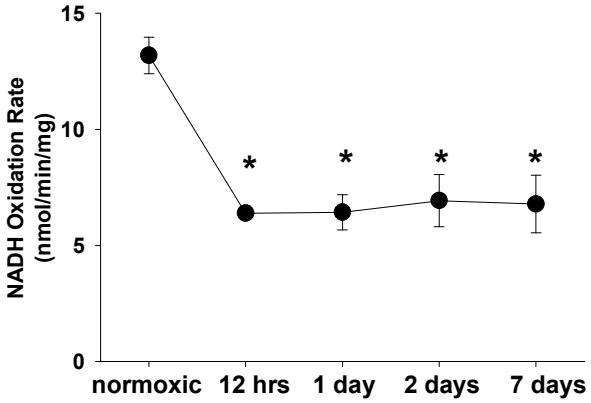

Figure 5.6 Rotenone-sensitive NADH oxidation rates in lung homogenate from rats exposed to room air (n=12), 85% O_2 for 12 hours (n=10), 85% O_2 for 24 hours (n=4), 85% O_2 for 48 hours (n=6) and 7 days (n=7) respectively. Values are mean ± SE. * Rates significantly different from the normoxic rate.

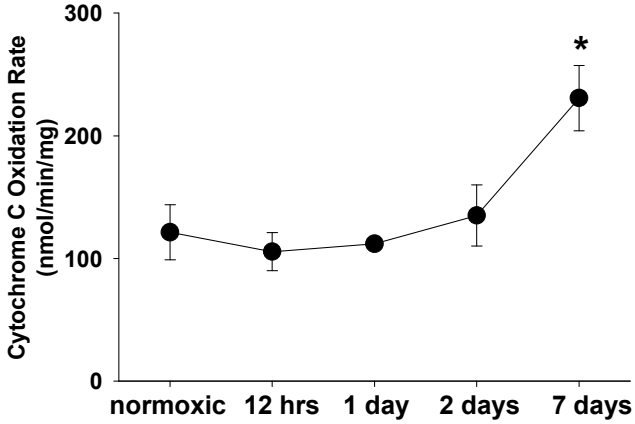

Figure 5.7 Cytochrome C oxidation rates in lung homogenate from rats exposed to room air (n=12), 85% O_2 for 12 hours (n=9), 85% O_2 for 24 hours (n=4), 85% O_2 for 48 hours (n=6) and 7 days (n=7) respectively. Values are mean ± SE. * Rates significantly different from the normoxic rate.

	Complex I (nmol/min/mg protein)	Complex IV (nmol/min/mg protein)
Normoxic (n=12)	13.18±0.78	121±22
12 h (n=10)	6.39±0.25*	106±16
24 h (n=4)	6.42±0.76*	112±23
48 h (n=6)	6.92±1.12*	135±25
7 days (n=7)	6.78±1.24*	231±27*

Table 5.3 The activities of complex I and IV in lung homogenates of rats exposed to 85% O_2 for 0 hour (n=12), 12 hours (n=10), 24 hours (n=4), 48 hours (n=6) and 7 days (n=7), respectively. Values are mean ± SE. * Values significantly different from the normoxic value.

5.3.4 Effect of Rat Exposure to 85% O_2 on Lung Rate of H_2O_2 Release

Figure 5.8 A shows that, in the presence of HRP, the absorbance at 571 nm of reservoir samples collected at different sampling time over a 30-min lung recirculation period through a normoxic rat lung increased linearly. Thus, the corresponding resorufin concentrations and hence H_2O_2 concentrations increased linearly with time at a rate ~ 0.8 μM/min (or 16 nmol/min for the whole lung H_2O_2 release). Since the perfusate can produce H_2O_2 via spontaneous reaction, a fraction of this rate is lung independent. Figure 5.8 B shows that, in the presence of HRP, H_2O_2 concentration in background sample increased linearly with time at a rate ~0.1 μM/min (2 nmol/min for the whole lung H_2O_2 release). Thus, the lung-dependent H_2O_2 production rate is ~ 0.7 μM /min (14 nmol/min for the whole lung H_2O_2 release).

The above experiments were repeated without the addition of HRP in the perfusate. Figure 5.8 C shows that, in the absence of HRP, H_2O_2 concentration in the reservoir also increases linearly at a rate ~0.5 μM/min (10 nmol/min for the whole lung H_2O_2 release). This suggests that rat lungs have endogenous peroxidase activity on the luminal surface of the pulmonary endothelium. Figure 5.8 D shows that, in the absence of HRP in the perfusate, the rate of resorufin formation in the background sample (i.e. not recirculated through the lung) is virtually zero.

Figure 5.9 shows the effect of redox enzyme inhibitors on normoxic lung rate of H_2O_2 release. Rotenone slightly decreased the detectable rate of H_2O_2 release (Figure 5.9 A) and antimycin A had no effect on the release rate of H_2O_2 (Figure 5.9 B). Figure 5.9 C shows that apocynin decreased the detected rate of H_2O_2 release by ~90% which is consistent with the results

of the benchtop experiments, presumably due to apocynin's H_2O_2 scavenging property. Figure 5.9 D shows that DEM decreased the rate of H_2O_2 release by ~87%, though the expected result of DEM was that depleting glutathione (GSH) by DEM would increase the rate of H_2O_2 released into the vascular space since GSH is the main cytosolic H_2O_2 scavenger.

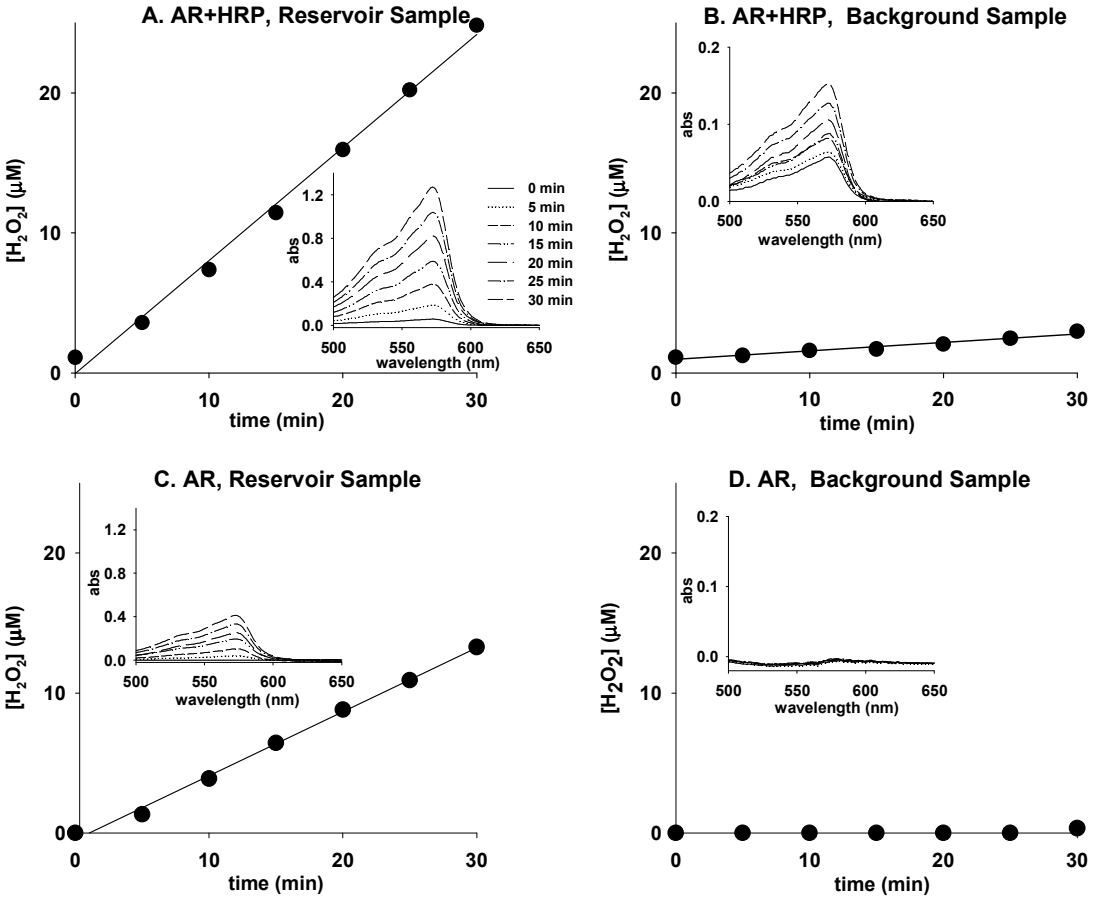

Figure 5.8 H_2O_2 release time course and spectra of reservoir or background samples during lung recirculation. The perfusate is KRB buffer containing 5% dextran, 50 μM AR. A: The H_2O_2 concentration and its corresponding spectra of reservoir samples during lung recirculation in the presence of 5U HRP. 1 ml reservoir sample was taken every 5 min. B: The H_2O_2 concentration and its corresponding spectra of background sample in the presence of 5U horseradish peroxidase. The background sample was incubated at 37°C and measured every 5 min. C: The H_2O_2 concentration and its corresponding spectra of reservoir samples during lung recirculation in the absence of 5U HRP. 1 ml reservoir sample was taken every 5 min. D: The H_2O_2 concentration and its corresponding spectra of background sample in the absence of 5U HRP. The background sample was incubated at 37°C and measured every 5 min.

Figure 5.10 shows that hyperoxic ventilation (95% O_2, 5% CO_2) increased the detectable rate of H_2O_2 release by ~20% as compared to lungs ventilated with normoxic gas mixture (15% O_2,

5% CO_2, and balance N_2).

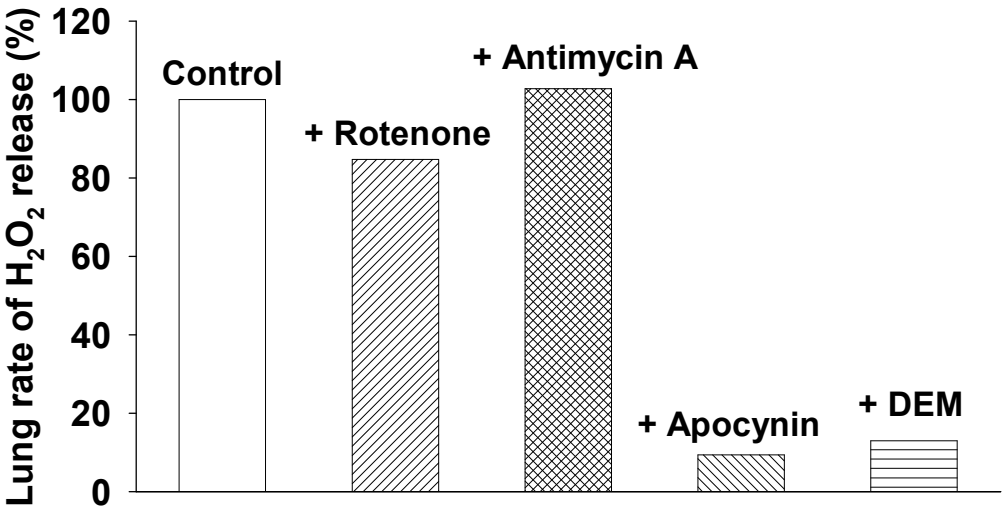

Figure 5.9 H_2O_2 release rate during amplex red recirculation with inhibitors passage through normoxic lungs for control, in the presence of 20 μM rotenone, 10 μM antimycin A, 1 mM apocynin and 6 mM DEM respectively.

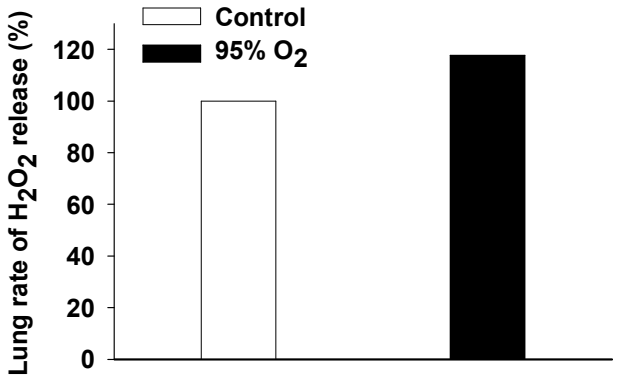

Figure 5.10 H_2O_2 release rate during amplex red recirculation with 95% O_2 and 5% CO_2 ventilation.

Effect of Rat Exposure to 85% O_2 on the Lung Rate of H_2O_2 Release

To investigate the effect of rat exposure to 85% O_2 on the lung rate of H_2O_2 release, AR recirculation experiments were repeated for lungs from rats exposed to 85% O_2 for 48 hours (initiation phase) or 7 days (adaptation phase).

Figure 5.11 shows that lung rates of H_2O_2 release from rats exposed to room air, 85% O_2

for 48 hours or 7 days using the above AR-H_2O_2 assay with HRP. The activity of endogenous peroxidase in lungs exposed to room air, 85% O_2 were estimated by AR-H_2O_2 recirculation assay without HRP (Figure 5.12). The results show that exposure to 85% O_2 for 48 hours had no significant effect on the rate of H_2O_2 release in the absence or presence of HRP as compared to normoxic lungs, while exposure to 85% O_2 for 7 days decreased lung rate of H_2O_2 release by 35~ 40% in the presence or absence of HRP (Table 5.4). Table 5.4 shows that the lung rates of H_2O_2 release (nmol/min) normalized to lung dry weight (nmol/min/g) or perfused capillary surface area (nmol/min). Normalizing the rates to lung dry weight assumes that all the lung cells are contributing equally to the H_2O_2 released into the perfusate. On the other hand, normalizing the rates to perfused surface area assumes that the capillary endothelial cells are the main source of H_2O_2 released into the perfusate. For lungs of rats exposed to 85% O_2 for 7 days, the rate of H_2O_2 release per gram of dry lung weight was ~60% smaller than that for normoxic lungs, whereas the rates normalized to perfused capillary surface were not significantly different from that for normoxic lungs.

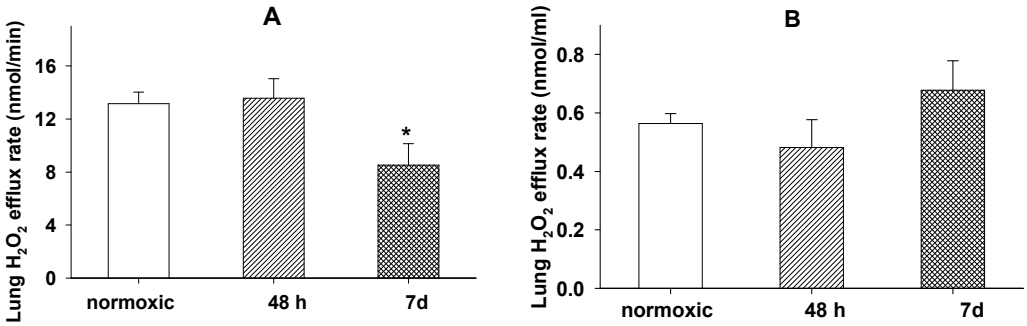

Figure 5.11 Lung H_2O_2 release rates from rat lungs during AR recirculation with HRP. A: Lung H_2O_2 release rate during 50 μM AR recirculation in the presence of 5U HRP from rat exposed to room air (n=9), 85% O_2 for 48 hours (n=6) and 7 days (n=4) respectively. B: Lung H_2O_2 release rate in Figure A normalized to lung perfused surface area. Values are mean ± SE. * Rates significantly different from the normoxic rate.

5.4 Discussion and Conclusions

In this study, the measurement of the efflux rate of CoQ_1H_2 during CoQ_1 arterial infusion was used to determine how early following rat exposure to 85% O_2 this decrease in complex I activity occurred. The results of this study reveal that rat exposure to 85% O_2 for 24 hours, but not 12 hours, decreased CoQ_1H_2 efflux rate during CoQ_1 infusion. Quantitative analysis based on the mathematical model described in chapter 4 indicated a ~30% decrease in the capacity of complex I

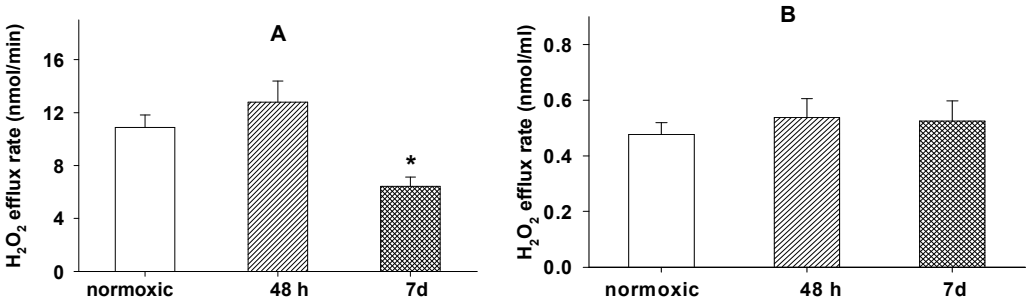

Figure 5.12 H_2O_2 release rates from rat lungs during AR recirculation. A: Lung H_2O_2 release rate during 50 μM AR recirculation from rat exposed to room air (n=5), 85% O_2 for 48 hours (n=4) and 7 days (n=4) respectively. B: Lung H_2O_2 release rate in Figure A normalized to lung perfused surface area. Values are mean ± SE. * Rates significantly different from the normoxic rate.

Rats	AR+HRP recirculation			AR recirculation		
	nmol/min	nmol/ml	nmol/min/g	Nmol/min	nmol/ml	nmol/min/g
Normoxic	13.2±0.9	0.56±0.03	59.8±3.9	10.9±0.93	0.48±0.04	49.5±4.1
48 h	13.6±1.5	0.48±0.09	64.8±7.1	12.8±1.61	0.54±0.07	61.0±7.6
7 d (n=7)	8.5±1.6*	0.68±0.10	23.0±4.3*	6.4±0.71*	0.53±0.07	17.3±1.9*

Table 5.4 H_2O_2 release rates from isolate rat lung during AR recirculation with or without HRP. The concentration of AR was 50 μM and the concentration of HRP was 5U. For AR+HRP recirculation, normoxic rats n=9; 85% 48 h rats n=6; 85% 7 days rats n=4. For AR recirculation, normoxic rats n=5; 85% 48 h rats n=5; 85% 7 days rats n=4. Values are mean ± SE. * Significantly different from normoxic values.

mediated CoQ_1 reduction, and hence in complex I activity, in lungs from rats exposed to 85% O_2 for 24 hours as compared to normoxic lungs. Complex I activity in lung homogenates was also

lower for lungs of rats exposed to 85% O_2 for 24 hours. Previously, Bassett et al. showed that rats exposed to 100% O_2 for 24 hours resulted in a NAD-linked but not FAD-linked decrease in ADP-stimulated rate of respiration in lung homogenate (Bassett, Bowen & Reichenbaugh, 1992). Since NAD ($NADH/NAD^+$) is the substrate for complex I while FAD ($FADH_2/FAD^+$) is the substrate for complex II, this result suggested a decrease in complex I activity, consistent with the results of this study. In summary, the decrease in lung complex I activity is detectable after 24-hour exposure to 85% O_2 and hence is a relatively early metabolic consequence of hyperoxic exposure. It occurs prior to the gross cellular and hemodynamic changes which are not detectable for at least 72 hours of hyperoxic exposure. Therefore, complex I could be an early index of the initiation phase of hyperoxic lung injury, and a target for imaging residue detection biomarkers such as ^{125}I-iodorotenone (VanBrocklin, Hanrahan & Enas, 2007).

Although rats exposed to 85% O_2 for 12 hours had no significant effect on lung efflux rate of CoQ_1H_2 during CoQ_1 infusion, it did result in a ~50% decrease in complex I activity in lung tissue homogenates as compared to normoxic lungs. One possible explanation for this apparent inconsistency could be due to the assumption that the lung activities of complex III and NQO1 were not affected by exposure to 85% O_2 for <48 hours. Cai et al. measured mRNA expression of complex III of lungs from premature newborn rats exposed to 85% O_2 and found that the expression of complex III increased after 1 and 4 days exposure to 85% O_2 but not for 2 or 3 days compared to the expression in lungs of normoxic rats (Cai, Chang & Li, 2008). This result suggested that the assumption that complex III activity was not affected by exposure to 85% O_2 for 12 hours because it was not affected by exposure to 85% O_2 for 48 hours may not be true, and hence would need to be evaluated in the future. The activity of complex III could be evaluated

using lung infusion with DQH_2 or CoQ_1H_2 which are the substrates of complex III.

In the present study, it is clear that there were no differences in complex IV activity of lung homogenates from rat exposure to 85% O_2 for 24, or 48 hours compared to normoxic rats. However, the results regarding the effect of rat exposure to 85% O_2 for 12 hours on complex IV activity in lung homogenates show a big variance, with 4 rats of 9 rats suggesting a ~50% decrease and other 5 rats suggesting no change as compared to normoxic lungs. Arab et al. (2010) demonstrated that a ~40% decrease in complex IV activity occurred in cultured human cardiomyocytes after 3-hour exposure to hypoxia (95% N_2/5% CO_2) (Arab, Wang & Bausch, 2010). This decrease in complex IV activity was reversible (Arab et al., 2010). Arab's study suggests that complex IV could respond to a change in oxygen supply quickly and the adjustment of complex IV activity could be a way to adjust O_2 consumption and further ATP synthesis. Raam et al. demonstrated that both complex III and complex IV were part of mitochondrial supercomplex and hence functionally associated (Van Raam et al., 2008). Thus, a decrease in complex IV activity in lungs of rats exposed to 85% O_2 for 12 hours could slow down the flow of electron through complex III and hence decrease the capacity of complex III mediated CoQ_1H_2 oxidation; or reversely, the decrease in complex IV activity could be a subsequential response of a decrease in complex III activity. This could explain why the decrease in complex I measured in lung homogenate of rats exposed to 85% O_2 for 12 hours did not change the rate of CoQ_1H_2 efflux during CoQ_1 infusion.

An important aspect of this study is the development of an assay for detecting the rate of H_2O_2 release from an isolated perfused rat lung. Using the developed AR assay, the rate of H_2O_2 release from normoxic rat lungs in the absence or presence of HRP was 10 or 14 nmol/min,

respectively. This rate is relatively close to ~17 nmol/min/lung which is the sum of estimated H_2O_2 release rate from lung endothelium, epithelium and macrophages (Kinnula et al., 1991). Using ortho-phenylenediamine dihydrochloride (o-PD) as a probe of H_2O_2, Al-Medhi et al. estimated the rate of H_2O_2 release from an isolated perfused rat lungs was 3.8 nmol/min in the presence of 5U HRP (Al-Mehdi et al., 1997). This lower rate could be in part due to the difference in the experimental rats (300 g SD rats in this study V.S. 150 g SD rats in Al-Medhi's study) and the difference in the efficiencies of the two H_2O_2 probes (AR V.S. o-PD).

The AR-H_2O_2 assay requires the presence of a peroxidase. However, the results of the present study shows ~10 nmol/min H_2O_2 release during the recirculation of AR-containing perfusate in the absence of exogenous peroxidase (HRP). This result suggested the existence of endogenous peroxidase on the surface of the pulmonary capillary endothelium. This is consistent with the results of previous studies which demonstrated the presence of myeloperoxidase (MPO) on the endothelial surface which transmigrated from neutrophil cells to endothelial cells when intracellular adhesion molecule 1 (ICAM-1) were expressed on the endothelial surface (Hamada, Ikata & Katoh, 1996; Schuschke, Percival & Lominadze, 2002; Rhian, 2008; Heumüller et al., 2008). This might explain the decrease in detectable rate of lung H_2O_2 release in the presence of DEM in the perfusate since Nathens et al. had demonstrated that DEM could inhibit the expression of ICAM-1 of endothelial cells (Nathens, Marshall & Watson, 1996) and hence inhibit the expression of MPO on the endothelial surface, which in turn would inhibit MPO-mediated AR-H_2O_2 reaction. However previous studies on ICAM-1 expression were based on endothelial cells pre-exposure to DEM for 6 hours. A study whether 15-min pre-exposure to DEM on lung endothelial ICAM-1 expression has the similar effect is needed.

There are several cellular sources of H_2O_2, including NADPH oxidase, and mitochondrial complexes I and III. One way to evaluate the contribution of each of these sources to the measured rate of lung H_2O_2 release would be by manipulating the activities of these enzymes using metabolic inhibitors. Previous studies in isolated mitochondria, submitochondrial particles or cells demonstrated a 10- to 20-fold increase in the rate of ROS formation in the presence of AA as compared to that in the absence of AA (Ksenzenko, Konstantinov & Khomutov, 1983; Turrens & Boveris, 1997; Hansford, Hogue & Mildaziene, 1997; Starkov & Fiskum, 2001; Budinger, Tso & McClintock, 2002; Turrens, 2003; Chen et al., 2003; Li et al., 2003; Drechsel & Patel, 2009). On the other hand, the effect of rotenone on ROS generation is somewhat complicated. In submitochondrial particles, a rotenone-induced ROS production is observed (Turrens & Boveris, 1980; Krishnamcorthy & Hinkle, 1988; Hansford et al., 1997; Kwong & Sohal, 1998). In intact mitochondria, rotenone-induced ROS production requires a very high degree of reduction of redox carrier's upstream of the rotenone binding site (Kushnareva, Murphy & Andreyev, 2002; Li et al., 2003; Andreyev et al., 2005). A few studies observed a decrease in ROS formation with rotenone treatment in sheep pulmonary microvascular endothelial cell suspensions (Sander et al., 1993). However, the results of the present study show that inhibiting complex I by rotenone or complex III by antimycin A had no effect on the lung rate of H_2O_2 release. This result suggests that the detected H_2O_2 release might not originate in mitochondria. The decrease in the rate of H_2O_2 release by the GSH depleter DEM is opposite to the expected results and may be due to its effect on cellular surface adhesive molecules. Apocynin, a NADPH oxidase inhibitor, decreased the rate of H_2O_2 release by ~90%, but presumably due to its H_2O_2 scavenging property instead of its effect on NADPH oxidase. Hence, the effect of apocynin is not able to define the role of NADPH

oxidase on lung H_2O_2 release. The insensitivity of the lung rate of H_2O_2 release measured using the AR assay to inhibit complex I or III could be due to the insensitivity of this assay to intracellular sources of H_2O_2. Tan et al. pointed out that the cell impermeable AR was not a sensitive probe for intracellular H_2O_2 (Tan & Berridge, 2010). The insensitivity of AR to intracellular H_2O_2 might be due to transmembrane disequilibrium of H_2O_2 or to the magnitude and kinetics of H_2O_2 cellular gradients that limits its diffusion in and out of cells (Tan & Berridge, 2010). Alternatively, there are multiple cellular antioxidant mechanisms (e. g. catalase, glutathione peroxidase) and other peroxide sinks that could scavenge intracellular generated H_2O_2 and hence prevent it from reaching AR in the vascular space (Tan & Berridge, 2010). Therefore, AR recirculation assay may be a sensitive method to detect lung H_2O_2 release but not a sensitive method to estimate intracellular H_2O_2 formation.

The results of this study show that rat exposure to 85% O_2 for 48 hours had no effect on the lung rate of H_2O_2 release, though lung complex I activity decreased by ~50% compared to normoxic rats. On the other hand, rat exposure to 85% O_2 for 7 days (hyper-85) decreased the lung rate of H_2O_2 release by ~50%. As stated in chapter 4, hyper-85 lungs decreased perfused lung capillary surface area by ~50% and increased lung dry weight by ~70% as compared to normoxic lungs. If the source of H_2O_2 detected using this AR recirculation assay is the capillary endothelial cells, then the rate of H_2O_2 release would need to be normalized to the capillary surface area. If all lung tissue cells contribute to lung rate of H_2O_2 release, then normalizing the rate to lung dry weight would be appropriate. Table 5.4 shows that normalizing to perfused capillary surface area dissipates the difference between normoxic and hyper-85 lungs, while normalizing to lung dry weight augments the difference in the rate of H_2O_2 release between hyper-85 and normoxic lungs.

Additionally, the decrease in detectable lung rate of H_2O_2 release caused by DEM also suggests that endothelial surface played a role in the detectable H_2O_2 release.

CHAPTER 6. DIFFERENTIAL RESPONSES OF TARGETED LUNG REDOX ENZYMES TO RATS EXPOSURE TO 60% OR 85% O_2

6.1 Introduction

As stated in chapter 1.2, the rat model of lung O_2 toxicity is unique in that when adult rats are exposed to an adaptive 85% O_2 environment for 5-7 days, they acquire tolerance to the otherwise lethal effects of 100% O_2, in that if transferred to a 100% O_2 environment they survive for prolonged period (Crapo et al., 1980; Sjostorm & Crapo, 1983; Frank, Iqbal & Hass, 1989; Coursin, Cihla & Will, 1987; Audi et al., 2005). Conversely, rats exposed to 60% O_2 for 7 days become more susceptible to 100% O_2 as evidenced by a decrease in their subsequent survival time in 100% O_2 environment (Coursin et al., 1987; Hayatdavoudi et al., 1981). Elucidating the factors that contribute to this rat tolerance of or susceptibility to 100% O_2 could further our understanding of the pathogenesis of lung O_2 toxicity, and may lead to the identification of potential therapeutic targets for protecting lung tissue from the toxic effects of high O_2 (Audi et al., 2005; Crapo et al., 1974, 1980; Frank et al.,1989; Sjostrom et al., 1983).

Using indicator dilution methods and mathematical modeling developed in our studies, we have demonstrated that the redox active quinone compound duroquinone (DQ) is reduced to durohydroquinone (DQH_2) and DQH_2 is oxidized to DQ on passage through the pulmonary circulation of the isolated perfused rat lung (Audi et al., 2003, 2005). Based on inhibitor studies, NAD(P)H:quinone oxidoreductase 1 (NQO1) was implicated as the dominant DQ reductase and mitochondrial complex III as the dominant DQH_2 oxidase, and the capacities of the lung to reduce DQ to DQH_2 and oxidize DQH_2 to DQ were shown to be measures of lung NQO1 activity and complex III activity, respectively (Audi et al., 2003, 2005).

The results of chapter 4 show that rat exposure to 85% O_2 for 7 days (hyper-85) increased

NQO1 activity by ~200% and complex III activity by ~180% estimated from changes in the capacity of NQO1-mediated DQ reduction and complex III mediated DQH_2 oxidation, respectively, on passage through the pulmonary circulation. Furthermore, the results of chapter 4 showed mitochondrial complex IV activity in lung homogenates was ~90% higher for hyper-85 lungs compared to normoxic lungs. The objective of the current study was to evaluate the effects of a 7-day exposure of rats to 60% O_2 (hyper-60) on NQO1 and mitochondrial complexes III in the intact lung using duroquinone (DQ) and its hydroquinone (DQH_2), respectively, as indicator dilution probes. Demonstration that the activity of a particular redox enzyme is differentially altered by exposure to 60% O_2 and 85% O_2 would suggest its role in the development of the observed susceptibility or tolerance to 100% O_2.

6.2 Materials and Methods

6.2.1 Hyperoxic Exposure

Rats were exposed to 60% O_2 for 7 days (hyper-60) using the exposure chamber and protocol described in chapter 4.1.1.

6.2.2 Lung Preparation

The isolated perfused lung preparation and the lung ventilation-perfusion system are described in chapter 4.1.2.

6.2.3 Pulse Infusion Experimental Protocols

To determine the DQ reducing capacity of the lung, four 135-second long sequential arterial pulse infusions at DQ concentrations of 50, 100, 200, and 400 μM were carried out as described in chapter 4.2.3.

To determine the capacity of NQO1-mediated DQ reduction on passage through the pulmonary circulation, each lung was perfused for 5 min with perfusate containing antimycin A (10 μM). This was followed by four successive DQ pulse infusions, with the inhibitor present throughout the infusion protocol.

To evaluate the capacity of complex III mediated DQH_2 oxidation on passage through the pulmonary circulation, each lung was perfused for 5 min with perfusate containing dicumarol (400 μM) or dicumarol plus rotenone (20 μM). This was followed by four 135-second sequential DQH_2 infusions as described in chapter 4.2.3.

The perfused lung surface area was determined using the ACE substrate FAPGG as described in chapter 4.2.6.

The concentrations of DQ and DQH_2 in the venous effluent samples were determined as described in chapter 4.2.4. The steady state efflux rates of DQH_2 or DQ from the lung during DQ or DQH_2 arterial infusion were calculated as the product of the perfusate flow (10 ml/min) and the steady state venous effluent DQH_2 or DQ concentrations, respectively. The log mean DQH_2 or DQ concentration were determined as described in chapter 4.2.4.

6.2.4 Tissue Assay

i. Lung Homogenate NQO1 Activity & Immunoblot Analysis of NQO1

The measurements of lung homogenate NQO1 activity and lung mitochondrial complexes I and IV activities were carried out as previously described in chapter 4.2.6.

ii. Total Glutathione Content

The lungs were washed free of blood with buffer containing 10 mM HEPES, 5 mM glucose, and 5% dextran (~67 kDa), pH 7.4. The lungs were then removed from the perfusion system, dissected free from connective tissue, and weighed. A portion of the lung was dried for determination of total lung dry weight and lung wet-to-dry wt ratio. The remaining tissue was placed into 10 volumes (per lung wet weight) of 4 ^{o}C sulfosalicylic acid (5%), minced and homogenized as above. The homogenate was centrifuged (10,000 × g) at 4 ^{o}C for 20 min, and the supernatant was used to determine total lung glutathione content as described by Owens and Belcher (Owens & Belcher, 1965) and later modified by Tietze (Tietze, 1969) and Griffith (Griffith, 1980).

6.3 Results

6.3.1 Rat Body Weight, Lung Wet/Dry Weight, Perfused Surface Area, and Arterial Blood Hematocrit

Rats lost ~14% of their pre-exposure body weights (Figure 6.1) over the 7-day 85% O_2 exposure period (Crapo et al., 1980; Ramakrishna et al., 2010). Most of this weight loss occurred between days 2 and 6. On the other hand, rats exposed to 60% O_2 gained body weight steadily over the 7-day exposure period at a rate that is virtually the same as age-matched normoxic rats (Coursin et al., 1987).

Rat exposure to 85% O_2 for 7 days (hyper-85) increased lung wet weight by 87%, with no effect on wet/dry weight ratio as compared to normoxic lungs (Table 6.1). The lack of a difference in wet/dry weight ratios between normoxic and hyper-85 lungs (Table 6.1) is consistent with the finding of Crapo et al. that the increase in wet weight was due to increased tissue mass instead of

edema (Crapo et al., 1980). Hyper-60 lung wet weights or wet/dry weight ratios were not different from normoxic lungs (Table 6.1) (Hayatdavoudi et al., 1981).

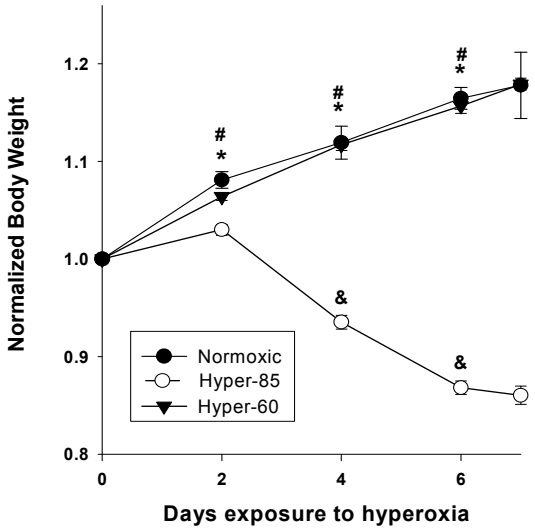

Figure 6.1 Rat body weights normalized to pre-exposure body weights at different time points during the 7-day exposure period to room air (normoxic), 60% O_2 (hyper-60), or 85% O_2 (hyper-85). Values are mean ± SE (n = 6, 33 and 34 for normoxic, hyper-60, and hyper-85 rats, respectively). $^{*,\ \#,\ \&}$Indicates normalized weights at a given time are significantly different from normalized weights at the previous time point for normoxic, hyper-60, or hyper-85 rats, respectively.

	B.W. (g)	W. W. (g)	W/D ratio	*PS* (ml/min)	Hct (%)
Normoxic	316 ± 4	1.22 ± 0.03	5.56 ± 0.09	24.7 ± 1.7	43.5 ± 0.4
Hyper-60	302 ± 2	1.31 ± 0.02	5.45 ± 0.05	25.1 ± 1.4	33.5 ± 0.6*
Hyper-85	311 ± 2	2.29 ± 0.08* $^{\&}$	5.72 ± 0.08	10.7 ± 0.8* $^{\&}$	50.1 ± 0.8* $^{\&}$

Table 6.1 Rat information of normoxic rats, hyper-85 rats and hyper-60 rats. *PS* (permeability surface area product), measure of ACE mediated FAPGG hydrolysis and an index of perfused capillary surface area. For normoxic lungs, n = 38, 38, 31, 19, and 27 for body wt, lung wet wt, wet/dry ratio, *PS*, and Hct, respectively, where 38 is the total number of normoxic rats studied. For hyper-60 lungs, n =38, 38, 29, 18, and 23 for pre-exposure body wt, lung wet wt, wet/dry ratio, *PS*, and Hct, respectively, where 38 is the total number of hyper-60 rats studied. For hyper-85 lungs, n = 41, 41, 28, 20, and 27 for pre-exposure body weight (B.W.), lung wet weight (W.W), lung wet/dry ratio (W/D ratio), *PS* (permeability-surface area product), and Hct (hematocrit), respectively, where 41 is the total number of hyper-85 rats studied. Values are mean ± SE. *: significantly different from normoxic values; *&: significantly different from normoxic and hyper-60 values, respectively.

Exposure to 85% O_2 for 7 days decreased *PS* (ml/min), an index of perfused capillary endothelial surface area, by 56% as compared to normoxic lungs (Table 6.1). This is consistent with the 50% decrease in capillary volume and endothelial surface area measured morphometrically (Crapo et al., 1980, Crapo 1974, Ramakrishna et al., 2010). The *PS* values for

hyper-60 and normoxic lungs were not different. This observation supports presentation of morphometric measures of capillary volume and endothelial surface area in hyper-60 lungs (Hayatdavoudi et al., 1981).

Rat exposure to 85% O_2 and 60% O_2 had a differential effect on aortic blood hematocrit (Table 6.1). Exposure to 85% O_2 increased hematocrit by 16% while exposure to 60% O_2 decreased it by 12% as compared to normoxic lungs (Crapo et al., 1980). There was no significant difference in the isolated lung perfusion pressure at 10 ml/min among the three groups of lungs (Ramakrishna et al., 2010).

6.3.2 Lung Infusion Experimental Results

The capacities of hyper-60 and hyper-85 lungs to reduce DQ to DQH_2 during DQ infusion were both higher than that of normoxic lungs (Figure 6.2). For both O_2 levels, the steady state DQH_2 efflux rates during the arterial infusion of DQ at the two highest concentrations were on average 37% higher than in normoxic lungs. For all three lung groups, lung treatment with dicumarol (NQO1 inhibitor) decreased the rate of DQH_2 efflux by > 95% during the infusion of DQ at the highest concentration (data not shown). This is consistent with NQO1 being the dominant reductase of DQ on passage through the pulmonary circulation of normoxic, hyper-60, and hyper-85 lungs (Audi et al., 2004, 2005).

To evaluate the capacity of the lung to oxidize DQH_2, we measured the steady state rate of DQ efflux during DQH_2 infusion in the presence of dicumarol to inhibit DQ reduction (Figure 6.3). For hyper-60 and hyper-85 lungs, the steady state rates of DQ efflux during DQH_2 infusion at the two highest concentrations were 40% higher than in normoxic lungs (Figure 6.3). For all three groups of lungs, treatment with antimycin A (complex III inhibitor) decreased the rate of DQ

efflux to nearly zero during DQH_2 infusion at the highest concentration (data not shown). This is consistent with DQH_2 oxidation on passage through normoxic and hyperoxic lungs occurring predominately via the hydroquinone oxidase-cytochrome c reductase activity of complex III (Audi et al., 2004, 2005; Merker, Audi & Bongard, 2006).

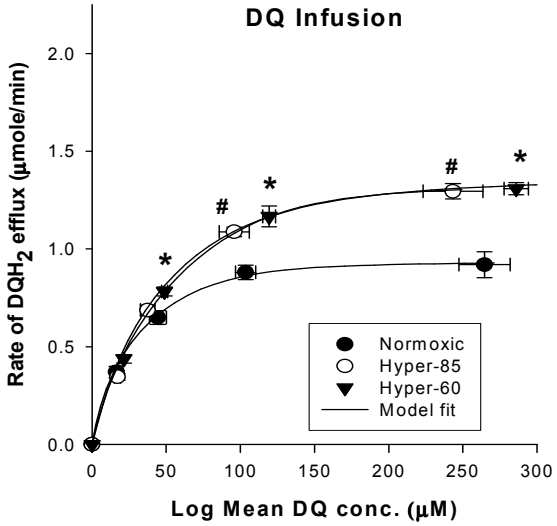

Figure 6.2 The relationship between the steady state rate of DQH_2 efflux and the log mean DQ concentrations , for normoxic lungs (n = 4), hyper-85 lungs (n = 5), and hyper-60 lungs (n = 5). Values are mean ± SE. The solid lines are model fits to the mean values of the data. * Hyper-60 rates significantly different from the normoxic rates at the same log mean DQ concentrations. # Hyper-85 rates significantly different from the normoxic rates at the same log mean DQ concentrations.

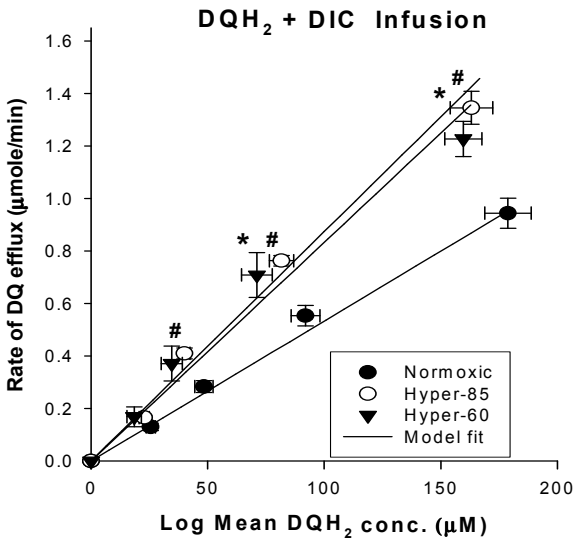

Figure 6.3 The relationship between the steady state rate of DQ efflux and the log mean DQH_2 concentrations , which are the effective intravascular DQH_2 concentrations during DQH_2 arterial infusion in the presence of dicumarol (DIC, 400 µM), for normoxic lungs (n = 6), hyper-85 lungs (n = 6), and hyper-60 lungs (n = 4). Values are mean ± SE. The solid lines are model fits to the mean values of the data. * Hyper-60 rates significantly different from the normoxic rates at the same log mean DQH_2 concentrations. # Hyper-85 rates significantly different from the normoxic rates at the log mean DQH_2 concentrations.

To evaluate the effect of rat exposure to 60% O_2 or 85% O_2 on NQO1 mediated DQ reduction, the rate of DQH_2 efflux during DQ infusion was measured in the presence of antimycin A to inhibit DQH_2 oxidation (Figure 6.4). As expected, the rates of DQH_2 efflux in the presence of

antimycin A were higher than those measured in the absence of antimycin A (Figure 6.2) over the range of infused DQ concentrations. Moreover, both O_2 levels increased the rate of DQH_2 efflux during DQ infusion at the two highest concentrations in the presence of antimycin A as compared to normoxic lungs, but the increase was larger for the hyper-85 lungs (52%) than for the hyper-60 lungs (23%) (Figure 6.4).

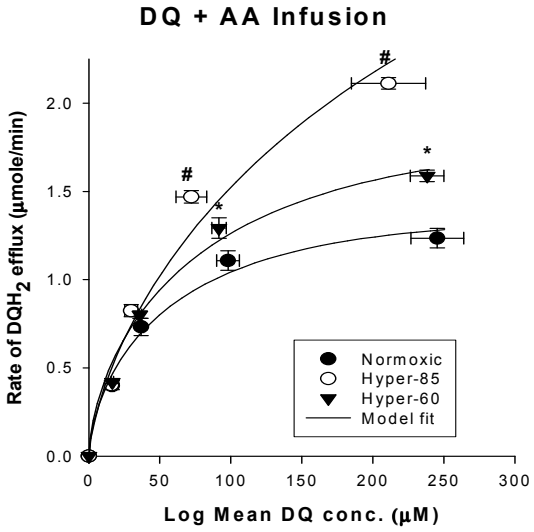

Figure 6.4 The relationship between the steady state rate of DQH_2 efflux and the log mean DQ concentrations, which are the effective intravascular DQ concentrations during DQ arterial infusion in the presence of antimycin A (AA, 10 µM), for normoxic lungs (n = 5), hyper-85 lungs (n = 5), and hyper-60 lungs (n = 5). Values are mean ± SE. The solid lines are model fits to the mean values of the data. * Hyper-60 rates significantly different from the normoxic rates at the same log mean DQ concentrations. # Hyper-85 rates significantly different from the normoxic rates at the same log mean DQ concentrations.

To evaluate the effect of rat exposure to 85% O_2 or 60% O_2 on mitochondrial complex III mediated DQH_2 oxidation, the rate of DQ efflux during DQH_2 infusion was measured in the presence of dicumarol and rotenone. Again, rotenone was added to minimize competition between DQH_2 and reduced endogenous coenzyme Q_9 hydroquinone (CoQ_9H_2) for oxidation via complex III. Figure 6.5 shows that for hyper-85 lungs, the steady state rates of DQ efflux during DQH_2 infusion at the two highest concentrations in the presence of dicumarol plus rotenone were about 30% higher than those in normoxic lungs. For all three groups of lungs, the rate of DQ efflux during DQH_2 infusion at the highest concentration in the presence of antimycin A along with dicumarol and rotenone was virtually zero. This further supports that complex III is the dominant site for DQH_2 oxidation on passage through the pulmonary circulation of all three groups of lungs.

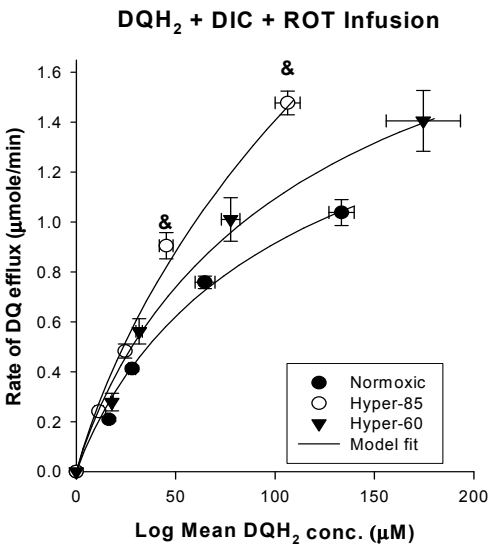

Figure 6.5 The relationship between the steady state rate of DQ efflux and the log mean DQH_2 concentrations, which are the effective intravascular DQH_2 concentrations during DQH_2 arterial infusion in the presence of dicumarol (DIC, 400 µM) plus rotenone (ROT, 20 µM), for normoxic lungs (n = 4), hyper-85 lungs (n = 4), and hyper-60 lungs (n = 4). Values are mean ± SE. The solid lines are model fits to the mean values of the data. & Hyper-85 rates significantly different from the normoxic rates at the same log mean DQH_2 concentrations.

6.3.3 Tissue Assay Results

Table 6.2 shows that rat exposure to 85% O_2 increased NOQ1 homogenate activity per lung by 72%, but had no effect on NQO1 activity per mg of protein. Exposure to 60% O_2 on the other hand had no effect on NQO1 activity in homogenate per lung or per mg of protein.

	Homogenate NQO1 Activity (µmol/min/lung)	Homogenate NQO1 Activity (nmol/min/mg protein)
Normoxic	26.5 ± 1.7	670 ± 80
Hyper-60	34.8 ± 2.0	737 ± 63
Hyper-85	45.6 ± 4.7 *,&	538 ± 43

Table 6.2 Lung homogenate NQO1 activity of normoxic, hyper-85, hyper-60 rats. Values are mean ± SE. n = 7, 10, and 7 for normoxic, hyper-60, and hyper-85 lungs, respectively. *& indicate value significantly different from the corresponding normoxic and hyper-60 values, respectively.

We also measured the activities of mitochondrial complexes I and IV in lung tissue homogenates. Table 6.3 shows that mitochondrial complex I activities normalized to protein were about 50% lower in P2 fractions derived from hyper-85 and hyper-60 lungs than normoxic lungs. Complex IV activity per mg of protein increased in only hyper-85 lung homogenates by 90% as compared to normoxic lungs (Table 6.3).

	Complex I activity (nmol/min/mg protein)	Complex IV activity (nmol/min/mg protein)
Normoxic	13.2 ± 2.3	232 ± 16
Hyper-60	6.5 ± 0.8 *	202 ± 46
Hyper-85	6.8 ± 1.2*	439 ± 51 *

Table 6.3 Mitochondrial complexes I and IV activities measured in mitochondrial fractions. Values are mean ± SE. For complexes I and IV activities, n = 5, 5, and 7 for normoxic, hyper-60, and hyper-85 lungs, respectively. * Indicates value significantly different from the corresponding normoxic value.

Table 6.4 shows that total glutathione content (oxidized plus reduced glutathione) per lung and per gram of dry lung weight increased by 101% and 20%, respectively, in hyper-85 lungs only.

	(GSH + GSSG) (μmol/lung)	(GSH + GSSG) (μmol/ g dry wt)
Normoxic	2.34 ± 0.17	10.23 ± 0.55
Hyper-60	3.09 ± 0.14	11.96 ± 0.77
Hyper-85	4.70 ± 0.39 *&	12.21 ± 0.47 *

Table 6.4 Total lung glutathione (GSH+GSSG) content. Reduced (GSH) and oxidized (GSSG) glutathione. Values are mean ± SE. n = 8, 5, and 7 for normoxic, hyper-60, and hyper-85 lungs, respectively. *& indicate value significantly different from the corresponding normoxic and hyper-60 values, respectively.

Western blots were carried out to estimate the expression of NQO1 protein in normoxic or hyper-85 lungs. There was an ~200% increase in NQO1 protein density in hyper-85 lungs and ~300% increase in hyper-60 lung (Figure 6.6). The quantitative results are listed in Table 6.5.

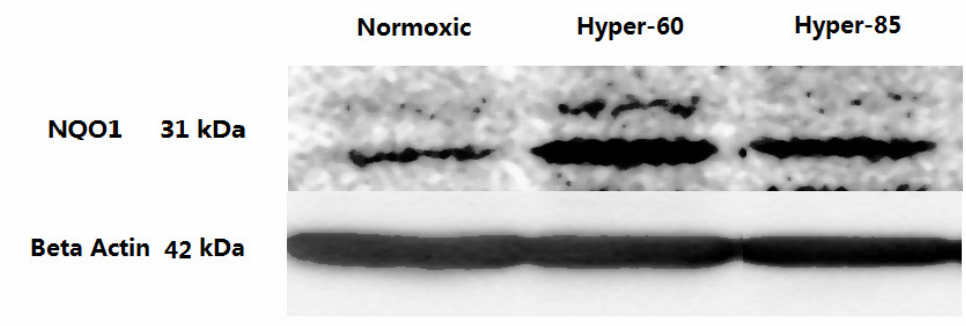

Figure 6.6 Western blots of NQO1. 1st column: normoxic rats, n=10; 2nd column: rats exposed to 60%

O_2 for 7 days, n=10; 3rd column: rats exposed to 85% O_2 for 7 days, n=12.

	Normoxic	Hyper-60	Hyper-85
NQO1 Band Intensity (%)	100	394±91*	298±85 *

Table 6.5 NQO1 band intensity of lung homogenate from normoxic rats (n=10), hyper-60 rats (n=10) and hyper-85 rats (n=12). *: significant different from the value of normoxic rats.

6.4 Kinetic Analysis of DQ/DQH_2 Pulse Infusion Data

The data in Figures 6.2-6.5 are the net result of a) DQ and DQH_2 interactions with competing nonlinear tissue redox processes, b) DQ and DQH_2 interactions with protein (i.e., BSA) in the vascular space, and c) capillary perfusion kinematics (i.e., a heterogeneous distribution, $h_c(t)$, of capillary transit times). Thus, for quantitative interpretation of the data in Figures 6.2-6.5 we utilized a kinetic model that accounts for DQ and DQH_2 tissue and vascular interactions as well as the distribution of capillary transit times (Audi et al., 2004, 2005, 2008). The model used to estimate parameters descriptive of the activities of NQO1 and complex III in the intact lung from the data in Figure 6.2-6.5 has been described in chapter 4.4.2.

The governing differential equations of the single capillary element model are the basis of the whole organ model which accounts for the distribution of pulmonary capillary transit times, $h_c(t)$. Previously, we determined $h_c(t)$ for normoxic rat lungs and hyper-85 lungs (Ramakrishna et al., 2010). These values were used in the kinetic analysis of the normoxic and hyper-85 lung data (Chapter 4). For hyper-60 lungs, $h_c(t)$ was assumed to be the same as that determined for normoxic lungs. This is based on results in Table 6.1 that show exposure to 60% O_2 for 7 days had no effect on perfused capillary surface area (*PS*), and on previous results that showed rat exposure to 60% O_2 for 7 days had no significant effect on morphometrically-measured lung capillary endothelial surface area and capillary volume (Hayatdavoudi et al., 1981).

Estimation of Model Parameters:

The unknown model parameters under steady-state conditions are V_{max1}, K_{m1a}, V_{max2}, K_{m2a}, and k_{ox} in Equation 4.7~4.10. The values of these parameters for each of the three groups of lungs were estimated using the following approach. First, the values of V_{max1} and K_{m1a}, parameters descriptive of NQO1-mediated DQ reduction, were determined. This was done by fitting the steady-state solution of the organ model to the steady state rates of DQH_2 efflux during DQ infusion in the presence of antimycin A (Figure 6.4), which corresponded to setting V_{max2} to zero in Equations (E4.3-4.4). The estimated values of these model parameters are given in Table 6.6. Rat exposure to 85% O_2 for 7 days increased V_{max1} by ~200%. The estimated values of V_{max1} for hyper-60 lungs tended to be higher than those for normoxic lungs, but the mean difference was not significant (one way ANOVA). For all three groups of lungs, the estimated value of K_{m1a} was 1 μM, which was the lower bound set for this parameter in the least squares fitting procedure. K_{m1a} is an intrinsic property of the enzyme and hence would be expected to be the same for all three groups of lungs.

	V_{max1} (μmol/min)	V_{max1} (μmol/min/g dry wt)	K_{ma1} (μM)
Normoxic	1.38± 0.07	6.4 ± 0.3	1.0
Hyper-60	1.84 ± 0.06	7.8 ± 0.5	1.0
Hyper-85	4.11 ± 0.39 *&	10.8 ± 0.7 *&	1.0

Table 6.6 Values of model parameters descriptive of NQO1-mediated DQ reduction in normoxic and hyperoxic lungs estimated from the steady-state DQH_2 efflux rates during DQ infusion in the presence of antimycin A. Values are mean ± SE. n = 5 for all three groups. V_{max1} is the maximum DQ reduction rate; K_{ma1} is the apparent Michaelis-Menten constant. *& significantly different from normoxic and hyper-60 values, respectively.

For a given lung, parameters descriptive of complex III-mediated DQH_2 oxidation (V_{max2} and K_{m2a}) were estimated by fitting the steady state solution of the organ model to the steady state

rates of DQ efflux during DQH_2 infusion in the presence of dicumarol and rotenone (Figure 6.5), with V_{max1} was set to zero in Equations (E4.3-4.4) to account for the presence of dicumarol (NQO1 inhibitor). Results in Table 6.7 show that exposure to 85% O_2 increased V_{max2} by ~180%, with no significant effect on K_{m2a}, compared to normoxic lungs. The estimated values of V_{max2} and K_{m2a} for hyper-60 lungs were not different from those estimated for normoxic lungs.

	V_{max2} (μmol/min)	V_{max2} (μmol/min/g dry wt)	K_{ma2} (μM)
Normoxic	1.67 ± 0.10	8.7 ± 0.7	42 ± 2
Hyper-60	2.07 ± 0.09	8.8 ± 0.5	38 ± 6
Hyper-85	4.65 ± 0.36 *&	13.6 ± 1.8 *&	36 ± 11

Table 6.7 Values of model parameters descriptive of complex III mediated DQH_2 oxidation in normoxic and hyperoxic lungs estimated from the steady-state DQ efflux rates during DQH_2 infusion in the presence of dicumarol plus rotenone. Values are mean ± SE. n = 4 for all three groups. V_{max2} is the maximum DQH_2 oxidation rate; K_{ma2} is the apparent Michaelis-Menten constant. *& significantly different from normoxic and hyper-60 values, respectively.

The value of k_{ox} was estimated by fitting the solution of the steady state organ model, with V_{max1} set to zero in Equations (E4.5-4.6), to the steady state rates of DQH_2 efflux during DQ infusion in the presence of dicumarol (Figure 6.3). Table 6.8 shows that rat exposure to 60% O_2 or 85% O_2 for 7 days increased the estimated value of k_{ox} by ~70% and ~140%, respectively, as compared to normoxic lungs.

	k_{ox} (ml/min)	k_{ox} (ml/min/g dry wt)
Normoxic	6.38 ± 0.60	27.6 ± 2.9
Hyper-60	10.84 ± 1.25 *	43.1 ± 4.0 *#
Hyper-85	15.16 ± 1.58 *&	35.0 ± 8.4

Table 6.8 Parameters descriptive of DQH_2 oxidation capacity. Values are mean ± SE. n = 6, 4 and 6 for normoxic hyper-60 and hyper-85 lungs, respectively. k_{ox} is rate of DQH_2 oxidation on passage through the pulmonary circulation. *&, # significantly different from normoxic, hyper-60, and hyper-85 values,

respectively.

A second estimate of the values of V_{max1} and K_{m1a} for normoxic and hyperoxic lungs was obtained by fitting the steady state organ model solution to the steady state rates of DOH_2 efflux during DQ infusion in the absence of inhibitors (Figure 6.2), with k_{ox} in Equations (E4.5-4.6) set to the mean values in Table 6.8. The estimated values of V_{max1} for hyper-60 and hyper-85 lungs were ~80% and 140% higher than that estimated for normoxic lungs, respectively (Table 6.9).

	V_{max1} (μmol/min)	V_{max1} (μmol/min/g dry wt)	K_{ma1} (μM)
Normoxic	1.46 ± 0.10	7.2 ± 0.8	4.4 ± 1.4
Hyper-60	2.64 ± 0.08*	11.8 ± 0.5*	12.5 ± 2.1$^{*\#}$
Hyper-85	3.52 ± 0.12$^{*\&}$	10.1 ± 0.6*	6.4 ± 1.6

Table 6.9 Values of model parameters descriptive of NQO1-mediated DQ reduction in normoxic and hyperoxic lungs estimated from the steady-state DQH_2 efflux rates during DQ infusion. Values are mean ± SE. n = 4, 5 and 5 for normoxic hyper-60 and hyper-85 lungs, respectively. V_{max1} is the maximum DQ reduction rate; K_{ma1} is the apparent Michaelis-Menten constant. The DQH_2 oxidation rate, k_{ox}, was set to the mean value in Table 6.6. $*^{\&, \#}$ significantly different from normoxic, hyper-60, and hyper-85 values, respectively.

For normoxic and hyper-85 lungs, the values of V_{max1} in Table 6.9 vs. Table 6.6, i.e. estimated from the steady state rates of DQH_2 efflux during DQ infusion in the absence or presence, respectively, of antimycin A were not different. This is consistent with the hypothesis that the dominant effect of antimycin A is on complex III- mediated DQH_2 oxidation. However, for hyper-60 lungs, the estimated values of V_{max1} were statistically different for the two approaches. In the discussion below, we speculate on possible reasons for this difference.

6.5 Discussion and Conclusions

The results of the present study demonstrate that rat exposure to 85% O_2 or 60% O_2 for 7 days increases the capacity of the lung to reduce DQ to DQH_2 by 37%. Inhibitor studies and

kinetic analysis revealed that for hyper-85 lungs this increase can be accounted for by a 140% increase in the capacity (V_{max1}) of NOQ1 mediated DQ reduction and a 138% increase in the rate (k_{ox}) of DQH_2 oxidation on passage through the pulmonary circulation. For hyper-60 lungs, the 37% increase in the rate of DQH_2 efflux during DQ infusion can be accounted for by an 80% and 70% increase in V_{max1} and k_{ox}, respectively. Moreover, kinetic analysis revealed that the capacity (V_{max2}) of complex III mediated DQH_2 oxidation increased by ~180% in hyper-85 lungs, with no change in hyper-60 lungs.

In addition to increasing V_{max1}, V_{max2}, and k_{ox}, rat exposure to 85% O_2 for 7 days increased lung dry weight (Table 6.1), presumably due to a large increase in the number of interstitial cells (Crapo et al., 1974, 1980). This brought into question whether the estimated increase in these extensive kinetic parameters was simply the result of an increase in tissue mass (i.e., more cells). As shown in Tables 6.6 and 6.8, the increase in the dry weight of hyper-85 lungs cannot account for all of the increase in the values of V_{max1} and V_{max2} since the values of V_{max1} and V_{max2} per gram of dry lung are respectively 40% and 56% higher than corresponding values for normoxic lungs. However, for hyper-85 lungs the increase in k_{ox} may be accounted for by the increase in dry lung weight (Table 6.8). The above results suggest that rat exposure to 85% O_2 for 7 days induced an increase of 40% and 56% in the lung activities of NQO1 and complex III per gram of dry lung weight, respectively.

Normalizing the above extensive parameters to lung dry weight assumes that all lung cells are accessible to DQ and DQH_2 on their passage through the pulmonary circulation. This assumption is based on the amphipathic nature of these redox active quinone compounds, which have high octanol:water partition coefficients along with significant water solubility (Audi et al.,

2004, 2005, 2008; Merker 2004, 2006). As a result, these compounds rapidly equilibrate between blood and tissue during passage through the pulmonary capillary bed (Audi et al., 2004, 2005, 2008).

As described above, for normoxic and hyper-85 lungs, the estimates of V_{max1} obtained using two independent data sets, i.e. DQH_2 efflux rates during DQ infusion in the absence or presence of antimycin A, are not significantly different (Tables 6.6 and 6.9). However, for hyper-60 lungs the difference in the estimated values of V_{max1} obtained from the two data sets is 42%. One possible reason for this difference might be that treatment of hyper-60 lungs with antimycin A not only inhibited complex III mediated DQH_2 oxidation, but also partially inhibited NQO1 mediated DQ reduction or other DQ reductase(s) (Von & Bohrer, 1975). In addition to inhibiting DQH_2 oxidation, antimycin A would be expected to suppress ATP production via oxidative phosphorylation. This impairment to oxidative ATP production could stimulate anaerobic glycolysis (Ahmad, White & Chang, 2001; Allen, Guo & White, 1998; Allen & White, 1998a; Schoonen, Wanamarta & Moorsel, 1990). This in turn would divert glucose-6-phosphate from the pentose phosphate pathway, the main source of NADPH for NOQ1 (Bongard et al., 2009). Although isolated NQO1 can utilize either NADH or NADPH as a reducing cofactor (Ross, Kepa & Winski, 2000), Bongard et al. (Bongard et al., 2009) demonstrated that NADPH is the endogenous NQO1 electron donor in cultured bovine pulmonary arterial endothelial cells. This suggests that for hyper-60 lungs the rate of NAPDH production in the presence of antimycin A may not be sufficient to maintain the maximum capacity of NQO1 for DQ reduction that is measurable in the absence of antimycin A (Figures 6.2 and 6.4). This explanation is consistent with previous studies which demonstrated that rat exposure to 85% O_2 for 7 days, but not 60% O_2

increased lung glucose-6-phosphate dehydrogenase and hexokinase activities as compared to normoxic lungs (Table 6.9) (Allen 1998, Hayatdavoudi et al., 1981). Glucose-6-phosphate is the substrate for the pentose phosphate pathway and hexokinase catalyzes the phosphorylation of intracellular glucose to glucose-6-phosphate, an important step for the cellular uptake of glucose. In addition, exposure to 85% O_2, but not 60% O_2 increased total glutathione content per lung and per gram of dry lung weight as compared to normoxic lungs (Table 6.4).

Figure 6.8 shows high correlation between NQO1 homogenate activity and the capacity (V_{max1}) of NQO1 mediated DQ reduction in normoxic, hyper-60, and hyper-85 lungs. However, the increase in V_{max1} is larger than the increase in NQO1 homogenate activity in hyper-60 and hyper-85 lungs. One possible reason for this difference may be that hyperoxia-induced changes in key aspects of the intact lung environment that may regulate NQO1 activity (e.g., availability of electron donors and their accessibility to the enzyme) are not preserved in lung homogenates (Audi et al., 2005). Another reason may be that other dicumarol-inhibitable reductase(s) besides NQO1 contribute to DQ reduction during its passage through the pulmonary circulation (Von & Bohrer, 1975; Gonzales-Aragon, Ariza & Villalba, 2007; Zhu & Beattie, 1988). This could be evaluated by using a different NQO1 inhibitor, e.g.5-methoxy-1,2-dimethyl-3-[(4-nitrophenoxy)methyl]indol-4,7-dione (ES936), that inhibits NQO1 by an alternative mechanism (Bongard et al., 2009). Previously, we showed that both dicumarol and ES936 equally inhibited DQ reduction in cultured bovine pulmonary artery endothelial cells (Merker et al., 2006). Although NQO1 is predominantly a cytosolic enzyme (> 90%), non-cytosolic NQO1activity has been previously reported (Beattie, Japa & Howton, 1992; Gonzales-Aragon et al., 2007; Tan & Berridge, 2010). Thus, another reason for the above difference may be that these O_2 levels induced

an increase in NQO1 activity in the non-cytosolic fraction of the lung tissue which was not preserved in the tissue homogenate used for the NQO1 assay. Several studies have evaluated the role of NQO1 in protection against pulmonary O_2 toxicity (Cho et al. 2002; Whitney et al., 1993). Whitney et al. (1993) found that treatment with dicumarol (NQO1 inhibitor) did not diminish the survivability of adapted adult rats in 100% O_2, and that the induction of NQO1 did not significantly improve the survivability of adult rats exposed to lethal O_2 levels. The results with dicumarol treatment may be in part because dicumarol has such a high affinity for plasma proteins that only a small fraction would be taken up by the lung in vivo (Whitney 1993). Cho et al. (2002)

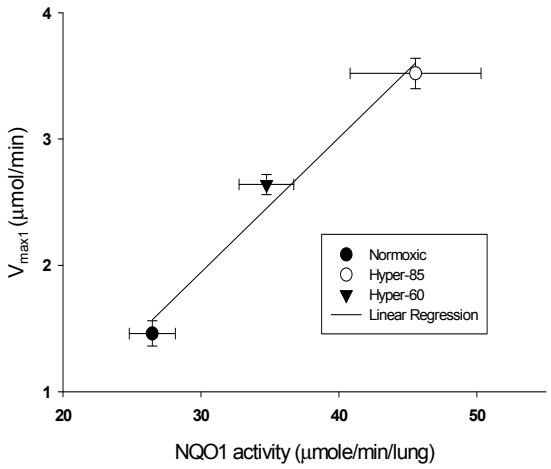

Figure 6.7 Relationship between total NQO1 activity in lung tissue homogenates (Table 6.2) and the capacity (V_{max1}) of NQO1 mediated duroquinone (DQ) reduction (Table 6.8) on passage through the pulmonary circulation of normoxic, hyper-60, or hyper-85 lungs. Values are mean ± SE. Solid line is linear model fit (r^2 = 0.975).

showed that mice deficient in the transcription factor Nrf2, which is involved in the induction of phase II enzymes including NQO1, had significantly lower lung NQO1 mRNA expression and were significantly more sensitive to hyperoxia (> 95% O_2 for 72 hours) than wild type mice. Furthermore, they showed that exposure of wild type mice to hyperoxia increased their lung homogenate NQO1 activity. Unlike rats, mice do not develop tolerance to 100% O_2 following exposure to 85% O_2 (Capellier, Maupoil & Boussat, 1999; Crapo et al., 1974). Previously we demonstrated that rat exposure to 85% O_2 for 21 days, but not for 2 days, increased the capacity of

NQO1 mediated DQ reduction on passage through the lungs, and suggested a potential role for NQO1 in rat tolerance to 100% O_2. One of the objectives of this study was to determine if rat exposure to 60% O_2 for 7 days or 85% O_2 for 7 days has a differential effect on the lung activity of NQO1. Demonstration that the activity of a redox enzyme is differentially altered by exposure to 60% O_2 versus 85% O_2 would be suggestive of a role in conferring susceptibility or tolerance to 100% O_2. However, the results of this study reveal that both hyperoxic O_2 levels appear to increase NQO1 activity in the intact lung.

Previous studies have suggested complex I as a site of DQ reduction (Fato, Bergamini & Leoni, 2008; Zhu & Beattie, 1988). This raises the question of whether the increase in the DQ efflux rate during DQH_2 infusion in the presence of rotenone plus dicumarol (Figure 6.5) versus dicumarol alone (Figure 6.3) is due to inhibition of complex I mediated DQ reduction or an increase in DQH_2 oxidation. The latter has to do with the fact that inhibiting complex I results in more oxidized state of complex III. The results of the present study demonstrate that NQO1 is the dominant reductase of DQ on passage through the pulmonary circulation since lung treatment with dicumarol decreased the rate of DQH_2 efflux during DQ infusion by > 95% for all three groups of lungs. Thus, complex I cannot be contributing significantly to the reduction of DQ on passage through the rat lung. Moreover, Table 6.3 shows that exposure to 60% O_2 or 85% O_2 resulted in a ~50% decrease in complex I activity in lung tissue homogenate. Hence, complex I activity cannot account for the increase in DQ reduction capacity of hyper-60 and hyper-85 lungs. Furthermore, Audi et al. showed in a previous study that the rate of DQH_2 efflux during DQ infusion in the presence of potassium cyanide (KCN) was the same as that in the presence of KCN plus rotenone (Audi et al., 2004). Again, inhibition of mitochondrial complex IV by KCN reduces complex III

and as a result inhibits complex III mediated DQH_2 oxidation (Audi et al., 2004, 2005, 2008). These results suggest that the rotenone effect on the steady state rate of DQ efflux during DQH_2 infusion (Figures 6.3 and 6.5) is predominantly on DQH_2 oxidation rate, rather than on DQ reduction rate. Again, the difference in the rate of DQ efflux during DQH_2 infusion in the presence of dicumarol (Figure 6.3) as compared to that in the presence of dicumarol plus rotenone (Figure 6.5) is consistent with competition between infused DQH_2 and complex I generated coenzyme Q_9 hydroquinone (CoQ_9H_2) for complex III mediated oxidation. Hence, this difference is a measure of the capacity of complex I for generating reducing equivalent (CoQ_9H_2) and of lung tissue rotenone-sensitive O_2 consumption. Previously, we estimated the rate of rotenone-sensitive O_2 consumption in normoxic lungs to be ~1.4 μmol/min/gram dry lung wt (Audi et al., 2003). This rate (which needs to be multiplied by two for comparison with the difference in DQ efflux rate in Figure 6.8) is comparable with the maximum difference in DQ efflux rate (~2.4 μmol/min/gram dry lung wt) in normoxic lungs (Figure 6.8).

For hyper-85 lungs, the difference in DQ efflux rate (Figure 6.8) was comparable to that for normoxic lungs. However, for hyper-60 lungs the difference was ~ 50% smaller than that for normoxic lungs (Figure 6.8). This suggests a potential decrease in the capacity of complex I for generated CoQ_9H_2 in hyper-60 lungs as compared to normoxic and hyper-85 lungs. This could be due to a decrease in lung tissue complex I activity and/or decrease in the rate of the metabolic coenzyme NADH supplied to complex I. Table 6.3 shows that exposure to 85% O_2 or 60% O_2 for 7 days decreased lung complex I activity (per mg of protein) by ~50% . This decrease appears to have no significant effect on the capacity of complex I for generating CoQ_9H_2 in hyper-85 lungs (Figure 6.8) suggesting a possible increase in the rate of NADH supplied to complex I to

compensate for the decrease in complex I activity. This would be consistent with an increase in tissue activities of glucose transporters and hexokinase in lungs of rats exposed to 85% O_2 for 7 days. For hyper-60 lungs, the decrease in complex I activity (Table 6.3) is proportional to the decrease in the rate of complex I generated CoQ_9H_2 (Figure 6.8).

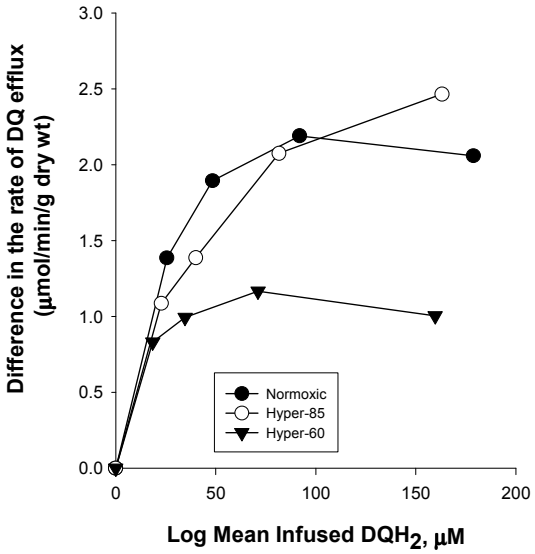

Figure 6.8 The relationship between the difference in steady state rates of DQ efflux during DQH_2 infusion in the presence of dicumarol plus rotenone (Figure 6.5) and dicumarol alone (Figure 6.3) and the log mean DQH_2 concentrations, for normoxic lungs, hyper-85 lungs, and hyper-60 lungs respectively. Model-based interpolation was used to determine the rates of DQ efflux in the presence of dicumarol plus rotenone (Figure 6.5) at the same log mean DQH_2 concentrations as in Figure 6.3.

Rat exposure to 85% O_2, but not to 60% O_2, for 7 days increased lung activities of complexes III and IV by 56% and 90%, respectively. This may be a compensatory mechanism to counter the potential effects of the decrease in lung complex I activity on mitochondrial ATP production (Desquiret, Gueguen & Malthiery, 2008). The increase in lung complexes III and IV activities could also be a means of decreasing ROS production at complex III, which involves the donation of electrons from ubisemiquinone to molecular O_2 since the higher the respiration rate the less time the electrons are delayed at critical leakage sites such as complex III (Li et al., 2004). Additional studies would be needed to evaluate the effect of this increase in complexes III and IV on mitochondrial ATP and ROS production.

Ratner et al. demonstrated that exposure of neonatal mice to hyperoxia (75% O_2 for 72

hours) decreases complex I activity by ~70%, and that this decrease compromises mitochondrial oxidative phosphorylation and contributes to alveolar development arrest (Ratner et al., 2009). Based on these results, they concluded the decrease in complex I plays a key role in lung O_2 toxicity. In the present study, exposure to 60% O_2 or 85% O_2 for 7 days decreased complex I activity by ~ 50%. However, for hyper-85 lungs the effect of this decrease on oxidative phosphorylation may have been countered by an increase in the lung activities of glucose transporters and hexokinase upstream from complex I, and by increases in the activities of complexes III and IV downstream from complex I (Table 6.9).

The results of the present study demonstrate an increase in lung tissue total glutathione (GSH) content per mg of protein in hyper-85 lungs as compared to normoxic lungs (Table 6.4). This is consistent with an increase in γ-glutamyltransferase activity in tissue homogenates of hyper-85 lungs, but not hyper-60 lungs, reported by Van Klaveren et al. (Table 6.9) (Van, Dinsdale & Pype, 1997). This enzyme is important for the uptake of substrates for intracellular GSH synthesis. However, in the same study Van Klaveren et al. reported no increase in GSH level in hyper-85 tissue homogenates per mg protein, which is different from the results in the present study (Van et al., 1997). This difference may be in part due to differences in rat strains (Wistar vs. Sprague-Dawley) and/or the methods used to measure tissue GSH content. The increase in GSH content in hyper-85 lung homogenates measured in the present study is potentially important since GSH is the major mechanism for scavenging H_2O_2 in endothelial cells, and since H_2O_2 is the most cytotoxic ROS in endothelial cells, which are a primary target of lung O_2 toxicity (Suttorp, Toepfer & Roka, 1986).

	Hyper-60	**Hyper-85**	**Reference**
NQO1 (per g of dry wt)	+ 64%	+40%	Present study

Complex III (per g dry wt)	NS	+56%	Present study
Complex I (per mg protein)	-51%	-49%	Present study
Complex IV (per mg protein)	NS	+90%	Present study
ACE	NS	-57%	Present study
k_{ox} (per g dry wt)	+56%	NS	Present study
Lung glutathione content (per g dry wt)	NS	+20	Present Study
G-6-PDH (per g dry wt)	NS	+68%	(Hayatdavoudi et al., 1981)
Hexokinase (per mg protein)	NA	+44%	(Allen 2001)
γ-glutamyltransferase (μU/mg)	NS	220%	(Van 1997)

Table 6.9 Summary of the effect of rat exposure to 60% or 85% O_2 for 7 days compared with normoxic rats on cell surface, cytosolic, and mitochondrial enzymes. K_{ox} (ml/min/g dry wt) is the rate of DQH_2 oxidation on passage through the pulmonary circulation. ACE, angiotensin converting enzyme; G-6-PDH, glucose 6 phosphate dehydrogenase. NS and NA, not significant and not available, respectively.

In conclusion, the results demonstrate that NQO1 activity increased in both hyper-60 and hyper-85 lungs, whereas complexes III activity increased in hyper-85 lungs only. This increase along with the increase in complex IV activity in hyper-85 lungs could be to counter the effects the depression in complex I activity might have on cellular energy homeostasis and/or mitochondrial ROS production, and hence be potentially important to the tolerance to 100% O_2 observed in hyper-85 rats. These results demonstrate the utility of these two hyperoxic models and indicator dilution methods for furthering our understanding of the pathogenesis of lung O_2 toxicity, and for providing insights into the underlying mechanisms of rat tolerance and susceptibility to 100% O_2.

CHAPTER 7. RHODAMINE DYES AS EXTRACELLULAR PROBES OF MITOCHONDRIAL AND PLASMA MEMBRANE POTENTIALS IN INTACT BOVINE PULMONARY ARTERIAL ENDOTHELIAL CELLS

7.1 Introduction

Pulmonary endothelial mitochondrial membrane potential ($\Delta\Psi_m$) and plasma membrane potentials ($\Delta\Psi_p$) are implicated in bioenergetic, metabolic and signaling processes which contribute to lung function under physiologic and pathophysiologic conditions (Chatterjee, Chapman & Fisher, 2008; Han, Moon & You, 2010; Madesh, Hawkins & Milovanova, 2005; Ruchko, Gorodnya & Ledoux, 2005; Wu, Jian & Xu, 2009; You & Park, 2010). For instance, $\Delta\Psi_m$ is the major component of the mitochondrial electrochemical transmembrane potential, and as such is involved in pulmonary endothelial mitochondrial ATP generation, regulation of calcium homeostasis, apoptosis, nitric oxide signaling and other functions (Dedkova & Blatter, 2005; Solaini, Sgarbi & Lenaz, 2007; Sud, Wells & Sharma, 2008; Terminella, Tollefson & Kroczynski, 2002). Dissipation of $\Delta\Psi_m$ is considered a hallmark of mitochondrial dysfunction in various cell types, including in pulmonary endothelial cells exposed to oxidative stresses (Han et al., 2010; Madesh et al., 2005; Mungunsukh, Griffin & Lee, 2010; Ruchko et al., 2005; You & Park, 2010). On the other hand, pulmonary endothelial $\Delta\Psi_p$ is implicated in regulating channel mediated calcium entry as a key signaling response to mechanical stimuli, vasoactive substances, oxidative stress, ischemia and hypoxia (Cannell & Sage, 1989; Chatterjee et al., 2006; Koliwad, Kunze & Elliott, 1996; Paffett, Jo & Pak, 2007; Stevens et al., 1994; Wu et al., 2009; Zhang, Chatterjee & Wei, 2008). Since the pulmonary capillary endothelium is a primary and early target of lung O_2 toxicity, the ability to quantify $\Delta\Psi_m$ and $\Delta\Psi_p$ is important for characterizing biochemical mechanisms underlying pulmonary endothelial responses to oxidative stress (e.g. hyperoxia), and

to evaluate the utility of therapeutics directed at restoration of normal mitochondrial function.

While various techniques have been reported for evaluating $\Delta\Psi_m$ in different cell types, a typical approach has been to use cationic fluorescent dyes that accumulate in the mitochondrial matrix driven by the voltage gradient across the inner mitochondrial membrane (Ehrenberg, Montana & Wei, 1988; Huang, Camara & Stowe, 2007; Scaduto & Grotyohann, 1999; Solaini, Sgarbi & Lenaz, 2007; Ward 2010). Such studies generally have involved measurements of fluorescence intensity within cells or isolated mitochondria. Because such measurements are easily confounded by the propensity of the dyes to undergo self-aggregation and quenching, photobleaching and/or to exert phototoxic effects, the outcomes have been predominately confined to qualitative changes in $\Delta\Psi_m$ (Ehrenberg et al., 1988; Huang et al., 2007; Huser & Blatter, 1999; Scaduto et al., 1999; Solaini et al., 2007; Ward 2010). In addition, the vast majority of studies have involved mitochondrial isolation, cell permeabilization or other conditions that have little relevance for intact cells, and yet, when intact cells have been studied, the contributions of processes other than $\Delta\Psi_m$ (e.g., the multi-drug transporter Pgp and/or $\Delta\Psi_p$) to dye disposition have often been overlooked (Baracca, Sgarbi & Solaini, 2003; Duchen et al., 2003; Huang et al., 2007; Nicholls et al., 2006; Yeheskely, Regev & Katzir, 2009).

The goal of this study was to develop a means to quantify $\Delta\Psi_m$ and $\Delta\Psi_p$ in intact pulmonary endothelial cells using two common membrane potential sensitive cationic fluorescent dyes, rhodamine 123 (R123) and tetramethylrhodamine ethyl ester (TMRE). The overall approach was to focus on the impact of the pulmonary arterial endothelial cells in culture on the extracellular concentrations of the dyes under a range of experimental conditions designed to separate the contributions of $\Delta\Psi_m$, $\Delta\Psi_p$ and Pgp to the net effect of the cells on the dyes. A kinetic

model was developed to interpret the data and to obtain parameter values for $\Delta\Psi_m$, $\Delta\Psi_p$ and Pgp for both dyes. R123 and TMRE were selected because whereas TMRE is more cell membrane permeable than R123, both have relatively strong fluorescence quantum yields, low sensitivity to changes in the cellular environment and undergo membrane potential-dependent changes in distribution across both the mitochondrial and plasma membranes (Duchen et al., 2003; Enrenberg et al., 1988; Loetchutinat, Saengkhae & Marbeuf, 2003; Solaini et al., 2007; Ward 2010). Thus, one concept was that the utility of the proposed approach for quantifying $\Delta\Psi_m$ and $\Delta\Psi_p$ in pulmonary arterial endothelial cells would be revealed by the consistency of the parameter values obtained from the studies with two dyes that have both distinct (i.e. different membrane permeabilities) and common (i.e. mitochondrial and plasma membrane potentials) properties.

7.2 Materials and Methods

Materials

Fetal bovine serum was purchased from Hyclone Laboratories (Logan, UT, USA), RPMI 1640 tissue culture medium and tetramethyrhodamine ethyl ester (TMRE) from Invitrogen (Carlsbad, CA), Biosilon microcarrier beads from Nunc (Roskilde, Denmark) and the protein assay reagent from Bio-Rad Laboratories (Hercules, CA). The multi-drug efflux transporter P-glycoprotein (Pgp) inhibitor *N*-(4-[2-(1,2,3,4-tetrahydro-6,7-dimethoxy-2-isoquinolinyl) ethyl]-phenyl)- 9,10-dihydro-5-methoxy-9-oxo-4 acridine carboxamide (GF120918) was generously supplied by GlaxoSmithKline (Research Triangle Park, NC). Rhodamine 123 (R123) and other chemicals unless specifically noted were purchased from Sigma Chemical (St. Louis, MO).

7.2.1 Endothelial Cell Culture

Bovine pulmonary arterial endothelial cells were isolated from segments of calf pulmonary artery obtained from a local slaughterhouse and cultured to confluence on gelatin coated (2% vol/wt) Biosilon (polystyrene) microcarrier beads (230 μm mean diameter; 160 cm^2/ml beads) in RPMI-1640 medium supplemented with 10% fetal calf serum, 100 U/ml penicillin, 100 μg/ml streptomycin and 30 mg/ml L-glutamine as previously described (Merker, Bongard & Linehan, 1997). The control cells were grown in room air, and exposure of the cells to hyperoxia (95% O_2, 5% CO_2, 48 hours) was carried out as previously described (Merker et al., 2006, 2007).

7.2.2 Measurement of Rhodamine Dye Concentrations in Extracellular Medium

For experiments with R123 or TMRE, ~0.40 ml of settled confluent cell-coated beads (~59 cm^2 cell surface area) or ~0.17 ml of confluent cell coated beads (~28 cm^2 cell surface area), respectively (128,000 cells/cm^2 surface area), were washed free of the culture medium by resuspension in Hanks balanced salt solution containing 5.5 mM glucose and 10 mM 4-(2-hydroxyethyl)-1-piperazineethanesulfonic acid (HEPES), pH 7.4, warmed to 37^oC (HBSS/HEPES), as previously described (Merker, Olson & Bongard, 1998). The cell-coated beads were allowed to settle (settling time ~ 15 sec), the supernatant was discarded, and the washing procedure repeated two more times. The washed cell-coated beads were then resuspended in 10mm x 10mm x 48mm acrylic fluorometric cuvettes containing 2.5 or 3.0 ml HBSS/HEPES 37^oC (“control medium”) and R123 or TMRE (10, 30 and 100 nM). Immediately, the beads were allowed to settle to the bottom of the cuvette, and the fluorescence intensity in the medium above

the settled cell-coated beads was measured (R123, λ_{ex} = 490 nm, λ_{em} = 525 nm; TMRE, λ_{ex} = 530 nm, λ_{em} = 573 nm) using a Perkin Elmer LS55 luminescence spectrometer. The dye concentrations ($[R_e]$) in the extracellular medium were calculated from a standard curve prepared on the same day in the same medium used in cell experiments. After the initial measurements (t = 0 min), the cell-coated bead suspension was then placed on a Nutator mixer at 37^{o}C. Periodically the mixing was stopped, the cell-coated beads were allowed to settle to the bottom of the cuvette and fluorescence intensity in the medium above the settled beads was measured. The same protocol was also carried out using the protonophore CCCP (0.1, 0.2, 0.3 and 5 μM), high K^+ (138 mM KCl/5 mM NaCl) and/or the Pgp inhibitor GF120918 (2.5 μM) and in the absence of cells, the latter to determine the contribution of nonspecific dye interactions with the plasticware.

7.2.3 Additional Measurements

To assess cellular viability, total cellular and medium lactate dehydrogenase (LDH) activity were measured at the end of each experiment, to determine % LDH release into the medium as previously described (Merker et al., 1998). Cell protein was measured using the Bio-Rad protein assay, and cell bead weights were obtained by drying and weighing the beads at the end of each experiment (Merker et al., 1998).

7.3 Results

7.3.1 Cell Protein, Cell Surface Area

Microcarrier bead surface area, cell protein, cell protein/cm^2 cell culture area and % total cell LDH released into the medium at the end of the experiments, expressed as mean ± SE., for all R123 experiments combined were 59.00 ± 1.20 cm^2, 1.54 ± 0.06 mg, 26.09 ± 1.04 μg/cm^2 and

2.73 ± 0.24%, respectively (n = 55). For all TMRE experiments, the combined values were 28.31 ± 0.77 cm^2, 0.74 ± 0.03 mg, 26.35 ± 0.85 μg/cm^2 and 2.68 ± 0.20% (n = 68), respectively. There were no detectable differences between values for these parameters in control and inhibitor-treated experimental groups ($p > 0.05$).

7.3.2 Time Course of Changes in the Extracellular Concentrations of R123 and TMRE in the Absence and Presence of Various Inhibitors

Figure 7.1 shows R123 (A) and TMRE (B) concentrations in the medium ($[R_e]$) surrounding the pulmonary arterial endothelial cell-coated beads, normalized to the initial dye concentrations. In the presence of the cells, the normalized $[R_e]$ for both dyes decreased throughout their respective incubation periods in a manner that was independent of dye concentration. For R123, the normalized $[R_e]$ fell continually throughout the 120 min incubation period (Figure 7.1 A). For TMRE, it reached a steady-state within ~ 30 min that was maintained throughout the 60 min incubation period (Figure 7.1 B). The decreases in the normalized $[R_e]$ over time were cell dependent since there was relatively very little change in the absence of cells (Figures 7.1 A and B). Thus, the decreases in dye concentration in the extracellular medium were interpreted as dye uptake by the cells.

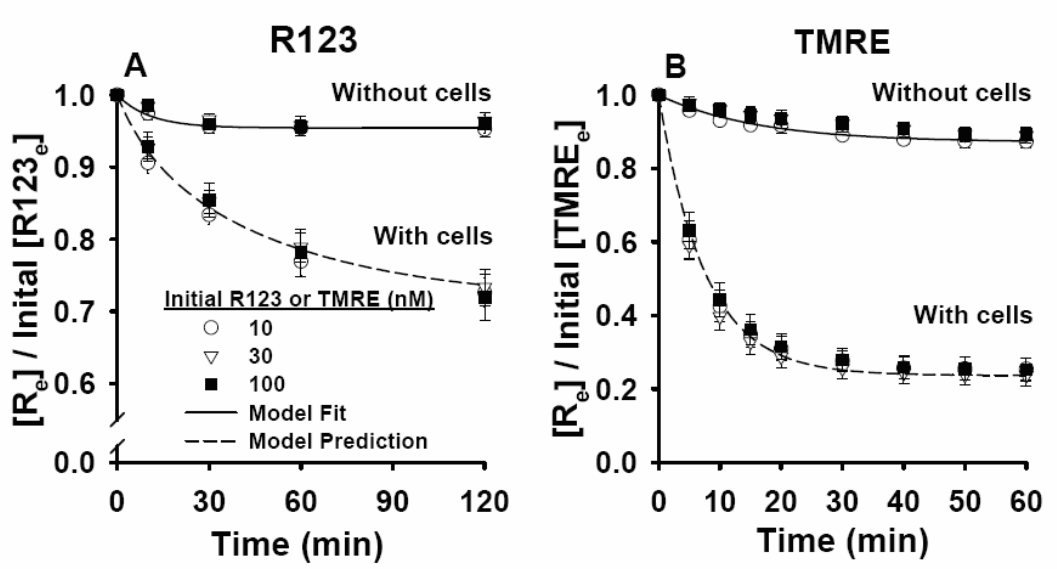

Figure 7.1 Normalized concentrations of R123 and TMRE in the medium surrounding the pulmonary arterial endothelial cell-coated beads vs. time. (A) Medium containing R123 (10, 30 and 100 nM) or (B) TMRE (10, 30 and 100 nM) was added to the cell coated beads and the dye concentrations in the medium ($[R_e]$) measured over time. The measured dye concentrations were normalized to the initial dye concentrations. Also shown are the normalized (A) R123 or (B) TMRE concentrations in the medium over time in the absence of cells. The symbols represent data without cells (n=3) and data with cells (n=4). The solid line is Equation (8) fit to the data and the dashed lines are model predictions using the parameter values in Table 7.1.

TMRE uptake was more rapid than R123 because it is more highly cell membrane permeant (Duchen et al., 2003; Loetchutinat et al., 2003). Accordingly, $[R_e]$ for TMRE reached the steady state more rapidly than the R123 data, thereby allowing the time course for TMRE studies to be comparatively shorter. We also used fewer cells (i.e., a lower cell coated bead surface area) for TMRE than for R123 studies (28 vs. 59 cm^2 confluent cell coated beads) because if we used the higher number for TMRE also, the cellular uptake of TMRE was so extensive that $[R_e]$ would rapidly approach zero, decreasing the sensitivity (i.e., dynamic range) of the measurement to experimental manipulation. On the other hand, if we used the lower surface area for the R123 studies, the time course required to obtain sufficient data to interpret would be too long to be consistent with high cell viability. The dye concentrations selected for further study were within the linear dye concentration vs. fluorescence intensity range, i.e., below the

aggregation threshold concentration for both dyes (10 nM for R123 and 20 nM for TMRE; data not shown) (Duchen et al., 2003; Huang et al., 2007).

The next step was to separate the contributions of $\Delta\Psi_m$, $\Delta\Psi_p$ and Pgp to the net effect of the cells on $[R_e]$. The approach was to use the protonophore CCCP, high K^+ or GF120918. CCCP was primarily directed at dissipation of $\Delta\Psi_m$ and high K^+ at $\Delta\Psi_p$ (Adams et al., 2004; Basuroy, Bhattachcharya & Leffler, 2009; Chatterjee et al., 2008; Carpo et al., 1980). GF120918 was used as the Pgp inhibitor (Roerig, Audi & Ahlf, 2004; Ward, 2010).

With regard to the concentrations of modulators used, 5 μM CCCP has been used to target the mitochondrial respiratory chain in cerebral microvascular endothelial cells (Basuroy et al., 2009). The high $[K^+]$ (143 mM; replacement of NaCl in the experimental buffer with KCl) was used to accomplish complete $\Delta\Psi_p$ depolarization, as specified by the Nernst equation, and as used for simultaneous determination of cell membrane potentials using microscopic measurements of rhodamine dyes (Farkas, Wei & Febbroriello, 1989; He & Curry, 1995). 2.5 μM GF120918 was based on our previous studies demonstrating that the maximum effect of GF120918 on rhodamine 6G accumulation in the perfused rabbit lung was attained at 2 mM (Roerig et al., 2004).

As can be seen in Figures 7.2A and B, the effects of the treatments on the $[R_e]$ vs. time progress curves for R123 and TMRE were qualitatively similar but quantitatively different. In general, CCCP and high K^+ attenuated the fall in $[R_e]$ for both dyes, whereas GF120918 had the opposite effect (Figures 7.2 A and B). The overall implication was that dissipation of $\Delta\Psi_m$ or $\Delta\Psi_p$ with CCCP or high K^+, respectively, decreased the extent of dye uptake by the cells. On the other hand, Pgp inhibition had the apparent effect of increasing dye uptake, but this was presumably via blockade of dye transport out of the cells (Katzir, Yeheskely & Regev, 2010; Yeheskely et al.,

2009).

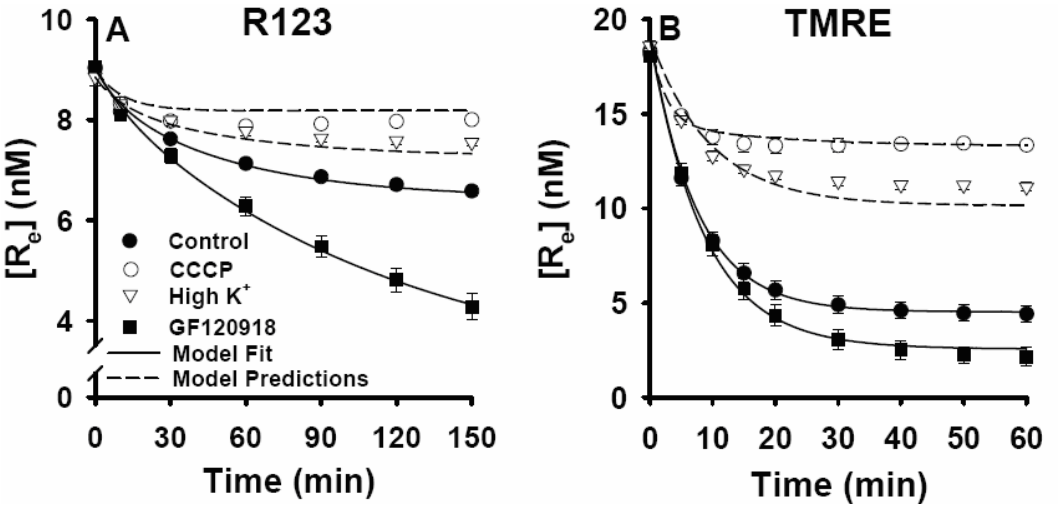

Figure 7.2 Effects of CCCP, high K+ and GF120918 on the concentrations of R123 and TMRE in the medium surrounding the cell-coated beads. The symbols represent the medium concentrations, [R_e], (mean ± SE) for the following number (n) of experiments: (A) control, 11; CCCP, 10; high K^+, 4; GF120918, 5; (B) all conditions, 8. The solid lines are the model fit to the data and the dashed lines are the model predictions using the Table 7.1 parameter values.

In Figures 7.3 A and C, [R_e] vs. time for R123 or TMRE, respectively, was measured for control and CCCP treated cells. As in Figure 7.2, the fall in [R_e] for R123 and TMRE was attenuated in the presence of CCCP. At the time point indicated by the dotted vertical lines, CCCP was added to both control cells and to the cells that had been treated with CCCP from the beginning of the experiment. The latter was to control for any effect of experimental time course on the addition of CCCP.

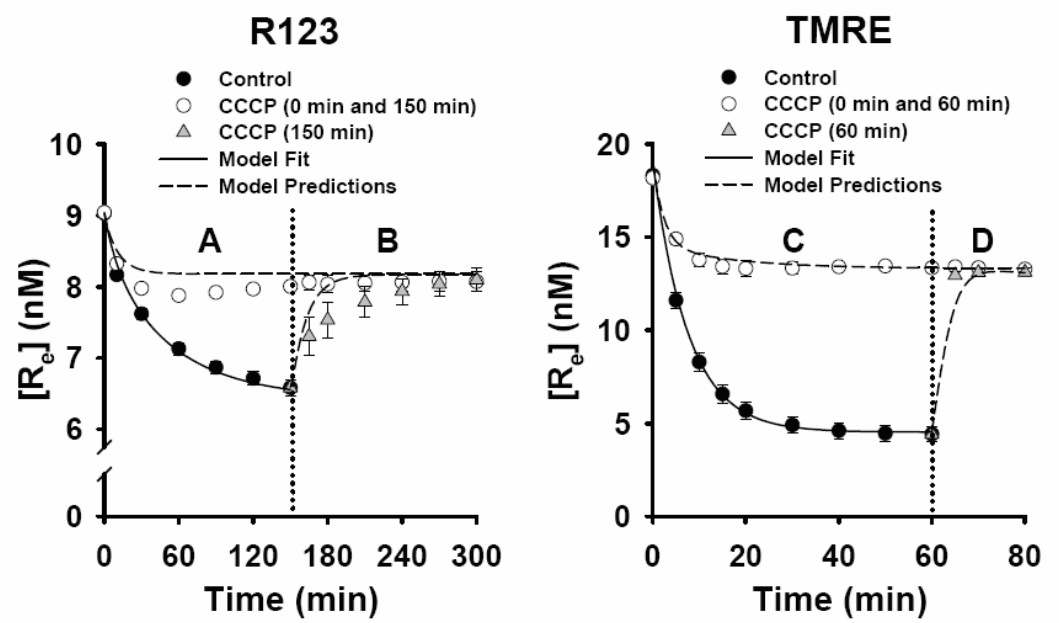

Figure 7.3 Effects of CCCP on the concentrations of R123 and TMRE in the medium surrounding the cell-coated beads. A: [R_e] for R123 in samples containing R123 only (closed circles, n = 11) or R123 + CCCP (open circles, n = 4). At the time represented by the dotted vertical line (150 min). B: CCCP was added to 4 of R123 samples (shaded triangles) and to all the R123 + CCCP samples (open circles). C: [R_e] for TMRE (closed circles, n = 4) or TMRE + CCCP (open circles, n = 4). At the time represented by the dotted vertical line (60 min). D: CCCP was added to all 4 TMRE samples (shaded triangles) and all 4 of the TMRE + CCCP samples (open circles). The symbols are the data (means ± SE) and the solid lines are the model fit to the data. The dashed lines are model predictions using the Table 7.1 parameter values.

For the control cells that had been allowed to accumulate the dyes in the absence of CCCP, [R_e] increased when CCCP was added, approaching that for cells that had been treated with CCCP from the beginning of the experiment (Figures 7.3 B and D). That is, CCCP not only blocked dye uptake by the cells if it was present from the beginning of the experiments, it also caused cell-accumulated dye to be released into the medium. With regard to the differences between the two dyes, TMRE is taken up more rapidly and to a proportionately greater extent by control cells than is R123, as also seen in Figure 7.2. In addition, when CCCP was added to cells that had already accumulated dye, TMRE efflux into the medium from the cells was more rapid than for R123, as reflected in the more rapid increase in [R_e] for TMRE than for R123 (Figures 7.3 D and B, respectively).

The data in Figures 7.2 and 7.3 implied that $\Delta\Psi_m$, $\Delta\Psi_p$ and Pgp all contributed to the net effect of the cells on $[R_e]$ for R123 and TMRE. Since kinetic model parameters are not estimable from a single data set or experimental condition we designed an experimental data set to contain sufficiently discriminating data to distinquish between effects of $\Delta\Psi_m$, $\Delta\Psi_p$ and Pgp on $[R_e]$. Figures 7.4 A and B show the effects of progressive, cumulative inhibition of Pgp, $\Delta\Psi_p$ and $\Delta\Psi_m$ on the $[R_e]$ vs. time progress curves for R123 and TMRE, respectively, using GF120918 only, GF120918 + high K^+ or GF120918 + high K^+ + CCCP.

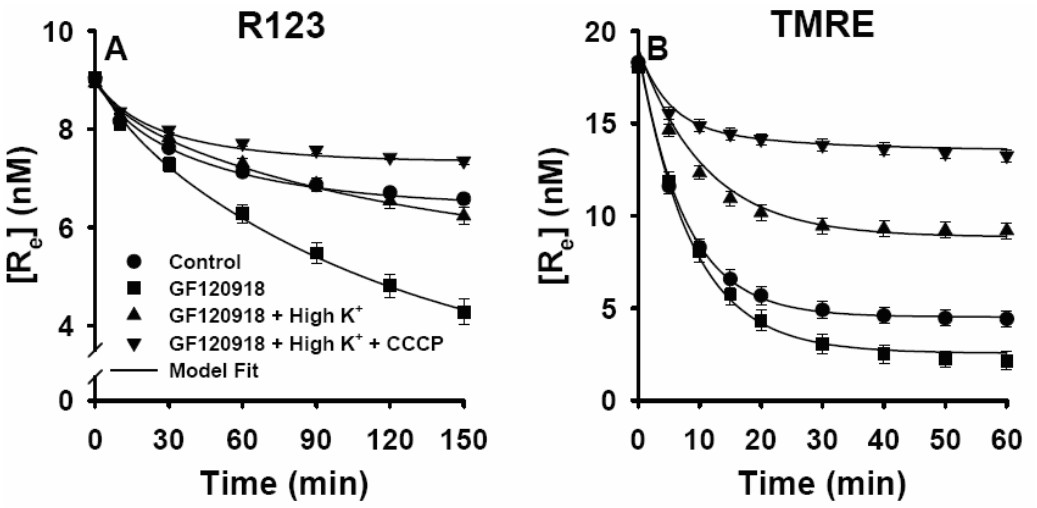

Figure 7.4 Cumulative inhibition of processes contributing to dye fate on the R123 and TMRE concentrations in the medium surrounding the cell- coated beads. The symbols are the data (means ± SE) for the following number (n) of experiments: (A) cell medium R123 concentrations for control, 11; GF120918, 5; GF120918 + high K^+, 4; GF120918 + high K^+ + CCCP, 4; (B) all conditions, 8. The $[R_e]$ data for control and GF120918 are the same as those in Figures 7.2 and 7.3. The solid lines are the model fit to data.

To take into account the possibility that CCCP might also depolarize $\Delta\Psi_p$, an additional study was carried out. Figure 7.5 A and B show the impact of CCCP on $[R_e]$ for R123 or TMRE, respectively, in the presence of GF120918 and absence of high K^+. Under these conditions, which include blocking any effect of Pgp, and without the high K^+ that would depolarize $\Delta\Psi_p$, any impact of CCCP on $\Delta\Psi_p$ should be unmasked.

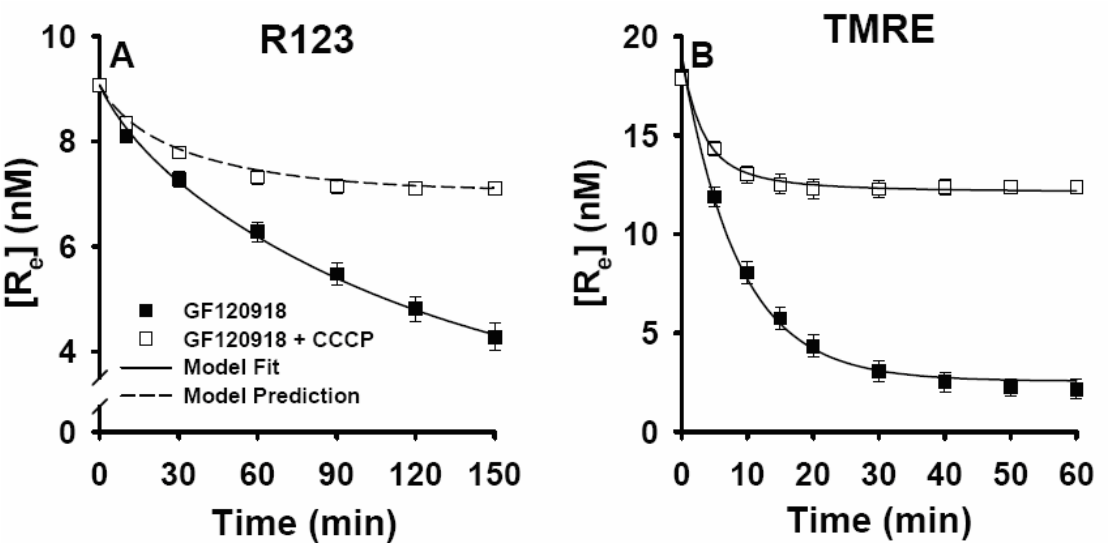

Figure 7.5 The impact of CCCP on R123 and TMRE concentrations when the contribution of Pgp is minimized with GF120918. The experimental medium did not contain high K^+. The symbols are the data (means ± SE) for the following number (n) of experiments: A: GF120918, n=5; GF120918 + CCCP, n=5; B: all conditions, n=8. The symbols are the data (means ± SE), the solid lines are the model fits to the data, and the dashed line is a model prediction.

7.4 Data Analysis

7.4.1 Kinetic Model for the Disposition of Rhodamine Dyes in Endothelial Cells

A mathematical model was developed to quantify the contributions of $\Delta\Psi_m$, $\Delta\Psi_p$ and Pgp to $[R_e]$ for R123 and TMRE. The model includes three regions, the extracellular medium, cytoplasm and mitochondrial matrix, with volumes V_e, V_c, and V_m, respectively (Figure 7.6). The dye flux across plasma (J_1) or inner mitochondrial membrane (J_2) is represented by a modified one-dimensional Goldman–Hodgkin-Katz equation (Huang et al., 2007). Because the fractional loss of dye from the extracellular medium in Figure 7.1 is dose-independent, Pgp-mediated dye efflux from V_c to V_e is hypothesized to follow first-order kinetics (Loetchutinat et al., 2003). Moreover, the model allows for slowly equilibrating nonspecific dye interactions with the cuvette (B_e) within V_e, and rapidly equilibrating nonspecific dye interactions with binding sites B_c and B_m

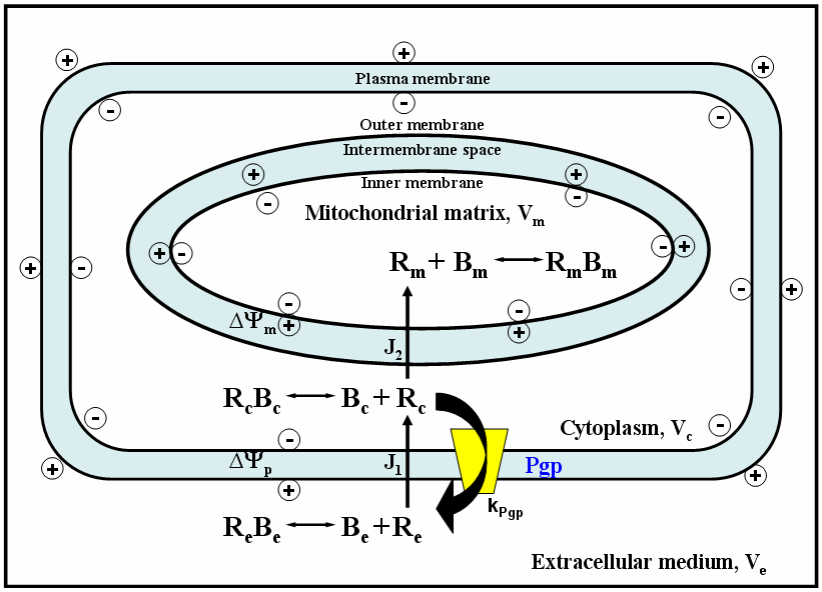

Figure 7.6 A schematic representation of the kinetic model of the disposition of R123 or TMRE in pulmonary arterial endothelial cells and the extracellular medium. V_e, V_c, and V_m are volumes of medium, cytoplasm and mitochondrial matrix, respectively. R_e, R_c and R_m are the free R123 or TMRE concentrations in the medium, cytoplasm and mitochondrial matrix, respectively. Within the medium, the dyes participate in nonspecific binding interactions with the fluorometric cuvette (B_e). The dyes also participate in nonspecific rapidly equilibrating interactions with binding sites B_c and B_m within V_c and V_m, respectively. R_cB_c and R_mB_m are the concentrations of bound dye in the cytoplasm and mitochondrial matrix, respectively. J_1 and J_2 are dye fluxes across plasma cell membrane and inner mitochondrial membrane, respectively. $\Delta\Psi_m$ and $\Delta\Psi_p$ are mitochondrial and plasma membrane potential, respectively; K_{Pgp} is the conductance of Pgp mediated dye release from the cells.

within V_c and V_m, respectively. Then, variations in dye concentrations in V_e, V_c and V_m with time are described by the ordinary differential equations

$$\frac{d[R_e]}{dt} = \frac{K_{Pgp}}{V_e}[R_c] - \frac{S_1 J_1}{V_e} - \overline{k}_1[R_e] + k_{-1}[R_eB_e] \tag{E7.1}$$

$$\frac{d[R_c]}{dt} = -\frac{K_{Pgp}}{V_1}[R_c] - \frac{S_1 J_1}{V_1} - \frac{S_2 J_2}{V_1} \tag{E7.2}$$

$$\frac{d[R_m]}{dt} = \frac{S_2 J_2}{V_2} \tag{E7.3}$$

$$\frac{d[R_eBe]}{dt} = \overline{k}_1[R_e] - k_{-1}[R_eB_e] \tag{E7.4}$$

where

$$J_1 = \frac{\alpha P_1 \Delta\overline{\Psi_p}}{e^{\alpha\Delta\overline{\Psi_p}} - 1}\left(e^{\alpha\Delta\overline{\Psi_p}}[R_e] - [R_c]\right) \quad \text{(E7.5)}$$

$$J_1 = \frac{\alpha P_2 \Delta\Psi_m}{e^{\alpha\Delta\Psi_m} - 1}\left(e^{\alpha\Delta\Psi_m}[R_c] - [R_m]\right) \quad \text{(E7.6)}$$

$[R_e](t)$, $[R_c](t)$ and $[R_m](t)$ are dye concentrations in V_e, V_c, and V_m, respectively, at time t; $[R_eB_e](t)$ is the dye concentration bound to cuvette at time t; $\alpha = ZF/RT = 0.0374\ mV^{-1}$ at 37 ^oC is a constant dependent on the universal gas constant (R), Faraday constant (F), dye valence (Z), and absolute temperature (T) (Huang et al., 2007); K_{Pgp} (ml/min) is Pgp mediated dye release from the cells, and P_1S_1 (ml/min) and P_2S_2 (ml/min) are products of dye permeabilities (P) across plasma and mitochondrial membranes, respectively, and the surface areas (S) of these membranes $V_1 = \left(1 + \frac{k_2[B_c]}{k_{-2}}\right) V_c$ (ml) and $V_2 = \left(1 + \frac{k_3[B_m]}{k_{-3}}\right) V_m$ (ml) are apparent cytoplasm and mitochondrial matrix volumes, respectively, where k_i and k_{-i} are dye association and dissociation rate constants, respectively, with B_c (i = 2) and B_m (i = 3), respectively; $\overline{k_1} = k_1[B_e]$ (min^{-1}) and k_{-1} (min^{-1}) are rate constants for dye-cuvette binding and unbinding, respectively, and $[B_e]$ is the concentration of cuvette dye binding sites.

Although typically thought of as a mitochondrial uncoupler, the protonophore carbonylcyanide p-trifluoromethoxyphenylhydrazone (FCCP) depolarizes both bovine aortic endothelial and cultured neuronal cell $\Delta\Psi_p$ in a concentration dependent manner (Nicholls et al., 2006; Park et al., 2002). Because CCCP is also an uncoupling protonophore, and the 5 μM CCCP concentration used in our study is in the range reported for the FCCP induced plasma membrane depolarization, we used model simulations to evaluate whether CCCP might have such an effect in the present study (not shown). The result was that the effect of CCCP on $[R_e]$ for both dyes was

greater than what could be accounted for solely by dissipation of only $\Delta\Psi_m$, as described by the empirical equation

$$\Delta\overline{\Psi_p} = \delta\ \Delta\Psi_p + (1-\delta)\Delta\Psi_p e^{-\frac{t}{\tau}} \qquad \text{(E7.7)}$$

where (1-δ) is the $\Delta\Psi_p$ fraction dissipated by CCCP and τ the associated time constant (min) such that in the absence of CCCP, δ = 1 and $\Delta\overline{\Psi_p} = \Delta\Psi_p$.

To break the high correlation between V_2 and $\Delta\Psi_m$ in the model, the V_2/V_1 ratio was set to 0.02, consistent with a lower bound measured for this ratio in rat pulmonary endothelium (Oldendorf, Cornford & Brown, 1977). Then, $\Delta\Psi_m$ $\Delta\Psi_p$, V_1, K_{Pgp}, P_1S_1, P_2S_2, δ , τ, $\overline{k_1}$ and k_{-1} are the unknown model parameters. The model governing differential equations were solved numerically using the MATLAB (MathWords, Inc) function "ode45" which is based on an explicit Runge-Kutta formula.

7.4.2 Estimation of Model Parameters

In the absence of cells, Equations (E7.1 – 7.4) become

$$\frac{[R_e](t)}{[R_e]_0} = \frac{1}{\overline{k_1} + k_{-1}}\left(k_{-1} + \overline{k_1}e^{-(\overline{k_1}+k_{-1})t}\right) \qquad \text{(E7.8)}$$

where $[R_e]_0$ is the initial (t = 0) dye concentration and $[R_e](t)$ is the concentration at time t. Fitting E7.8 to the without cell data in Figure 7.1 gives $\overline{k_1}$ and k_{-1} as 4.3 x 10^{-3} min^{-1} and 8.9 x 10^{-2} min^{-1}, respectively, for R123 and 7.9 x 10^{-3} min^{-1} and 5.4 x 10^{-2} min^{-1}, respectively, for TMRE. The fitting procedure was implemented in MATLAB using function "lsqcurvefit" which solves a non-linear curve fitting problem in the least-squares sense using the Levenberg-Marquardt algorithm.

Estimation of the values of model parameters descriptive of the contributions of

membrane potentials and Pgp to changes in $[R_e]$ vs. time requires a collection of data sets that provides sufficiently discriminating information about these cellular processes.

Thus for each dye, the values of $\Delta\Psi_m$, $\Delta\Psi_p$, V_1, K_{Pgp}, P_1S_1 and P_2S_2 were obtained by fitting the solution of Equations (E7.1 – 7.4) simultaneously to the mean $[R_e]$ versus time data in Figure 7.4. The hypothesis was that $\Delta\Psi_m$, $\Delta\Psi_p$ and K_{Pgp} could be set to zero in the presence of CCCP, high K^+ or GF120918, respectively. In addition, it was hypothesized that in the presence of CCCP + high K^+, any effect of CCCP on $\Delta\Psi_p$ would be negligible, allowing to be set to one in Equation (E 7.7). The parameter values and the 95% confidence intervals (C.I.) are given in Table 7.1 (Bates & Watts, 1983). The Figure 7.4 B data do not have sufficient temporal resolution to provide a value for P_2S_2 for TMRE other than an upper bound set in the non-linear regression algorithm.

The means ± 95% C.I. for the parameters δ and τ were determined to be 0.25 ± 0.02 and 2.3 ± 0.7 min, respectively, by fitting the solution of model Equations (E7.1-7.4) to the GF120918 plus CCCP data for TMRE in Figure 7.5 B with K_{Pgp} and $\Delta\Psi_m$ set to zero, and with $\Delta\Psi_m$ and other parameters set to the values shown in Table 7.1. Model simulations revealed that the effect of CCCP on $\Delta\Psi_p$ is more apparent in the presence of GF120918 than under any other experimental condition studied.

Model simulations based on Equations (E7.1-7.4) revealed that increasing or decreasing the V_2/V_1 ratio by 50% changed $\Delta\Psi_m$ by +10 mV and 18 mV, respectively, consistent with previous estimates of the sensitivity of $\Delta\Psi_m$ to the V_2/V_1 ratio (Nicholls 2005). Model simulations further demonstrated that values for $\Delta\Psi_p$ and K_{Pgp} are insensitive to changes in the V_2/V_1 ratio.

7.4.3 Model Predictions (Validation)

The kinetic model was evaluated by testing its ability to predict $[R_e]$ under experimental conditions that were not used for estimating model parameters in Table 7.1. The Table 7.1 values were used to generate model predictions for data sets in Figures 7.2, 7.3 and 7.5 (dashed lines). The values for δ and τ, which quantify a time-dependent CCCP mediated $\Delta\Psi_p$ depolarization, obtained from the TMRE data in Figure 7.5B were used to predict the effect of CCCP on the R123 $[R_e]$ vs. time curve in the presence of CCCP + GF120918 (Figures 7.6 A). That this prediction was a reasonable explanation of the R123 CCCP + GF120918 data provided support for the hypothesis of a depolarizing effect of CCCP on $\Delta\Psi_p$ under the study conditions.

7.4.4 Steady State Analysis for Mitochondrial Membrane Potential

Following the addition of the dye along with GF120918 and CCCP to high K^+ medium, the steady state dye concentrations in V_e, V_1 and V_2 should be equal to that in the medium, $[R_e]_{s1}$.

$$[R_e] = [R_c] = [R_m] = [R_e]_{s1} \quad \text{(E7.9)}$$

Using mass balance,

$$[R_e]_{s0}\, V_e = [R_e]_{s1}\, (V_e + V_1 + V_2) \quad \text{(E7.10)}$$

where $[R_e]_{s0}$ is the steady state value of dye concentration in the medium following the addition of dye in the absence of cells (Figure 7.1).

Following the addition of dye along with GF120918 to high K^+ medium, the steady state dye concentrations in V_e and V_1 should be equal and different from that in V_2. Thus, using mass balance

$$[R_e]_{s0}\, V_e = [R_e]_{s2}\, (V_e + V_1) + [R_m]_s\, V_2 \quad \text{(E7.11)}$$

where $[R_e]_{s2}$ and $[R_m]_s$ are the respective steady state dye concentrations within V_e and V_2, following the addition of dye + GF120918 to high K^+ medium. $[R_e]_{s2}$ and $[R_m]_s$ can be related to $\Delta\Psi_m$ using the Nernst equation.

$$\Delta\Psi_m = \frac{1}{\alpha}\ln\frac{[R_e]_{s2}}{[R_m]_s} \qquad \text{(E7.12)}$$

Using algebraic manipulations, Equations (E7.1-7.4) lead to the following equation:

$$\Delta\Psi_m = \frac{1}{\alpha}\ln\left(\frac{\beta([R_e]_{s0}-[R_e]_{s1})[R_e]_{s2}}{[R_e]_{s0}((1+\beta)[R_e]_{s1}-[R_e]_{s2}-\beta[R_e]_{s1}[R_e]_{s2})}\right) \qquad \text{(E7.13)}$$

where α is the ratio V_2/V_1, $[R_e]_{S0}$ is the steady-state $[R_e]$ in the absence of cells, $[R_e]_{s2}$ is the steady-state $[R_e]$ for high K^+ + GF120918, $[R_e]_{s1}$ is the steady-state $[R_e]$ for high K^+ + GF120918 + CCCP.

Since $[R_e]$ for TMRE reaches steady-state over the experimental time period (~30 min, Figures 7.1 – 5), we reasoned that steady-state analysis could be used to estimate $\Delta\Psi_m$ under just two experimental conditions, high K^+ + GF120918 and high K^+ + GF120918 + CCCP, using the above algebraic equation (E7.13), the $\Delta\Psi_m$ determined is −124 ± 6 mV (mean ± SE).

Figures 7.7 and 7.8 exemplify the use of steady state TMRE data and steady state data analysis to evaluate the effect of a physiological stimulus on the $\Delta\Psi_m$ response to uncoupling with CCCP. The studies included GF120918 and high K^+ to eliminate the contributions of $\Delta\Psi_p$ and Pgp to TMRE fate, thereby isolating and emphasizing the impact of $\Delta\Psi_m$. Figure 7.7 shows $[R_e]$ vs. time data for control (room air) and hyperoxia-exposed cells in which the CCCP concentration varies from none (Figure 7.7 A) to 0.1, 0.2, 0.3 and 5.0 μM in Figures 7B-E, respectively. Figures 7.7 A and E show that the steady state $[R_e]$ is nearly the same for hyperoxia-exposed and control cells in the absence of CCCP and at the highest CCCP concentration (5 μM). However, at

intermediate CCCP concentrations, the steady state [R_e] appears higher for hyperoxia-exposed than control cells (Figures 7.7 B, C and D). Figure 7.8 shows the $\Delta\Psi_m$ for control, room air and hyperoxia-exposed cells calculated from E7.13 and the Figure 7.7 [R_e] vs. time data at each CCCP concentration. As anticipated from Figure 7.7, the resting $\Delta\Psi_m$ and the $\Delta\Psi_m$ at 5 μM CCCP are not detectably different, but the hyperoxia-exposed cell $\Delta\Psi_m$ is more sensitive to the depolarizing effects of uncoupling with CCCP.

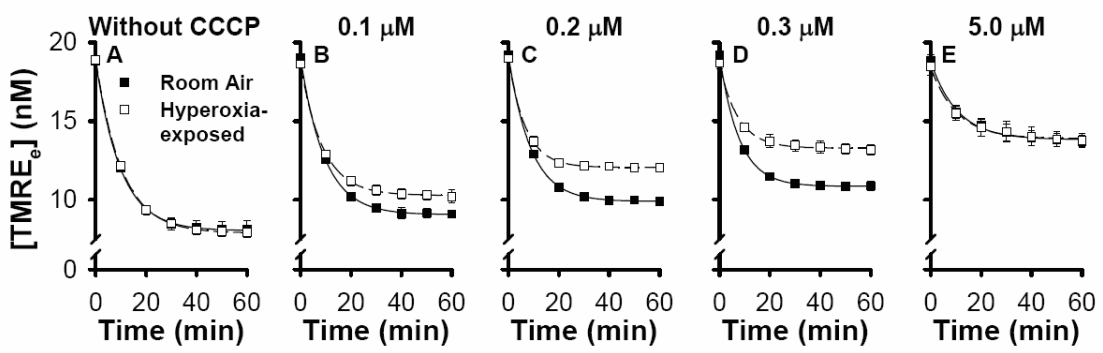

Figure 7.7 The impact of varying concentrations of CCCP on TMRE concentrations in the medium surrounding control (room air) and hyperoxia-exposed pulmonary arterial endothelial cells. The experiments were carried out in the presence of GF120918 and high K^+ without CCCP or with 0.1, 0.2, 0.3 or 5.0 μM CCCP. The symbols are the mean ± SE for n = 3 determinations at each CCCP concentration.

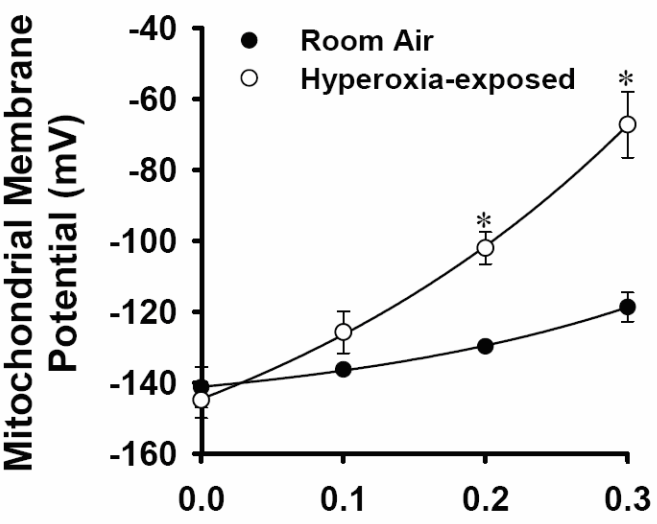

Figure 7.8 Hyperoxia-exposed cell $\Delta\Psi_m$ is more sensitive to CCCP induced depolarization than control (room-air) cells. The symbols represent the values for $\Delta\Psi_m$ obtained using the steady state TMRE data from Figure 7.7 and Equation. *Significantly different from control room air values at the same CCCP concentration, t-test, $P < 0.05$

	$\Delta\Psi_m$ (mV)	$\Delta\Psi_p$ (mV)	P_1S_1 (μl/min/cm^2)	P_2S_2 (μl/min/cm^2)	K_{Pgp} (μl/min/cm^2)	V_1 (μl/cm^2)
R123	-130 ± 7	-36 ± 4	0.17 ± 0.02	0.18 ± 0.20	0.41 ± 0.07	7.4 ± 0.8
TMRE	-133 ± 4	-49 ± 4*	5.20 ± 0.79*	37.67 ± 47.81	1.92 ± 0.41*	30.5 ± 3.8*

Table 7.1 Kinetic model parameter values of rhodamine model: Kinetic model parameter values ± asymptotic 95% confidence intervals (C.I.) $\Delta\Psi_m$ and $\Delta\Psi_p$ are mitochondrial and plasma membrane potentials, respectively; P_1S_1 and P_2S_2 are permeability-surface area products descriptive of R123 or TMRE conductance across plasma and mitochondrial membranes, respectively; K_{Pgp} is the constant rate of Pgp mediated release of R123 or TMRE from the cells; V_1 is the apparent volume of cell cytoplasm. Parameter values were obtained by fitting the model solution to the mean values of the extracellular R123 or TMRE concentration ($[R_e]$) versus time data in Figure 7.4. * Significantly different than value for the same parameter obtained using R123 data; *t*-test, $P < 0.05$.

7.5 Discussion and Conclusions

The present study was based on the general hypothesis that changes in the concentrations of rhodamine dyes in the medium surrounding the intact pulmonary arterial endothelial cells ($[R_e]$) would be sensitive to perturbations in $\Delta\Psi_m$ and $\Delta\Psi_p$. The study reveals that the observed changes in *extracellular* dye disposition in response to the perturbations were highly predictable based on previous measurements of *intracellular* rhodamine dye disposition using the same or very similar kinds of perturbations, albeit in different cell types, e.g., in (Farkas et al., 1989). Taken together with the knowledge that such intracellular dye measurements had been used to quantify $\Delta\Psi_m$ and $\Delta\Psi_p$, our reasoning was that the extracellular dye concentration vs. time kinetic data would also contain this quantitative information.

A key challenge in unlocking this quantitative information was that the net effect of the cells on the rhodamine dye concentrations in the medium involved multiple interacting processes. A general strategy in this situation is to use inhibitors and treatment conditions to provide discriminating data relevant to these processes, and kinetic modeling to obtain values for kinetic parameters descriptive of the individual processes involved. We used a variety of treatment conditions and inhibitors to target the processes hypothesized to be involved in dye disposition,

and a computational model to interpret the data.

Computational modeling provides an integrated framework for quantifying the qualitative features of the data, as well as a means to evaluate mechanistic hypotheses regarding the processes that produce the data (Beard, Bassingthwaighte & Greene, 2005). Generally speaking, computational models make use of physical laws (e.g., mass balance) together with existing models of subsystems (e.g., Goldman-Katz equation) to describe the interactions among the components of a more complex system (e.g., intact cells) (Beard et al., 2005). Our model incorporates mass balance, the Goldman-Katz equation, and linear kinetics to describe the cellular disposition of the rhodamine dyes within the cells and the medium. The model is distinct from, and complementary to, certain already existing models for evaluating cell membrane potentials in that it allows for contributions of additional cellular processes to dye disposition (e.g., Pgp), utilizes extracellular dye concentration data (rather than microscopic measurements of intracellular dye) and takes advantage of an entire intact cell population (instead of individual cells or isolated mitochondria) (Ward 2010).

In general, model parameters are not estimable from a single data set or experimental condition (Audi et al., 2003; Merker et al., 2004). Instead, a diverse set of experimental protocols are needed to provide sufficiently discriminating data to break correlations between the contributing processes. In the present study, the data sets used to obtain the parameter values consist of concentration data for two different dyes under four experimental conditions, as a function of time (Figure 7.4). The model provided a good fit to the data for the two different dyes, and the values obtained for $\Delta\Psi_m$ and $\Delta\Psi_p$ were consistent for the two dyes. They were also consistent with values reported for pulmonary arterial endothelial cells in culture using an array of

other approaches (discussed in more detail below). Since the values representing Pgp activity (K_{pgp}) and dye permeability surface area product (*PS*) are determined by physical and chemical properties of the dyes rather than by intrinsic properties of the cells, they are not expected to be the same for R123 and TMRE. However, as anticipated from the reported higher cell membrane permeability of TMRE, the values of P_1S_1 and P_2S_2 (normalized to cell surface area) for TMRE are higher than those for R123 (Table 7.1) (Duchen et al., 2003; Loetchutinat et al., 2003).

To our knowledge, the values for $\Delta\Psi_m$ of 130 ± 7 mV and133 ± 4 mV (means ± 95% C.I.) using R123 and TMRE, respectively, obtained in the present study are the first quantification of $\Delta\Psi_m$ for bovine pulmonary artery endothelial cells in culture. Previous studies of bovine aortic endothelial cells using the potential sensitive triphenylphosphonium ion yielded a $\Delta\Psi_m$ of 220 mV (OMalley, Fink & Ross, 2006). However, it is difficult to make a comparison because the latter studies involved isolated mitochondria under hyperpolarizing conditions (e.g., in the presence of oligomycin) (OMalley et al., 2006).

The study further showed that steady state analysis of TMRE data can be used to obtain values for $\Delta\Psi_m$ that were consistent with the values obtained from transient kinetic R123 and TMRE data. An application of the steady state approach to quantify the impact of hyperoxic exposure on pulmonary endothelial $\Delta\Psi_m$ was demonstrated, and to our knowledge, provides the first quantitative assessment of the impact of an oxidative stress on pulmonary endothelial cell $\Delta\Psi_m$. Hyperoxic exposure was selected as the stress because elevated O_2 is the most common treatment for respiratory failure, yet is injurious to the lung, with endothelial cells being a primary and early target (Crapo, Barry & Foscue, 1980; Moody, Simon & Johns, 2001).

For the hyperoxia-exposed cells, resting $\Delta\Psi_m$ was not different from control (room-air)

cells, but hyperoxia-exposed cell $\Delta\Psi_m$ was more sensitive to depolarization via uncoupling. It should be emphasized that the effect of hyperoxic exposure on pulmonary endothelial mitochondria would not have been revealed by measuring only the resting $\Delta\Psi_m$ or if we had used only a single commonly used CCCP concentration (5 μM) to depolarize the mitochondria. Previous studies have reported various indications of mitochondrial dysfunction in hyperoxia exposed rat lung, pulmonary endothelial cells in culture and other cell types (Ahmad et al., 2006; Audi et al., 2005, 2008; Bassett et al., 1986, 1989; Merker et al., 1996, 2007; Pruji, Schoonen & Joenje, 1992; Schoonen et al., 1990). In this context, the present observations are consistent with a hyperoxia-induced mitochondrial deficiency.

Previous methods for evaluating stimulation or stress induced alterations in pulmonary endothelial cell $\Delta\Psi_m$ using rhodamines or ratiometric probes have in general provided only indices of relative changes, estimated from changes in fluorescence intensity (Dedkova & Blatter, 2005; Han et al., 2010; Huser et al., 1999; Mungunsukh et al., 2010; You & Park, 2010). A common pitfall in interpreting such data is that the logarithmic form of the Nernst equation specifies that changes in fluorescence intensity (and, for ratiometric dyes, ratios derived from such changes) are not linearly proportional to changes in $\Delta\Psi_m$ (Nicholls, 2000). In this context, the ratiometric dye, 5,5',6,6'-tetrachloro-1,1',3,3'-tetraethylbenzimidazolylcarbocyanineiodide (JC-1), exists in a monomeric form, with an emission wavelength of 527 nm (green) when excited at 490 nm, but, when the dye accumulates in polarized mitochondria, it forms aggregates associated with a large shift in emission wavelength, to 590 nm (red) (Di, Blank & Colonna, 1995). Changes in green/red fluorescence ratio have been useful in giving a semi-quantitative picture of the impact of various stimuli on $\Delta\Psi_m$. However, aside from the apparently few attempts that have been made to quantify

the association between these ratios and $\Delta\Psi_m$ in isolated mitochondria, the quantitative relationship between any given ratio change and the corresponding change in $\Delta\Psi_m$ in mV in intact cells is not generally considered (Di et al., 1995). Our approach could be viewed as complementary to that of JC-1 wherein it would provide a means for quantitative interpretation of changes in green/red fluorescence ratios.

The values for $\Delta\Psi_p$ obtained in the present study were 36 ± 4 mV and 49 ± 4 mV (means ± 95% C.I.) using R123 and TMRE, respectively (Table 7.1). The difference between the two may be attributable to the longer experimental time course needed to overcome the lower membrane permeability of R123 as compared to TMRE (as represented by *PS* products in Table 7.1). Previous estimates of cultured bovine pulmonary arterial endothelial $\Delta\Psi_p$ made using whole-cell patch clamp have yielded mean values of 26 mV to 67 mV (Adams et al., 2004; Campbell et al., 1991; Johns et al., 1987; Koliwad et al., 1996; Voets et al., 1996). The variation may be attributable to differences in culture conditions or from error arising from leakage currents (Adams et al., 2004; Campbell et al., 1991). The issue of leakage currents has been addressed by rejecting cells displaying resting potentials below a set seal resistance, narrowing the range in values from 56 mV to 67 mV (Adams et al., 2004; Campbell et al., 1991; Johns et al., 1987). Issues to consider when comparing these values with those obtained in the present study include that the "whole cell" patch clamp studies were carried out at room temperature, used estimated values based on reversal potentials and involved rupturing the plasma membrane and cell dialysis with pipette solutions. In contrast, we carried out our studies at 37^{o}C using a non-destructive protocol. An additional point is that patch clamp focuses on relatively small numbers of individual cells, which reveals heterogeneity within the population, while our approach is directed at entire cell

populations (Campbell et al., 1991; Cannell et al., 1989; Duchen et al., 2003; Koliwad et al., 1996).

Previous measurements of $\Delta\Psi_m$ and $\Delta\Psi_p$ using rhodamine dyes have commonly not taken into account that they are also Pgp substrates (Mandala, Serck & Martino, 1999; Ward et al., 2007, 2010; Yeheskely et al., 2009). For cell types that have few or no multidrug transporters, this may be of minimal importance, but multidrug transporters perform a key function in the pulmonary endothelium, which is in direct contact with blood borne pharmacological, physiological and toxicological substances. In the present study, the effect of increasing or decreasing K_{Pgp} by 50% on the dye concentration in the mitochondria [R_m] would be a ~45% increase or ~40% decrease for R123 and a 12% increase or 8% decrease for TMRE. These effects could be misinterpreted to represent changes in $\Delta\Psi_m$ and/or $\Delta\Psi_p$. This concept may be of particular importance in studying cell injury, which has been observed to affect Pgp protein levels in brain endothelial cells (Robertson, Kania & Hladky, 2009).

Previous experimental and theoretical studies have been carried out for simultaneous assessment of $\Delta\Psi_m$ and $\Delta\Psi_p$ in a variety of non-endothelial mammalian cell types using rhodamine dyes and other probes (Farkas et al., 1989; Ward et al., 2000, 2007). Among these, Nicholls used a proprietary $\Delta\Psi_p$ indicator, PMPI, along with tetramethylrhodamine methyl ester to monitor changes in both membrane potentials in cultured neurons (Nicholls et al., 2006; Park et al., 2002). The combination of probes allowed for a means to account for the impact of changes in $\Delta\Psi_p$ on the rhodamine dye disposition (Nicholls et al., 2006; Park et al., 2002). Ward et al. developed an elegant computational model to interpret intracellular rhodamine dye fluorescence measurements in terms of transmembrane potentials for cultured cerebellar neuronal and granular cells (Ward et al., 2000, 2007). The Ward et al. and Nicholls studies accounted for the impact of

$\Delta\Psi_m$, $\Delta\Psi_p$, membrane permeability and mitochondrial volume fraction, but not for effects of Pgp on dye disposition (Nicholls et al., 2006; Park et al., 2002; Ward 2000, 2007). In contrast to our approach, the latter modeling approaches relied on input of initial values for $\Delta\Psi_m$ and $\Delta\Psi_p$ obtained in separate studies. A MATLAB based public web service, TOXI-SIM, was developed as a tool for implementing the Ward et al. model, the output of which is information on changes in $\Delta\Psi_m$ and $\Delta\Psi_p$ relative to fixed initial values (Huber et al., 2009). The approach described in the present study may be viewed as complementary in that it could provide initial values for the TOXI-SIM tool. This would allow for quantitative assessment of changes in pulmonary endothelial plasma and mitochondrial membrane potentials, including under conditions in which changes are rapid relative to the time scale of the present studies.

In summary, we took several approaches to optimize utility of rhodamine dyes for assessing $\Delta\Psi_m$ and $\Delta\Psi_p$ in intact pulmonary arterial endothelial cells. Dye concentrations were maintained in the linear range of fluorescence intensity vs. concentration, overcoming many of the complexities associated with interpreting contributions of quenching and dequenching to the signals. Solid microcarrier bead cell cultures optimized the cell surface to medium volume ratio, maximizing the impact of the cells on substances in the medium. Additionally, since the cell coated beads rapidly (within ~15 sec) settle out of suspension, medium fluorescence measurements are made without exposing cells to light or requiring dissociation from the culture surface.

In conclusion, this study presents a unique approach for quantification of $\Delta\Psi_m$ and $\Delta\Psi_p$ in intact pulmonary endothelial cells, and for evaluating the impact of various stresses (e.g. hyperoxia) on the bioenergetic properties of the pulmonary endothelial cells.

CHAPTER 8. CONCLUSIONS, FUTURE DIRECTIONS AND CLINICAL IMPLICATIONS

8.1 Conclusions and Future Directions

The long-term objectives of this study are to elucidate the underlying mechanisms of rat tolerance to 100% O_2 and to further understand the mechanisms involved in lung O_2 toxicity. A series of experiments were performed wherein rats were exposed to either 85% O_2 or 60% O_2, or cultured endothelial cells exposed to 95% O_2.

The results of this study demonstrate that rat exposure to 85% O_2 for 7 days (hyper-85) decreases the lung activity of complex I. This decrease is detectable following just 12 hours of exposure and persists for at least 7 days of exposure. The results also show that a comparable decrease in complex I activity occurs in lung homogenates of rats exposed to 60% O_2 for 7 days (hyper-60). Previous studies demonstrate that the decrease in complex I activity can impair oxidative phosphorylation, decrease ATP production, and hence negatively impact ATP-dependent cellular functions (Paradies et al., 2004; Chen et al., 2003). Thus, the decrease in complex I activity appears to be an initial event in the sequential events in lung O_2 toxicity and hence highly important pathologically.

The results of this study demonstrate that lung activities of complexes III and IV increase in lungs of rats exposed to 85% O_2 for 7 days, but not for 2 days. This suggests that the increase in the activities of complexes III and IV, which are the downstream components in the electron transport chain, might be a result of the decreased complex I activity. The increase in the activities of complexes III and IV might serve to accelerate the electron transfer through complex III and hence reduce the electron leakage at complex III, the primary site of mitochondrial ROS formation. These increases are not detectable in hyper-60 lungs which are 100% O_2 susceptible, suggesting

the role of complexes III and IV in rat tolerance of 100% O_2. However, additional studies would be needed to ascertain their specific role in this tolerance. Previous studies on hypoxia indicate "Damage occurring in mitochondria during ischemia is associated with a loss of respiratory activity of complex I in the electron transport chain; the activity of complex III is also altered but this occurs at later time point" (Janssens, Delaive & Houbion, 2000, P1514), which is interestingly consistent with the results in this hyperoxic study. Thus, both an increase in O_2 supply (hyperoxia) and a decrease in O_2 supply (hypoxia), which are models of pulmonary oxidative stress, induce a loss of the activity of complex I and a subsequent change in complex III. This suggests a potential common mechanism of adaptation to a change in O_2 supply. Additional studies using hypoxic rats could help to determine this common mechanism.

Our experiments showed that exposure to 85% O_2 for 7 days, but not 2 days, increases the activity of the cytosolic anti-oxidant enzyme NQO1. A comparable increase in NQO1 protein expression was measured in lungs of rats exposed to 85% O_2 for 7 days, which suggests that the increase in NQO1 activity in these lungs might be due to an increase in NQO1 protein expression. However, since a similar increase was also measured in lungs of rats exposed to 60% O_2 for 7 days, this increase in NQO1 activity by itself is not sufficient to account for the tolerance of rats exposed to 85% O_2 for 7 days to 100% O_2.

An important outcome of this study is the development of a novel approach for quantitative estimation of the mitochondrial membrane potential ($\Delta\Psi_m$) in intact cells using cationic rhodamine dyes. In normoxic cultured bovine pulmonary arterial endothelial cells (BPAEC), we estimated $\Delta\Psi_m$ to be ~-130 mV. This was done using two different dyes, R123 and TMRE, which yielded estimates without statistically difference, suggesting the reliability of our

newly-developed approach. Preliminary results using this approach indicate that endothelial cells exposed to 95% O_2 for 48 hours were able to maintain normal $\Delta\Psi_m$ but with an increased sensitivity to a mitochondrial uncoupler, an indicator of endothelial mitochondrial dysfunction. Additional studies would be needed to evaluate the effect of prolonged exposure to hyperoxia on $\Delta\Psi_m$ and the impact of a change in $\Delta\Psi_m$ on mitochondrial bioenergetics.

8.2 Clinical Implications

An important outcome from this study is the acquisition of data regarding the mechanisms of rat tolerance of 100% O_2 toxicity that may translate rapidly into clinical therapeutic strategies. For instance, the results of this study highlight the critical role of mitochondria, especially the complexes of mitochondrial electron transport chain, in lung O_2 toxicity and O_2 tolerance, and points to the mitochondrial electron transport chain as a target for protecting the lung from hyperoxia-induced injury. Thus drugs that can counter the hyperoxia-induced depression in complex I on mitochondrial ATP production may provide protection against O_2 toxicity. Aescine, a venotropic drug used in the treatment of chronic peripheral ischemia, has been shown to decrease endothelial cell death and to protect endothelial cells against the hyperoxia-induced decrease in ATP content and the injury caused by mitochondrial metabolic inhibitors (Janssens, Delaive & Houbiion, 2000). This suggests the potential utility of aescine for countering hyperoxia-induced mitochondrial dysfunction.

Metformin, a mild complex I inhibitor and widely used Type II diabetes drug, has been shown to provide a protective role against endotoxin-induced acute lung injury (Zmijewski, Lorne & Zhao, 2008). Using bovine heart mitochondria, Nadanaciva et al. demonstrated that metformin not only decreased the activity of complex I but also slightly increased the activity of complex IV

(Nadanaciva, Bernal & Aggeler, 2007). The effect of metformin on the activities of complexes I and IV is consistent with the changes we observed in O_2 tolerant hyper-85 rats. This might explain how metformin protects the lung against endotoxin-induced acute injury, and suggests that metformin might could be a potential drug to induce O_2 tolerance. However, since metformin inhibits complex I and hence mitochondrial ATP production, this stimulates glycolysis and result in lactic acidosis, which occurs in approximately 1% of cases (Price, 2003; Spiller & Quadrani, 2004). Thus, additional studies are needed to validate the comprehensive effect of metformin on lung O_2 toxicity.

Presently, there is no clinical means for detecting early lung O_2 injury secondary to hyperoxia, i.e., before injury can be detected by CT scans. An important outcome of this study is that the depression in complex I activity could be a key and early event in lung O_2 toxicity, i.e., occurring prior to significant structural, hemodynamic or morphometric changes. This suggests that new strategies for early identification of O_2 injury ought to focus on methods for evaluating changes in complex I activity. I^{123}-iodorotenone, a radioiodinated rotenone analog, is a lipophilic, neutral single-photon emission computed tomography (SPECT) imaging biomarker that binds to the ubiquinione site of complex I (VanBrocklin et al., 2007). This biomarker was developed to assess myocardial perfusion in vivo but also showed significant quantifiable uptake in the lung (VanBrocklin et al., 2007). Thus, I^{123}-iodorotenone could be used to detect a hyperoxia-induced decrease in complex I activity as an early index of lung O_2 injury. Since, I^{123}-iodorotenone is an analog of rotenone, a potent inhibitor of complex I, a study on the potential toxic effect of I^{123}-iodorotenone is also needed.

The redox sensitive, SPECT imaging agent hexamethylpropyeneamine oxime (^{99m}Tc–HMPAO) is an FDA-approved cerebral blood flow imaging agent (Inoue, Nakagawa & Goto, 2003), but there is evidence that it also serves as a marker of lung injury (Suga, Uchisako & Nishigauchi, 1994; Hang, Shiau & Hsu, 2003). For instance, increased HMPAO uptake has been reported in subclinical lung injury due to chemotherapy, irradiation lung injury, diabetes and smoking injuries in the absence of significant perfusion impairment or x-ray abnormalities (Suga et al., 1994; Chang et al., 2004). Previous studies have shown that the cellular uptake of HMPAO is dependent on intracellular GSH content and other factors, including mitochondrial dysfunction (Jacquier, Polla & Slosman, 1996; Shimura, Musya & Hashimoto, 2000). The results of this study demonstrate an increase in GSH content in lungs of hyper-85 rats, but not hyper-60 rats. Preliminary data by Drs. Clough and Audi suggest an increase in the lung uptake of HMPAO in lungs of hyper-85 rats, but not hyper-60 rats (Clough, Haworth & Audi, 2010). Based on these results, the ability of lung tissue to increase its capacity to generate GSH as measured by HMPAO uptake may be indicative of the ability of a critically ill patient to tolerate sustained exposure to O_2 at high fractions (Chang, Liu and Lin, 2004). In contrast, a patient with the same O_2 requirement and no increase in HMPAO uptake could be at a much higher risk for irreversible lung injury. In this case, the patient with evidence of enhanced susceptibility to hyperoxia would be a candidate for more invasive and expensive therapies (e.g., extracorporeal membrane oxygenation) or acceptance of lower arterial O_2 tension.

Exposure to >95% O_2 causes lung O_2 toxicity with a 4~22 hours latent period in which no overt clinical manifestations of toxicity can be detected (Bitterman, 2009). The duration of this latent period is inversely proportional to the level of inspired O_2. Most clinicians believe that the

treatment with 50%~60% O_2 is relatively safe for humans (Clark & Lambertsen, 1971; Bitterman, 2009). Though there is no substantial morphologic or structural change in lungs of rats exposed to 60% O_2 (Crapo et al., 1980, Hayatdavoudi et al., 1981), this study demonstrated a decrease in complex I activity and an increase in NQO1 activity in these lungs. These biochemical changes suggest the potential for toxicity caused by 60% O_2 exposure, and hence 60% O_2 therapy in the clinic might not be as safe as clinicians currently believe.

BIBLIOGRAPHY

Adams DJ and Hill MA. (2004) Potassium channels and membrane potential in the modulation of intracellular calcium in vascular endothelial cells. *J Cardiovasc Electrophysiol* 15: 598-610.

Ahmad A, Ahmad S, Chang LY, Schaack J and White CW. (2006) Endothelial Akt activation by hyperoxia: role in cell survival. *Free Radic Biol Med* 40: 1108-1118.

Ahmad S, White CW, Chang LY, Schneider BK and Allen CB. (2001) Glutamine protects mitochondrial structure and function in oxygen toxicity. *Am J Physiol Lung Cell Mol Physiol* 280: L779-791.

Allen CB, Guo XL and White CW. (1998) Changes in pulmonary expression of hexokinase and glucose transporter mRNAs in rats adapted to hyperoxia. *Am J Physiol* 274: L320-329.

Allen CB and White CW. (1998) Glucose modulates cell death due to normobaric hyperoxia by maintaining cellular ATP. *Am J Physiol* 274: L159-164.

Al-Mehdi AB, Shuman H and Fisher AB. (1997) Intracellular generation of reactive oxygen species during nonhypoxic lung ischemia, *Am J Physiol*, 272: L294-300.

Al-Mehdi AB, Shuman H and Fisher AB. (1997a) Oxidant generation with k+-induced depolarization in the isolated perfused lung, *Free Radi Biol Med*, 23: 47-56.

Altemeier WA and Sinclair SE. (2007) Hyperoxia in the intensive care unit: why more is not always better, *Curr Opin Crit Care*. 13: 73-78.

Andreyev AY, Kushnareva YE and Starkov AA (2005) Mitochondrial metabolism of reactive oxygen species, *Biochemistry (Moscow),* 70: 200-214.

Arab A, Wang J, Bausch K, von Schmadel K, Bode C and Hehrlein C (2010) Transient hyperoxic reoxygenation reduces cytchrome C oxidase activity by increasing superoxide dismutase and nitric oxide. *J Biol Chem* 285: 11172-11177

Armstrong JS, Steinauer KK, Hornung B, Irish JM, Lecane P, Birrell GW, Peehl DM, and Knox SJ (2002) Role of glutathione depletion and reactive oxygen species generation in apoptotic signaling in a human B lymphoma cell line. *Cell Death Differ* 9:252-263.

Audi SH, Linehan JH, Krenz GS and Dawson CA. (1998**)** Accounting for the heterogeneity of capillary transit times in modeling multiple indicator dilution data. *Ann Biomed Eng* 26: 914-930.

Audi SH, Dawson CA, Ahlf SB and Roerig DL. (2001) Oxygen dependency of monoamine oxidase activity in the intact lung. *Am J Physiol Lung Cell Mol Physiol* 281: L969-981.

Audi SH, Zhao H, Bongard RD, Hogg N, Kettenhofen NJ, Kalyanaraman B, Dawson CA and Merker MP. (2003) Pulmonary arterial endothelial cells affect the redox status of coenzyme Q_0. *Free Radic Biol Med* 34: 892-907.

Audi SH, Bongard RD, Krenz GS, Rickaby DA, Haworth ST, Eisenhauer J, Roerig DL and Merker MP. (2005) Effect of chronic hyperoxic exposure on duroquinone reduction in adult rat lungs. *Am J Physiol Lung Cell Mol Physiol* 289: L788-L797.

Audi SH, Merker MP, Krenz GS, Ahuja T, Roerig DL and Bongard RD. (2008) Coenzyme Q_1 redox metabolism during passage through the rat pulmonary circulation and the effect of hyperoxia. *J Appl Physiol* 105: 1114-1126.

Bao L, Avshalumov MV, Patel JC, Lee CR, Miller EW, Chang CJ and Rice ME (2009) Mitochondria are the source of hydrogen peroxide for dynamic brain-cell signaling. *J Neurosci* 29: 9002-9010.

Baracca A, Sgarbi G, Solaini G and Lenaz G. (2003) Rhodamine 123 as a probe of mitochondrial membrane potential: evaluation of proton flux through F(0) during ATP synthesis. *Biochim Biophys Acta* 1606: 137-146.

Barja G (2002) The quantitative measurement of H2O2 generation in isolated mitochondria. *J Bioenerg Biomembr* 34: 227-234.

Bass L and Ribinson PJ. (1981) Effects of capillary heterogeneity on rates of steady uptake of substances by the intact liver. *Microvasc Res* 22: 43-57.

Bassett DJ and Bowen-Kelly E. (1986) Pyruvate metabolism of perfused rat lungs after exposure to 100% oxygen. *J Appl Physiol* 60: 1605-1609.

Bassett DJ, Bowen-Kelly E and Reichenbaugh SS. (1989) Rat lung glucose metabolism after 24 h of exposure to 100% oxygen. *J Appl Physiol* 66: 989-996.

Bassett DJ, Bowen-Kelly E and Reichenbaugh SS (1992) Lung mitochondrial function following oxygen exposure and diethyl maleate-induced depletion of glutathione, *Toxicol Appl Pharamacol*. 115: 161-167.

Bassingthwaighte J, Goresky CA and Linehan JH (1998) *Whole Organ Approaches to Cellular Metabolism: Permeation, Cellular Uptake, and Product Formation*. New York: Springer.

Basuroy S, Bhattacharya S, Leffler CW and Parfenova H. (2009) Nox4 NADPH oxidase mediates oxidative stress and apoptosis caused by TNF- in cerebral vascular endothelial cells. *Am J Physiol Cell Physiol* 296: C422-C432.

Bates DM and Watts DG. (1983) *Non-linear Regression Analysis and its Applications*. New York.

Beattie DS, Japa S, Howton M and Zhu QS. (1992) Direct interaction between the internal NADH: ubiquinone oxidoreductase and ubiquinol:cytochrome c oxidoreductase in the reduction of exogenous quinones by yeast mitochondria. *Arch Biochem Biophys* 292: 499-505.

Beard DA, Bassingthwaighte JB and Greene AS. (2005) Computational modeling of physiological systems. *Physiol Genomics* 23: 1-3.

Beasly DMG and Glass WI (1998) Cyanide poisoning : pathophysiology and treatment recommendations, *Occup Med* 48: 427-431.

Behnke AR, Johnson FS, Poppen JR and Motley EP (1935) The effect of oxygen on man at pressures from 1 to 4 atmospheres. *Am J Physiol* 110:565-572.

Belinsky SA, Kauffman FC and Thurman RG (1989) Interactions between glycolysis and mixed function oxidation: studies with 7-ethoxycoumarin in perfused livers from β -naphthoflavone-treated rats. *Mol Pharmcol* 35: 512-518.

Beyer RE, Segura-Aguilar J, Di Bernardo S, Cavazzoni M, Fato R, Fiorentini D, Galli MC, Setti M, Landi L and Lenaz G (1996) The role of DT-diaphorase in the maintenance of the reduced antioxidant form of coenzyme Q in membrane systems. *Proc Natl Acad Sci U S A* 93: 2528-2532.

Bienert GP, Schjoerring JK and Jahn TP (2006) Memranbe transport of hydrogen peroxide *Biochim Biophys Acta* 1758: 994-1003.

Bitterman H. (2009) Bench-to-bedside review: oxygen as a drug. *Crit Care* 13:205-212.

Block ER and Fisher AB (1977) Depression of serotonin clearance by rat lungs during oxygen exposure. *J Appl physiol* 42: 33-38.

Bongard RD, Merker MP, Shundo R, Okamoto Y, Roerig DL, Linehan JH and Dawson CA (1995) Reduction of thiazine dyes by bovine pulmonary arterial endothelial cells in culture. *Am J Physiol Lung Cell Mol Physiol* 269: L78-L84.

Bongard RD, Lindemer BJ, Krenz GS and Merker MP (2009) Preferential utilization of NADPH as the endogenous electron donor for NAD(P)H:quinone oxidoreductase 1 (NQO1) in intact pulmonary arterial endothelial cells. *Free Radic Biol Med* 46: 25-32.

Boveris A, Oshino R, Erecinska M and Chance B (1971) Reduction of mitochondrial components by durohydroquinone. *Biochim Biophys Acta* 245: 1-16.

Brand MD (2010) The sites and topology of mitochondrial superoxide production. *Experimental*

Gerontology 45: 466-472.

Brueckl C, Kaestle S. Kerem A, Habazettl H, Krombach F, Kuppe H and Kuebler WM (2006) Hyperoxia-induced reactive oxygen species formation in pulmonary capillary endothelial cells in situ. *Am J Respir Mol Biol*, 34: 453-463.

Budinger GR, Tso M, McClintock DS, Dean DA, Sznajder JI and Chandel NS (2002) Hyperoxia-induced apoptosis does not require mitochondrial reactive oxygen species and is regulated by Bc1-2 protein. *J Biol Chem* 227: 15654-15660.

Cadenas E, Boveris A, Ragan CI and Stoppani AO (1977) Production of superoxide radicals and hydrogen peroxide by NADH-ubiquinone reductase and ubiquinol-cytochrome c reductase from beef-heart mitochondria. *Arch Biochem Biophys* 180: 248-257.

Cadenas E (1995**)** Antioxidant and prooxidant functions of DT-diaphorase in quinone metabolism. *Biochem Pharmacol* 49: 127-140.

Cai C, Chang L, Li W and Liu W (2008) Effects of hyperoxia on mitochondrial multienzyme complex III and V in premature newborn rat lung, *J Huazhong Univ Sci Technol* 28: 207-210.

Caldwell PR, Lee WL Jr, Schildkraut HS and Archibald ER (1966) Changes in lung volume, diffusing capacity and blood gases in men breathing oxygen. *J. Appl. Physiol*, 21: 1477-1483.

Campbell DL, Strauss HC and Whorton AR. (1991) Voltage dependence of bovine pulmonary artery endothelial cell function. *J Mol Cell Cardiol* 23 Suppl 1: 133-144.

Campian JL, Qian M, Gao X and Eaton JW (2004) Oxygen tolerance and coupling of mitochondrial electron transport. *J Biol Chem* 279: 46580-46587.

Campian JL, Gao X, Qian MW and Eaton JW (2007) Cytochrome c oxidase activity and oxygen tolerance. *J Biol Chem* 282: 12430-12438.

Cannell MB and Sage SO (1989) Bradykinin-evoked changes in cytosolic calcium and membrane currents in cultured bovine pulmonary artery endothelial cells. *J Physiol* 419: 555-568.

Capellier G, Maupoil V, Boussat S, Laurent E and Neidhardt A (1999) Oxygen toxicity and tolerance. *Minerva Anestesiol* 65: 388-392.

Carvalho CR, Depaula P, Schettino G, Maranhao B and Bethlem EP (1998) Hyperoxia and lung disease, *Pulmonary Medicine* 4: 300-304.

Carvalho PA, Chiu ML, Kronauge JF (1992) Subcellular distribution and analysis of technetium-99m-sestamibi myocardial retention. *J Nucl Med* 33: 1516-1522.

Cehovic GA, Hatton KW and Fahy BG (2009) Adult respiratory distress syndrome, *International Anesthesiology Clinics*, 27: 83-95.

Chandel NS (2010) Mitochondrial complex III: an essential component of universal oxygen sensing machinery? *Respir Physiol Neurobiol*. 174:175-81.

Chang MC, Pralle A, Lsacoff EY and Chang CJ (2004) A selective, cell-permeable potical probe for hydrogen peroxide in living cells. *J Am Chem Soc*. 126: 15392–15393.

Chang CT, Liu FY, Lin CC, Wang TY, Lee CC and Kao A (2004) Usefulness of technтium-99m hexamethylpropylene amine oxime lung scan to detect subclinical lung injury in patients with noninsulin-dependent diabetes mellitus. *J Diabetes Complications* 18: 229-232.

Chatterjee S, Levitan I, Wei Z and Fisher AB (2006) K_{ATP} channels are an important component of the shear-sensing mechanism in the pulmonary microvasculature. *Microcirculation* 13:633-644.

Chatterjee S, Chapman KE and Fisher AB (2008) Lung ischemia: a model for endothelial mechanotransduction. *Cell Biochem Biophys* 52: 125-138.

Chen Q, Vazquez EJ, Moghaddas S, Hoppel CL and Lesnefsky EJ (2003) Production of reactive oxygen species by mitochondria: central role of complex III. *J Biol Chem* 278:36027-36031

Chicco AJ and Sparagna GC (2007) Role of cardiolipin alterations in mitochondrial dysfunction and disease. *Am J Physiol Cell Physiol* 292: C33-C44.

Cho HY, Jedlicka AE, Reddy SP, Kensler TW, Yamamoto M, Zhang LY and Kleeberger SR (2002**)** Role of NRF2 in protection against hyperoxic lung injury in mice. *Am J Respir Cell Mol Biol* 26: 175-182.

Chow CW, Herrera AM, Suzuki T and Downey GP (2003) Oxidative stress and acute lung injury. *Am J Respir Cell Mol Biol* 29: 427-431.

Clark JM and Lambertsen CJ (1967) Pulmonary oxygen tolerance and the rate of development of pulmonary oxygen toxicity in man at 2 atmospheres inspired PO_2, *Underwater Physiology* 439-451.

Clark JM and Lambertsen CJ (1971) Pulmonary oxygen toxicity: a review. *Pharmacol Rev* 23: 37-133.

Clough AV, Haworth S, Audi SH, Molthen R, Roerig D (2010) Differential lung uptake of 99mTc-HMPAO and 99mTc-duramycin in the chronic hyperoxia rat model of lung injury.

Small Animal SPECT Imaging Conference, University of Arizona, Tucson, AZ.

Coursin DB, Cihla HP, Will JA and McCreary JL (1987**)** Adaptation to chronic hyperoxia. Biochemical effects and the response to subsequent lethal hyperoxia. *Am Rev Respir Dis* 135: 1002-1006.

Crane P, Laliberte R and Heminway S (1993) Effect of mitochondrial viability and metabolism on technetium-99m-sestamibi myocardial retention. *Eur J Nucl Med* 20: 20-25.

Crapo JD and Tierney DF (1974) Superoxide dismutase and pulmonary oxygen toxicity. *Am J Physiol* 226: 1401-1407.

Crapo JD, Peters-Golden M, Marsh-Salin J and Shelburne JS (1978) Pathologic changes in the lungs of oxygen-adapted rats: a morphometric analysis. *Lab Invest* 39: 640-653.

Crapo JD, Barry BE, Foscue HA and Shelburne J (1980) Structural and biochemical changes in rat lungs occurring during exposures to lethal and adaptive doses of oxygen. *Am Rev Resp Dis* 122: 123-143.

Crapo JD, Freeman BA, Barry BE, Turrens JF and Young SL (1983) Mechanisms of hyperoxic injury to the pulmonary microcirculation, *Physiologist*, 26: 170-176.

Davis WB, Rennard SI, Bitterman PB and Crystal RG (1983) Pulmonary oxygen toxicity. Early reversible changes in human alveolar structures induced by hyperoxia. *N Engl J Med* 309: 878-883.

Dawson CA, S.H. Audi, G.S. Krenz and D.L. Roerig (2003) Endothelium and compound transfer in: molecular nuclear medicine: the challenge of genomics and proteomics to clinical practice, edited by Feinendegen LES, Eckelman WC, Bahk YW and Wagner JN. *New York*: *Springer*, 201-216.

Dedkova EN and Blatter LA. (2005) Modulation of mitochondrial Ca^{2+} by nitric oxide in cultured bovine vascular endothelial cells. *Am J Physiol Cell Physiol* 289: C836-C845.

Desquiret V, Gueguen N, Malthiery Y, Ritz P and Simard G (2008) Mitochondrial effects of dexamethasone imply both membrane and cytosolic-initiated pathways in HepG2 cells. *Int J Biochem Cell Biol* 40: 1629-1641.

Di LF, Blank PS, Colonna R, Gambassi G, Silverman HS, Stern MD and Hansford RG (1995) Mitochondrial membrane potential in single living adult rat cardiac myocytes exposed to anoxia or metabolic inhibition. *J Physiol* 486 (Pt 1): 1-13.

Di VF and Azzone GF (1982) Activation of site I redox-deriven H^+ pump by exogenous quinones in intact mitochondria. *J Biol Chem*, 257: 4106-4113.

Dickman KG and Mandel LJ (1990) Differential effects of respiratory inhibitors on glycolysis in proximal tubules. *Am J Physiol.* 258: F1608-15.

Dinkova-Kostova AT and Talalay P (2000) Persuasive evidence that quinone reductase type 1 (DT diaphorase) protects cells against the toxicity of electrophiles and reactive forms of oxygen. *Free Radic Biol Med* 29: 231-240.

Djurhuus R, Svardal AM and Thorsen E (1999) Glutathione in the cellular defense of human lung cells exposed to hyperoxia and high pressure. *Undersea Hyperb Med* 26: 75-85.

Drechsel DA and Patel M (2009) Differential contribution of the mitochondrial respiratory chain complexes to reactive oxygen species production by redox cycling agents implicated in parkinsonism. *Toxicological Sciences* 112: 427-434.

Duchen MR, Surin A and Jacobson J (2003) Imaging mitochondrial function in intact cells. *Methods Enzymol* 361: 353-389.

Ehrenberg B, Montana V, Wei MD, Wuskell JP and Loew LM (1988) Membrane potential can be determined in individual cells from the nernstian distribution of cationic dyes. *Biophys J* 53: 785-794.

Factor P, Dumasius A, Saldias F, Brown LA and Sznajder JI (2000) Adenovirus-mediated transfer of an Na^+/K^+-ATPase $ß_1$ submit gene improves alveolar fluid clearance and survival in hyperoxic rats. *Human Gene Therapy*, 11: 2231-2242.

Farkas DL, Wei MD, Febbroriello P, Carson JH and Loew LM (1989) Simultaneous imaging of cell and mitochondrial membrane potentials. *Biophys J* 56: 1053-1069.

Fatma N, Kubo E, Toris CB, Stamer WD, Camras CB and Singh DP (2009) PRDX6 attenuates oxidative stress- and TGFbeta-induced abnormalities of human trabecular meshwork cells, *Free Radic Res* 43: 783-95.

Fato R, Bergamini C, Leoni S and Lenaz G (2008) Mitochondrial production of reactive oxygen species: role of complex I and quinone analogues. *Biofactors* 32: 31-39.

Fisher AB and Beers MF (2008) Hyperoxia and acute lung injury. *Am J Physiol Lung Cell Mol Physiol* 295: L1066; author reply L1067.

Fisher AB, Forman HJ and Glass M (1984) Mechanisms of pulmonary oxygen toxicity. *Lung* 162: 255-259.

Franco R, Panayiotidis MI and Cidlowski JA (2007) Glutathione depletion is necessary for apoptosis in lymphoid cells independent of reactive oxygen species formation. *J Biol Chem*

282:30452-30465

Franco R and Cidlowski JA (2009) Apoptosis and glutathione: beyond an antioxidant. *Cell Death Differ* 16:1303-1314.

Frank L, Summerville J and Massaro D (1980) Protection from oxygen toxicity with endotoxin. Role of the endogenous antioxidant enzymes of the lung. *J Clin Invest* 65: 1104-1110.

Frank L, Iqbal J, Hass M and Massaro D (1989) New "rest period" protocol for inducing tolerance to high O_2 exposure in adult rats. *Am J Physiol* 257: L226-231.

Freeman BA and Crapo JD (1981) Hyperoxia increases oxygen radical production in rat lungs and lung mitochondria. *J Biol Chem* 256: 10986-10992.

Fridovich I (1983) Superoxide radical: an endogenous toxicant. *Annu Rev Pharmacol Toxicol* 23: 239-257.

Fridovin I and Freeman B (1986) Antioxidant defenses in the lung. *Annu Rev Physiol* 48: 693-702.

Genova ML, Bianchi C and Lenaz G (2005) Supercomplex organization of the mitochondrial respiratory chain and the role of the Coenzyme Q pool: pathophysiological implications. *Biofactors* 25: 5-20

Gomi F and Matsuo M (2002) Effects of 60% oxygen inhalation on the survival and antioxidant enzyme activities of young and old rats. *Mech Ageing Dev* 123:1295-1304

González AD, Ariza J and Villalba JM (2007) Dicumarol impairs mitochondrial electron transport and pyrimidine biosynthesis in human myeloid leukemia HL-60 cells. *Biochem Pharmacol* 73: 427-439

Griffith DE, Holden WE, Morris JF, Min LK and Krishnamurthy GT (1986) Effects of common therapeutic concentrations of oxygen on lung clearance of 99mTc DTPA and bronchoalveolar lavage albumin concentration. *Am Rev Respir Dis* 134: 233-237.

Griffith OW (1980) Determination of glutathione and glutathione disulfide using glutathione reductase and 2-vinylpyridine. *Anal Biochem* 106: 207-212.

Hamada Y, Ikata T, Katoh S, Nakauchi K, Niwa M, Kawai Y and Fukuzawa K (1996) Involvement of an intercellular adhesion molecule 1-dependent pathway in the pathogenesis of secondary changes after spinal cord injury in rats. *J Neurochem* 66: 1525-1531.

Han YH, Moon HJ, You BR and Park WH (2010) Propyl gallate inhibits the growth of calf pulmonary arterial endothelial cells via glutathione depletion. *Toxicol In Vitro* 24: 1183-1189.

Han YH, Kim SH, Kim SZ and Park WH. (2008) Intracellular GSH levels rather than ROS levels are tightly related to AMA-induced HeLa cell death. *Chem Biol Interact* 171:67-78

Hang LW, Shiau YC, Hsu WH, Tsai JJ, Yeh JJ and Kao A (2003) Increased lung uptake of technetium-99m hexamethylpropylene amine oxime in diffuse infiltrative lung disease. *Respiration* 70: 479-483.

Hansford RG, Hogue BA and Mildaziene V (1997) Dependence of H_2O_2 formation by rat heart mitochondria on substrate availability and donor age. *J Bioenerg Biomembr* 29: 89-95.

Haughland R (2002) Handbook of Fluorescent Compounds and Research Products, 9th Ed. *Molecular Probes, Inc.*

Hayatdavoudi G, O'Neil JJ, Barry BE, Freeman BA and Crapo JD (1981) Pulmonary injury in rats following continuous exposure to 60% O_2 for 7 days. *J Appl Physiol* 51: 1220-1231.

He P and Curry FE (1995) Measurement of membrane potential of endothelial cells in single perfused microvessels. *Microvasc Res* 50: 183-198.

Heumüller S, Wind S, Barbosa ES, Schmidt H, Busse R, Schroder K, Brandes RF (2008), Apocynin is not an inhibitor of vascular NADPH oxidases but an antioxidant. *Hypertension* 51: 211-217.

Higgins DS Jr and Greenamyre JT (1996) [3H]dihydrorotenone binding to NADH:ubiquinone reductase (complex I) of the electron transport chiain: an autoradiographic study. *J Neurosci* 16: 3807-3816

Ho YS. (2002) Transgenic and knockout models for studying the role of lung antioxidant enzymes in defense against hyperoxia. *Am J Respir Crit Care Med* 166: S51-56.

Ho YS, Dey MS and Crapo JD (1996) Antioxidant enzyme expression in rat lungs during hyperoxia. *Am J Physiol* 270: L810-818.

Huang L, Yappert MC, Jumblatt MM and Borchman D (2008) Hyperoxia and thyroxin treatment and the relationships between reactive oxygen species generation, mitochondrial membrane potential and cardiolipin in human lens epithelial cell cultures. *Current Eye Research* 33: 575-586.

Huang LS, Cobessia D, Tung EY and Berry EA (2005) Binding of the respiratory chain inhibitor antimycin to the mitochondrial bc1 complex: a new crystal structure reveals an altered intramolecular hydrogen-binding pattern, *J Mol Biol* 351: 573–597.

Huang M, Camara AK, Stowe DF, Qi F and Beard DA (2007) Mitochondrial inner membrane electrophysiology assessed by rhodamine-123 transport and fluorescence. *Ann Biomed Eng* 35: 1276-1285.

Huber HJ, Plchut M, Weisova P, Dnssmann H, Wenus J, Rehm M, Ward MW and Prehn JHM (2009) TOXI-SIM--A simulation tool for the analysis of mitochondrial and plasma membrane potentials. *J Neurosci Methods* 176: 270-275.

Huser J and Blatter LA (1999) Fluctuations in mitochondrial membrane potential caused by repetitive gating of the permeability transition pore. *Biochem J* 343: 311-317.

Hyde RW and Rawson AJ (1969) Unintentional iatrogenic oxygen pneumonitis-response to therapy. *Ann Intern Med*, 71: 517-531.

Inoue K, Nakagawa M, Goto R, Kinomura S, Sato T, Sato K and Fukuda H (2003) Regional differences between 99mTc-ECD and 99mTc-HMPAO SPET in perfusion changes with age and gender in healthy adults. *Eur J Nucl Med Mol Imaging* 20: 1489-1497.

Jacquier SM, Polla BS and Slosman DO (1996) Oxido-reductive state: the major determinant for cellular retention of technetium-99m-HMPAO. *J Nucl Med* 37:1413-1416.

Janssens D, Delaive E, Houbion A, Eliaers F, Remacle J and Michiels C (2000) Effect of venotropic drugs on the respiratory activity of isolated mitochondria and in endothelial cells. *Br J Pharmacol* 130: 1513-1524.

Johns A, Lategan TW, Lodge NJ, Ryan US, van BC and Adams DJ (1987) Calcium entry through receptor-operated channels in bovine pulmonary artery endothelial cells. *Tissue Cell* 19: 733-745.

Joffe N and Simon M (1969) Pulmonary oxygen toxicity in the adult. *Radiology* 92: 460-465.

Kapanci Y, Tosco Rm, Eggermann J and Gould VE (1972) Oxygen Pneumonitis is Man. *Chest* 62:162-169

Katzir H, Yeheskely-Hayon D, Regev R and Eytan GD (2010) Role of the plasma membrane leaflets in drug uptake and multidrug resistance. *FEBS J* 277: 1234-1244.

Kim V, Benditt JO, Wise RA and Sharafkhaneh A (2008) Oxygen therapy in chronic obstructive pulmonary disease. *Proc Am Thorac Soc* 5: 513-518.

Kim YJ (2004) The influence of NaCl and carbonylcynaide-m-chlorophenylhydrazone on the production of extracellular proteases in a marine Vibrio strain. *J Microbiol* 42: 156-159.

Kimball RE, Reddy K, Peirce TH, Schwartz LW, Mustafa MG and Cross CE (1976) Oxygen toxicity: augmentation of antioxidant defense mechanisms in rat lung. *Am J Physiol* 230: 1425-1431.

Kinnula VL, Everitt JI, Whorton AR and Crapo JD (1991) Hydrogen peroxide production by

alveolar type II cells, alveolar macrophages, and endothelial cells. *Am J Physiol* 261: L84-91

Koliwad SK, Kunze DL and Elliott SJ (1996) Oxidant stress activates a non-selective cation channel responsible for membrane depolarization in calf vascular endothelial cells. *J Physiol* 491 (Pt 1): 1-12.

Kraus RJ and Ganther HE (1980) Reaction of cyanide with glutathione peroxidase. *Biochem Biophys Res Commun* 96: 1116-1122.

Krishna R and Mayer LD (2000) Multidrug resistance (MDR) in cancer Mechanisms, reversal using modulators of MDR and the role of MDR modulators in influencing the pharmacokinetics of anticancer drugs. *Eur J Pharm Sci* 11: 265–283.

Krishnamoorthy G and Hinkle PC (1988) Studies on the electron transfer pathway, topography of iron-sulfur centers, and site of coupling in NADH-Q oxidoreductase. *J Biol Chem.* 263: 17566-75.

Ksenzenko M, Konstantinov AA, Khomutov GB, Tikhonov AN and Ruuge EK. (1983) Effect of electron transfer inhibitors on superoxide generation in the cytochrome bc1 site of the mitochondrial respiratory chain. *FEBS Lett.* 155: 19-24.

Kushnareva Y, Murphy AN and Andreyev A. (2002) Complex I-mediated reactive oxygen species generation: modulation by cytochrome c and NAD(P)+ oxidation-reduction state. *Biochem J.* 368(Pt 2): 545-53.

Kümin A, Huber C, Rulicke T, Wolf E and Werner S (2006) Peroxiredoxin 6 is a potent cytoprotective enzyme in the epidermis. *Am J Pathol* 169: 1194-205.

Kwong LK and Sohal RS (1998) Substrate and site specificity of hydrogen peroxide generation in mouse mitochondria. *Arch Biochem Biophys*. 350: 118-26.

Labinskyy N, Csiszar A, Orosz Z, Smith K, Rivera A, Buffenstein R and Ungvari1 Z (2006) Comparison of endothelial function, O_2^- and H_2O_2 production, and vascular oxidative stress resistance between the longest-living rodent, the naked mole rat, and mice, *Am J Physiol Heart Circ Physiol* 291: H2698–H2704.

Lenaz G (2001) The mitochondrial production of reactive oxygen species: mechanisms and implications in human pathology. *IUBMB Life* 52: 159-164.

Lenaz G, Fato R, Baracca A and Genova ML. (2004) Mitochondrial quinone reductases: complex I. *Methods Enzymol* 382: 3-20.

Li J, Gao X, Qian M and Eaton JW (2004**)** Mitochondrial metabolism underlies hyperoxic cell damage. *Free Radic Biol Med* 36: 1460-1470.

Li N, Ragheb K, Lawler G, Sturgis J, Rajwa B, Melendez JA, Robinson JP (2003) Mitochondrial complex I inhibitor rotenone induces apoptosis through enhancing mitochondrial reactive oxygen species production. *J Biol Chem.* 278: 8516-8525.

Lind C, Cadenas E, Hochstein P and Ernster L (1990) DTdiaphorase: purification, properties and function. *Methods Enzymol* 186: 287-301.

Lindemer BJ, Bongard RD, Hoffmann R, Baumgardt S, Gonzalez FJ and Merker MP (2011) Genetic evidence for NAD(P)H:Quinone Oxidoreductase 1 catalyzed quinone reduction on passage through the mouse pulmonary circulation. *Am J Physiol Lung Cell Mol Physiol* EPub

Loetchutinat C, Saengkhae C, Marbeuf-Gueye C and Garnier-Suillerot A (2003) New insights into the P-glycoprotein-mediated effluxes of rhodamines. *Eur J Biochem* 270: 476-485.

Madari H and Panda D (2003) Dicumarol: a unique microtubule stabilizing natural product that is synergistic with taxol. *Cancer Res* 623: 1214-1220.

Madesh M, Hawkins BJ, Milovanova T, Bhanumathy CD, Joseph SK, RamachandraRao SP, Sharma K, Kurosaki T and Fisher AB (2005) Selective role for superoxide in InsP3 receptor-mediated mitochondrial dysfunction and endothelial apoptosis. *J Cell Biol* 170: 1079-1090.

Mandala M, Serck-Hanssen G, Martino G and Helle KB (1999) The fluorescent cationic dye rhodamine 6G as a probe for membrane potential in bovine aortic endothelial cells. *Anal Biochem* 274: 1-6.

Manevich Y and Fisher AB (2005) Peroxiredoxin 6, a 1-Cys peroxiredoxin, functions in antioxidant defense and lung phospholipid metabolism. *Free Radic Biol Med* 38:1422-32.

Mantell LL, Horowitz S, Davis JM and Kazzaz JA (1999**)** Hyperoxia-induced cell death in the lung--the correlation of apoptosis, necrosis, and inflammation. *Ann N Y Acad Sci* 887: 171-180.

Matute BG, Frevert CW and Martin TR (2008) Animal models of acute lung injury. *Am J Physiol Lung Cell Mol Physiol* 295:379-399.

Mays JB and Benson AM (1992) Inhibition of mouse glutathione transferases and glutathione peroxidase II by dicoumarol and other ligands. *Biochem Pharmacol* 44: 921-925.

Merker MP, Armitage IM, Audi SH, Kakalis LT, Linehan JH, Maehl JR, Roerig DL and Dawson CA (1996) Impact of angiotensin-converting enzyme substrate conformation on fractional hydrolysis in the lung. *Am J Physiol Lung Cell Mol Physiol* 270: L251-L259.

Merker MP, Bongard RD, Linehan JH, Okamoto Y, Vyprachticky D, Brantmeier BM, Roerig DL and Dawson CA (1997) Pulmonary endothelial thiazine uptake: separation of cell surface reduction from intracellular reoxidation. *Am J Physiol Lung Cell Mol Physiol* 272: L673-L680.

Merker MP, Olson LE, Bongard RD, Patel MK, Linehan JH and Dawson CA (1998) Ascorbate-mediated transplasma membrane electron transport in pulmonary arterial endothelial cells. *Am J Physiol Lung Cell Mol Physiol* 274: L685-L693.

Merker MP, Bongard RD, Kettenhofen NJ, Okamoto Y and Dawson CA (2002) Intracellular redox status affects transplasma membrane electron transport in pulmonary arterial endothelial cells. *Am J Physiol Lung Cell Mol Physiol* 282: L36-L43.

Merker MP, Bongard RD, Krenz GS, Zhao H, Fernandes V, Kalyanaraman B, Hogg N and Audi SH (2004) Impact of pulmonary arterial endothelial cells on duroquinone redox status. *Free Radic Biol Med* 37: 86-103.

Merker MP, Audi SH, Bongard RD, Lindemer BJ and Krenz GS (2006) Influence of pulmonary arterial endothelial cells on quinone redox status: effect of hyperoxia induced NAD(P)H quinone oxidoreductase 1 (NQO1). *Am J Physiol Lung Cell Mol Physiol* 290: L607-L619.

Merker MP, Audi SH, Lindemer BJ, Krenz GS and Bongard RD (2007) Role of mitochondrial electron transport complex I in coenzyme Q_1 reduction by intact pulmonary arterial endothelial cells and the effect of hyperoxia. *Am J Physiol Lung Cell Mol Physiol* 293: L809-L819.

Minamiya Y (1995) Endotoxin-induced hydrogen peroxide production in intact pulmonary circulation of rat. *Am J Respir Crit Care Med* 152: 348-384.

Moody EJ, Simon BA and Johns RA (2001) Therapeutic Gases. In: *The Pharmacological Basis of Therapeutics*, edited by Hardman JG, Limbird LE and Gilman AG. New York: McGraw-Hill.

Muller FL (2000) The nature and mechanism of superoxide production by the electron transport chain: its relevance to aging. *J Amer Aging Assoc* 23: 227-253.

Muller FL, Liu Y and Remmen HV (2004) Complex III releases superoxide to both sides of the inner mitochondrial membrane. *J Biol Chem* 279: 49064-49073.

Mungunsukh O, Griffin AJ, Lee YH and Day RM (2010) Bleomycin induces the extrinsic apoptotic pathway in pulmonary endothelial cells. *Am J Physiol Lung Cell Mol Physiol* 298: L696-L703.

Nadanaciva S, Bernal A, Aggeler R, Capaldi R and Will Y (2007) Target identification of drug induced mitochondrial toxicity using immunocapture based OXPHOS activity assays. *Toxicol In Vitro* 5: 902-911.

Nagato A, Silva FL, Silva AR, Bezerra FS, Oliveira ML, Bello KA, Cristovao PL and Santos VS (2009) Hyperoxia-induced lung injury is dose dependent in wistar rats. *Exp Lung Res* 35: 713-728.

Nathens AB, Marshall JC, Watson RW, Dackiw AP and Rostein OD (1996) Diethylmaleate attenuates endotoxin-induced lung injury. *Surgery* 120: 362-366.

Nicholls DG and Budd SL (2000) Mitochondria and neuronal survival. *Physiol Rev* 80: 315-360.

Nicholls DG (2005) Commentary on: 'old and new data, new issues: the mitochondrial Deltapsi' by H. Tedeschi. *Biochim Biophys Acta* 1710: 63-65.

Nicholls DG (2006) Simultaneous monitoring of ionophore- and inhibitor-mediated plasma and mitochondrial membrane potential changes in cultured neurons. *J Biol Chem* 281: 14864-14874.

Nici L, Dowin R, Gilmore HM, Jamieson JD and Ingbar DH (1991) Upregulation of rat lung Na-K-ATPase during hyperoxic injury. *Am. J. Physiol* 261: L307-L314.

O'Brodovich HM and Mellins RB (1985) Bronchopulmonary dysphasia. Unresolved neonatal acute lung injury. *Am Rev Respir Dis* 132: 694-709.

Oldendorf WH, Cornford ME and Brown WJ (1977) The large apparent work capability of the blood-brain barrier: a study of the mitochondrial content of capillary endothelial cells in brain and other tissues of the rat. *Ann Neurol* 1: 409-417.

O'Malley Y, Fink BD, Ross NC, Prisinzano TE and Sivitz WI (2006) Reactive oxygen and targeted antioxidant administration in endothelial cell mitochondria. *J Biol Chem* 281: 39766-39775.

Ortega AL, Mena S and Estrela JM (2011) Glutathione in cancer cell death. *Cancer* 3:1285-1310

Otterbein LE and Choi AM (2002) The saga of leucine zippers continues: in response to oxidative stress. *Am J Respir Cell Mol Biol* 26: 161-163.

Owens CW and Belcher RV (1965) A Colorimetric Micro-Method for the Determination of Glutathione. *Biochem J* 94: 705-711.

Paffett ML, Naik JS, Resta TC and Walker BR (2007) Reduced store-operated Ca^{2+} entry in

pulmonary endothelial cells from chronically hypoxic rats. *Am J Physiol Lung Cell Mol Physio* 293: L1135-L1142.

Paradies G, Petrosillo G, Pistolese M, Di VN, Federici A and Ruggiero FM (2004) Decrease in mitochondrial complex I activity in ischemic/reperfused rat heart: involvement of reactive oxygen species and cardiolipin. *Circ Res* 94: 53-59

Park KS, Jo I, Pak K, Bae SW, Rhim H, Suh SH, Park J, Zhu H, So I and Kim KW (2002) FCCP depolarizes plasma membrane potential by activating proton and Na^+ currents in bovine aortic endothelial cells. *Pflugers Arch* 443: 344-352.

Park WH, Han YW, Kim SH and Kim SZ (2007) An ROS generator, antimycin A, inhibits the growth of HeLa cells via apoptosis. *J Cell Biochem* 102: 98-109.

Phua J, Badia JR, Adhikari NK, Friedrich JO, Fowler RA, Singh JM, Scales DC, Stather DR, Li A, Jones A, Gattas DJ, Hallett D, Tomlinson G, Stewart TE and Ferguson ND (2009) Has mortality from acute respiratory distress syndrome decreased over time?: A systematic review. *Am J Respir Crit Care Med* 179: 220-227.

Preusch PC, Siefel D, Gibson NW and Ross D (1991) A note on the inhibition of DT-diaphorase by dicumarol *Free Radic Bio Med* 11: 77-80.

Price G. (2003) Metformin lactic acidosis, acute renal failure and rofecoxib. *Br J Anaesth* 91: 909-910.

Pruijn FB, Schoonen WG and Joenje H (1992) Inactivation of mitochondrial metabolism by hyperoxia-induced oxidative stress. *Ann N Y Acad Sci* 663: 453-455.

Radjendirane V, Joseph P, Lee YH, Kimura S, Klein-Szanto AJ, Gonzalez FJ and Jaiswal AK (1998) Disruption of the DT diaphorase (NQO1) gene in mice leads to increased menadione toxicity. *J Biol Chem* 273: 7382-7389.

Ramakrishna M, Gan Z, Clough AV, Molthen RC, Roerig DL and Audi SH (2010) Distribution of Capillary Transit Times in Isolated Lungs of Oxygen-Tolerant Rats. *Ann Biomed Eng*. 38: 3449-3465.

Ragaller M and Richter T (2010) Acute lung injury and acute respiratory distress syndrome. *J Emerg Trauma Shock* 3: 43-51.

Ratcliffe P, Ebert B, Firth J, Gleadle J, Maxwell P, Nagao M, O Rourke J, Pugh C and Wood S (1997) Oxygen regulated gene expression: erythropoietin as a model system. *Kidney Int.* 51:514-526.

Ratner V, Starkov A, Matsiukevich D, Polin RA and Ten VS (2009) Mitochondrial dysfunction

contributes to alveolar developmental arrest in hyperoxia-exposed mice. *Am J Respir Cell Mol Biol* 40: 511-518.

Rhian MT (2008) Apocynin, NADPH oxidase, and vascular cells: a complex matter. *Hypertension* 51: 172-174.

Robertson SJ, Kania KD, Hladky SB and Barrand MA (2009) P-glycoprotein expression in immortalised rat brain endothelial cells: comparisons following exogenously applied hydrogen peroxide and after hypoxia-reoxygenation. *J Neurochem* 111: 132-141.

Roerig DL, Audi SH and Ahlf SB (2004) Kinetic characterization of P-glycoprotein mediated efflux of rhodamine 6G in the intact rabbit lung. *Drug Metab Dispos* 32: 953-958.

Rogers LK, Tipple TE, Nelin LD and Welty SE (2009) Differential responses in the lungs of newborn mouse pups exposed to 85% or >95% oxygen. *Pediatr Res* 65: 33-38.

Ross D, Kepa JK, Winski SL, Beall HD, Anwar A and Siegel D (2000) NAD(P)H:quinone oxidoreductase 1 (NQO1): chemoprotection, bioactivation, gene regulation and genetic polymorphisms. *Chem Biol Interact* 129: 77-97.

Ross D, Siegel D, Beall H, Prakash AS, Mulcahy RT and Gibson NW (1993) DT-diaphorase in activation and detoxification of quinones. Bioreductive activation of mitomycin C. *Cancer Metastasis Rev* 12: 83-101.

Rourke B, Cortassa S and Aon MA (2005) Mitochondrial ion channels: gatekeepers of life and death *Am Physiol Soc* 20: 303-313.

Ruchko M, Gorodnya O, LeDoux SP, Alexeyev MF, Al-Mehdi AB and Gillespie MN (2005) Mitochondrial DNA damage triggers mitochondrial dysfunction and apoptosis in oxidant-challenged lung endothelial cells. *Am J Physiol Lung Cell Mol Physio* 288: L530-L535.

Rugolo M and Lenaz G (1987) Monitoring of the mitochondrial and plasma membrane potentials in human fibroblasts by tetraphenylphosphonium ion distribution. *J Bioenerg Biomembr* 19: 705-718.

Sander SP, Zweier JL, Kuppusamy P, Harrison SJ, Bassett DJ, Gabrielson EEW and Sylvester JT (1993) Hyperoxic sheep pulmonary microvascular endothelial cells generate free radicals via mitochondrial electron transport. *J Clin Invest* 91: 46-52.

Saugstad OD (2007) Optimal oxygenation at birth and in the neonatal period. *Neonatology* 91: 319-322.

Scaduto RC and Grotyohann LW (1999) Measurement of mitochondrial membrane potential using fluorescent rhodamine derivatives. *Biophys J* 76: 469-477.

Schoonen WG, Wanamarta AH, van der Klei-van Moorsel, Jakobs C and Joenje H (1990) Respiratory failure and stimulation of glycolysis in Chinese hamster ovary cells exposed to normobaric hyperoxia. *J Biol Chem* 265: 1118-1124.

Schuschke DA, Percival SS, Lominadze D, Sarri JT and Lentsch AB (2002) Tissue-spcific ICAM-1 expression and neutrophil transmigration in the copper-deficient rat. *Inflmmation* 26: 297-303.

Seddon B and Mcvitte J (1974) The effect of inhibitors on the electron-transport chain of Bacillus brevis: Evidence for branching of the NADH oxidase respiratory chain. *J Gen Microbiol* 84: 386-390.

Semenza G (1994) Regulation of erythropoietin production. New insights into molecular mechanisms of oxygen hemeostasis. *Hematol. Oncol. Clin. North Am*. 8: 863-884.

Semenza G (2007) Life with oxygen. *Science* 318: 62-64.

Seral C, Michot JM, Chanteux H, Leclercq MP, Tulkens PM and Bambeke FV (2003) Influence of P-glycoprotein inhibitors on accumulation of macrolides in J774 murine macrophages. Antimicrob Agents Chemother 43: 1047–1051.

Shimura N, Musya A, Hashimoto T, Kojima S, Kubodera A and Sasaki T (2000) Usefulness of (99m)Tc-d,I-HMPAO for estimation of GSH content in tumor tissues. *Nucl Med Biol* 27: 577-580.

Siegel D and Ross D (2000) Immunodetection of NAD(P)H:quinone oxidoreductase 1 (NQO1) in human tissues. *Free Radic Biol Med* 29: 246-253.

Siegel D, Gustafson DL, Dehn DL, Han JY, Boonchoong P, Berliner LJ and Ross D (2004) NAD(P)H:quinone oxidoreductase 1: role as a superoxide scavenger. *Mol Pharmacol* 65: 1238-1247.

Sjostrom K and Crapo JD (1983) Structural and biochemical adaptive changes in rat lungs after exposure to hypoxia. *Lab Invest* 48: 68-79.

Solaini G, Sgarbi G, Lenaz G and Baracca A (2007) Evaluating mitochondrial membrane potential in cells. *Biosci Rep* 27: 11-21.

Song C, Al-Mehdi AB and Fisher AB (2001) An immediate endothelial cell signaling response to lung ischemia. *Am J Physiol Lung Cell Mol Physiol* 281: L993-L1000.

Spiller HA and Quadrani DA (2004) Toxic effects from metformin exposure. *Ann Pharmacother* 38: 776-780.

Starkov AA and Fiskum G (2001) Myxothiazol induces H_2O_2 production from mitochondrial respiratory chain. *Biochem Biophys Res Commun.* 281: 645-50.

Stevens T, Cornfield DN, McMurtry IF and Rodman DM (1994) Acute reductions in PO_2 depolarize pulmonary artery endothelial cells and decrease $[Ca^{2+}]_i$. *Am J Physiol* 266: H1416-H1421.

Storrie B and Madden EA (1990) Isolation of subcellular organelles. *Methods Enzymol* 182: 203-225.

Sud N, Wells SM, Sharma S, Wiseman DA, Wilham J and Black SM (2008) Asymmetric dimethylarginine inhibits HSP90 activity in pulmonary arterial endothelial cells: role of mitochondrial dysfunction. *Am J Physiol Cell Physiol* 294: C1407-C1418.

Suga K, Uchisako H, Nishigauchi K, Shimizu K, Kume N, Yamada N and Nakanishi T (1994) Technetium-99m-HMPAO as a marker of chemical and irradiation lung injury: experimental and clinical investigations. *J Nucl Med* 25: 1520-1527.

Suttorp N, Toepfer W and Roka L (1986) Antioxidant defense mechanisms of endothelial cells: glutathione redox cycle versus catalase. *Am J Physiol* 251: C671-680.

Suzy AA and Serpil CE (2002) Antixodiant responses to oxidant-mediated lung diseases. *Am J Physiol Lung Cell Mol Physiol* 283: L246–L255.

Talpade DJ, Greene JG, Higgins DS Jr and Greenamyre JT (2000) In vivo labeling of mitochondrial complex I (NADH:ubiquinone oxidoreductase) in rat brain using [(3)H]dihydrorotenone. *J Neurochem* 75: 2611-21.

Tan AS and Berridge MV (2010) Evidence for NAD(P)H:quinone oxidoreductase 1 (NQO1)-mediated quinone-dependent redox cycling via plasma membrane electron transport: A sensitive cellular assay for NQO1. *Free Radic Biol Med* 48: 421-429.

Terminella C, Tollefson K, Kroczynski J, Pelli J and Cutaia M (2002) Inhibition of apoptosis in pulmonary endothelial cells by altered pH, mitochondrial function, and ATP supply. *AJP - Lung Cellular and Molecular Physiology* 283: L1291-L1302.

Thompson RJ, Buttigieg J, Zhang M and Nurse CA (2007) A rotenone-sensitive site and H_2O_2 are key components of hypoxia-sensing in neonatal rat adrenomeduliary chromaffin cells. *Neuroscience* 145: 130–141.

Tietze F (1969) Enzymic method for quantitative determination of nanogram amounts of total and oxidized glutathione: applications to mammalian blood and other tissues. *Anal Biochem* 27: 502-522.

Townsend DM, Tew KD and Tapiero H. (2003) The importance of glutathione in human disease. *Biomed Pharmacother* 57:145-55.

Turrens JF and Boveris A (1980) Generation of superoxide anion by the NADH dehydrogenase of bovine heart mitochondria. *Biochem J.* 191: 421-7.

Turrens JF (1997) Superoxide production by the mitochondrial respiratory chain. *Biosci Rep.* 17:3-8.

Turrens JF (2003) Mitochondrial formation of reactive oxygen species. *J Physiol* 552 (Pt 2): 335-344.

VanBrochlin HF, Hanrahan SM, Enas JD, Nandanan E and ONeil JP (2007) Mitochondrial avid radioprobes. Preparation and evaluation of 7'(Z)-$^{[125]}$iodorotenone and 7'(Z)-$^{[125]}$iodorotenol. *Nucl Med Biol* 34: 109-116.

Van Klaveren RJ, Dinsdale D, Pype JL, Demedts M and Nemery B (1997) Changes in gamma-glutamyltransferase activity in rat lung tissue, BAL, and type II cells after hyperoxia. *Am J Physiol* 273: L537-547.

Van Raam BJ, Sluiter W, de Wit E, Roos D, Verhoeven AJ and Kuijpers Tw (2008) Mitochondrial membrane potential in human neutrophils is maintained by complex III activity in the absence of supercomplex organization. *PLoS One* 3: e2013

Voets T, Droogmans G and Nilius B (1996) Membrane currents and the resting membrane potential in cultured bovine pulmonary artery endothelial cells. *J Physiol* 497 (Pt 1): 95-107.

Von JG and Bohrer C (1975) Inhibition of electron transfer from ferrocytochrome b to ubiquinone, cytochrome c1 and duroquinone by antimycin. *Biochim Biophys Acta* 387: 409-424.

Wang L, Leggas M, Goswami M, Empey PE and McNamara PJ (2008) N-(4-[2-(1,2,3,4-tetrahydro-6,7-dimethoxy-2-isoquinolinyl)ethyl]-phenyl)-9,10-dihydro-5-methoxy-9-oxo-4-acridine carboxamide (GF120918) as a chemical ATP-binding cassette transporter family G member 2 (Abcg2) knockout model to study nitrofurantoin transfer into milk. *Drug Metab Dispos* 36: 2591-2596.

Wang Y, Manevich Y, Feinstein SI and Fisher AB (2004) Adenovirus-mediated transfer of the 1-cys peroxiredoxin gene to mouse lung protects against hyperoxic injury. *Am J Physiol Lung Ce*ll *Mol Physiol* 286: L1188-1193.

Wang Y, Feinstein SI, Manevich Y, Ho YS and Fisher AB (2004b) Lung injury and mortality with hyperoxia are increased in peroxiredoxin 6 gene-targeted mice. *Free Radic Biol Med* 37: 1736-1743.

Ward MW (2010) Quantitative analysis of membrane potentials. *Methods Mol Biol* 591: 335-351.

Ward MW, Huber HJ, Weisova P, Dussmann H, Nicholls DG and Prehn JH (2007) Mitochondrial and plasma membrane potential of cultured cerebellar neurons during glutamate-induced necrosis, apoptosis, and tolerance. *J Neurosci* 27: 8238-8249.

Ward MW, Rego AC, Frenguelli BG and Nicholls DG (2000) Mitochondrial membrane potential and glutamate excitotoxicity in cultured cerebellar granule cells. *J Neuroscience* 20: 7208-7219.

Welch BE, Morgan TJ and Clamann HG (1963) Time concentration effects in relation to oxygen toxicity in man. *Federation Proc* 22: 1053-1056

Whitney PL and Frank L (1993) Does lung NAD(P)H:quinone reductase (DT-diaphorase) play an antioxidant enzyme role in protection from hyperoxia? *Biochim Biophys Acta* 1156: 275-282.

Wilhelm J, Vankova M, Maxova H and Kova AI (2003) Hydrogen peroxide production by alveolar macrophages is increased and its concentration is elevated in the breath of rats exposed to hypoxia: relationship to lung lipid peroxidation *Physiol Res* 52: 327-332.

Williams JA (1970) Origin of transmembrane potentials in non-excitable cells. *J Theor Biol* 28: 287-296.

Wosilait WD, Ryan MP and Byington KH (1981) Uptake of anticoagulants by isolated rat hepatocytes. *Drug Metab Dispos* 9: 80-84.

Wu S, Jian MY, Xu YC, Zhou C, Al-Mehdi AB, Liedtke W, Shin HS and Townsley MI (2009) Ca^{2+} entry via α1G and TRPV4 channels differentially regulates surface expression of P-selectin and barrier integrity in pulmonary capillary endothelium. *Am J Physiol Lung Cell Mol Physiol* 297: L650-L657.

Yeheskely-Hayon D, Regev R, Katzir H and Eytan GD (2009) Competition between innate multidrug resistance and intracellular binding of rhodamine dyes. *FEBS J* 276: 637-648.

You BR and Park WH (2010) The effects of antimycin A on endothelial cells in cell death, reactive oxygen species and GSH levels. *Toxicol In Vitro* 24: 1111-1118.

Ysuf K, Ronald T, Jacques E and Victor EG (1972) Oxygen pneumonitis is man. *Chest* 62: 162-169.

Zhang H, Huang HM, Carson RC, Mahmood J, Thomas HM and Gibson GE (2001) Assessment of membrane potentials of mitochondrial populations in living cells. *Anal Biochem* 298: 170-180.

Zhang Q, Chatterjee S, Wei Z, Liu WD and Fisher AB (2008) Rac and PI3 kinase mediate endothelial cellreactive oxygen species generation during normoxic lung ischemia. *Antioxidants & Redox Signaling* 10: 679-689.

Zhou M, Diwu Z, Panchuk VN and Haugland RP (1997) A stable nonfluorescent derivative of resorufin for the fluorometric determination of trace hydrogen peroxide: applications in detecting the activity of phagocyte NADPH oxidase and other oxidases *Anal Biochem* 253: 162-169.

Zhu H, Jia Z, Mahaney JE, Ross D, Misra HP, Trush MA and Li Y (2007) The highly expressed and inducible endogenous NAD(P)H:quinone oxidoreductase 1 in cardiovascular cells acts as a potential superoxide scavenger. *Cardiovasc Toxicol* 7: 202-211.

Zhu QS and Beattie DS (1988) Direct interaction between yeast NADH-ubiquinone oxidoreductase, succinate-ubiquinone oxidoreductase, and ubiquinol-cytochrome c oxidoreductase in the reduction of exogenous quinones. *J Biol Chem* 263: 193-199.

Zmijewski JW, Lorne E, Zhao X, Tsuruta Y, Sha Y, Liu g, Siegal GP and Abraham E (2008) Mitochondrial respiratory complex I regulates neutrophil activation and severity of lung injury. *Am J Respir Crit Care Med*. 178: 168-179.

APPENDIX I - Recipes

Krebs-ringer bicarbonate buffer (KRB)

Stock solutions:
KCl 0.07 g/ ml H_2O
$CaCl_2 \cdot 2H_2O$ 0.0737 g/ ml H_2O
$MgSO_4 \cdot 7H_2O$ 0.058 g/ ml H_2O
KH_2PO_4 0.032 g/ ml H_2O

Buffer composition
0.5 ml of each stock / 100 buffer
NaCl 0.69 g/100 ml buffer
Dextrose 0.1 g/100 ml buffer
NaHCO3 0.21 g/100 ml buffer

5% Bovine Serum Albumin Perfusate (BSA)

5 g BSA / 100 ml KRB
PH 7.4

5% Dextran Perfusate (KD)

5 g dextran / 100 ml KRB
PH 7.4

Perfusate containing FAPGG

Stock
0.75 mg FAPGG/ ml ETOH
2. 9 mg ZnSO4.7H2O / ml H2O

Perfusate composition
0.1 ml FAPGG stock / 12 ml perfusate
132 µl ZnSO4 stock / 12 ml perfusate

Perfusate containing Rotenone

Stock
Rotenone 3.944 mg/ ml DMSO

20 µM Perfusate
20 µl rotenone stock / 10 ml perfusate

Perfusate containing Dicumarol

Stock
Dicumarol 43.7 mg/ ml DMSO

400 µM Perfusate
310 µl dicumarol stock to 10 ml perfusate

Perfusate containing Antimycin A

Stock
2.743 mg antimycin A/ ml DMSO

10 µM Perfusate
200 µl antimycin A stock/ 10 ml perfusate

Perfusate containing KCN

Stock
130 mg KCN/ ml H_2O

2 mM Perfusate
100 µl KCN stock/ 10 ml prepared perfusate

Perfusate containing CoQ_1

Stock
5 mg CoQ_1 / ml DMSO

400 µM Perfusate
20.4 µl CoQ_1 stock/ 10 ml perfusate

Perfusate containing DQ

stock
3.284 mg DQ / ml DMSO

400 μM perfusate
20.4 μl DQ stock/ 10 ml perfusate

Perfusate containing CoQ_1H_2

Stock
5 mg CoQ_1 / ml DMSO
4 mg NaOH / ml H_2O
0.2 ml 1M HCl / ml H_2O
27 mg KBH_4 / ml NaOH stock
37 mg EDTA / ml H_2O
CoQ_1H_2 stock:

Take 375 μl CoQ_1 stock into a 0.65 ml micro centrifuge tube
Add 15 μl KBH_4 stock into the tube, keep reacting in darkness for 1 hour.
Add 75 μl HCl stock, mixes slowly
Add 5 μL EDTA stock, keep reacting in darkness for 30 min

400 μM Perfusate
25.56 μl CoQ_1H_2 stock/ 10 ml perfusate

Perfusate containing DQH_2

Stock
3.284 DQ / ml DMSO
4 mg NaOH / ml H_2O
0.2 ml 1M HCl / ml H_2O
27 mg KBH_4 / ml NaOH stock
37 mg EDTA / ml H_2O
DQH_2 stock:

Take 375 μl DQ stock into a 0.65 ml micro centrifuge tube
Add 15 μl KBH_4 stock into the tube, keep reacting in darkness for 1 hour.
Add 75 μl HCl stock, mixes slowly
Add 5 μL EDTA stock, keep reacting in darkness for 30 min

400 μM Perfusate
25.56 μl DQH_2 stock/ 10 ml perfusate

Perfusate containing Amplex Red

Stock
5 mg amplex red / 1.943 ml DMSO

50 µM perfusate
50 µl amplex red stock/10 ml perfusate

Perfusate containing apocynin

Stock
apocynin 16.62 mg / ml ETOH

1 mM perfusate
100 µl apocynin stock / 10 ml perfusate

Perfusate containing Diethylmaleate

Stock
0.1 ml 97% DEM / ml DMSO

6 mM perfusate
100 µl stock/10 ml perfusate

Perfusate containing horseradish peroxidase

Stock
2 mg horseradish peroxidase / ml H2O

5U perfusate
100 µl stock/10 ml perfusate

APPENDIX II - Data Processing Codes

A. Codes for estimation of tube-binding coefficient

A.1 tube_model.m

```
function tube_model
% Function:       Find the optimized value for the parameters
% Input:          experimental data
% Output:         optimized value of parameters
% Format of input data:
%                 1st column: sampling time
%                 2nd column: normalized [R]e at corresponding sampling time without cells
% By Z Gan, updated on 04-17-2011

clear global
close all

% open data file
infile = 'tube.txt';
fid = fopen(infile, 'r');
if fid < 1
   input('invalid filename, press any key to end the program.', 's');
else
   % get data
   expdata = textscan(fid,'%f %f');
   fclose(fid);
   mtime = (expdata{1})';
   tube = (expdata{2})';

   % set initial values
   k1 = 0.0004382;  % Rate constant for dye-cuvette binding (min^-1 nM^-1)
   k2 = 0.00079704; % Rate constant for dye-cuvette unbinding (min^-1)

   % define parameters which will be optimized
   p0 = [k1 k2];
   % define lower and upper bound
   lb = [0 0];
   ub = [1 1];

   % define time points used for optimization
   tdata = mtime;

   % define data used for optimization
```

```
    ydata = tube;

    % define the optimization options
    options=optimset('TolX',1e-8,'MaxFunEvals',3000);

    % fitting model to input data and find out the optimized values for parameters
    [p, ssd, residual,exitflag,output,lambda,nJa] = lsqcurvefit(@solve_tube, p0, tdata, ydata, lb, ub,
options);

    % calculate correlation matrix
    [Q,R]=qr(nJa);
    R1 = R(1:length(p), :);
    h=inv(R1'*R1);
    for i=1:length(p)
        for j=1:length(p)
            cc(i,j)=h(i,j)/(h(i,i)*h(j,j))^0.5;
        end
    end

    % calculate confidence interval
    s2=ssd/(length(ydata)-length(p));
    for i = 1:length(p)
        seb(i)=(s2^0.5)*(h(i,i)^0.5);
    end
    ci=seb.*2.01

    % display the estimated values and related results
    fprintf('   k1 = %f ml/min\n', p(1));
    fprintf('   k2 = %f ml/min\n', p(2));
    fprintf('   ci = %f %f \n', ci);
    fprintf('   ssd = %f \n', ssd);

end
```

A.2 slove_tube.m

```
function yy = solve_tube (p,t)
% Function: calculate [R]e according to given parameters
% Input:    p: parameters
%           t: sampling time
% Output:   An array of [R]e
% By Z Gan, updated on 04-17-2011

k1 = p(1);
```

```
k2 = p(2);

% calculate [R]e based on tubing-binding model
for i=1:length(t)
   Y11(i)= (k2+k1*exp(-(k1+k2)*t(i)))/(k1+k2);
end

% return [R]e
yy = [Y11];
end
```

B. Codes for rhodamine distribution model

B.1 optimize_rhodamine.m

```
function optimize_rhodamine
% Function:      Find the optimized value for the parameters
% Input:         experimental data
% Output:        optimized value of parameters
% By Z Gan, updated on 04-14-2011
% Format of input data:
%   1st column: sampling time
%   2nd column: [R]e at corresponding sampling time with cells only
%   3rd column: [R]e at corresponding sampling time with cells in the presence of CCCP
%   4th column: [R]e at corresponding sampling time with cells in the presence of GF
%   5th column: [R]e at corresponding sampling time with cells in the presence of HK
%   6rd column: [R]e at corresponding sampling time with cells in the presence of CCCP and GF
%   7th column: [R]e at corresponding sampling time with cells in the presence of CCCP and HK
%   8th column: [R]e at corresponding sampling time with cells in the presence of GF and HK
%   9th column: [R]e at corresponding sampling time with cells in the presence of CCCP, HK,GF

clear global
close all
global params tt cccp150tt n data0 nCond nPara vmratio

% index of optimization loop
n = 0;
v1 = 2.65;              % volume of extracellular solution (ml)
k1b = 0.0043;           % Rate constant for dye-cuvette unbinding (nM^-1 min^-1)
km1 = 0.0897;           % Rate constant for dye-cuvette unbinding (min^-1)
zf_rt = 0.0374158;      % const of RT/ZF
ps1 = 0.094;            % PS product of rhodamine dye for plasma membrane (ml/min)
ps2 = 0.0105;           % PS product of rhodamine dye for mitochondrial membrane (ml/min)
v2  = 0.44;             % volume of cytoplasma (ml)
```

```
v3  = 0.0088;          % volume of mitochondria (ml)
vmaxkm = 0.025;        % Kpgp, P-glycoprotein mediated dye efflux rate (ml/min)
delp = 35;             % plasma membrane potential (mV)
delm = 130;            % mitochondrial membrane potential (mV)
vmratio = 0.02;        % the ratio between cytosol volume and mitochondrial volume

%open file, read experimental data to be fit
infile = 'ndata9.dat';
fid = fopen(infile, 'r');
if fid < 1
   input('invalid filename, press any key to end the program.', 's');
else
   %open data file
   data150 = textscan(fid,'%f %f %f %f %f %f %f %f %f %f %f');
   fclose(fid);
   %get data
   tt = (data150{1})';    %  sampling time
   cell=(data150{2})';   % data for cells + dye only
   cccp=(data150{3})'; % data for cells+ dye + CCCP
   gf = (data150{4})';   % data for cells+ dye + GF
   hk = (data150{5})';  % data for cells+ dye + HK
   cccpgf=(data150{6})'; % data for cells+ dye + CCCP+GF
   cccphk = (data150{7})'; % data for cells+ dye + CCCP+HK
   gfhk = (data150{8})'; % data for cells+ dye + GF+HIK
   cccpgfhk = (data150{9})'; % data for cells+ dye + CCCP+GF+HK

   % get the initial value of each array
   data0=[cell(1) cccp(1) gf(1) hk(1) cccpgf(1) cccphk(1) gfhk(1) cccpgfhk(1)];

   % define all parameters for the model
   params = [ps1, ps2, v2, v3, vmaxkm, delp, delm, k1b, km1, zf_rt, v1];

   % define the data which will be used to estimate parameters
   indata = [cell gf  gfhk  cccpgfhk];

   % define the corresponding sampling time points
   ttdata = [tt tt tt tt ];

   % define the parameters which will be estimated
   p0 = [ps1, ps2, v2, vmaxkm, delp, delm];

   % define the lower bound of parameters
   lb = [0.0001, 0.0001, 0.0001, 0.0001, 0.0001, 0.0001];
```

```
    % define the upper bound of parameters
    ub = [10 10 10 10 200 300];

    % define the optimization options
    options = optimset('TolX',1e-8,'MaxFunEvals',3000);

    % fitting model to input data and find out the optimized values for parameters
    [p, ssd, residual,exitflag,output,lambda,nJa] = lsqcurvefit(@solve_rhodamine, p0, ttdata, indata,
lb, ub, options);

    % calculate correlation coefficient
    [Q,R]=qr(nJa);
    R1 = R(1:length(p), :);
    h=inv(R1'*R1);
    for i=1:length(p)
        for j=1:length(p)
            cc(i,j)=h(i,j)/(h(i,i)*h(j,j))^0.5;
        end
    end

    % calculate confidence interval
    s2=ssd/(length(indata)-length(p));
    for i = 1:length(p)
        seb(i)=(s2^0.5)*(h(i,i)^0.5);
    end
    tt=2.01;  % constant for freedom 40-60
    ci=seb.*tt;

    % display the optimized values of parameters and related results
    fprintf('result:\n   PS1 = %f ml/min\n', p(1));
    fprintf('   PS2 = %f ml/min\n', p(2));
    fprintf('   V2 = %f ml\n', p(3));
    fprintf('   V3 = %f ml\n', vmratio*p(3));
    fprintf('   VmaxKm = %f ml/min\n', p(4));
    fprintf('   PMP = %f mV\n', p(5));
    fprintf('   MMP = %f mV\n', p(6));
    fprintf('   SSD = %f\n', ssd);
    ci

end
```

B.2 slove_rhodamine.m

```
function Cmatch = solve_rhodamine(p, ttdata)
% Function:       calculate [R]e with given parameters
```

```
% Input:          p: given parameters
%                 ttdata: sampling time
% Output:         An array of [R]e
% By Z.Gan, updated on 04-17-2011

%declare global variables
global  params tt cccp150tt n data0 nCond nPara vmratio

% show the index of optimization loops
n=n+1
% show the values of parameters during optimization process
p

% set a small constant instead of zero, provent from dividing by zero
nSmall = 0.001;

% define an available to store updated parameters
parameter_values1 = params;
parameter_values1(1) = p(1);       % ps1
parameter_values1(2) = p(2);       % ps2
parameter_values1(3) = p(3);       % v2
parameter_values1(4) = vmratio*p(3);% v3
parameter_values1(5) = p(4);       % vmaxkm
parameter_values1(6) = p(5);       % delp
parameter_values1(7) = p(6);       % delm

% define the optimization options
options=odeset('RelTol', 1e-7);

% calculate [R]e without inhibitors with given parameters
temp = parameter_values1;
y110  = [data0(1),  0,  0, 0]';
[T11,Y11] = ode45(@rhodamine, tt, y110, options, temp);
CELL = Y11(:,1);

% calculate [R]e in the presence of GF with given parameters
temp = parameter_values1;
% set Vmaxkm for Pgp to 0
temp(5) = 0;
y110  = [data0(3),  0,  0, 0]';
[T11,Y11] = ode45(@rhodamine, tt, y110, options, temp);
GF=Y11(:,1);

% calculate [R]e in the presence of GF and HK with given parameters
```

```
temp = parameter_values1;
% set Vmaxkm for Pgp to 0; Set plasma membrane potential close to 0
temp(5) = 0.0;
temp(6) = nSmall;
y110  = [data0(7),  0,  0, 0]';
[T11,Y11] = ode45(@rhodamine, tt, y110, options, temp);
GFHK=Y11(:,1);

% calculate [R]e in the presence of GF,HK and CCCP with given parameters
temp = parameter_values1;
% set Vmaxkm for Pgp to 0; set plasma membrane potential close to 0
% set mitochondrial membrane potential close to 0
temp(5) = 0;                    % vamxkm=0
temp(6) = nSmall;               % delp =0
temp(7) = nSmall;               % delm =0
y110  = [data0(8),  0,  0, 0]';
[T11,Y11] = ode45(@rhodamine, tt, y110, options, temp);
CCCPGFHK=Y11(:,1);

% return [R]e under above selected conditions
Cmatch = [CELL' GF' GFHK' CCCPGFHK'];
end
```

B.3 rhodamine.m

```
function dydt = rhodamine(time, y, parameters)
% Function: calculated [R]e at a specific time with given parameters based on rhodamine
distribution model
% Input:   time: sampling time
%          y: concentrations of rhodamine in extracellular medium,
%             cytosol, mitochondria and bound to tubing
%          parameters: an array of constants for rhodamine distribution
%          model
% Output: [R]e
% By Z Gan, updated on 04-14-2011

% rhodamine concentration in mediu (nM)
C1    = y(1);
% rhodamine concentration in cytoplasm (nM)
C2    = y(2);
% rhodamine concentration in mitochondrial matrix (nM)
C3    = y(3);
% bound rhodamine (nM)
C1P   = y(4);
```

```
ps1       = parameters(1);   % PS product of rhodamine dye for plasma membrane (ml/min)
ps2       = parameters(2);   % PS product of rhodamine dye for mitochondrial membrane (ml/min)
v2        = parameters(3);  % volume of cytoplasma (ml)
v3        = parameters(4);  % volume of mitochondrial (ml)
vmaxkm    = parameters(5); % Kpgp, P-glycoprotein mediated dye efflux rate (ml/min)
delp      = parameters(6);  % plasma membrane potential (mV)
delm      = parameters(7);  % mitochondrial membrane potential (mV)
k1b       = parameters(8);  % Rate constant for dye-cuvette unbinding (nM^-1 min^-1)
km1       = parameters(9);  % Rate constant for dye-cuvette unbinding (min^-1)
alfa      = parameters(10); % const of RT/ZF
v1        = parameters(11); % volume of extracellular solution (ml)

% rhodamine distribution model
constp0 = exp(alfa*delp);
constp1 = ps1*alfa*delp*constp0/(constp0-1);
constp2 = ps1*alfa*delp/(constp0-1);

constm0 = exp(alfa*delm);
constm1 = ps2*alfa*delm*constm0/(constm0-1);
constm2 = ps2*alfa*delm/(constm0-1);

a11 = -k1b - constp1/v1;
a12 =  vmaxkm/v1 + constp2/v1;
a13 =  0;
a14 =  km1;

a21 =  constp1/v2;
a22 = -vmaxkm/v2 - constp2/v2 - constm1/v2;
a23 =  constm2/v2;
a24 =  0;

a31 =  0;
a32 =  constm1/v3;
a33 = -constm2/v3;
a34 =  0;

a41 =  k1b;
a42 =  0;
a43 =  0;
a44 = -km1;

dC1dt   = a11*C1 + a12*C2 + a13*C3 + a14*C1P;
dC2dt   = a21*C1 + a22*C2 + a23*C3 + a24*C1P;
dC3dt   = a31*C1 + a32*C2 + a33*C3 + a34*C1P;
```

```
dC1Pdt  = a41*C1 + a42*C2 + a43*C3 + a44*C1P;

% return resulting [R]e in extracellular medium, cytosol, mitochondria and
% bound to tubing
dydt = [dC1dt; dC2dt; dC3dt; dC1Pdt];
```

B.4 simulate_ rhodamine.m

```
function simulate_rhodamine
% Function:     simulate [R]e with given parameters
% Input:        none
% Output:       a datafile containing simulated data for 9 conditions
% By Z Gan, updated on 04-17-2011

clear global

% define constant
v1 = 2.65;              % volume of extracellular solution (ml)
k1b = 0.004286;         % Rate constant for dye-cuvette unbinding (nM^-1 min^-1)
km1 = 0.089737;         % Rate constant for dye-cuvette unbinding (min^-1)
zf_rt = 0.0374158;      % const of ZF/RT
ps1 = 0.005;            % PS product of rhodamine dye for plasma membrane (ml/min)
ps2 = 0.005;            % PS product of rhodamine dye for mitochondrial membrane (ml/min)
v2  = 0.2;              % volume of cytoplasma (ml)
v3  = 0.02;             % volume of mitochondria (ml)a
vmaxkm = 0.02;          % Kpgp, P-glycoprotein mediated dye efflux rate (ml/min)
delp = 50;              % plasma membrane potential (mV)
delm = 160;             % mitochondrial membrane potential (mV)
vmratio = 0.02;         % the ratio between cytosol volume and mitochondrial volume

% define constants for rhodamine models
params = [ps1, ps2, v2, v3, vmaxkm, delp, delm, k1b, km1, zf_rt, v1];

% define sampling time
tt = [0 10 30 60 90 120 150];

% define given values for simulation parameters
p = [0.009777  0.007747   0.443182  0.025156   35.772977   127.937142];

% define inital value of [R]e (when t=0)
data0 =[9.0270    9.0378    9.0591    8.8482    9.0830    8.9201    8.9470    8.9872    9.0270];

params(1) = p(1);       % ps1
params(2) = p(2);       % ps2
params(3) = p(3);       % v2
```

```
params(4) = p(3)*vmratio;   % v3
params(5) = p(4);           % vmaxkm
params(6) = p(5);           % delp
params(7) = p(6);           % delm

% define a small number instead of zero
nSmall = 0.001;

% define sampling time points
tt =0:1:300;
% define a time avariable for adding CCCP after 150 minutes
cccp150tt=150:1:300;

% define the optimization options
options = odeset ('RelTol', 1e-6);

% calculate [R]e without inhibitors with given parameters
temp = params;
y110  = [data0(1),  0,  0, 0]';
[T11,Y11] = ode45(@rhodamine, tt, y110, options, temp);
CELL = Y11(:,1);

% calculate [R]e adding CCCP after 150 minutes
temp = params;
temp(7)=nSmall;
y110 = [Y11(151,1), Y11(151,2), Y11(151,3), Y11(151,4)];
[T11,Y11] = ode45(@rhodamine, cccp150tt, y110, options, temp);
CELL150 = [CELL(1:151); Y11(2:151,1)];

% calculate [R]e in the presence of CCCP with given parameters
% set mitochondrial membrane potential to 0
temp = params;
temp(7) = nSmall;
y110  = [data0(2),  0,  0, 0]';
[T11,Y11] = ode45(@rhodamine,tt, y110, options, temp);
CCCP = Y11(:,1);

% calculate [R]e in the presence of GF with given parameters
% set Kpgp to 0
temp = params;
temp(5) = 0;
y110  = [data0(3),  0,  0, 0]';
[T11,Y11] = ode45(@rhodamine,tt, y110, options, temp);
GF=Y11(:,1);
```

```
% calculate [R]e in the presence of HK with given parameters
% set plasma membrane potential to 0
temp = params;
temp(6) = nSmall;
y110  = [data0(4),  0,  0, 0]';
[T11,Y11] = ode45(@rhodamine,tt, y110, options, temp);
HK=Y11(:,1);

% calculate [R]e in the presence of CCCP and GF with given parameters
% set mitochondrial membrane potential, Kpgp to 0
temp = params;
temp(5) = 0;
temp(7) = nSmall;
y110  = [data0(5),  0,  0, 0]';
[T11,Y11] = ode45(@rhodamine, tt, y110, options, temp);
CCCPGF=Y11(:,1);

% calculate [R]e in the presence of CCCP and HK with given parameters
% set mitochondrial membrane potential, plasma membrane potential to 0
temp = params;
temp(7) = nSmall;
temp(6) = nSmall;
y110  = [data0(6),  0,  0, 0]';
[T11,Y11] = ode45(@rhodamine,tt, y110, options, temp);
CCCPHK=Y11(:,1);

% calculate [R]e in the presence of GF and HK with given parameters
% set Kpgp, plasma membrane potential to 0
temp = params;
temp(5) = 0.0;
temp(6) = nSmall;
y110  = [data0(7),  0,  0, 0]';
[T11,Y11] = ode45(@rhodamine,tt, y110, options, temp);
GFHK=Y11(:,1);

% calculate [R]e in the presence of GF, CCCP and HK with given parameters
% set Kpgp, plasma membrane potential and mitochondrial membrane potential to 0
temp = params;
temp(7)=nSmall;
temp(5)=0;
temp(6)=nSmall;
y110  = [data0(8),  0,  0, 0]';
[T11,Y11] = ode45(@rhodamine,tt, y110, options, temp);
```

```
CCCPGFHK=Y11(:,1);

% save simulated data
str1 = input('Would you like to save these results, input the file name or input 0: ', 's');
if str1 == '0';
else
   fid = fopen(str1,'w');
   for i = 1:length(tt)
     fprintf(fid,'%f\t%f\t%f\t%f\t%f\t%f\t%f\t%f\t%f\t%f\t%f\t%f\n',tt(i),CELL(i),CCCP(i), GF(i), HK(i),
CCCPGF(i), CCCPHK(i), GFHK(i), CCCPGFHK(i), CELL150(i));
  end
   fclose(fid);
end
end
```

C. Codes for rhodamine steady state model

C.1 steady_delm_calculation.m

```
function  steady_delm_calculation
% Function:       calculate mitochondrial membrane potential according to steady_state model
% Input:          [R]e
% output:         mitochondrial membrane potential
% Created by Z Gan, updated on 04-20-2011

% steady_state concentration of medium R123 without cells ;
% intial Re=9.0 nM, @150 minutes, it is about 0.9522*Re
Res0=8.5698;
% steady_state concentration of medium R123 with cells in the presence of GF+HK+CCCP (nM)
Res1=7.3991;
% steady_state concentration of medium R123 with cells in the presence of GF+HK (nM)
Res2=5.1121;
% The ratio between Vm and Vc
beta=0.02;
% const of ZF/RT,
alfa=0.0374158;
% extracelluar volume, ml
Ve=2.65;
% steady state model
Vc = (Res0-Res1)*Ve/Res1/(1+beta)
Rms = (Res0*Ve-Res2*Ve-Res2*Vc)/(Vc*beta)
delm = log(Res2/Rms)/alfa
% display the result
fprintf('When beta= %f, MMP = %f mV\n', beta, delm);
end
```

D. Codes for CoQ_1/CoQ_1H_2 metabolism model

D.1 gan_fitCoQ1.m

```
% Function:     estimate Vmax and Km of complex I, complex III, NQO1 and other reductase %
%               by fitting CoQ1 distribution model to experimental data
% Input:        experimental data
% Output:       estimated values of Vmax(s) and Km(s)
% Created by Zhuohui Gan on 12-2010, updated on 04-20-2011

clear variables
global n

%Parameter entry
redo1 = 1;
while(redo1)
  % Enter parameters
  par = gan_GetCoQ1Parameters();
  if par == -9999
     disp('Error during parameter acquirement.');
     return;
  else
   homorg = par(17);  % 0: hetergenous  1: homogenous
   % calculate peclet
   for i = 1:(2-homorg)  % why pe calculated before adjustment of tibar, tcbar?
     pe(i) = gan_Peclet(par(3*i-2),par(3*i-1));
     if (pe(i) <= 0)
        disp(['    when tibar=' num2str(par(3*i-2)) '   vari must be <' num2str(par(3*i-1))]);
     else
        redo1 = 0;
     end
   end
  end
end

% define all constants or parameters
tibar   = par(1); % non-capillary mean transit time (sec)
vari    = par(2); % variance of non-capillary
avsi    = par(3); % shift for tibar
tcbar   = par(4); % capillary mean transit time (sec)
varc    = par(5); % variance of capillary
avsc    = par(6); % shift for tcbar
vmax1   = par(7); % m-m vmax for NQO1 mediated Q reduction (umol/min)
akm1    = par(8); % m-m constant for NQO1 mediated Q reduction (uM)
```

```
vmax2   = par(9); % m-m vmax for complex III mediated QH oxidation (umol/min)
akm2    = par(10); % m-m constant for complex III mediated QH oxidation (uM)
qf1     = par(11); % virtual capillary volume (ml)
qf2     = par(12); % virtual lung tissue volume (ml)
alb1    = par(13); % apperant binding ratio between Q-Pc and Q-Pe for quinone (a1/a2)
alb2    = par(14); % apperant binding ratio between QH-Pc and QH-Pe for hydroquione (a3/a4)
qdot    = par(15); % flow (ml/s)
dose    = par(16); % infused probe concentration  (uM)
homog   = par(17); % homogenous or hetergenous 1=homogenous
dt      = par(18); % time resolution (sec)
tinj    = par(19); % total inject time (for input, sec)
tsp     = par(20); % delay time (for input, sec)
tfinal  = par(21); % time when the venous sample was collected (sec)
alpha   = par(22); % constant for input function
qflag   = par(23); % 1=Q, 0=QH
vmax3   = par(24); % m-m vmax for complex I mediated Q reduction (umol/min)
akm3    = par(25); % m-m constant for complex I mediated Q reduction (uM)
vmax4   = par(26); % m-m vmax for other Q reduction (umol/min)
akm4    = par(27); % m-m constant for other Q reduction (uM)

% check the initial setting for the program
if (tcbar <= 0)
  disp('    tcbar <0, so program stopped.')
  return;
end
if (tfinal <= 0)
  disp('    tfinal<=0, Program stopped.')
  return;
end
if qflag==1
   disp('   Your infused probe is quione.');
elseif qflag==0
   disp('   Your infused probe is hydroquione..');
else
   disp('   Your infused probe flag is mistaken,quit program.');
   return;
end

%initialized variables
ndim = round(tfinal/dt);   % # points of time axis
npdes = 3;                 % # of pdes for 1 model
fcmin = 0.01;              % covered area
dx      = dt/tcbar;        % normalized deltx , deltz
qc      = qdot*tcbar;      % capillary volume (ml)
```

```
delx    = dx*tcbar;          % consider the delay into mean transit time
tibar = tibar + avsi;
tcbar = tcbar + avsc;

% set up pe, tihat
if homorg ==1
   pei = pe(1);
   pec = 0;
   tihat   = tibar/(1+2/pei); % the parameter for the input function.
else
   pei = pe(1);
   pec = pe(2);
   tihat   = tibar/(1+2/pei); % the parameter for the input function.
   tchat = tcbar/(1+2/pec);
end

hcpdf = zeros(1,ndim); % capillary transit time distribution
hnpdf = zeros(1,ndim); % non-capillary transit time distribution
if (homorg==1)
  % if it is a homogeneous organ
  iend = 1/dx + 0.001; % the last spacial point
  test = 1.0/dx - iend;
  if (test > 0.001)
    disp(['    For a homogenous organ, 1/dx must be an integer, now 1/dx=' num2str(1/dx)]);
    disp(['    With this dx, capillary mmt will be changed to ' num2str(iend*delx)]);
    C_ok = input('Continue or Start over (C = continue)? ','s');
    if (C_ok == 'C' | C_ok == 'c')
      tcbar = iend*delx;
    else
      return;
    end
  end
  ibeg = iend; % since it is homogenous, so no scalar required
else
  % if it is not a hetergeneous organ
  disp(['    dose=' num2str(dose)]);
  % capillary distribution function
  hcpdf = hcpdfunc(ndim,delx,avsc,tchat,pec);
  % find the begin and the end, but for hetergenous organ, ibeg ==1
  [ibeg,iend] = begendfunc(hcpdf,ndim,fcmin);
  %Renormalize hc(t) to unit area
  hcpdf = hcpdf(2:ndim); % get rid of the first point, because
  % from first point to iend point, which is supposed to be 99.9% covered.
  hcpdf = hcpdf(1:iend);
```

```
  % to get an interget for the area under the capillary function
  ac = trapz(hcpdf)*dt;
  % rescale ,so 100% area
  hcpdf = hcpdf./(ac/delx);

  %Noncapillary transport function
  qd = qdot*tihat; % non-capillary volume
  hnpdf = gan_hnpdfunc(ndim, par, qd); %non-capillary input function
  hnpdf = hnpdf(2:ndim);
  ibeg = 1;
  disp(['    ibeg=' num2str(ibeg) '      iend=' num2str(iend)]);
end

captmin = ibeg*delx;
captmax = iend*delx;
disp(['    min/max capillary times are [ ' num2str(captmin) '  ' num2str(captmax)  ' ]']);
if (iend == ndim)
  disp('    iend=dimenssion..!');
end

%set-up of nx
nxy =round (3*captmax/dt);
nfinala = round(tfinal/dt) + 1;
nx = iend + 1;
if (nx > nxy)
  disp(['    dx is too small, required dx >= ' num2str(1/nxy)]);
  return;
else
  disp(['    nx = ' num2str(nx)]);
end

%Initial conditions when t = 0
par_var    = par;
par_var(1)  = tibar;
par_var(4)  = tcbar;
par_var(23) = qflag;
par_var(24) = nfinala;
par_var(25) = nx;
par_var(26) = nxy;
par_var(27) = ndim;
par_var(28) = ibeg;
par_var(29) = iend;
par_var(30) = pec;
par_var(31) = pei;
```

```
par_var(32) = qc;
par_var(33) = delx;
par_var(34) = vmax3;
par_var(35) = akm3;
par_var(36) = vmax4;
par_var(37) = akm4;
par_var(38) = npdes;

% sampling time series
t = [0:dt:(tfinal-dt)];

% load experimental data
redo2=1;
in_con=[];      % infused dye concentration (uM)
log_con = [];  % log mean concentration (uM)
out_con = [];  % efflux metabolic product concentration (uM)
cond = [];  % infused condition
rate = [];    % the efflux rate of metabolic product (umol/min)
while redo2==1
  datafile = input ('Please enter the file which contains data:  ', 's');
  fid = fopen(datafile, 'r');
  if (fid==-1)
     temp = input('invalid file name, quit (0) or continue (1)?  ');
     if (temp==1)
     else
        return;
     end
  else
     fclose(fid);
     % the required format of data file:
     % Quinone infusion: [QH]v+[Q]v, log mean of [QH]v+[Q]v, [QH]v, QHv
     % Hydroquinone infusion:    [QH]v, log mean of [QH]v, [Q]v, Qv
     load(datafile);
     data=eval(datafile(1:(length(datafile)-4)));
     tempin = data(:,1);  % infused concentration
     templog = data(:,2);  % log mean concenctration
     tempout = data(:,3); ; % efflux product concentration, QHv or Qv
     temprate = data(:,4);   % efflux product rate, umol/min
     %  The infusion  condition
     tempname = char(datafile(1:(length(datafile)-6)));

     in_con= [in_con tempin'];
     log_con = [log_con templog'];
     out_con = [out_con tempout'];
```

```
      rate = [rate temprate'];
      tempcondi=[];
      for tempi= 1:length(tempin)
         tempcondi{tempi}=upper(tempname);
      end
      cond = [cond tempcondi];
      % for multiple-condition fitting
      temp = input (' Do you want to load more data? Yes (1) No (0)?  ');
      if (temp==1)
      else
       redo2=0;
      end
   end
end

% define parameters that want to be evaluated;
npara=input ('Please enter parameters you want to estimate, \n Vmax1 -> NQO1, Vmax2 ->
complex III, Vmax3 -> complex I, Vmax4-> others\n1: Vmax4 Km4; \n2: Vmax1 Km1; \n3:
Vmax2 Km2; \n4: Vmax1 Km1 Vmax3 Km3:\n5: Vmax2 Km2 Vmax4 Km4 \n6: Vmax1,2,3,4
and their kms \n7: Vmax3 Km3 \n8: Vmax1,2,3 and their kms \n9: Vmax3\n your choice:  ');
par_var(39) = npara;
switch npara
case 1
    p0 = [vmax4 akm4];
    lb = [0.0001];
    ub = [2000 ];
case 2
    p0 = [vmax1 akm1];
    lb = [0.0001 0.0001];
    ub = [2000 2000];
case 3
    p0 = [vmax2 akm2];
    lb = [0.0001 0.0001];
    ub = [2000 2000];
case 4
    p0 = [vmax1 akm1 vmax3 akm3];
    lb = [0.0001, 0.0001, 0.0001, 0.0001];
    ub = [2000 2000 2000 2000];
case 5
    p0 = [vmax2 akm2 vmax4 akm4];
    lb = [0.0001 0.0001 0.0001 0.0001];
    ub = [2000 2000 2000 2000];
case 6
    p0 = [vmax1 akm1 vmax2 akm2 vmax3 akm3 vmax4 akm4];
```

```
    lb = [0.0001 0.0001 0.0001 0.0001 0.0001 0.0001 0.0001 0.0001];
    ub = [2000 2000 2000 2000 2000 2000 2000 2000];
case 7
    p0 = [vmax3 akm3];
    lb = [0.0001];
    ub = [2000 ];
case 8
    p0 = [vmax1 akm1 vmax2 akm2 vmax3 akm3];
    lb = [0.0001 0.0001 0.0001 0.0001 0.0001 0.0001];
    ub = [2000 2000 2000 2000 2000 2000];
case 9
    p0 = [vmax3];
    lb = [0.0001];
    ub = [2000];
otherwise
    disp('The parameters you want to estimate is unclear. Quit Program...');
    return;
end

options=optimset('TolFun', 1e-8, 'TolX', 1e-8,'MaxFunEvals',1400);
% Seeking for the optimized parameters by fitting the model to experimental data
n=0;
 [p, SSD, residual,exitflag,output,lambda,nJa] = lsqcurvefit(@gan_solveCoQ1, p0, in_con, rate, lb,
ub, options,par_var,hcpdf, cond);

% calculate correlation coefficient
 [Q,R]=qr(nJa);
R1 = R(1:length(p), :);
h=inv(R1'*R1);
for i=1:length(p)
    for j=1:length(p)
        cc(i,j)=h(i,j)/(h(i,i)*h(j,j))^0.5;
    end
end
cc
SSD

% calculate confidence interval
s2=SSD/(length(in_con)-length(p));
for i = 1:length(p)
    seb(i)=(s2^0.5)*(h(i,i)^0.5);
end

switch npara
```

```
case 1
    tt=2.07;
    ci=seb.*tt
    disp(['    vmax4= ' num2str(p(1))]);
    disp(['    km4= ' num2str(p(2))]);
    par_var(36) = p(1);  % update vmax4
    par_var(37) = p(2);  % update vmax4
case 2
    tt=2.07;
    ci=seb.*tt
    disp(['    vmax1= ' num2str(p(1))]);
    disp(['    km1= ' num2str(p(2))]);
    par_var(7) = p(1);  % update vmax1
    par_var(8) = p(2);  % update km1
case 3
    tt=2.07;
    ci=seb.*tt
    disp(['    vmax2= ' num2str(p(1))]);
    disp(['    km2= ' num2str(p(2))]);
    par_var(9) = p(1);  % update vmax2
    par_var(10) = p(2);  % update km2
case 4
    tt=2.07;
    ci=seb.*tt
    disp(['    vmax1= ' num2str(p(1))]);
    disp(['    km1= ' num2str(p(2))]);
    disp(['    vmax3= ' num2str(p(3))]);
    disp(['    km3= ' num2str(p(4))]);
    par_var(7) = p(1);  % update vmax1
    par_var(8) = p(2);  % update km1
    par_var(34) = p(3);  % update vmax3
    par_var(35) = p(4); % update km3
case 5
    tt=2.07;% 4 data points, 4 variable;
    ci=seb.*tt
    disp(['    vmax2= ' num2str(p(1))]);
    disp(['    km2= ' num2str(p(2))]);
    disp(['    vmax4= ' num2str(p(3))]);
    disp(['    km4= ' num2str(p(4))]);
    par_var(9) = p(1);  % update vmax2
    par_var(10) = p(2);  % update km2
    par_var(36) = p(3);  % update vmax4
    par_var(37) = p(4); % update km4
case 6
```

```
    tt=2.07;% 4 data points, 4 variable;
    ci=seb.*tt
    disp(['    vmax1= ' num2str(p(1))]);
    disp(['    km1= ' num2str(p(2))]);
    disp(['    vmax2= ' num2str(p(3))]);
    disp(['    km2= ' num2str(p(4))]);
    disp(['    vmax3= ' num2str(p(5))]);
    disp(['    km3= ' num2str(p(6))]);
    disp(['    vmax4= ' num2str(p(7))]);
    disp(['    km4= ' num2str(p(8))]);
    par_var(7) = p(1);  % update vmax1
    par_var(8) = p(2);  % update km1
    par_var(9) = p(3);  % update vmax2
    par_var(10) = p(4); % update km2
    par_var(34) = p(1);  % update vmax3
    par_var(35) = p(2);  % update km3
    par_var(36) = p(3);  % update vmax4
    par_var(37) = p(4); % update km4
case 7
    tt=2.07; % 4 data points, 1 variable
    ci=seb.*tt
    disp(['    vmax3= ' num2str(p(1))]);
    disp(['    km3= ' num2str(p(2))]);
    par_var(34) = p(1);  % update vmax1
    par_var(35) = p(2);  % update vmax1
otherwise
    tt=2.07;  % constant for freedom 40-60
    ci=seb.*tt;
    p
end

% ask whether a simulation is required.
temp = input('Do you want to run a simulation? Yes(1) No(0)  ');
if temp == 0
    return;
end

% determine the time point of efflux (as tfinal for simulation)
redo3=1;
while redo3==1
    temp = input('Input the time point you want to pick up the efflux concentration: ');
    if temp>0
        t = temp;
    else
```

```
        disp('invalid time point.')
        t = 99999;
    end

    if (t/dt)> ndim
        temp = input ('Your time point is either too big or mistaken, Do you want to try again, Y(1), N(0)?  ');
        if temp==0
            return;
        end
    else
        redo3=0;
    end
end

% calculate the dose-dependent simulation based on new parameters.
m = int16(t/dt);
dose_interval =5;
num_dose =80;
for i=1:(num_dose+1);
    % initialize yold, ynew
    yold = zeros(npdes,nxy); % concentrations of probes (r, oxidized, reduced)at a given time t
    ynew = zeros(npdes,nxy); % concentrations of probes(r, oxidized, reduced)at a given time t+dt
    par_var(16)=(i-1)*dose_interval;
    [cr,cq,cqh,istop] = gan_CoQ1(ndim, par_var, yold, ynew, hcpdf);
    mQ(i)=cq(m);
    mQH(i)=cqh(m);
end

dose = 0:dose_interval:num_dose*dose_interval;
plot(dose,mQ,dose,mQH);
legend('Q', 'QH');

% save simulated results
conc_save = [dose; mQ; mQH; mQ+mQH];
save_sims = input('Save simulated data? Yes [1] No[0] ');
if save_sims == 1,
  gan_SaveData(conc_save, dose_interval);
elseif save_sims ~= 0,
    disp(['Unexpected entry.  Program will complete without saving. ']);
end
disp(['Program completed']);
```

D.2 gan_getCoQ1Parameters.m

```
function param = gan_GetCoQ1Parameters()
% Function:       Acquire the initial setting for all parameters in the model
% Input:          none
% output:         an array containing initial values for all parameters
% Created by Z Gan, updated on 04-20-2011

stop_flag = 0;
get_parms = 1;
par =[];
% Vmax1, Km1: NQO1 mediated CoQ1 reduction
% Vmax2, Km2: complex III mediated CoQ1H2 oxidation
% Vmax3, Km3: complex I mediated CoQ1 reduction
% Vmax4, Km4: other CoQ1 reduction
while(get_parms),
  T_or_F = input('Enter "t" for Term or "f" for file: ','s');
  if ((T_or_F == 't') | (T_or_F == 'T')),
    % define input dlg
    prompt1 = {'hn MTT (s):','hn VAR :','hn AVS (s):','hc MTT (s):','hc VAR:','hc AVS (s):',...
      'Vmax1 (nmol/s): NQO1', 'Km1 (uM): NQO1', 'Vmax2(nmol/s): complex III', 'Km2(uM):
complex III','QF1:','QF2:','alb1:','alb2:'};
    prompt2 = {'Qdot:','Dose:','homo? 1=Yes 0=No','dt','tinj:','tsp:','tfinal',...
      'alpha', 'Q? 1=Q 0=QH','Vmax3(nmol/s): complex I', 'Km3 (uM): complex
I','Vmax4(nmol/s): other reductase', 'Km4(uM): other reductase'};
    %       tibar  vari   avsi   tcbar  varc   avsc   vmax1 km1 vmax2 km2   qf1 qf2   alb1 alb2
    defs1 = {'1.3333','0.4444','0.6667','0.8333','0.4444','0.00','19.5',
'13.4','76.7','75.9','25.26','28.55','14.6','16.5'};
    %       qdot dose homog  dt    tinj   tsp   tfinal   alpha  Q/QH Vmax3   Km3   Vmax4  km4
    defs2 = {'0.5','100','0','0.01','47','4.0490','47','0.5530','1','36.1','33.7','14.3','65.6'};

    %acquire parameters from inputdlg
    temp = inputdlg(prompt1,'Enter Parameter Values (1/2)',1,defs1);
    par1 = str2num(char(temp));
    temp = inputdlg(prompt2,'Enter Parameter Values (2/2)',1,defs2);
    par2 = str2num(char(temp));

    % check whether all inputs are number.
    non_number=0;
    if(length(par1)<1) ||length(par2)<1
       non_number=1;
    end

    % Inquiry if there is a non-number, what to do next step
    if non_number>0
```

```
    msgbox('you have 1 or more non-number parameters,Please retry.','Warning','warn')
else
  par = [par1; par2];
  % save paramters to a file if need
  save_ck = input('Save parameter file? Yes [1] No [0]  ');
  if save_ck == 1,
  fcell = { 'hn MTT(s):      ', 'hn VAR(s):      ', 'hn AVS:        ','hc MTT(s):      ',...
          'hc VAR:        ', 'hc AVS:        ', 'Vmax1:         ','Km1:            ',...
          'Vmax2:         ', 'Km2:           ', 'QF1:           ','QF2:            ',...
          'alb1:          ', 'alb2:          ', 'Qdot:          ','Dose:           ',...
          'homo? 1=Yes 0=No', 'dt            ', 'tinj:          ','tsp:            ',...
          'tfinal         ', 'alpha          ', 'Q? 1=Q 0=QH    ','Vmax3:          ',...
          'Km3:           ', 'Vmax4:         ', 'Km4:           '};
  ffield = {'p1','p2','p3','p4','p5','p6','p7','p8','p9','p10','p11','p12','p13',...
       'p14','p15','p16','p17','p18','p19','p20','p21','p22','p23','p24','p25','p26','p27'};
  fpar = cell2struct(fcell,ffield,2);
  pno = length(par);
  repeat = 1;
  while(repeat),
     s_fname = input('Enter filename to save parameters: ','s');
     fid_r = fopen(s_fname,'r');
     file_save = 0;
     if fid_r ~= -1,
        fclose(fid_r);
        file_save = input('Filename already exists. Enter new name [1] or write over [0]? ');
        if file_save == 0,
           fid_w = fopen(s_fname,'w');
           fprintf(fid_w,' %i\n',pno);
           for i = 1:pno
              eval(['fprintf(fid_w," %s     %8.4f\n",fpar.p' int2str(i) ...
              ', par(' int2str(i) '));']);
           end
           fclose(fid_w);
           repeat = 0;
        end
     else
        fid_w = fopen(s_fname,'w');
        fprintf(fid_w,' %i\n',pno);
        for i = 1:pno
           eval(['fprintf(fid_w," %s     %8.4f\n",fpar.p' int2str(i) ...
           ', par(' int2str(i) '));']);
        end
        fclose(fid_w);
        repeat = 0;
```

```
        end
      end  % end of while
    end  % end of if
    % change the control for the loop
    get_parms = 0  ;
    param =  par;
   end
  elseif ((T_or_F == 'f') | (T_or_F == 'F')),
    par=gan_ReadParameters;
    if par==-9999
     param =-9999;
    else
     param =par;
     if length(par)<1
       msgbox('You give up to set up parameters. This may cause sequential
error.','Warning','warn')
      else
       for i = 1:length(par),
         eval(['clear line_p' int2str(i) '; clear p' int2str(i) '; clear sp' int2str(i) ';' ]);
       end
      end
    end
    prompt1 = {'hn MTT (s):','hn VAR (s):','hn AVS:','hc MTT (s):','hc VAR (s):','hc AVS:',...
      'Vmax1 (nmol/s, NQO1):', 'Km1 (uM):', 'Vmax2 (nmol/s, complexIII):', 'Km2 (uM):','QF1
(ml):','QF2 (ml):','alb1:','alb2:'};
    prompt2 = {'Qdot (flow, ml/s):','Dose (uM):','homo? 1=Yes 0=No','dt(s):','tinj (s):','tsp
(s):','tfinal (s):',...
      'alpha', 'Q? 1=Q 0=QH','Vmax3 (nmol/s, complex I):', 'Km3 (uM):','Vmax4 (nmol/s, other):',
'Km4 (uM):'};
    %       tibar  vari   avsi   tcbar  varc   avsc  vmax1 km1 vmax2 km2  qf1 qf2  alb1 alb2
    defs1 = {num2str(par(1)),num2str(par(2)),num2str(par(3)),num2str(par(4)),num2str(par(5)),...
          num2str(par(6)),num2str(par(7)),num2str(par(8)),num2str(par(9)),num2str(par(10)),...
          num2str(par(11)),num2str(par(12)),num2str(par(13)),num2str(par(14))};
    %       qdot    dose homog  dt   tinj   tsp   tfinal    alpha  Q/QH Vmax3 Km3 Vmax4 km4
defs2={num2str(par(15)),num2str(par(16)),num2str(par(17)),num2str(par(18)),num2str(par(19)),...
         num2str(par(20)),num2str(par(21)),num2str(par(22)),num2str(par(23)),num2str(par(24)),...
         num2str(par(25)),num2str(par(26)),num2str(par(27))};
    %acquire parameters from inputdlg
    temp = inputdlg(prompt1,'Enter Parameter Values (1/2)',1,defs1);
    par1 = str2num(char(temp));
    temp = inputdlg(prompt2,'Enter Parameter Values (2/2)',1,defs2);
    par2 = str2num(char(temp));
    par = [par1; par2];
    param = par;
```

```
    get_parms = 0;
  else
    get_parms = input('Invalid entry.  Retry? [1] or Quit [0] ');
    stop_flag = 1;
    param = -9999;
  end
end
```

D.3 gan_simCoQ1.m

```
% Function:       simulate the efflux rate of CoQ1 or CoQ1H2 with a given set of  parameters
% Input:          none
% output:         simulated results
% Created by Z Gan, updated on 04-20-2011

clear all
global tchat
global pec

%Parameter entry , update on 07-28-2010 by Gan
redo1 = 1;
while(redo1)
  % Enter parameters
  par = gan_GetCoQ1Parameters();
  if par == -9999
     disp('Error during parameter acquirement.');
     return;
  else
   homorg = par(17); % 0: hetergenous  1: homogenous
   % calculate peclet
   for i = 1:(2-homorg)
    pe(i) = gan_Peclet(par(3*i-2),par(3*i-1));
    if (pe(i) <= 0)
      disp(['    when tibar=' num2str(par(3*i-2)) '   vari must be <' num2str(par(3*i-1))]);
    else
      redo1 = 0;
    end
   end
  end
end

% define all constants or parameters
tibar   = par(1); % non-capillary mean transit time, sec
vari    = par(2); % variance of non-capillary
```

```
avsi    = par(3); % shift for tibar
tcbar   = par(4); % capillary mean transit time, sec
varc    = par(5); % variance of capillary
avsc    = par(6); % shift for tcbar
vmax1   = par(7); % m-m vmax for NQO1 mediated Q reduction (umol/min)
akm1    = par(8); % m-m constant for NQO1 mediated Q reduction (uM)
vmax2   = par(9); % m-m vmax for complex III mediated QH oxidation (umol/min)
akm2    = par(10); % m-m constant for complex III mediated QH oxidation (uM)
vf1     = par(11); % virtual capillary volume (ml)
vf2     = par(12); % virtual tissue volume (ml)
alb1    = par(13); % apperant binding ratio between Q-Pc and Q-Pe for quinone (a1/a2)
alb2    = par(14); % apperant binding ratio between QH-Pc and QH-Pe for hydroquione (a3/a4)
qdot    = par(15); % flow (m/s)
dose    = par(16); % infused probe concentration (uM)
homog   = par(17); % homogenous or hetergenous 1=homogenous
dt      = par(18); % time resolution (sec)
tinj    = par(19); % total inject time (for input, sec)
tsp     = par(20); % delay time (for input, sec)
tfinal  = par(21); % total simulation time (sec)
alpha   = par(22); % constant for input function
qflag   = par(23); % 1=Q, 0=QH
vmax3   = par(24); % m-m vmax for complex I mediated Q reduction (umol/min)
akm3    = par(25); % m-m constant for complex I mediated Q reduction (uM)
vmax4   = par(26); % m-m vmax for other Q reduction (umol/min)
akm4    = par(27); % m-m constant for other Q reduction (uM)

% basic check of the setting for the model initial value
if (tcbar <= 0)
  disp('    tcbar <0, so program stopped.')
  return;
end
if (tfinal <= 0)
  disp('    tfinal<=0, Program stopped.')
  return;
end

 %initialized variables
ndim = round(tfinal/dt); % # points of time axis
npdes = 3;  % # of pdes for 1 model
fcmin = 0.01;  % covered area
dx      = dt/tcbar;  % normalized deltx , deltz
qc      = qdot*tcbar; % capillary volume
delx    = dx*tcbar;
```

```
% consider the delay into mean transit time
tibar = tibar + avsi;
tcbar = tcbar + avsc;

% set up pe, tihat
if homorg ==1
   pei = pe(1);
   pec = 0;
   tihat   = tibar/(1+2/pei); % the parameter for the input function.
else
   pei = pe(1);
   pec = pe(2);
   tihat   = tibar/(1+2/pei); % the parameter for the input function.
   tchat  = tcbar/(1+2/pec);
end

%set-up of cap trans. func. as vector, min and max cap trans. times
hcpdf = zeros(1,ndim); % capillary transit time distribution
hnpdf = zeros(1,ndim); % non-capillary transit time distribution
if (homorg==1)
  % if it is a homogeneous organ
  iend = 1/dx + 0.001; % the last spacial point
  test = 1.0/dx - iend;
  if (test > 0.001)
    disp(['    For a homogenous organ, 1/dx must be an integer, now 1/dx=' num2str(1/dx)]);
    disp(['    With this dx, capillary mmt will be changed to ' num2str(iend*delx)]);
    C_ok = input('Continue or Start over (C = continue)? ','s');
    if (C_ok == 'C' | C_ok == 'c')
      tcbar = iend*delx;
    else
      return;
    end
  end
  ibeg = iend; % since it is homogenous, so no scalar required
else
  % if it is not a hetergeneous organ
  disp(['    dose=' num2str(dose)]);
  % capillary distribution function
  hcpdf = hcpdfunc(ndim,delx,avsc,tchat,pec);
  % find the begin and the end, but for hetergenous organ, ibeg ==1
  [ibeg,iend] = begendfunc(hcpdf,ndim,fcmin);
  %Renormalize hc(t) to unit area
  hcpdf = hcpdf(2:ndim); % get rid of the first point, because
  % from first point to iend point, which is supposed to be 99.9% covered.
```

```
  hcpdf = hcpdf(1:iend);
  % to get an interget for the area under the capillary function
  ac = trapz(hcpdf)*dt;
  % rescale ,so 100% area
  hcpdf = hcpdf./(ac/delx);

  %Noncapillary transport function
  qd = qdot*tihat; % non-capillary volume
  hnpdf = gan_hnpdfunc(ndim, par, qd); %non-capillary input function
  hnpdf = hnpdf(2:ndim);
  ibeg = 1;
  disp(['    ibeg=' num2str(ibeg) '      iend=' num2str(iend)]);
end
 captmin = ibeg*delx;
captmax = iend*delx;
disp(['    min/max capillary times are [ ' num2str(captmin) '  ' num2str(captmax)  ' ]']);
if (iend == ndim)
  disp('    iend=dimenssion..!');
end

%set-up of nx
nxy =round (3*captmax/dt);
nfinala = round(tfinal/dt) + 1;
nx = iend + 1;
if (nx > nxy)
  disp(['    dx is too small, required dx >= ' num2str(1/nxy)]);
  return;
else
  disp(['    nx = ' num2str(nx)]);
end

%Initial conditions when t = 0
par_var     = par;
par_var(1)  = tibar;
par_var(4)  = tcbar;
par_var(24) = nfinala;
par_var(25) = nx;
par_var(26) = nxy;
par_var(27) = ndim;
par_var(28) = ibeg;
par_var(29) = iend;
par_var(30) = pec;
par_var(31) = pei;
par_var(32) = qc;
```

```
par_var(33) = delx;
par_var(34) = vmax3;
par_var(35) = akm3;
par_var(36) = vmax4;
par_var(37) = akm4;
par_var(38) = npdes;

t = [0:dt:(tfinal-dt)];
myway = input('Input the way you to acquire doses: manual input(0), data file(1), auto input(2)? ');
% determine the input approach of doses which need simulated
switch myway
  case 0 % input infusion dose one by one manually
    num = input('How many doses for this simulation? ');
    if num>=1
       for i=1:num
          disp(['please input your No.' num2str(i)  '  dose']);
          temp = input('must be a number   ','s');
          if str2num(temp)>=0
             temp=str2num(temp);
          else
             temp=0;
          end
          dose(i)=temp;
       end
    end
  case 1  % load infusion doses from an experimental data file
    redo2=1;
    while redo2==1
       datafile = input ('Please enter the file which contains data:', 's');
       fid = fopen(datafile, 'r');
       if (fid==-1)
          temp = input('invalid file name, quit (0) or continue (1)?');
          if (temp==1)
          else
             return;
          end
       else
          fclose(fid);
          redo2=0;
       end
    end
    % the file name must be end with .txt or .dat.
    load(datafile);
    data=eval(datafile(1:(length(datafile)-4)));
```

```
    dose = data(:,1);  % infused concentration
    num = length(dose);
  case 2  % generate doses automatically based on start-end dose and dose interval
    dose0 = input ('Please input the start dose:  ','s');
    dose1 = input ('Please input the end dose:  ', 's');
    interval = input('Please input dose interval:  ', 's');
    dose0 = str2num(dose0);
    dose1 = str2num(dose1);
    interval = str2num(interval);
    if (dose0>dose1)
       disp('The end dose can not be less than the start dose.');
    elseif (dose0<0)
       disp('Dose can not be less than 0.');
    end
    num = int16((dose1-dose0)/interval);
    dose = dose0:interval:(dose0+num*interval);
    num = length(dose);
  otherwise
    disp('You did not select a proper way. Quit the program..');
    return;
end

% Calculate efflux concentrations based on input concentrations.
for i=1:num
       par_var(16)=dose(i);  % set up dose
       % initialize avaiable
       cr = zeros(1,ndim); % concentration of reference probe
       cq = zeros(1,ndim); % concentration of oxidized probe
       cqh = zeros(1,ndim); % concentration of reduced probe
       % initialize yold, ynew
       yold = zeros(npdes,nxy); % concentrations of probes(r, oxidized, reduced)at a given time t
       ynew = zeros(npdes,nxy); % concentrations of probes(r, oxidized, reduced)at a given time
t+dt
       % calculate the result
       [cr,cq,cqh,istop] = gan_CoQ1(ndim, par_var, yold, ynew, hcpdf);
       mCr(i,1:ndim)=cr;
       mCq(i,1:ndim)=cq;
       mCqh(i,1:ndim)=cqh;
end

% display the results
switch myway
    case 2
       redo3=1;
```

```
    while redo3 ==1
      ptime = input('input the time point you want to collect sample. \n');
      if ptime>tfinal
        disp('The time you selected is longer than tfinal. Try again');
        redo3=1;
      elseif ptime<0
        disp('Time can not be less than 0.');
        redo3=1;
      elseif (0<ptime) && (ptime<=tfinal)
        redo3=0;
      else
        disp('Your input may have some mistake. Quit program now.')
        redo3=1;
      end
      if redo3==1
        temp = input('Do you want to try again, Yes(1) No(0)?');
        if temp ==1
          redo3=1;
        else
          redo3=0;
          return;
        end
      end
    end
    tpoint = int16(ptime/dt);
    for i=1:num
      mcr(i) = mCr(i,tpoint);
      mcq(i) = mCq(i,tpoint);
      mcqh(i)= mCqh(i,tpoint);
    end
    plot(dose,mcr,dose,mcq,dose,mcqh);
    legend('Ref', 'Q', 'QH') ;
    save_sims = input('Save simulated data? Yes [1] No[0] ');
    if save_sims == 1,
      conc_save = [double(dose); mcr; mcq; mcqh];
      gan_SaveData(conc_save, interval);
    end
  otherwise
    for i=1:num
      mcr = mCr(i,1:ndim);
      mcq = mCq(i,1:ndim);
      mcqh= mCqh(i,1:ndim);
      subplot(1,num,i);
      plot(t,mcr,t,mcq,t,mcqh);
```

```
        legend('Ref', 'Q', 'QH') ;
        title(num2str(dose(i)));
    end
    % save the results
    save_sims = input('Save simulated data? Yes [1] No[0] ');
    if save_sims == 1,
        for i=1:num
            mcr = mCr(i,1:ndim);
            mcq = mCq(i,1:ndim);
            mcqh= mCqh(i,1:ndim);
            conc_save = [double(t); mcr; mcq; mcqh];
            gan_SaveData(conc_save, dt);
        end
    elseif save_sims ~= 0,
        disp(['Program will complete without saving. ']);
    end
end
disp(['Program completed']);
```

D.4 gan_solveCoQ1.m

```
function Cmatch = gan_solveCoQ1(p, in_con, par_var, hcpdf, cond)
%this function is called by gan_fit.m, using to solve the pde set.
% Function:     solve the PDE sets and return steady_state efflux value with a given set of
%               parameters
% Input:        p: variables for the model
%               in_con: infused doses
%               par_var: parameters for the model
%               hcpdf: capillary distribution
%               cond: infusion conditions
% output:       an array of steady_state efflux values
% Created by Z Gan, updated on 04-20-2011

%declare global variables
global  n

mparameters =  par_var;
qflag = par_var(23);
nxy = par_var(26);
ndim = par_var(27);
npdes = par_var(38);
npara = par_var(39);
flow = par_var(15);
```

```
switch npara
   case 1
      mparameters(36) = p(1);      % vmax4
      mparameters(37) = p(2);      % km4
   case 2      % 2 parameters
      mparameters(7) = p(1);      % vmax1
      mparameters(8) = p(2);      % km1
   case 3      % 4 parameters
      mparameters(9) = p(1);      % vmax2
      mparameters(10) = p(2);      % km2
   case 4      % 4 parameters
      mparameters(7) = p(1);      % vmax1
      mparameters(8) = p(2);      % km1
      mparameters(34) = p(3);      % vmax3
      mparameters(35) = p(4);      % km3
   case 5      % 4 parameters
      mparameters(9) = p(1);      % vmax2
      mparameters(10) = p(2);      % km2
      mparameters(36) = p(3);      % vmax4
      mparameters(37) = p(4);      % km4
   case 6      % 6 parameters
      mparameters(7) = p(1);      % vmax1
      mparameters(8) = p(2);      % km1
      mparameters(9) = p(3);      % vmax2
      mparameters(10) = p(4);      % km2
      mparameters(34) = p(5);      % vmax3
      mparameters(35) = p(6);      % km3
      mparameters(36) = p(7);      % vmax4
      mparameters(37) = p(8);      % km4
   case 7
      mparameters(34) = p(1);      % vmax3
      mparameters(35) = p(2);      % km3
   case 8      % 6 parameters
      mparameters(7) = p(1);      % vmax1
      mparameters(8) = p(2);      % km1
      mparameters(9) = p(3);      % vmax2
      mparameters(10) = p(4);      % km2
      mparameters(34) = p(5);      % vmax3
      mparameters(35) = p(6);      % km3
   case 9
      mparameters(34) = p(1);      % vmax3
   otherwise
end
```

```
% progress control.....
n=n+1
p
% adjust the parameters based on infusion condition
numDose = length(in_con);
for i=1:numDose
   temppara = mparameters;
   temppara(16)=in_con(i); % dose
   yold = zeros(npdes,nxy); % concentrations of probes(r, oxidized, reduced)at a given time t
   ynew = zeros(npdes,nxy); % concentrations of probes(r, oxidized, reduced)at a given time t+dt
   if (strcmp(cond{i},'COQ1DIC') ||strcmp(cond{i},'COQ1DIC21') ||
strcmp(cond{i},'COQ1DIC85') || strcmp(cond{i},'COQ1DIC60'))
         temppara(7) = 0;       % vmax1=0, NQO1 inhibited
         temppara(23)= 1;       % infused CoQ1
   elseif (strcmp(cond{i},'COQ1ROT') ||strcmp(cond{i},'COQ1ROT21')
||strcmp(cond{i},'COQ1ROT85') ||strcmp(cond{i},'COQ1ROT60'))
         temppara(34) = 0;      % vmax3=0, COMPLEX I INHIBITED
         temppara(23)= 1;       % infused CoQ1
   elseif (strcmp(cond{i},'COQ1DICROT') ||strcmp(cond{i},'COQ1DICROT21') ||
strcmp(cond{i},'COQ1DICROT85') || strcmp(cond{i},'COQ1DICROT60'))
         temppara(34) = 0;      % vmax3=0, COMPLEX I INHIBITED
         temppara(7) = 0;       % vmax1=0, NQO1 inhibited
         temppara(23)= 1;       % infused CoQ1
elseif(strcmp(cond{i},'COQ1AA')||strcmp(cond{i},'COQ1AA21')||strcmp(cond{i},'COQ1AA85')
||strcmp(cond{i},'COQ1AA60'))
         temppara(9) = 0;       % vmax2=0, COMPLEX III inhibited
         temppara(23)= 1;       % infused CoQ1
   elseif(strcmp(cond{i},'COQ1KCN')||strcmp(cond{i},'COQ1KCN21')||
strcmp(cond{i},'COQ1KCN85') || strcmp(cond{i},'COQ1KCN60'))
         temppara(9) = 0;       % vmax2=0, COMPLEX III inhibited
         temppara(23)= 1;       % infused CoQ1
   elseif(strcmp(cond{i},'COQ1H2DICROT')||strcmp(cond{i},'COQ1H2DICROT21')||
strcmp(cond{i},'COQ1H2DICROT85') || strcmp(cond{i},'COQ1H2DICROT60'))
         temppara(34) = 0;      % vmax3=0, COMPLEX I INHIBITED
         temppara(7) = 0;       % vmax1=0, NQO1 inhibited
         temppara(23)= 0;       % infused CoQ1H2
   else
   end
   % Calculate steady_state efflux values
   [cr, cq, cqh, istop] = gan_CoQ1(ndim, temppara, yold, ynew, hcpdf);
   mQ(i)=cq(ndim);
   mQH(i)=cqh(ndim);
   % pick up the right value corresponding to its infusion condition
   if (temppara(23)==1)
```

```
      mResult(i)= mQH(i);
   else
      mResult(i)= mQ(i);
   end
end

% adjust efflux rate from nmol/s to umol/min
temp = flow*60/1000;
Cmatch = mResult.*temp;
```

D.5 gan_saveData.m

```
function gan_SaveData(conc_save, dt)
% Function:       save simulated data
% Input:          conc_save: simulated data
%                 dt: sampling time interval
% output:         a file containing simulated data
%                 numbers should follow the format of 6.3 12.5 12.5 12.5
%                 1st column: time or dose
%                 2nd column: infused concentration
%                 3rd column: [Q]v
%                 4th column: [QH]v
% Created by Z Gan 0n 07-2010, updated on 04-20-2011

disp([' ']);
disp(['Current stepsize is:']);
disp([dt]);
% inquiry whether adjust step size, if yes, adjust corresponding data
change_dt = input('Change stepsize for output file? Yes [1] No[0]  ','s');
change_flag = 1;
if change_dt == '1',
  while(change_flag),
     new_dt = input('Enter new step size: ');
     if new_dt < dt,
        disp(['New stepsieze cannot be smaller than original']);
     elseif new_dt == dt,
        n_conc_save = conc_save;
        change_flag = 0;
     else
        index_dt = round(new_dt/dt);
        n_dt = index_dt * dt;
        disp(['New stepsize has been rounded to ' ]);
        disp([n_dt]);
        disp([' ']);
```

```
        for i = 1:index_dt:size(conc_save,2)
          n_conc_save(:,(i-1)/index_dt + 1) = conc_save(:,i);
        end
        change_flag = 0;
      end
    end
elseif change_dt ~= '0',
  temp = input('Unexpected entry. Do you want to try again ? Yes [1] No[0]  ');
  if temp ==1
    new_dt = input('Enter new dt (Must be a positive number) : ');
  end
  n_conc_save = conc_save;
else
  n_conc_save = conc_save;
end

 % save data into a file
repeat = 1;
while(repeat),
  save_dat = input('Enter filename to save data: ','s');
  fid_r = fopen(save_dat,'r');
  file_save = 0;

  if fid_r ~= -1,
    fclose(fid_r);
    file_save = input('Filename already exists. Enter new name [1] or write over [0]?  ');
  else
    fid_w = fopen(save_dat,'w');
    fprintf(fid_w,'%6.3f\t %12.5f\t %12.5f\t %12.5f\n',n_conc_save);
    fclose(fid_w);
    repeat = 0;
  end

  if file_save == 0,
    fid_w = fopen(save_dat,'w');
    fprintf(fid_w,'%6.3f\t %12.5f\t %12.5f\t %12.5f\n',n_conc_save);
    fclose(fid_w);
    repeat = 0;
  end
end
```

D.6 gan_getPeclet.m

```
function [pe] = gan_Peclet(t,v)
```

```
% Function:      calculate peclet numbers
% Input:         t: mean transit time
%                v: variance of transit time
% output:        peclet numbers
% Created by Z Gan 0n 07-2010, updated on 04-20-2011
% Use Rugani's codes as reference
d = v/(t^2);
a = 1 - 2*d;
b = 1 + 4*d;
pe = (a + sqrt(b))/d;
```

D.7 begendfunc.c

```
// Function:      find out the begin and the end of capillary distribution
// Input:         hcpdf: capillary distribution function
//                ndim: total number of sampling points
//                fcmin: uncovered area% under capillary distribution function
// output:        ibeg: the index of begin of capillary distribution
//                iend: the index of end of capillary distribution
// Created by Z Gan 0n 07-2010, updated on 04-20-2011

#include <math.h>
#include "mex.h"
void begendfunc(double *ibeg, double *iend, double *hcpdf, int ndim, double fcmin)
{
   double mmax(double *, int);
   double hmx;
   int i;
   // find out the maximum
   hmx = mmax(hcpdf, ndim);
   // find out the begin
   for (i=0;i<ndim;i++)
   {
      if(*(hcpdf + i) > hmx*fcmin) // fcmin =0.001, so 99.9% conserved
      {
         *ibeg = i;
         break;
      }
   }
   // find out the end
   for (i=ndim-1;i>=0;i--)
   {
      if(*(hcpdf + i) > hmx*fcmin)
      {
         *iend = i;
```

```
            break;
        }
    }
}
 // sub-function used to figure out the maximum in a data series
double mmax(double *hcpdf, int ndim)
{
    int i;
    double amax;

    amax = -pow(10,30);
    for (i=0;i<ndim;i++)
    {
        if(amax < *(hcpdf+i))
            amax = *(hcpdf+i);
    }
    return(amax);
}
// Gateway function to use C in matlab
void mexFunction(int nlhs, mxArray *plhs[], int nrhs, mxArray *prhs[])
{
    double *hcpdf;
    double fcmin;
    int ndim;
    double *ibeg, *iend;

    if (nrhs != 3){
        mexErrMsgTxt("Three input arguments required.");
    }
    else if (nlhs != 2){
        mexErrMsgTxt("Two output argument requrired.");
    }

    plhs[0] = mxCreateDoubleMatrix(1, 1, mxREAL);
    plhs[1] = mxCreateDoubleMatrix(1, 1, mxREAL);
    hcpdf = mxGetPr(prhs[0]);
    ndim = mxGetScalar(prhs[1]);
    fcmin = mxGetScalar(prhs[2]);
    ibeg = mxGetPr(plhs[0]);
    iend = mxGetPr(plhs[1]);
    begendfunc(ibeg, iend, hcpdf, ndim, fcmin);
}
```

D.8 gan_hnpdfunc.c

```
// Function:        construct non-capillary distribution function
// Input:           par: parameters for the model
//                  fcmin: uncovered area% under capillary distribution function
// output:          hnpdf: non-capillary distribution
// Created by Z Gan 0n 07-2010, updated on 04-20-2011

#include <math.h>
#include "mex.h"
void gan_hnpdfunc(double *hnpdf, int n, double *par, double qd)
{
   double a, t, dose, dt, tsp, tinj, alpha, avsi;
   int i;

   dose    = *(par+15);
   dt      = *(par+17);
   tinj    = *(par+18);
   tsp     = *(par+19);
   alpha   = *(par+21);
   avsi    = *(par+2);
   a       = dose/qd;

   for (i=0; i<n; i++){
      t=dt*i-avsi;
      if (t<tsp)
      {
         *(hnpdf+i)=0;
      }else if((t>=tsp) && (t<(tsp+tinj)))
      {
         *(hnpdf+i)=a *(1- exp(-alpha*(t-tsp)))/tinj;
      }else
      {
         *(hnpdf+i)=a *(exp(-alpha*(t-tsp-tinj))-exp(-alpha*(t-tsp)))/tinj;
      }
   }
}

//  Gateway function                                                    */
void mexFunction(int nlhs, mxArray *plhs[], int nrhs, mxArray *prhs[])
{
   double *hnpdf, *par;
   double qd;
   int ndim;
   if (nrhs != 3){
      mexErrMsgTxt("Seven input arguments required.");
```

```
    }
    else if (nlhs != 1){
        mexErrMsgTxt("One output argument requrired.");
    }
    ndim = mxGetScalar(prhs[0]);
    plhs[0] = mxCreateDoubleMatrix(ndim, 1, mxREAL);
    hnpdf = mxGetPr(plhs[0]);
    par = mxGetPr(prhs[1]);
    qd = mxGetScalar(prhs[2]);
    gan_hnpdfunc(hnpdf, ndim, par, qd);
}
```

D.9 gan_hcpdfunc.c

```
// Function:        construct capillary distribution function
// Input:           delx: x interval
//                  capsft: shift of capillary transit time
// output:          hcpdf: capillary distribution
// Created by Z Gan 0n 07-2010, updated on 04-20-2011

#include <math.h>
#include "mex.h"
void hcpdfunc(double *hcpdf, int n, double delx, double capsft,
        double tchat, double pec)
{
    double hc(double, double, double);
    double hct1, hct2, xi;
    int i;

    for (i=0;i<n;i++)
    {
        xi = delx*i-capsft;
        hct1 = hc(xi-delx/2, tchat, pec);
        hct2 = hc(xi+delx/2, tchat, pec);
        *(hcpdf+i) = (delx/2)*(hct1+hct2);
    }
}
// calculate hct based on random-walk function
double hc(double t, double tchat, double pec)
{
    double rwf(double, double);
    double hct, rwft;
    rwft = rwf(t/tchat,pec);
    hct = rwft/tchat;
    return(hct);
```

```
}
// random-walk function
double rwf(double s, double p)
{
   double rwft, sq, pi, ex;
   pi = 3.1415926535897932;
   if (s <= 0)
   {
      rwft = 0;
   }
   else
   {
      sq = sqrt(p/(4*pi*s));
      ex = exp((-p*(1-s)*(1-s))/(4*s));
      rwft = sq*ex;
   }
   return(rwft);
}

//  Gateway function
void mexFunction(int nlhs, mxArray *plhs[], int nrhs, mxArray *prhs[])
{
   double *hcpdf;
   double delx, capsft, tchat, pec;
   int n;
   if (nrhs != 5){
      mexErrMsgTxt("Five input arguments required.");
   }
   else if (nlhs != 1){
      mexErrMsgTxt("One output argument requrired.");
   }

   n = mxGetScalar(prhs[0]);
   plhs[0] = mxCreateDoubleMatrix(n, 1, mxREAL);
   hcpdf = mxGetPr(plhs[0]);
   delx = mxGetScalar(prhs[1]);
   capsft = mxGetScalar(prhs[2]);
   tchat = mxGetScalar(prhs[3]);
   pec = mxGetScalar(prhs[4]);
   hcpdfunc(hcpdf, n, delx, capsft, tchat, pec);
}
```

D.10 gan_CoQ1.c

```
// Function:        calculate efflux values based on mathematical model
```

```
// Input:          yold: old efflux values
//                 ynew: new efflux values
//                 par_var: parameters for the model
// output:         cr: concentration of Q+QHold efflux values
//                 cq: concentration of quinone
//                 cqh: concentration of hydroquinone
//                 istop: the sign of stop
// Created by Z Gan 0n 07-2010, updated on 04-20-2011

#include <math.h>
#include "mex.h"
int homorg, ibeg, iend, nx, nxy, ndim, qflag, nfinala;
double tibar, vari, avsi, tcbar, varc, avsc, qdot, dose, dt, delx, qc, pei, pec;
double qf1, qf2, vmax1, vmax2, akm1, akm2, vmax3, akm3, vmax4, akm4, alb1, alb2, f1,f2;
double alpha, tfinal, tinj, tsp, tihat, qd;

void gan_main(double *par_var, double *yold, double *ynew, double *hcpdf, double *cr, double
*cq, double *cqh, double *istop)
{
   int i, m;
   double tout, crsum, cqsum, cqhsum, hcj, rbar, qbar, qhbar, rchem, qchem, qhchem, fchem1,
fchem2, a1, a2;
   double square(double, double);
   // define all parameters
   tibar      = *(par_var+0);
   vari       = *(par_var+1);
   avsi       = *(par_var+2);
   tcbar      = *(par_var+3);
   varc       = *(par_var+4);
   avsc       = *(par_var+5);
   vmax1      = *(par_var+6);
   akm1       = *(par_var+7);
   vmax2      = *(par_var+8);
   akm2       = *(par_var+9);
   qf1        = *(par_var+10);
   qf2        = *(par_var+11);
   alb1       = *(par_var+12);
   alb2       = *(par_var+13);
   qdot       = *(par_var+14);
   dose       = *(par_var+15);
   homorg     = *(par_var+16);
   dt         = *(par_var+17);
   tinj       = *(par_var+18);
   tsp        = *(par_var+19);
```

```
tfinal     = *(par_var+20);
alpha      = *(par_var+21);
qflag      = *(par_var+22);
nfinala    = *(par_var+23);
nx         = *(par_var+24);
nxy        = *(par_var+25);
ndim       = *(par_var+26);
ibeg       = *(par_var+27);
iend       = *(par_var+28);
pec        = *(par_var+29);
pei        = *(par_var+30);
qc         = *(par_var+31);
delx       = *(par_var+32);
vmax3      = *(par_var+33);
akm3       = *(par_var+34);
vmax4      = *(par_var+35);
akm4       = *(par_var+36);

// calculate public constant
tihat = tibar/(1+2/pei);
qd    = qdot*tihat;
// constants f1, 1-f1
f1 = qc/(qc+qf1/alb1);
f2 = qc/(qc+qf2/alb2);
// constants for chemical parts
fchem1 = dt/(qc+qf1/alb1);
fchem2 = dt/(qc+qf2/alb2);

*istop = ndim;
// loop at time axis
for (i=0;i<=ndim;i++)
{
   tout = i*dt;  // actual time, second
   if (tout >= tfinal)  // stop
   {
      *istop =i;
      break;
   }
   // calculate boundary
   if (qflag ==1)  // inject quinone
   {
      *yold=square((tout-avsi), dose*tinj); // normalization factor was removed '/areaa';
      *(yold+nxy)=square((tout-avsi), dose*tinj);
      *(yold+2*nxy)=0;
```

```
}
else    // inject hydroquinone
{
   *yold=square((tout-avsi), dose*tinj); //  /areaa;
   *(yold+nxy)=0;
   *(yold+2*nxy)=square((tout-avsi), dose*tinj);
}

// calculate next time point, f1, f2, qchem, qhchem represent the model.
for (m=1; m<=nx;m++)
{   //average
   rbar  = 0.5*(*(yold+m)+*(yold+m-1));
   qbar  = 0.5*(*(yold+nxy+m)+*(yold+nxy+m-1));
   qhbar = 0.5*(*(yold+2*nxy+m)+*(yold+2*nxy+m-1));
   // chemistry
   rchem = 0;
   // *****  The model key equations *****
   // vmax1: NQO1; vmax2: complex III; vmax3: complex I; vmax4: other reductase
   a1 = vmax1/(akm1+qbar)+vmax3/(akm3+qbar)+vmax4/(akm4+qbar);
   a2 = vmax2/(akm2+qhbar);
   qchem = fchem1*(-qbar*a1+qhbar*a2);
   qhchem= fchem2*(qbar*a1-qhbar*a2);
   // ynew
   *(ynew+m)= *(yold+m-1);
   *(ynew+nxy+m)= (1-f1)**(yold+nxy+m)+f1**(yold+nxy+m-1)+qchem;
   *(ynew+2*nxy+m)= (1-f2)**(yold+2*nxy+m)+f2**(yold+2*nxy+m-1)+qhchem;
}

// adjust the value according the type of flow distribution
if (homorg==1) // if homogenous distribution
{
   *(cr+i)=*(ynew+nx-1);
   *(cq+i)=*(ynew+nxy+nx-1);
   *(cqh+i)=*(ynew+2*nxy+nx-1);
}
else // if heterogenous distribution
{
   crsum=0;
   cqsum=0;
   cqhsum=0;
   for (m=ibeg-1; m<nx-2; m++)
   {
      hcj = *(hcpdf+m);
      crsum = crsum + hcj**(ynew+m+1);
```

```
            cqsum = cqsum + hcj**(ynew+nxy+m+1);
            cqhsum = cqhsum + hcj**(ynew+2*nxy+m+1);
         }
         *(cr+i)=crsum;
         *(cq+i)=cqsum;
         *(cqh+i)=cqhsum;
      }

      // clean negative value and update yold
      for (m=0; m<=nx; m++)
      {
         if(*(ynew+m)<0) // no negative value is allowed.
            *(ynew+m)=0;
         if(*(ynew+nxy+m)<0)
            *(ynew+nxy+m)=0;
         if(*(ynew+2*nxy+m)<0)
            *(ynew+2*nxy+m)=0;
         *(yold+m)=*(ynew+m);
         *(yold+nxy+m)=*(ynew+nxy+m);
         *(yold+2*nxy+m)=*(ynew+2*nxy+m);
      }
   }
}

// sub-function which simulates a square function
double square(double t, double a)
{
   double hit;
   if (t<tsp)
   {
      hit=0;
   }else if((t>=tsp) && (t<(tsp+tinj)))
   {
      hit=a*(1- exp(-alpha*(t-tsp)))/tinj;
   }else
   {
      hit=a*(exp(-alpha*(t-tsp-tinj))-exp(-alpha*(t-tsp)))/tinj;
   }
   return(hit);
}



// Gateway function
```

```
void mexFunction(int nlhs, mxArray *plhs[], int nrhs, const mxArray *prhs[])
{
   double *cr, *cq, *cqh, *par_var, *yold, *ynew, *hcpdf, *istop;
   int n;

   if (nrhs != 5){
      mexErrMsgTxt("5 input arguments required.");
   }
   else if (nlhs != 4){
      mexErrMsgTxt("4 output argument requrired.");
   }
   n = mxGetScalar(prhs[0]);
   plhs[0] = mxCreateDoubleMatrix(n, 1, mxREAL);
   plhs[1] = mxCreateDoubleMatrix(n, 1, mxREAL);
   plhs[2] = mxCreateDoubleMatrix(n, 1, mxREAL);
   plhs[3] = mxCreateDoubleMatrix(1, 1, mxREAL);
   cr = mxGetPr(plhs[0]);
   cq = mxGetPr(plhs[1]);
   cqh = mxGetPr(plhs[2]);
   istop = mxGetPr(plhs[3]);
   par_var = mxGetPr(prhs[1]);
   yold = mxGetPr(prhs[2]);
   ynew = mxGetPr(prhs[3]);
   hcpdf = mxGetPr(prhs[4]);
   gan_main(par_var, yold, ynew, hcpdf, cr, cq, cqh,istop);
}
```

E. Codes for DQ/DQH$_2$ metabolism model

E.1 gan_fitDQ.m

```
% Function:     estimate Vmax and Km of complex III, NQO1
%               by fitting DQ distribution model to experimental data
% Input:        experimental data
% Output:       estimated values of Vmax(s) and Km(s)
% Created by Zhuohui Gan on 12-2010, updated on 04-20-2011
% Using Rugani's codes as a reference

clear all
close all
global n

% get initial values for all parameters
redo1 = 1;
while(redo1)
```

```
  % Enter parameters
  par = gan_GetDQParameters();
  if par == -9999
     disp('Error during parameter acquirement.');
     return;
  else
   homorg = par(17); % 0: hetergenous  1: homogenous
   % calculate peclet
   for i = 1:(2-homorg)  % why pe calculated before adjustment of tibar, tcbar?
     pe(i) = gan_Peclet(par(3*i-2),par(3*i-1));
     if (pe(i) <= 0)
        disp(['    when tibar=' num2str(par(3*i-2)) '   vari must be <' num2str(par(3*i-1))]);
     else
        redo1 = 0;
     end
   end
  end
end

% define all constants
tibar   = par(1); % non-capillary mean transit time, sec
vari    = par(2); % variance of non-capillary
avsi    = par(3); % shift for tibar
tcbar   = par(4); % capillary mean transit time, sec
varc    = par(5); % variance of capillary
avsc    = par(6); % shift for tcbar
vmax1   = par(7); % m-m vmax for NQO1 mediated Q reduction, nmol/min
akm1    = par(8); % m-m constant for NQO1 mediated Q reduction, uM
vmax2   = par(9); % m-m vmax for complex III mediated QH oxidation, nmol/min
akm2    = par(10); % m-m constant for complex III mediated QH oxidation, uM
qf1     = par(11); % virtual capillary volume, ml
qf2     = par(12); % virtual tissue volume, ml
alb1    = par(13); % apperant binding ratio between Q-Pc and Q-Pe for quinone (a1/a2)
alb2    = par(14); % apperant binding ratio between QH-Pc and QH-Pe for hydroquione (a3/a4)
qdot    = par(15); % flow cm/s
dose    = par(16); % initial , uM
homog   = par(17); % homogenous or hetergenous 1=homogenous
dt      = par(18); % time resolution, sec
tinj    = par(19); % total inject time (for input), sec
tsp     = par(20); % delay time (for input), sec
tfinal  = par(21); % time when the venous sample was collected, sec
alpha   = par(22); % constant for input function
qflag   = par(23); % 1=Q, 0=QH
ratio   = 1;
```

```
% check basic setting
if (tcbar <= 0)
  disp('    tcbar <0, so program stopped.')
  return;
end
if (tfinal <= 0)
  disp('    tfinal<=0, Program stopped.')
  return;
end
if qflag==1
   disp('   Your infused probe is quione.');
elseif qflag==0
   disp('   Your infused probe is hydroquione..');
else
   disp('   Your infused probe flag is mistaken,quit program.');
   return;
end

%initialized variables
ndim = round(tfinal/dt); % # points of time axis
npdes = 3;  % # of pdes for 1 model
fcmin = 0.01;  % covered area
dx     = dt/tcbar;  % normalized deltx , deltz
qc     = qdot*tcbar; % capillary volume
delx    = dx*tcbar;
% consider the delay into mean transit time
tibar = tibar + avsi;
tcbar = tcbar + avsc;

% set up pe, tihat
if homorg ==1
   pei = pe(1);
   pec = 0;
   tihat   = tibar/(1+2/pei); % the parameter for the input function.
else
   pei = pe(1);
   pec = pe(2);
   tihat   = tibar/(1+2/pei); % the parameter for the input function.
   tchat = tcbar/(1+2/pec);
end

%set-up of cap trans. func. as vector, min and max cap trans. times
hcpdf = zeros(1,ndim); % capillary transit time distribution
```

```
hnpdf = zeros(1,ndim); % non-capillary transit time distribution
if (homorg==1)
  % if it is a homogeneous organ
  iend = 1/dx + 0.001; % the last spacial point
  test = 1.0/dx - iend;
  if (test > 0.001)
    disp(['    For a homogenous organ, 1/dx must be an integer, now 1/dx=' num2str(1/dx)]);
    disp(['    With this dx, capillary mmt will be changed to ' num2str(iend*delx)]);
    C_ok = input('Continue or Start over (C = continue)? ','s');
    if (C_ok == 'C' | C_ok == 'c')
      tcbar = iend*delx;
    else
      return;
    end
  end
  ibeg = iend; % since it is homogenous, so no scalar required
else
  % if it is not a hetergeneous organ
  disp(['    dose=' num2str(dose)]);
  % capillary distribution function
  hcpdf = hcpdfunc(ndim,delx,avsc,tchat,pec);
  % find the begin and the end, but for hetergenous organ, ibeg ==1
  [ibeg,iend] = begendfunc(hcpdf,ndim,fcmin);
  %Renormalize hc(t) to unit area
  hcpdf = hcpdf(2:ndim); % get rid of the first point, because
  % from first point to iend point, which is supposed to be 99.9% covered.
  hcpdf = hcpdf(1:iend);
  % to get an interget for the area under the capillary function
  ac = trapz(hcpdf)*dt;
  % rescale ,so 100% area
  hcpdf = hcpdf./(ac/delx);

  %Noncapillary transport function
  qd = qdot*tihat; % non-capillary volume
  hnpdf = gan_hnpdfunc(ndim, par, qd); %non-capillary input function
  hnpdf = hnpdf(2:ndim);
  ibeg = 1;
  disp(['    ibeg=' num2str(ibeg) '      iend=' num2str(iend)]);
end
captmin = ibeg*delx;
captmax = iend*delx;
disp(['    min/max capillary times are [ ' num2str(captmin) '  ' num2str(captmax)  ' ]']);
if (iend == ndim)
  disp('    iend=dimenssion..!');
```

```
end

%set-up of nx
nxy =round (3*captmax/dt);
nfinala = round(tfinal/dt) + 1;
nx = iend + 1;
if (nx > nxy)
  disp(['    dx is too small, required dx >= ' num2str(1/nxy)]);
  return;
else
  disp(['    nx = ' num2str(nx)]);
end

%Initial conditions when t = 0
par_var     = par;
par_var(1)  = tibar;
par_var(4)  = tcbar;
par_var(23) = qflag;
par_var(24) = nfinala;
par_var(25) = nx;
par_var(26) = nxy;
par_var(27) = ndim;
par_var(28) = ibeg;
par_var(29) = iend;
par_var(30) = pec;
par_var(31) = pei;
par_var(32) = qc;
par_var(33) = delx;
par_var(34) = npdes;

t = [0:dt:(tfinal-dt)];

% get all data
redo2=1;
in_con=[]; % infused dye concentration (uM)
log_con = [];% log mean concentration of infused dye (uM)
out_con = [];% efflux concentration of metabolic product (uM)
cond = [];% infused condition
rate = [];% efflux rate of metabolic product (umol/min)
while redo2==1
  datafile = input ('Please enter the file which contains data:  ', 's');
  fid = fopen(datafile, 'r');
  if (fid==-1)
     temp = input('invalid file name, quit (0) or continue (1)?  ');
```

```
    if (temp==1)
    else
      return;
    end
  else
    fclose(fid);

  end
  load(datafile);
  data=eval(datafile(1:(length(datafile)-4)));
  tempin = data(:,1);  % infused concentration, in_con = Qv+QHv
  templog = data(:,2);  % log mean concenctration, log_con=(in-Qv)/(log(in)-log(Qv))
  tempout = data(:,3); ; % efflux product concentration, QHv or Qv
  temprate = data(:,4);   % efflux product rate, umol/min
  tempname = char(datafile(1:(length(datafile)-4)));

  in_con= [in_con tempin'];
  log_con = [log_con templog'];
  out_con = [out_con tempout'];
  rate = [rate temprate'];
  tempcondi=[];
  for tempi= 1:length(tempin)
    tempcondi{tempi}=upper(tempname);
  end
  cond = [cond tempcondi];

  temp = input (' Do you want to load more data? Yes (1) No (0)?  ');
  if (temp==1)
  else
     redo2=0;
  end
end

% define parameters which wants to be evaluated;
npara=input ('Please enter parameters you want to estimate, \n Vmax1 -> NQO1, Vmax2 ->
complex III, Vmax3 -> complex I, Vmax4-> others\n0: ratio of vmax2\n1: Vmax1; \n2: Vmax1
and km1; \n3: Vmax2 and km2; \n4: Vmax1, km1,Vmax2, km2:  ');
par_var(35) = npara;
switch npara
case 0
   p0=[ratio];
   lb=[0];
   ub=[1];
case 1
```

```
    p0 = [vmax1];
    lb = [0.0001];
    ub = [1000 ];
case 2
    p0 = [vmax1 akm1];
    lb = [0.0001 0.0001];
    ub = [1000 1000];
case 3
    p0 = [vmax2 akm2];
    lb = [0.0001 0.0001];
    ub = [1000 1000];
case 4
    p0 = [vmax1 akm1 vmax2 akm2];
    lb = [0.0001, 0.0001, 0.0001, 0.0001];
    ub = [2000 2000 2000 2000];
otherwise
    disp('The parameters you want to estimate is unclear. Quit.');
    return;
end

options=optimset('TolFun', 1e-8, 'TolX', 1e-8,'MaxFunEvals',1400);
n=0;
[p, SSD, residual,exitflag,output,lambda,nJa] = lsqcurvefit(@gan_solveDQ, p0, in_con, out_con,
lb, ub, options,par_var,hcpdf, cond);
result=p

% calculate correlation coefficient
[Q,R]=qr(nJa);
R1 = R(1:length(p), :);
h=inv(R1'*R1);
for i=1:length(p)
    for j=1:length(p)
        cc(i,j)=h(i,j)/(h(i,i)*h(j,j))^0.5;
    end
end
cc
SSD

% calculate confidence interval
s2=SSD/(length(in_con)-length(p));
for i = 1:length(p)
    seb(i)=(s2^0.5)*(h(i,i)^0.5);
end
```

```
switch npara
case 1
   tt=3.182; % 4 data points, 1 variable
   ci=seb.*tt
   disp(['    vmax1= ' num2str(p(1))]);
   par_var(7) = p(1);  % update vmax1
case 2
   tt=4.303; % 4 data points, 2 variable
   ci=seb.*tt
   disp(['    vmax1= ' num2str(p(1))]);
   disp(['    km1= ' num2str(p(2))]);
   par_var(7) = p(1);  % update vmax1
   par_var(8) = p(2);  % update km1
case 3
   tt=4.303; % 4 data points, 2 variable
   ci=seb.*tt
   disp(['    vmax2= ' num2str(p(1))]);
   disp(['    km2= ' num2str(p(2))]);
   par_var(9) = p(1);  % update vmax1
   par_var(10) = p(2);  % update km1
case 4
   tt=12.706;% 4 data points, 4 variable;
   ci=seb.*tt
   disp(['    vmax1= ' num2str(p(1))]);
   disp(['    km1= ' num2str(p(2))]);
   disp(['    vmax2= ' num2str(p(3))]);
   disp(['    km2= ' num2str(p(4))]);
   par_var(7) = p(1);  % update vmax1
   par_var(8) = p(2);  % update km1
   par_var(9) = p(3);  % update vmax2
   par_var(10) = p(4); % update km2
otherwise
   tt=2.01;  % constant for freedom 40-60
   ci=seb.*tt;
   p
end

% ask whether a simulation is required.
temp = input('Do you want to run a simulation? Yes(1) No(0)  ');
if temp == 0
   return;
end

% determine the time point of efflux  (as tfinal for simulation)
```

```
redo3=1;
while redo3==1
   temp = input('Input the time point you want to pick up the efflux concentration: ');
   if temp>0
      t = temp;
   else
      disp('invalid time point.')
      t = 99999;
   end

   if (t/dt)> ndim
      temp = input ('Your time point is either too big or mistaken, Do you want to try again, Y(1),
N(0)?  ');
      if temp==0
         return;
      end
   else
      redo3=0;
   end
end

% calculate the dose-dependent simulation based on new parameters.
m = int16(t/dt);
dose_interval =10;
num_dose =40;
for i=1:(num_dose+1);
      % initialize yold, ynew
      yold = zeros(npdes,nxy); % concentrations of probes(r, oxidized, reduced)at a given time t
      ynew = zeros(npdes,nxy); % concentrations of probes(r, oxidized, reduced)at a given time
t+dt
      par_var(16)=(i-1)*dose_interval;
      [cr,cq,cqh,istop] = gan_main2(ndim, par_var, yold, ynew, hcpdf);
      mQ(i)=cq(m);
      mQH(i)=cqh(m);
end

dose = 0:dose_interval:num_dose*dose_interval;
plot(dose,mQ,dose,mQH);
legend('Q', 'QH');

% save simulated results
conc_save = [dose; mQ; mQH; mQ+mQH];
save_sims = input('Save simulated data? Yes [1] No[0] ');
if save_sims == 1,
```

```
  gan_SaveData(conc_save, dose_interval);
elseif save_sims ~= 0,
    disp(['Unexpected entry.  Program will complete without saving. ']);
end

disp(['Program completed']);
```

E.2 gan_getDQParameters.m

```
function param = gan_GetDQParameters()
% Function:       acquire all parameters
% Input:          none
% Output:         a list of parameter values
% Created by Zhuohui Gan on 12-2010, updated on 04-20-2011

stop_flag = 0;
get_parms = 1;
par =[];

% Vmax1, Km1: NQO1 mediated CoQ1 reduction
% Vmax2, Km2: complex III mediated CoQ1H2 oxidation
% Vmax3, Km3: complex I mediated CoQ1 reduction
% Vmax4, Km4: other CoQ1 reduction
while(get_parms),
  T_or_F = input('Enter "t" for Term or "f" for file: ','s');
  if ((T_or_F == 't') | (T_or_F == 'T')),
    % define input dlg
    prompt1 = {'hn MTT (s):','hn VAR (s):','hn AVS:','hc MTT (s):','hc VAR (s):','hc AVS:',...
      'Vmax1 (nmol/s, NQO1):', 'Km1 (uM):', 'Vmax2 (nmol/s, complexIII):', 'Km2 (uM):','QF1
(ml):','QF2 (ml):','alb1:','alb2:'};
    prompt2 = {'Qdot (flow, ml/s):','Dose (uM):','homo? 1=Yes 0=No','dt(s):','tinj (s):','tsp
(s):','tfinal (s):',...
      'alpha', 'Q? 1=Q 0=QH','Vmax3:(not used for DQ)', 'Km3:(not used for DQ)','Vmax4:(not
used for DQ)', 'Km4:(not used for DQ)'};
    %       tibar  vari   avsi   tcbar  varc   avsc  vmax1 km1 vmax2 km2  qf1 qf2  alb1 alb2
    defs1 = {'4.00','4.00','2.00','2.50','4.00','0.00','45', '3','20','38','10','4','25','4.17'};
    %       qdot    dose homog  dt   tinj   tsp   tfinal   alpha  Q/QH Vmax3 Km3 Vmax4 km4
    defs2 = {'0.1667','100','0','0.01','145','5.09706','140','0.20358','1','20','20','25','10'};

    %acquire parameters from inputdlg
    temp = inputdlg(prompt1,'Enter Parameter Values (1/2)',1,defs1);
    par1 = str2num(char(temp));
    temp = inputdlg(prompt2,'Enter Parameter Values (2/2)',1,defs2);
    par2 = str2num(char(temp));
```

```
% check whether all inputs are number.
non_number=0;
if(length(par1)<1) ||length(par2)<1
    non_number=1;
end

% Inquiry if there is a non-number, what to do next step
if non_number>0
   msgbox('you have 1 or more non-number parameters,Please retry.','Warning','warn')
else
  par = [par1; par2];
  % save paramters to a file if need
  save_ck = input('Save parameter file? Yes [1] No [0]  ');
  if save_ck == 1,
  fcell = { 'hn MTT(s):     ', 'hn VAR(s):     ', 'hn AVS:       ','hc MTT(s):     ',...
          'hc VAR:       ', 'hc AVS:       ', 'Vmax1:        ','Km1:           ',...
          'Vmax2:        ', 'Km2:          ', 'QF1:          ','QF2:           ',...
          'alb1:         ', 'alb2:         ', 'Qdot:         ','Dose:          ',...
          'homo? 1=Yes 0=No', 'dt            ', 'tinj:         ','tsp:           ',...
          'tfinal        ', 'alpha         ', 'Q? 1=Q 0=QH   ','Vmax3:         ',...
          'Km3:          ', 'Vmax4:        ', 'Km4:          '};
  ffield = {'p1','p2','p3','p4','p5','p6','p7','p8','p9','p10','p11','p12','p13',...
        'p14','p15','p16','p17','p18','p19','p20','p21','p22','p23','p24','p25','p26','p27'};
  fpar = cell2struct(fcell,ffield,2);
  pno = length(par);
  repeat = 1;
  while(repeat),
     s_fname = input('Enter filename to save parameters: ','s');
     fid_r = fopen(s_fname,'r');
     file_save = 0;
     if fid_r ~= -1,
        fclose(fid_r);
        file_save = input('Filename already exists. Enter new name [1] or write over [0]? ');
        if file_save == 0,
           fid_w = fopen(s_fname,'w');
           fprintf(fid_w,' %i\n',pno);
           for i = 1:pno
              eval(['fprintf(fid_w," %s     %8.4f\n",fpar.p' int2str(i) ...
              ', par(' int2str(i) '));']);
           end
           fclose(fid_w);
           repeat = 0;
        end
```

```
        else
          fid_w = fopen(s_fname,'w');
          fprintf(fid_w,' %i\n',pno);
          for i = 1:pno
            eval(['fprintf(fid_w," %s     %8.4f\n",fpar.p' int2str(i) ...
            ', par(' int2str(i) '));']);
          end
          fclose(fid_w);
          repeat = 0;
        end
      end  % end of while
    end  % end of if
    % change the control for the loop
    get_parms = 0  ;
    param =  par;
    end
  elseif ((T_or_F == 'f') | (T_or_F == 'F')),
    par=gan_ReadParameters;
    if par==-9999
      param =-9999;
    else
      param =par;
      if length(par)<1
        msgbox('You give up to set up parameters. This may cause sequential
error.','Warning','warn')
      else
        for i = 1:length(par),
          eval(['clear line_p' int2str(i) '; clear p' int2str(i) '; clear sp' int2str(i) ';' ]);
        end
      end
    end
    prompt1 = {'hn MTT (s):','hn VAR (s):','hn AVS:','hc MTT (s):','hc VAR (s):','hc AVS:',...
      'Vmax1 (nmol/s, NQO1):', 'Km1 (uM):', 'Vmax2 (nmol/s, complexIII):', 'Km2 (uM):','QF1
(ml):','QF2 (ml):','alb1:','alb2:'};
    prompt2 = {'Qdot (flow, ml/s):','Dose (uM):','homo? 1=Yes 0=No','dt(s):','tinj (s):','tsp
(s):','tfinal (s):',...
      'alpha', 'Q? 1=Q 0=QH','Vmax3:(not used for DQ)', 'Km3:(not used for DQ)','Vmax4:(not
used for DQ)', 'Km4:(not used for DQ)'};
    %       tibar  vari   avsi   tcbar  varc   avsc  vmax1 km1 vmax2 km2  qf1 qf2  alb1 alb2
    defs1 = {num2str(par(1)),num2str(par(2)),num2str(par(3)),num2str(par(4)),num2str(par(5)),...
          num2str(par(6)),num2str(par(7)),num2str(par(8)),num2str(par(9)),num2str(par(10)),...
          num2str(par(11)),num2str(par(12)),num2str(par(13)),num2str(par(14))};
    %       qdot    dose homog  dt   tinj   tsp   tfinal    alpha  Q/QH Vmax3 Km3 Vmax4 km4
```

```
    defs2 =
{num2str(par(15)),num2str(par(16)),num2str(par(17)),num2str(par(18)),num2str(par(19)),...

num2str(par(20)),num2str(par(21)),num2str(par(22)),num2str(par(23)),num2str(par(24)),...
        num2str(par(25)),num2str(par(26)),num2str(par(27))};

    %acquire parameters from inputdlg
    temp = inputdlg(prompt1,'Enter Parameter Values (1/2)',1,defs1);
    par1 = str2num(char(temp));
    temp = inputdlg(prompt2,'Enter Parameter Values (2/2)',1,defs2);
    par2 = str2num(char(temp));
    par = [par1; par2];
    param = par;
    % get param, quit the loop
    get_parms = 0;
  else
    get_parms = input('Invalid entry.  Retry? [1] or Quit [0] ');
    stop_flag = 1;
    param = -9999;
  end

end
```

E.3 gan_simDQ.m

```
 % Function:      simulate efflux value with a given set of parameters
% Input:          none
% Output:         a file containing simulated data
% Created by Zhuohui Gan on 12-2010, updated on 04-20-2011

clear all
global tchat
global pec

%Parameter entry , update on 07-28-2010 by Gan
redo1 = 1;
while(redo1)
  % Enter parameters
  par = gan_GetDQParameters();
  if par == -9999
     disp('Error during parameter acquirement.');
     return;
  else
   homorg = par(17); % 0: hetergenous  1: homogenous
   % calculate peclet
```

```
    for i = 1:(2-homorg)
        pe(i) = gan_Peclet(par(3*i-2),par(3*i-1));
     if (pe(i) <= 0)
       disp([' when tibar=' num2str(par(3*i-2)) ' vari must be <' num2str(par(3*i-1))]);
     else
       redo1 = 0;
     end
   end
  end
end

% define all constants or parameters
tibar  = par(1); % non-capillary mean transit time, sec
vari   = par(2); % variance of non-capillary
avsi   = par(3); % shift for tibar
tcbar  = par(4); % capillary mean transit time, sec
varc   = par(5); % variance of capillary
avsc   = par(6); % shift for tcbar
vmax1  = par(7); % m-m vmax for NQO1 mediated Q reduction
akm1   = par(8); % m-m constant for NQO1 mediated Q reduction
vmax2  = par(9); % m-m vmax for complex III mediated QH oxidation
akm2   = par(10); % m-m constant for complex III mediated QH oxidation
qf1    = par(11); % virtual capillary volume
qf2    = par(12); % virtual tissue volume
alb1   = par(13); % apperant binding ratio between Q-Pc and Q-Pe for quinone (a1/a2)
alb2   = par(14); % apperant binding ratio between QH-Pc and QH-Pe for hydroquione (a3/a4)
qdot   = par(15); % flow m/s
dose   = par(16); % infused concentration
homog  = par(17); % homogenous or hetergenous 1=homogenous
dt     = par(18); % time resolution
tinj   = par(19); % total inject time (for input)
tsp    = par(20); % delay time (for input)
tfinal = par(21); % total simulation time
alpha  = par(22); % constant for input function
qflag  = par(23); % 1=Q, 0=QH

% if mean transit time for capillary is less than 0, something wrong, stop
if (tcbar <= 0)
  disp('  tcbar <0, so program stopped.')
  return;
end

if (tfinal <= 0)
  disp('  tfinal<=0, Program stopped.')
```

```
  return;
end

%initialized variables
ndim = round(tfinal/dt);  % # points of time axis
npdes = 3;  % # of pdes for 1 model
fcmin = 0.01;  % covered area
dx      = dt/tcbar;  % normalized deltx , deltz
qc      = qdot*tcbar; % capillary volume
delx    = dx*tcbar;

% consider the delay into mean transit time
tibar = tibar + avsi;
tcbar = tcbar + avsc;

% set up pe, tihat
if homorg ==1
   pei = pe(1);
   pec = 0;
   tihat   = tibar/(1+2/pei); % the parameter for the input function.
else
   pei = pe(1);
   pec = pe(2);
   tihat   = tibar/(1+2/pei); % the parameter for the input function.
   tchat = tcbar/(1+2/pec);
end

%set-up of cap trans. func. as vector, min and max cap trans. times
hcpdf = zeros(1,ndim); % capillary transit time distribution
hnpdf = zeros(1,ndim); % non-capillary transit time distribution
if (homorg==1)
  % if it is a homogeneous organ
  iend = 1/dx + 0.001; % the last spacial point
  test = 1.0/dx - iend;
  if (test > 0.001)
    disp(['    For a homogenous organ, 1/dx must be an integer, now 1/dx=' num2str(1/dx)]);
    disp(['    With this dx, capillary mmt will be changed to ' num2str(iend*delx)]);
    C_ok = input('Continue or Start over (C = continue)? ','s');
    if (C_ok == 'C' | C_ok == 'c')
      tcbar = iend*delx;
    else
      return;
    end
  end
```

```
  ibeg = iend; % since it is homogenous, so no scalar required
else
  % if it is not a hetergeneous organ
  disp(['    dose=' num2str(dose)]);
  % capillary distribution function
  hcpdf = hcpdfunc(ndim,delx,avsc,tchat,pec);
  % find the begin and the end, but for hetergenous organ, ibeg ==1
  [ibeg,iend] = begendfunc(hcpdf,ndim,fcmin);
  %Renormalize hc(t) to unit area
  hcpdf = hcpdf(2:ndim); % get rid of the first point, because
  % from first point to iend point, which is supposed to be 99.9% covered.
  hcpdf = hcpdf(1:iend);
  % to get an interget for the area under the capillary function
  ac = trapz(hcpdf)*dt;
  % rescale ,so 100% area
  hcpdf = hcpdf./(ac/delx);

  %Noncapillary transport function
  qd = qdot*tihat; % non-capillary volume
  hnpdf = gan_hnpdfunc(ndim, par, qd); %non-capillary input function
  hnpdf = hnpdf(2:ndim);
  ibeg = 1;
  disp(['    ibeg=' num2str(ibeg) '      iend=' num2str(iend)]);
end
 captmin = ibeg*delx;
captmax = iend*delx;
disp(['    min/max capillary times are [ ' num2str(captmin) '  ' num2str(captmax)  ' ]']);
if (iend == ndim)
  disp('    iend=dimenssion..!');
end

%set-up of nx and the vector xbreak(i) of knots
nxy =round (3*captmax/dt);
nfinala = round(tfinal/dt) + 1;
nx = iend + 1;
if (nx > nxy)
  disp(['    dx is too small, required dx >= ' num2str(1/nxy)]);
  return;
else
  disp(['    nx = ' num2str(nx)]);
end

%Initial conditions when t = 0
par_var     = par;
```

```
par_var(1)  = tibar;
par_var(4)  = tcbar;
par_var(24) = nfinala;
par_var(25) = nx;
par_var(26) = nxy;
par_var(27) = ndim;
par_var(28) = ibeg;
par_var(29) = iend;
par_var(30) = pec;
par_var(31) = pei;
par_var(32) = qc;
par_var(33) = delx;
par_var(34) = npdes;

t = [0:dt:(tfinal-dt)];
myway = input('Input the way you to acquire doses: manual input(0), data file(1), auto input(2)? ');
% set up the dose
switch myway
  case 0
    num = input('How many doses for this simulation? ');
    if num>=1
       for i=1:num
          disp(['please input your No.' num2str(i)  '  dose']);
          temp = input('must be a number   ','s');
          if str2num(temp)>=0
             temp=str2num(temp);
          else
             temp=0;
          end
          dose(i)=temp;
       end
    end
  case 1
    redo2=1;
    while redo2==1
       datafile = input ('Please enter the file which contains data:', 's');
       fid = fopen(datafile, 'r');
       if (fid==-1)
          temp = input('invalid file name, quit (0) or continue (1)?');
          if (temp==1)
          else
             return;
          end
       else
```

```
            fclose(fid);
            redo2=0;
        end
    end
    % the file name must be end with .txt or .dat.
    load(datafile);
    data=eval(datafile(1:(length(datafile)-4)));
    dose = data(:,1);
    num = length(dose);
  case 2
    dose0 = input ('Please input the start dose:  ');
    dose1 = input ('Please input the end dose:  ');
    interval = input('Please input dose interval:  ');
    if (dose0>dose1)
        disp('The end dose can not be less than the start dose.');
    elseif (dose0<0)
        disp('Dose can not be less than 0.');
    end
    num = int16((dose1-dose0)/interval);
    dose = dose0:interval: (dose0+num*interval);
    num = length(dose);
  otherwise
    disp('You did not select a proper way. Quit the program..');
    return;
end

% Calculate efflux concentrations based on input concentrations.
for i=1:num
        par_var(16)=dose(i);  % set up dose
        % initialize avaiable
        cr = zeros(1,ndim); % concentration of reference probe
        cq = zeros(1,ndim); % concentration of oxidized probe
        cqh = zeros(1,ndim); % concentration of reduced probe
        % initialize yold, ynew
        yold = zeros(npdes,nxy); % concentrations of probes(r, oxidized, reduced)at a given time t
        ynew = zeros(npdes,nxy); % concentrations of probes(r, oxidized, reduced)at a given time
t+dt
        % calculate the result
        [cr,cq,cqh,istop] = gan_main2(ndim, par_var, yold, ynew, hcpdf);
        mCr(i,1:ndim)=cr;
        mCq(i,1:ndim)=cq;
        mCqh(i,1:ndim)=cqh;
end
```

```
% display the results
switch myway
   case 2
      redo3=1;
      while redo3 ==1
         ptime = input('input the time point you want to collect sample.');
         if ptime>tfinal
            disp('The time you selected is longer than tfinal. Try again');
            redo3=1;
         elseif ptime<0
            disp('Time can not be less than 0.');
            redo3=1;
         elseif (0<ptime) && (ptime<=tfinal)
            redo3=0;
         else
            disp('Your input may have some mistake. Quit program now.')
            redo3=1;
         end
         if redo3==1
            temp = input('Do you want to try again, Yes(1) No(0)?');
            if temp ==1
               redo3=1;
            else
               redo3=0;
               return;
            end
         end
      end
      tpoint = int16(ptime/dt);
      for i=1:num
        mcr(i) = mCr(i,tpoint);
        mcq(i) = mCq(i,tpoint);
        mcqh(i)= mCqh(i,tpoint);
      end
      plot(dose,mcr,dose,mcq,dose,mcqh);
      legend('Ref', 'Q', 'QH') ;
      save_sims = input('Save simulated data? Yes [1] No[0] ');
      if save_sims == 1,
         conc_save = [dose; mcr; mcq; mcqh];
         gan_SaveData(conc_save, interval);
      end
   otherwise
      for i=1:num
         mcr = mCr(i,1:ndim);
```

```
        mcq = mCq(i,1:ndim);
        mcqh= mCqh(i,1:ndim);
        subplot(1,num,i);
        plot(t,mcr,t,mcq,t,mcqh);
        legend('Ref', 'Q', 'QH') ;
        title(num2str(dose(i)));
    end
    % save the results
    save_sims = input('Save simulated data? Yes [1] No[0] ');
    if save_sims == 1,
        for i=1:num
            mcr = mCr(i,1:ndim);
            mcq = mCq(i,1:ndim);
            mcqh= mCqh(i,1:ndim);
            conc_save = [t; mcr; mcq; mcqh];
            gan_SaveData(conc_save, dt);
        end
    elseif save_sims ~= 0,
        disp(['Program will complete without saving. ']);
    end
end
disp(['Program completed']);
```

E.4 gan_solveDQ.m

```
function Cmatch = gan_solvepdes(p, in_con, par_var, hcpdf, cond)
% Function:     solve PDE sets with a given set of parameters
% Input:        in_con: infused concentration
%               par_var: parameters
%               hcpdf: capillary distribution
%               cond: infusion conditions
% Output:       a list of steady_state efflux values
% Created by Zhuohui Gan on 12-2010, updated on 04-20-2011

global  n

mparameters =  par_var;
qflag = par_var(23);
nxy = par_var(26);
ndim = par_var(27);
npdes = par_var(34);
npara = par_var(35);

switch npara
   case 0
```

```
        mparameters(9) = mparameters(9)*p(1); %vmax2 for the probe
    case 1        % 1 parameters
        mparameters(7) = p(1);        % vmax1
    case 2        % 2 parameters
        mparameters(7) = p(1);        % vmax1
        mparameters(8) = p(2);        % km1
    case 3        % 4 parameters
        mparameters(9) = p(1);        % vmax2
        mparameters(10) = p(2);       % km2
    case 4        % 4 parameters
        mparameters(7) = p(1);        % vmax1
        mparameters(8) = p(2);        % km1
        mparameters(9) = p(3);        % vmax2
        mparameters(10) = p(4);       % km2
    otherwise
end

% progress control.....
n=n+1
p
% adjust parameter based on the infusion condition
numDose = length(in_con);
for i=1:numDose
    temppara = mparameters;
    temppara(16)=in_con(i); % dose
    yold = zeros(npdes,nxy); % concentrations of probes(r, oxidized, reduced)at a given time t
    ynew = zeros(npdes,nxy); % concentrations of probes(r, oxidized, reduced)at a given time t+dt
    if (strcmp(cond{i},'DQH2DIC') ||strcmp(cond{i},'DQH2DIC21')||
strcmp(cond{i},'DQH2DIC85') || strcmp(cond{i},'DQH2DIC60'))
            temppara(7) = 0;        % vmax1=0, NQO1 inhibited
            temppara(23) = 0;       % infused DQH2
    elseif (strcmp(cond{i},'DQDICROT')||strcmp(cond{i},'DQDICROT21') ||
strcmp(cond{i},'DQDICROT85') || strcmp(cond{i},'DQDICROT60'))
            temppara(7) = 0;        % vmax1=0, NQO1 inhibited
            temppara(23) = 1;       % infused DQ
    elseif(strcmp(cond{i},'DQAA') ||strcmp(cond{i},'DQAA21') || strcmp(cond{i},'DQAA85') ||
strcmp(cond{i},'DQAA60'))
            temppara(9) = 0;        % vmax2=0, COMPLEX III inhibited
            temppara(23) = 1;       % infused DQ
    elseif(strcmp(cond{i},'DQKCN') ||strcmp(cond{i},'DQKCN21') || strcmp(cond{i},'DQKCN85')
|| strcmp(cond{i},'DQKCN60'))
            temppara(9) = 0;        % vmax2=0, COMPLEX III inhibited
            temppara(23) = 1;       % infused DQ
```

```
   elseif(strcmp(cond{i},'DQH2DICROT')||strcmp(cond{i},'DQH2DICROT21')||
strcmp(cond{i},'DQH2DICROT85') || strcmp(cond{i},'DQH2DICROT60'))
         temppara(7) = 0;       % vmax1=0, NQO1 inhibited
         temppara(23) = 0;      % infused DQH2
   elseif(strcmp(cond{i},'DQ')||strcmp(cond{i},'DQ21')|| strcmp(cond{i},'DQ85') ||
strcmp(cond{i},'DQ60'))
         temppara(23) = 1;      % infused DQ
   else
   end

   [cr, cq, cqh, istop] = gan_main2(ndim, temppara, yold, ynew, hcpdf);
   mQ(i)=cq(ndim);
   mQH(i)=cqh(ndim);
   % pick up the right value
   if (temppara(23)==1)
      mResult(i)= mQH(i);
   else
      mResult(i)= mQ(i);
   end

end
Cmatch = mResult;
```

E.5 Gan_main2.c

```
// Function:      calculate efflux values based on mathematical model for DQ/DQH2
// Input:         yold: old efflux values
//                ynew: new efflux values
//                par_var: parameters for the model
// output:        cr: concentration of Q+QHold efflux values
//                cq: concentration of quinone
//                cqh: concentration of hydroquinone
//                istop: the sign of stop
// Created by Z Gan 0n 07-2010, updated on 04-20-2011

#include <math.h>
#include "mex.h"

int homorg, ibeg, iend, nx, nxy, ndim, qflag, nfinala;
double tibar, vari, avsi, tcbar, varc, avsc, qdot, dose, dt, delx, qc, pei, pec;
double qf1, qf2, vmax1, vmax2, akm1, akm2, alb1, alb2, f1,f2;
double alpha, tfinal, tinj, tsp, tihat, qd;

void gan_main(double *par_var, double *yold, double *ynew, double *hcpdf, double *cr, double
*cq, double *cqh, double *istop)
```

```
{
   int i, m;
   double tout, crsum, cqsum, cqhsum, hcj, rbar, qbar, qhbar, rchem, qchem, qhchem, fchem1,
fchem2;
   double rwfhi(double);
   double square(double, double);

   // define all parameters
   tibar      = *(par_var+0);
   vari       = *(par_var+1);
   avsi       = *(par_var+2);
   tcbar      = *(par_var+3);
   varc       = *(par_var+4);
   avsc       = *(par_var+5);
   vmax1      = *(par_var+6);
   akm1       = *(par_var+7);
   vmax2      = *(par_var+8);
   akm2       = *(par_var+9);
   qf1        = *(par_var+10);
   qf2        = *(par_var+11);
   alb1       = *(par_var+12);
   alb2       = *(par_var+13);
   qdot       = *(par_var+14);
   dose       = *(par_var+15);
   homorg     = *(par_var+16);
   dt         = *(par_var+17);
   tinj       = *(par_var+18);
   tsp        = *(par_var+19);
   tfinal     = *(par_var+20);
   alpha      = *(par_var+21);
   qflag      = *(par_var+22);
   nfinala    = *(par_var+23);
   nx         = *(par_var+24);
   nxy        = *(par_var+25);
   ndim       = *(par_var+26);
   ibeg       = *(par_var+27);
   iend       = *(par_var+28);
   pec        = *(par_var+29);
   pei        = *(par_var+30);
   qc         = *(par_var+31);
   delx       = *(par_var+32);

   // calculate public constant
   tihat = tibar/(1+2/pei);
```

```
qd    = qdot*tihat;
// constants f1, 1-f1
f1 = qc/(qc+qf1/alb1);
f2 = qc/(qc+qf2/alb2);
// constants for chemical parts
fchem1 = dt/(qc+qf1/alb1);
fchem2 = dt/(qc+qf2/alb2);


*istop = ndim;
// loop at time axis
for (i=0;i<=ndim;i++)
{
   tout = i*dt;  // actual time, second
   if (tout >= tfinal)  // stop
   {
      *istop =i;
      break;
   }
   // calculate boundary
   if (qflag ==1)  // inject quinone
   {
      *yold=square((tout-avsi), dose*tinj); // normalization factor was removed '/areaa';
      *(yold+nxy)=square((tout-avsi), dose*tinj);
      *(yold+2*nxy)=0;
   }
   else    // inject hydroquinone
   {
      *yold=square((tout-avsi), dose*tinj); //  /areaa;
      *(yold+nxy)=0;
      *(yold+2*nxy)=square((tout-avsi), dose*tinj);
   }

   // calculate next time point, f1, f2, qchem, qhchem represent the model.
   for (m=1; m<=nx;m++)
   {   //average
      rbar  = 0.5*(*(yold+m)+*(yold+m-1));
      qbar  = 0.5*(*(yold+nxy+m)+*(yold+nxy+m-1));
      qhbar = 0.5*(*(yold+2*nxy+m)+*(yold+2*nxy+m-1));
      // chemistry
      rchem = 0;
      // vmax1: NQO1; vmax2: complex III
      qchem = -fchem1*vmax1*qbar/(akm1+qbar)+fchem1*vmax2*qhbar/(akm2+qhbar);
      qhchem= fchem2*vmax1*qbar/(akm1+qbar)-fchem2*vmax2*qhbar/(akm2+qhbar);
```

```
        // ynew
        *(ynew+m)= *(yold+m-1);
        *(ynew+nxy+m)= (1-f1)**(yold+nxy+m)+f1**(yold+nxy+m-1)+qchem;
        *(ynew+2*nxy+m)= (1-f2)**(yold+2*nxy+m)+f2**(yold+2*nxy+m-1)+qhchem;
    }

    // adjust the value according the type of flow distribution
    if (homorg==1) // if homogenous distribution
    {
        *(cr+i)=*(ynew+nx-1);
        *(cq+i)=*(ynew+nxy+nx-1);
        *(cqh+i)=*(ynew+2*nxy+nx-1);
    }
    else // if heterogenous distribution
    {
        crsum=0;
        cqsum=0;
        cqhsum=0;
        for (m=ibeg-1; m<nx-2; m++)
        {
            hcj = *(hcpdf+m);
            crsum = crsum + hcj**(ynew+m+1);
            cqsum = cqsum + hcj**(ynew+nxy+m+1);
            cqhsum = cqhsum + hcj**(ynew+2*nxy+m+1);
        }
        *(cr+i)=crsum;
        *(cq+i)=cqsum;
        *(cqh+i)=cqhsum;
    }

    // clean negative value and update yold
    for (m=0; m<=nx; m++)
    {
        if(*(ynew+m)<0) // no negative value is allowed.
            *(ynew+m)=0;
        if(*(ynew+nxy+m)<0)
            *(ynew+nxy+m)=0;
        if(*(ynew+2*nxy+m)<0)
            *(ynew+2*nxy+m)=0;
        *(yold+m)=*(ynew+m);
        *(yold+nxy+m)=*(ynew+nxy+m);
        *(yold+2*nxy+m)=*(ynew+2*nxy+m);
    }
}
```

```
}

// sub-function used to simulate a square input
double square(double t, double a)
{
   double hit;
   if (t<tsp)
   {
      hit=0;
   }else if((t>=tsp) && (t<(tsp+tinj)))
   {
      hit=a*(1- exp(-alpha*(t-tsp)))/tinj;
   }else
   {
      hit=a*(exp(-alpha*(t-tsp-tinj))-exp(-alpha*(t-tsp)))/tinj;
   }
   return(hit);
}

// for random-walk input
double rwfhi(double t)
{
   double rwf(double);
   double hit;

   double rwft, sq, pi, ex,s;
   pi = 3.1415926535897932;
   s=t/tihat;
   if (s <= 0)
   {
      rwft = 0;
   }
   else
   {
      sq = sqrt(pei / (4 * pi * s));
      ex = exp((-pei * (1-s) * (1-s)) / (4 * s));
      rwft = sq * ex;
   }

   hit = (dose/qd) * rwft;
   return(hit);
}

/*  Gateway function        */
```

```
void mexFunction(int nlhs, mxArray *plhs[], int nrhs, const mxArray *prhs[])
{
   double *cr, *cq, *cqh, *par_var, *yold, *ynew, *hcpdf, *istop;
   int n;

   if (nrhs != 5){
      mexErrMsgTxt("5 input arguments required.");
   }
   else if (nlhs != 4){
      mexErrMsgTxt("4 output argument requrired.");
   }
   n = mxGetScalar(prhs[0]);
   plhs[0] = mxCreateDoubleMatrix(n, 1, mxREAL);
   plhs[1] = mxCreateDoubleMatrix(n, 1, mxREAL);
   plhs[2] = mxCreateDoubleMatrix(n, 1, mxREAL);
   plhs[3] = mxCreateDoubleMatrix(1, 1, mxREAL);
   cr = mxGetPr(plhs[0]);
   cq = mxGetPr(plhs[1]);
   cqh = mxGetPr(plhs[2]);
   istop = mxGetPr(plhs[3]);
   par_var = mxGetPr(prhs[1]);
   yold = mxGetPr(prhs[2]);
   ynew = mxGetPr(prhs[3]);
   hcpdf = mxGetPr(prhs[4]);
   gan_main(par_var, yold, ynew, hcpdf, cr, cq, cqh,istop);
}
```

APPENDIX III – Glossary

AA = Antimycin A

ACE = Angiotensin converting enzyme

ALI = Acute lung injury

AR = Amplex red

ARDS = Acute respiratory distress syndrome

B_c = Dye binding sites within the cytoplasm

B_e = Dye cuvette bonding sites

B_m = Dye binding sites within mitochondrial matrix

BPAEC = Bovine pulmonary arterial endothelial cells

BSA = Bovine serum albumin

CCCP = Carbonyl cyanide 3-chlorophenylhydrazone

CoQ_9H_2 = endogenous coenzyme Q_9 hydroquinone

DCF = 2,7-dichlorofluorescein

DCPIP = 2,6-dichlorophenolindophenol

DQH_2 = Durohydroquinone

[DQ] (x,t), and [DQH_2] (x,t) = Vascular concentrations of free DQ and DQH_2, respectively, at distance x from the capillary inlet and time t (μM).

$[\overline{DQ}]$ = Total (free + BSA bound) vascular concentration of DQ (μM)

$[\overline{DQH_2}]$ = Total (free + BSA bound) vascular concentration of DQH_2 (μM)

ES936 = 5-methoxy-1,2-dimethyl-3-[(4-nitrophenol)methyl]-indole-4,7-dione

F = Faraday constant (coluomb/mol)

FCCP = Carbonylcyanide *p*-trifluoromethoxyphenylhydrazone

$h_c(t)$ = Capillary transit time distribution

FAPGG = N-[3-(2-Furyl) acryloyl]-Phe-Gly-Gly

GF120918 = *N*-(4-[2-(1,2,3,4-tetrahydro-6,7-dimethoxy-2-isoquinolinyl) ethyl]-phenyl)-9,10-dihydro-5-methoxy-9-oxo-4 acridine carboxamide

GSH = Glutathione

H_2O_2 = Hydrogen peroxide

HBSS = Hank's buffered salt solution

HEPES = 4-(2-hydroxyethyl)-1-piperazineethanesulfonic acid

HRP = Horseradish peroxidase

J_1 = Dye flux across plasma membrane (pmol/cm^2)

J_2 = Dye flux across inner mitochondrial membrane (pmol/cm^2)

k_1 = Rate constant for dye-cuvette binding (min^{-1} nM^{-1})

k_{-1} = Rate constant for dye-cuvette unbinding (min^{-1})

$\bar{k}_1 = k_1 [B_e]$ = Rate for dye-cuvette binding (min^{-1})

k_2 = Association rate constant of dye binding with B_c (min^{-1} nM^{-1})

k_{-2} = Dissociation rate constant of dye binding with B_c (min^{-1})

k_3 = Association rate constant of dye binding with B_m (min^{-1} nM^{-1})

k_{-3} = Dissociation rate constant of dye binding with B_m (min^{-1})

K_{m1a} = Apparent Michaelis-Menten constant for NQO1 mediated DQ reduction, (μM)

K_{m2a} = Apparent Michaelis-Menten constant for DQH_2 oxidation via complex III, (μM)

K_{Pgp} = Pgp mediated dye efflux rate (ml/min)

k_{ox} = NQO1 = NAD(P)H:quinone oxidoreductase 1

KCN = Potassium cyanide

KRB = Kreb's ringer bicarbonate buffer

KRB-Dex = Kreb's ringer bicarbonate buffer containg dextran

KRB-GO = Krebs' ringer bicarbonate buffer containing glucose and glucose oxidase

LDH = Lactate dehydrogenase

NADH = Nicotinamide adenine dinucleotide

o-PD = Ortho-phenylenediamine dihydrochloride

P_1 = Dye permeability across plasma membrane (cm/min)

P_2 = Dye permeability across mitochondrial membrane (cm/min)

P_1S_1 = Dye permeability-surface area product across plasma membrane (ml/min)

P_2S_2 = Dye permeability-surface area product across mitochondrial membrane (ml/min)

Pa = Pulmonary arterial pressure, (Torr)

Pgp = Multi-drug efflux pump p-glycoprotein

PS = Permeability-surface area product, (ml/min), which is a measure of rate of ACE mediated FAPGG hydrolysis, and an index of perfused capillary surface area

Q_i = quinone-reducing center

Q_o = quinol-oxidizing center

R = Universal gas constant (Joule K^{-1} mol^{-1})

R123 = Rhodamine 123

$[R_c](t)$ = Dye concentration in cytoplasm at time t (nM)

$[R_e](t)$ = Dye concentration in extracellular medium at time t (nM)

$[R_e]_{s0}$ = Dye steady-state concentration in extracellular medium in absence of BPAEC (nM)

$[R_e]_{s1}$ = Dye steady-state concentration in extracellular medium in presence of BPAEC, GF120918 and high potassium(nM)

$[R_e]_{s2}$ = Dye steady-state concentration in extracellular medium in presence of BPAEC, GF120918, high potassium, and CCCP (nM)

$[R_m](t)$ = Dye concentration in mitochondrial matrix at time t (nM)

$[R_m]_s$ = Dye steady-state concentration in mitochondrial matrix (nM)

ROS = Reactive oxygen species

Rot = Rotenone

S_1 = Surface area of plasma membrane (cm^2)

S_2 = Surface area of mitochondrial membrane (cm^2)

T = Absolute temperature (Kelvin)

TBST = Tris buffered saline with tween-20

TMRE = Tetramethyrhodamine ethyl ester

V_1 = Apparent cytoplasm volume (ml)

V_2 = Apparent mitochondrial matrix volume (ml)

V_c = Volume of the vascular region of the single capillary element model (ml)

V_c = Physical cytoplasm volume (ml) *[For rhodamine distribution model]*

V_e = Volume of the tissue region of the single capillary element model (ml)

V_e = Extracellular medium volume (ml) V_e = Extracellular medium volume (ml)

V_m = Physical mitochondrial matrix volume (ml)

V_{max1} = Maximum rate for DQ reduction via NQO1, (μmol/min)

V_{max2} = Maximum rate for DQH_2 oxidation via complex III, (μmol/min)

V_{F1}/α_1 = Virtual volume of distribution for DQ, (ml)

V_{F2}/α_2 = Virtual volume of distribution for DQH_2, (ml)

W = Convective transport velocity, (cm/min)

Z = Dye valence

Greek symbols

$\alpha = ZF/RT$ (mV^{-1})

$\beta = V_2/V_1$

δ = Fraction of $\Delta\psi_p$ not dissipated by CCCP

τ = Time constant of $\Delta\psi_p$ decay in presence of CCCP (min)

$\Delta\Psi_p$ = Plasma membrane potential (mV)

$\Delta\Psi_m$ = Mitochondrial membrane potential (mV)

α_1 and α_2 = Constants which account for the rapidly equilibrating interactions of DQ and DQH_2 with the 5% BSA (i.e., P_c) perfusate

α_3 and α_4 = Constants which account for the rapidly equilibrating interactions of DQ and DQH_2 with lung tissue sites of association, respectively

PUBLICATIONS

Z Gan, S.H. Audi, R.D. Bongard, M.P. Merker
Quantifying mitochondrial and plasma membrane potentials in intact pulmonary arterial endothelial cells based on extracellular disposition of rhodamine dyes.
American Journal of Physiology – lung cellular and molecular physiology, 300(5):L762-72, 2011.

Z Gan, DL Roerig, AV Clough, SH Audi
Differential responses of targeted lung redox enzymes to rat exposure to 60% or 85% oxygen.
Journal of Applied Physiology, 111(1): 95-107, 2011

M Ramakrishna, *Z Gan*, AV Clough, RC Molthen, DL Roerig, SH Audi
Distribution of capillary transit times in isolated lungs of oxygen tolerant rats
Annals of Biomedical Engineering, 38 (11), 3449-65, 2010.